# Regulation and function of the RPEL protein – Phactr1

**Maria Katarzyna Wiezlak**

University College London

and

Cancer Research UK London Research Institute

PhD Supervisor: Richard Treisman

A thesis submitted for the degree of

Doctor of Philosophy

University College London

May 2013

# Declaration

I Maria Wiezlak confirm that the work presented in this thesis is my own. Part of the work was performed in collaboration.

In Chapter 3, experiments presented in Figure 3.11 and parts of Figures 3.8, 3.10 and 3.15 were performed by Jessica Diring, a postdoc from the Transcription Laboratory at the London Research Institute. The structural analysis presented in Chapter 4 was performed in collaboration with Stephane Mouilleron, a postdoc from Neil McDonald's Laboratory (Structural Biology Laboratory at the London Research Institute). Of the work presented, I was involved in initial optimisation of complex formation and initial screens. Stephane Mouilleron performed majority of the crystallisation screens and the optimisation work at the crystallisation stage, collected the X-ray diffraction data and solved the crystal structures. He also performed SEC-MALLS analysis of the complexes. Where analyses were performed by Stephane Mouilleron, this is indicated in the figure legends. In Chapter 5, experiments presented in parts of Figures 5.3, 5.4, 5.5 and 5.6 were performed by Jasmine Abella, a postdoc from Michael Way's Laboratory (Cell Motility Laboratory at the London Research Institute).

All other experiments presented in this thesis were performed by the author. Where information has been derived from other sources, I confirm that this has been indicated in the thesis. Results presented in this thesis have been published in:

Wiezlak M, Diring J, Abella J, Mouilleron S, Way M, McDonald NQ, Treisman R. (2012). G-actin regulates shuttling and PP1 binding by the RPEL protein Phactr1 to control actomyosin assembly. Journal of Cell Science 125, 5860-5872.

Mouilleron S*, Wiezlak M*, O'Reilly N, Treisman R, McDonald NQ. (2012). Structures of the Phactr1 RPEL domain and RPEL motif complexes with G-actin reveal the molecular basis for actin binding cooperativity. Structure 20, 1960-70.

*equal contribution

# Abstract

Actin-binding proteins play well established roles in the regulation of actin dynamics and assembly of F-actin based structures involved in cell motility and adhesion. The Phosphatase and actin regulator (Phactr) family of proteins each contain four G-actin binding RPEL motifs and has been found to bind protein phosphatase 1 (PP1) via their C-terminal domain. Their function is not well established and it has been unclear whether G-actin can be their regulator. Members of the Phactr family are highly expressed in the nervous system and in some metastatic cancers.

The RPEL domain was previously shown to confer Rho-regulated nuclear shuttling and activation of Serum Response Factor (SRF) coactivator myocardin – related transcription factor A (MRTF-A, also known as MAL/MKL1). MRTF-A is cytoplasmic in unstimulated cells and accumulates in the nucleus upon activation of Rho-actin signalling.

In this thesis I show that activation of Rho-actin signalling by serum stimulation induces nuclear accumulation of Phactr1, but not other Phactr family members (Phactr2-4). Actin binding by the three Phactr1 C-terminal RPEL motifs is required for Phactr1 cytoplasmic localisation in resting cells. Phactr1 nuclear accumulation is Importin α–β-dependent. I also reveal that G-actin and Importin α–β bind competitively to nuclear import signals associated with the N- and C-terminal RPEL motifs in Phactr1. All four motifs are required for the inhibition of serum-induced Phactr1 nuclear accumulation by elevated G-actin. G-actin and PP1 bind competitively to the Phactr1 C-terminal region, and expression of Phactr1 C-terminal RPEL mutants that cannot bind G-actin induces actomyosin foci dependent on PP1 binding. In CHL-1 metastatic melanoma cells, Phactr1 exhibits actin-regulated subcellular localisation and is required for stress fibre assembly, motility, and invasiveness. These data support a role for Phactr1 in actomyosin assembly and suggest that Phactr1 G-actin sensing allows its coordination with F-actin availability.

## Acknowledgement

I would like to thank Richard Treisman for giving me the opportunity to work in his laboratory, for his supervision, support, and advice.

This work would never have been possible without the help of my collaborators. Many thanks to Stephane Mouilleron, who has been an excellent colleague and collaborator, always creative and helpful. I would also like to thank Jessica Diring, who offered her help with biochemical and mutational studies presented in Chapter 3. I am very grateful to Jasmine Abella, who helped with functional studies. Her experience and imaging skills greatly improved the work presented in Chapter 5.

I thank my thesis committee and collaborators, Neil McDonald and Michael Way, who offered their continuous support, help, and creativity during this project.

Work presented here would not be possible without the continuous help and advice of everyone in the lab. I thank Cyril for fruitful discussions, Diane and Patrick for great advice and comic relief, and Rob and Matthew for day-to-day help with almost everything! I also thank Ricky, Francesco, Anastasia, Charlie and past members of the lab. Special thanks go to Rafal, who helped me in the lab, when I started. Many thanks to Lucy, who has been extremely helpful with all the admin issues during my time at the LRI.

Thanks to Nicola O'Reilly for her expertise in peptide synthesis and to everyone in the LRI equipment park. Many thanks to Sally and Sophie (and Sabina and Erin), the graduate team at the LRI, for making this experience so enjoyable. I thank Cancer Research UK for funding.

Most importantly, would like to thank my family and friends. I would never have been able to do this work without my mom and my parents in law, who helped every day to take care of my little daughter Mia and were enormously supportive. I would also like to thank my grandpa, who encouraged me to pursue science.

Finally, I would like to thank my husband Jas, who has been extremely patient throughout my studies.

# Table of Contents

# Table of figures

# List of tables

# Abbreviations

| | |
|---|---|
| aa | amino acid |
| Abi1 | Abl-interactor 1 |
| ABP | actin binding protein |
| ADF-H | ADF-homology |
| ADP | adenosine diphosphate |
| AMP | adenosine monophosphate |
| Arp2/3 | actin-related protein 2/3 complex |
| ATP | adenosine triphosphate |
| bp | base pair |
| BSA | bovine serum albumin |
| CD | cytochalasin D |
| Cdc42 | cell division cycle 42, GTP binding protein |
| CDK | cyclin-dependent kinase |
| cDNA | complementary DNA |
| cGKIα | cyclic guanosine monophosphate -dependent protein kinase Iα |
| CIP | calf intestinal phosphatase |
| Cobl | cordon-bleu |
| CoIP | co-immunoprecipitation |
| Crm1 | chromosome region maintenance |
| DAPI | 4’,6’-diamidino-2-phenylindole |
| DMEM | Dulbecco's modified Eagle medium |
| DMSO | dimethyl sulfoxide |
| DNA | deoxyribonucleic acid |
| DNase | deoxyribonuclease |
| dNTP | deoxy-nucleotide triphosphate |
| DRC | DNA repair capacity |
| DTT | dithiothreitol |
| ECL | enhanced chemiluminescence |
| EDTA | ethylenediaminetetraacetic acid |
| EGTA | ethylene glycol tetraacetic acid |
| ELK1 | Ets-like transcription factor 1 |

| | |
|---|---|
| ENCCs | enteric neural crest cells |
| ENS | enteric nervous system |
| ENU | ethyl nitrosourea |
| ER | endoplasmic reticulum |
| ERK | extracellular signal regulated kinase |
| F-actin | filamentous actin |
| FCS | fetal calf serum |
| FH | formin homology |
| G-actin | globular actin |
| GADD34 | growth arrest and DNA damage protein |
| GAP | GTPase activating protein |
| GAPDH | glyceraldehyde 3-phosphate dehydrogenase |
| GDI | guanine nucleotide dissociation inhibitors |
| GDP | guanosine diphosphate |
| GEF | guanine nucleotide exchange factor |
| GFP | green fluorescent protein |
| GMF | glia maturation factor |
| GPCRs | G protein-coupled receptors |
| GSK3 | glycogen synthase kinase 3 |
| GST | glutathione S-transferase |
| GTP | guanosine triphosphate |
| GTPase | GTP hydrolase |
| GWAS | genome-wide association study |
| Hem-1 | hematopoietic protein 1 |
| HIV-1 | human immunodeficiency virus type 1 |
| HMECs | human mammary epithelial cells |
| HRP | horseradish peroxidase |
| HSCR | Hirschsprung disease |
| HSPC300 | haematopoietic stem/ progenitor cell protein 300 |
| HUVECs | human umbilical vein endothelial cells |
| ILK | integrin-linked kinase |
| IP | immunoprecipitation |

| | |
|---|---|
| IP3 | inositol-1, 4, 5-trisphosphate |
| IPTG | isopropyl-D-thiogalactopyranoside |
| IRSp53 | insulin receptor tyrosine kinase substrate p53 |
| JNK | c-Jun N-terminal kinase |
| kDa | kilodaltons |
| LatB | latrunculin B |
| LIMK | LIM kinase |
| LMB | leptomycin B |
| LZ | leucine zipper |
| MADS | MCM1, agamous, deficiens and SRF |
| MAL | megakaryocytic acute leukaemia |
| MAPK | mitogen-activated protein kinase |
| MAPKKKs | MAP kinase kinase kinases |
| MKL1 | megakaryoblastic leukaemia 1 |
| MLC | myosin light chain |
| MLCK | myosin light chain kinase |
| MLCP | myosin light chain phosphatase |
| MRCK | myotonic dystrophy kinase-related Cdc42-binding kinase |
| mRNA | messenger RNA |
| MRTF | myocardin related transcription factor |
| MYPT | myosin phosphatase targeting subunit |
| N-WASP | neural Wiskott-Aldrich syndrome protein |
| Nap1 | Nck-associated protein 1 |
| NIH3T3 | National Institute of Health 3T3 fibroblasts |
| NLS | nuclear localisation signal |
| NPF | nucleation promoting factor |
| PAGE | polyacrylamide gel electrophoresis |
| PAK | p21-activated kinase |
| PBS | phosphate buffered saline |
| PCR | polymerase chain reaction |
| PFAM | protein family database |
| PH | pleckstrin homology |

| | |
|---|---|
| Phactr | phosphatase and actin regulator |
| PIR121 | p53-inducible messenger RNA |
| PLD1 | phospholipase D1 |
| PP1 | protein phosphatase 1 |
| PtdInsI(4,5)P2 | phosphatidylinositol (4,5) bisphosphate |
| Rb | retinoblastoma |
| RNA | ribonucleic acid |
| RNP | ribonucleoprotein |
| ROCK | Rho kinase |
| RPEL motif | (RPxxxEL; PFAM 02755) |
| rpm | revolutions per minute |
| RPMI | Roswell Park Memorial Institute medium |
| RTK | receptor tyrosine kinase |
| s.e.m | standard error of the mean |
| SAP | SAF-AIB, Acinus, Pias |
| SAP1 | SRF accessory protein 1 |
| SAXS | small-angle X-ray scattering |
| SDS | sodium dodecyl sulfate |
| SEC | size exclusion chromatography |
| SEC-MALLS | SEC coupled to multi-angle laser light scattering |
| SNP | single-nucleotide polymorphism |
| Sra1 | steroid receptor RNA activator 1 |
| SRE | serum response element |
| SRF | serum response factor |
| SSH | suppression subtractive hybridizations |
| STOP genes | suppressors of tumorigenesis and/or proliferation |
| TAD | transactivation domain |
| Tat | transactivator of transcription |
| TBE | Tris/Borate/EDTA |
| TBS | Tris-Buffered Saline |
| TCF | ternary complex factor |
| Tβ4 | thymosin β4 |

| | |
|---|---|
| VEGF | vascular endothelial growth factor |
| VEGFR | vascular endothelial growth factor receptor |
| WASP | Wiskott-Aldrich syndrome protein |
| WAVE | Wiskott–Aldrich syndrome verprolin homologous protein |
| WH2 | WASP homology 2 |

v/v volume to volume
w/v weight to volume

Nucleotides:
A – adenosine
C – cytosine
G – guanosine
T – thymidine

The standard single-letter amino acid code and the International System of units (SI) were used.

# Chapter 1. Introduction

## 1.1 Functions of actin

Actin is one of the most abundant proteins in the cell. Diverse and complex actin functions result from its ability to polymerize. Actin polymerisation and de-polymerisation mechanisms are essential for the formation of a dynamic cytoskeleton. Its ability to form filaments provides force that can generate movement and establishes cell shape – two crucial characteristics that determine cell survival. Moreover, the capability of actin to crosslink its filaments with myosin explains the basis of cell contraction, adding yet another level of functional significance to this remarkable protein. Actin also emerges as a critical player in cell polarity and is involved in transcription regulation.

Here I review structures of monomeric and filamentous actin, describe signalling pathways that control actin turnover and discuss the basis of actin interaction with several binding partners. I also explain how the structures of actin complexes translate into function.

### 1.1.1 The dynamics of actin turnover

Actin was first isolated in 1940s during pioneering research on muscle contraction. Series of elegant experiments by Straub (1942) showed that actin exists in two main forms. The first form, called globular actin (G-actin), exists under low salt concentration, but in the presence of high salt it is able to polymerize and form actin filaments (F-actin). Straub found that actin, together with myosin, form a very regular network of filaments (accounting for more than half of the total protein content). In the 1960s, actin and myosin were again found in two different organisms, first in the parasite plasmodium (Hatano and Oosawa, 1966) and later in slime mold (Adelman and

Taylor, 1969). This early research revealed that viscous filaments found in muscle contain both actin and myosin. Those proteins formed a highly specialised system, which could be used to explain muscle contraction.

Monomeric actin, called G-actin is a 42kDa globular protein that binds either ATP or ADP (Figure 1.1). Main isoforms in vertebrates include cardiac, skeletal and smooth muscle α-isoforms and β- and γ-isoforms, found in both muscle and non-muscle cells. The subtle differences between actin isoform structures occur at the N-terminus (Herman, 1993). The first atomic resolution structure of G-actin was reported at 2.4 Å, bound to DNase I (Kabsch et al., 1990). This structural study revealed that over 40% of the G-actin structure is α-helical and that the nucleotide is bound in the deep cleft at the centre of G-actin (Figure 1.1 B). It also showed that $Mg^{2+}$ cation determines how strongly the nucleotide is bound. Several other structures of G-actin were reported bound to various actin-binding partners, like cofilin or profilin, reporting conformational changes upon binding different partners (for review, see (dos Remedios et al., 2003). With dimensions of around 55 Å x 55 Å x 35 Å, the actin monomer has four subdomains (Figure 1.1 A). In the actin filament, subdomains 1 and 3 are exposed at the barbed end and subdomains 2 and 4 are exposed at the pointed end. Subdomains 1 and 3 are structurally similar and many actin-binding proteins interact with G-actin within the target-binding cleft formed between those two subdomains (Figure 1.1 B) (Dominguez, 2007; Dominguez and Holmes, 2011). *In vivo*, G-actin binds $Mg^{2+}$ cation and ATP/ADP. The binding of ATP or ADP in the central part of the molecule is largely dependent on the communication between the nucleotide cleft and the target-binding cleft (Figure 1.1 B).

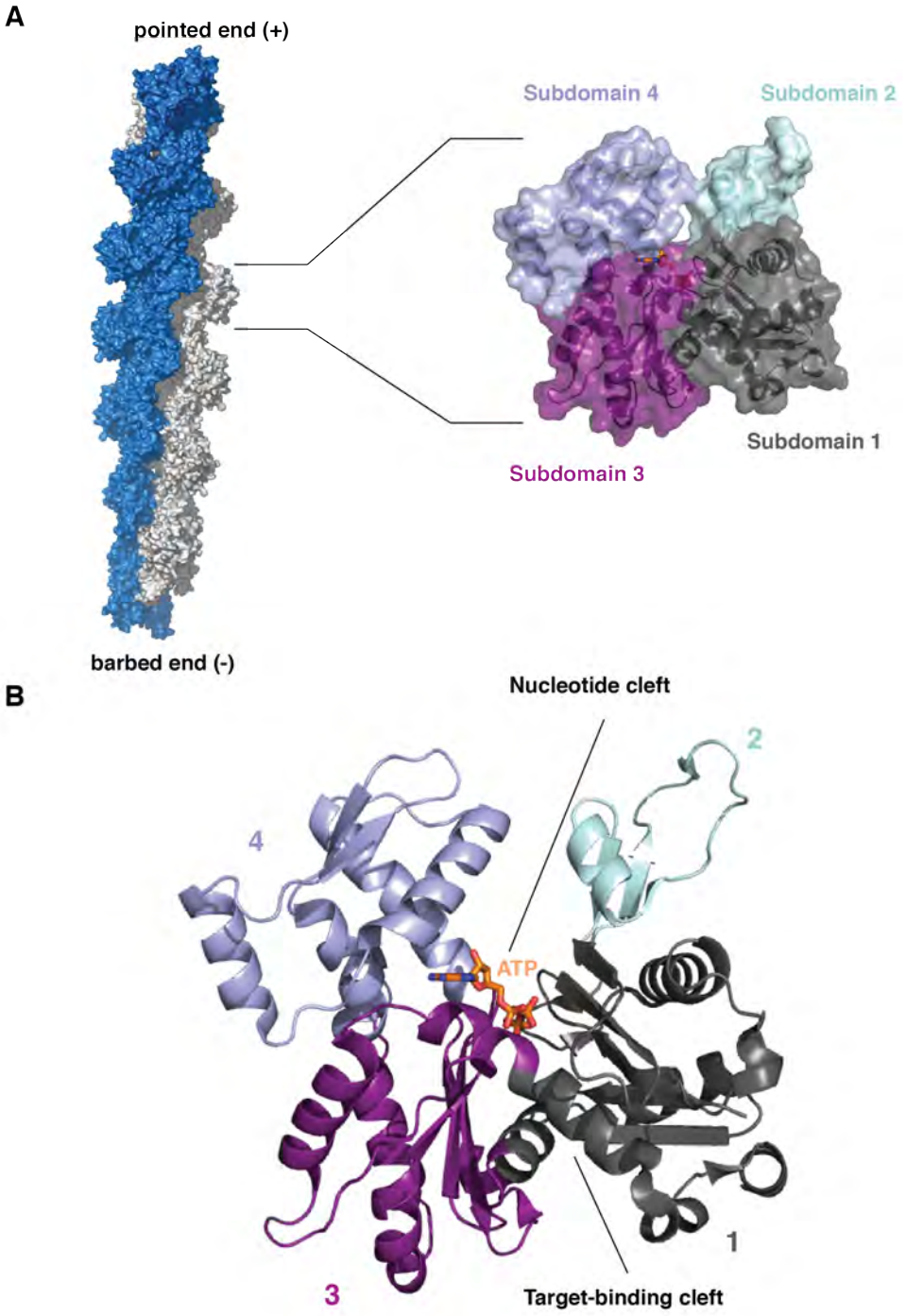
A
pointed end (+)
Subdomain 4
Subdomain 2
Subdomain 1
Subdomain 3
barbed end (-)
B
Nucleotide cleft
2
4
ATP
1
3
Target-binding cleft

**Figure 1.1 Monomeric and filamentous actin structure.**

**(A)** Left, atomic structure of actin filament, based on actin filament model of K.C. Holmes (Holmes et al., 1990); surface representation; the filament ends are labeled. Right, surface model of G-actin molecule indicating four subdomains (colour-labeled); subdomain 1 (residues 1-32, 70-144 and 338-372), subdomain 2 (residues 33-69), subdomain 3 (residues 145-180 and 270-337), subdomain 4 (residues 181-269). **(B)** Ribbon representation of G-actin structure indicating target-binding cleft between domains 1 and 3; ATP (orange) is bound within the nucleotide binding cleft; subdomains are colored as in A. Surface and cartoon structural models were assembled in PYMOL.

Filamentous actin (F-actin) was first described by Jean Hanson and Jack Lowy (Hanson and Lowy, 1964), nearly 50 years ago. They showed models, where F-actin is either a left-handed helix with a one-end start or a both-end start right-handed helix. The second model is a more conventional view of how F-actin is assembled, as later established by Kabsch (Holmes et al., 1990). Details of actin structure within the filament were recently deduced from X-ray fibre diagrams of F-actin and from electron microscopy, which led to atomic models of the actin filament (Fujii et al., 2010; Oda et al., 2009), for review see (Dominguez and Holmes, 2011).

There are three sequential phases of actin filament polymerisation (for review, see (Lodish H, 2000)). During the first phase actin assembles into short, unstable oligomers and once the oligomer reaches certain length (usually three or four subunits), it becomes more stable and is often referred to as 'nucleus'. During the second phase, the filament rapidly elongates by the addition of actin monomers to both of its ends. While the actin filament is growing, the concentration of G-actin monomers decreases until it is in equilibrium with the filament. This third phase is called a 'steady state', as there is no net change in the total mass of filaments and G-actin monomers exchange with subunits at the filament ends. Once the 'steady state' is reached, subunits continue to be added at the 'plus end' and lost form the 'minus end' (Lodish H, 2000). The two ends of an actin filament therefore exhibit different dynamics of subunit addition. The 'plus end' (also called the barbed end) elongates five to ten times faster then the 'minus end' (also called the pointed end). The length of the filament remains constant and the newly added subunits of G-actin are traveling through the filament, as if on a treadmill, until they reach the pointed end, where they dissociate. This process is therefore referred to as treadmilling, where one end of a filament grows in length while the other end shrinks (for review, see (Lodish H, 2000)).

Early studies suggested that ATP hydrolysis of bound nucleotide is strictly linked to actin polymerisation (Wegner, 1976). Subsequent studies showed however, that the kinetics of ATP hydrolysis and $P_i$ release are actually two separate events (Carlier et al., 1984; Pardee et al., 1982). It was shown that ATP hydrolysis occurs at

ten times higher rate than $P_i$ release. This suggested that the main intermediate in nucleotide hydrolysis is ADP-$P_i$-F-actin.

In a motile cell, treadmilling occurs faster then *in vitro,* where 3 μm of a filament is renewed in 2 hours (for pure actin) and accelerates by two orders of magnitude, mainly due to the activity of actin depolymerizing factor - cofilin (Carlier et al., 1999). Actin-binding partners tightly regulate actin turnover. Dynamic actin filament turnover and the interaction of actin filament with actin-binding proteins is crucial for cell morphology, like establishing cell shape and maintaining cellular symmetry. Actin polymerisation is also crucial for single cell migration and for collective cell movement. Moreover, cell behaviour aspects, like phagocytosis or cell contraction are dependent on actin turnover. Therefore, actin polymerisation must be tightly coupled to extracellular signals. Signalling pathways connecting these events are dependent on specific, abundant, signalling molecules called Rho-GTPases (for review, see (Etienne-Manneville and Hall, 2002)).

### 1.1.2 Actin control by Rho-GTPases

Actin turnover in the cell is dynamically regulated by extracellular signals. The Rho family of small GTPases play a critical role in the regulation of actin dynamics by extracellular signals. GTPases are proteins that control multiple cellular processes. They are often referred to as molecular switches because they cycle between two conformational states, one bound to GTP and other bound to GDP, as they are able to perform hydrolysis of GTP to GDP (Figure 1.2). Those two states are reflecting their active or inactive form respectively. Three types of regulators that are controlling the activity of Rho-GTPases are called: (1) guanine nucleotide exchange factors (GEFs), which load the Rho proteins with GTP, (2) GTPase activating proteins (GAPs), which stimulate the GTPase activity and (3) guanine nucleotide dissociation inhibitors (GDIs), which are responsible for preventing nucleotide exchange (Figure 1.2) (for review, see (Jaffe and Hall, 2005)). GTPases are small, monomeric proteins that can be divided into five different groups: Ras, Rab, Ran, Arf and Rho (Etienne-Manneville and Hall, 2002).

Because the activation of Rho GTPases leads to the assembly of dynamic actin cytoskeleton, they will be discussed here in more detail.

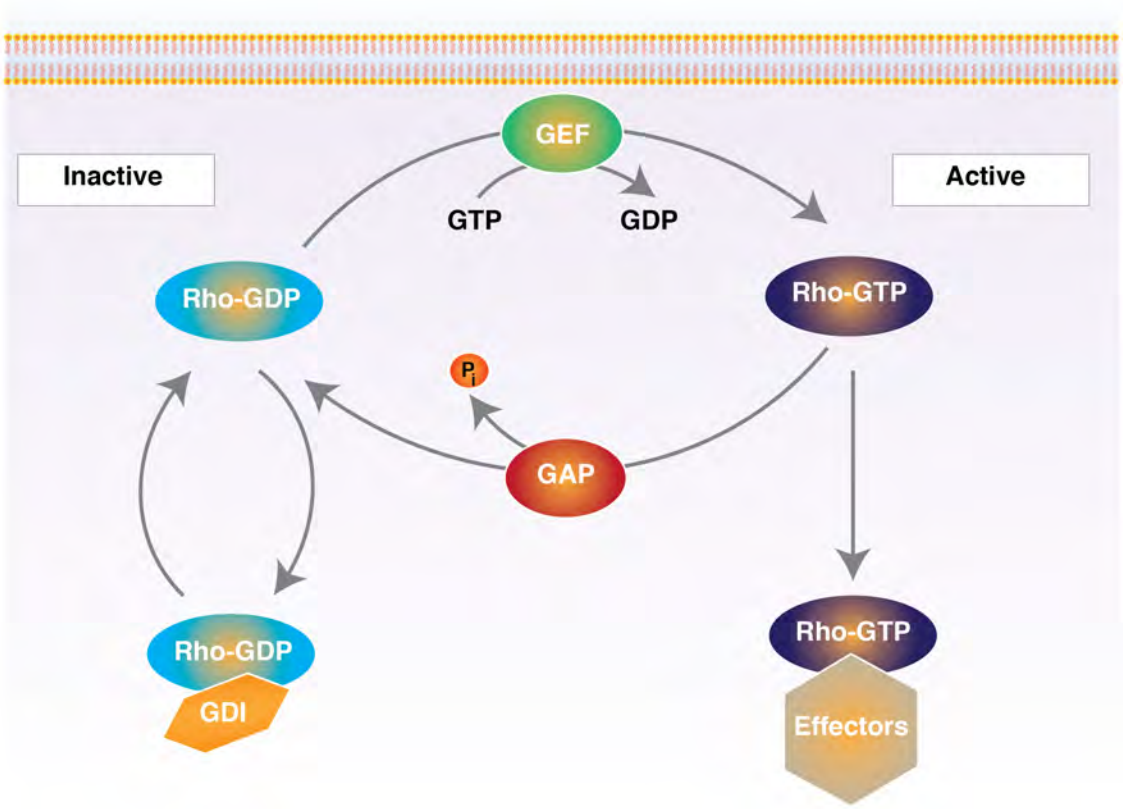


**Figure 1.2 The Rho GTPase cycle.**

The cycle between an active (GTP-bound) and an inactive (GDP-bound) conformation of Rho GTPases. In the active state (dark blue) Rho-GTPases interact with one of the multiple target proteins (effectors). GEFs (green) catalyse nucleotide exchange and mediate activation, GAPs (red) stimulate GTP hydrolysis leading to inactivation, GDIs (orange) prevent nucleotide exchange (for details, see text) (Etienne-Manneville and Hall, 2002).

Rho GTPases are a Ras-related family of GTPases, found in all eukaryotic cells. There are many families of Rho GTPases in mammals. The well-studied families include Rho, Rac and Cdc42 (some of them are represented by multiple isoforms). The best known are the three isoforms of Rho: A, B and C and three isoforms of Rac: 1, 2 and 3, but Rho-GTPase family has many more members. Those include for example RhoD, Rnd1 and 2, RhoE, Rif and others (Aspenstrom et al., 2004). In *Saccharomyces cerevisiae* there are five Rho proteins: Rho1, 2, 3, 4 and Cdc42. In worm *Caenorhabditis elegans* there are predicted to be ten Rho-GTPases and *Drosophila melanogaster* has eleven (for review, see (Etienne-Manneville and Hall, 2002)).

The first insight into the function of Rho GTPases, Rho and Rac was provided over twenty years ago. It was shown that Rho rapidly stimulates stress fibre and focal adhesion formation when microinjected into serum starved Swiss 3T3 cells (Ridley and Hall, 1992). Similar experiments with Rac showed induction of actin protrusions, which caused the growth of lamellipodia (Ridley et al., 1992). Related approaches showed that Cdc42 was also able to influence actin cytoskeleton by promoting the formation of actin-rich membrane extensions, called the filopodia (Nobes and Hall, 1995). These findings led to the proposal that all three members of Rho-GTPase family control distinct functions during the formation of actin cytoskeleton. They were predicted to be involved in regulating separate signal transduction pathways that connect receptors localised on the plasma membrane with various actin-based structures in the cell. Subsequently, Rho-GTPases were shown to be involved in regulating variety of different signalling pathways, like control of cell polarity, cell cycle progression, vesicular transport, enzymatic activity and transcription regulation. It is not clear, to what extent these functions are independent of their roles in controlling cytoskeleton, as most effectors of Rho-GTPases are cytoskeletal regulators.

Here, I will review how Rho-GTPases link extracellular signals with two important biochemical functions: formation of actin cytoskeleton and gene expression. I will explain how these important biochemical processes mediated by Rho-GTPases translate into biological functions.

#### *1.1.2.1 Rho-GTPases in regulation of actin dynamics*

Rho-GTPases control three crucial events in actin dynamics: actin nucleation through nucleation promoting factors (NPFs) and actin turnover through effectors like cofilin, ROCK or PAK.

Rho-kinase (ROCK) is the effector of the small GTPase Rho playing pivotal roles in cytoskeleton rearrangements. Rho-kinase is a serine/threonine kinase, structurally related to myotonic dystrophy kinase (DMPK) and to Cdc42-binding MRCK. There are two isoforms of ROCK kinase, ROCK1 and ROCK2 (referred to collectively as ROCK). The domain organisation of ROCK can be divided into three crucial parts, with the kinase domain being located at the N-terminus, a large coiled coil domain in the middle, containing the Rho-binding site and the pleckstrin homology (PH) domain at the C-terminus. Binding of Rho to ROCK activates its kinase activity (for review, see (Amano et al., 2010)). Structural studies of ROCK revealed a model of ROCK function that depends on the two extension regions flanking the kinase domain forming an intramolecular homodimer. This conformation of ROCK maintains its active form (Yamaguchi et al., 2006). Additionally, the domain that interacts with Rho forms a parallel structure supporting the view that active ROCK is a dimer (Chen et al., 2002). The C-terminal region of ROCK containing the PH domain can be engaged an intramolecular interaction with the catalytic N-terminal region of ROCK therefore inhibiting its kinase activity (Amano et al., 1997; Ishizaki et al., 1997; Leung et al., 1996). Moreover, proteolytic cleavage at the C-terminus of ROCK leads to apoptotic phenotypes like membrane blebbling caused by constitutive active ROCK (Coleman et al., 2001).

ROCK is ubiquitously expressed in all tissues, with ROCK1 being more abundant in liver, lung and testis, whereas ROCK2 in neural tissues and in muscles (Leung et al., 1996). Although very similar in amino acid content (64% homology), the two isoforms are implicated in mediating different functions. ROCK1 is involved in stress fibres assembly and ROCK2 was reported to mediate phagocytosis and cell

contractions. Both of those functions are reliant on the control of myosin light chain (MLC) phosphorylation (Yoneda et al., 2005).

Interestingly, mice carrying homozygous deletion of ROCK1 and ROCK2 show postnatal and embryonic lethality respectively (Shimizu et al., 2005). To better understand the function of ROCK *in vivo*, several small molecule inhibitors have been developed to selectively target ROCK. The two broadly used inhibitors are Fasudil and Y-27632, which act in an ATP-competitive manner. Both of those inhibitors induce a conformational change resulting from binding to the catalytic domain of ROCK, which results in its inhibition. Some ROCK inhibitors have been developed for pharmacological purposes and are now in clinical trials (for review, see (Amano et al., 2010)).

Rho is a specific activator of actin filament formation and actomyosin network formation and it influences cytoskeleton through two effectors, formin mDia and ROCK. Rho, through the activation of ROCK, mediates actomyosin crosslinking. ROCK is involved in specifically phosphorylating components of the myosin network, like myosin targeting subunit of myosin light chain phosphatase (MLCP) complex (MYPT) or MLC itself, which allows F-actin filaments to crosslink with myosin (Riento and Ridley, 2003) (described in detail in section: 'Actomyosin contractility'). In mammalian cells, diaphanous-related formin, mDia and in *Saccharomyces cerevisiae* formins Bni1 or Bnr1 are direct effectors of Rho. Activation of Rho by GTP, relieves an intramolecular auto-inhibitory interaction in these formins, which causes exposure of their actin-binding domains and subsequent actin nucleation (Pring et al., 2003; Watanabe et al., 1999; Zigmond, 2004). Cooperation of Rho effectors: ROCK and mDia, is essential for the formation of actomyosin bundles, like stress fibres.

Interestingly, the treatment of starved fibroblasts with either C3 transferase (Rho signalling inhibitor) (Morii and Narumiya, 1995) or Y-27632 leads to different effects on cell morphology. Y27632 treatment inhibited serum-induced stress fibre assembly and focal adhesion formation, as did C3 transferase treatment, but Y27632 additionally induced membrane ruffling. Analysis of this effect showed that Rho-mDia signal leads

to the activation of Rac signalling, which can than be supressed by ROCK (Tsuji et al., 2002). Opposing effects of mDia and ROCK were also suggested in the process of adherens junctions in epithelial tissues formation (Sahai and Marshall, 2002).

ROCK can also directly activate LIM kinase (LIMK) through phosphorylation, which has implications for cytoskeleton organisation. Firstly, LIMK is a direct kinase for cofilin, an F-actin severing factor. Cofilin is regulated on several levels, through changes in intracellular pH, protein-protein interactions and phosphorylation (described in section: 'Actin binding proteins and their roles'). Once phosphorylated by LIMK, cofilin becomes inactive and cannot disassemble actin filaments. Therefore, Rho is again signalling to promote F-actin formation. Rac and Cdc42 are also able to phosphorylate LIMK through their effector kinase, p-21-activated kinase (PAK). Phosphorylation of LIMK by PAK and subsequent phosphorylation of cofilin leads to inhibition of actin monomer dissociation from the pointed end of the filaments. As a consequence, cellular membrane protrusions are formed (for review, see (Jaffe and Hall, 2005)).

The Arp2/3 complex (described in section: 'Actin binding proteins and their roles') is a major activator of actin polymerisation. Rac and Cdc42 influence the formation of morphologically different structures at the plasma membrane, but the genesis of both lamellipodia and filopodia is similar. They arise through actin polymerisation events mediated by Arp2/3 acting together with nucleation promoting factors (NPFs). The Arp2/3 complex mediates dynamic actin branching, therefore allowing the actin network to grow and extend to form three-dimensional systems (for review, see (Jaffe and Hall, 2005)). Interestingly, both Rac and Cdc42 are able to activate branching through binding to different NPFs.

Active Cdc42 (Cdc42-GTP) can directly bind to an NPF of the Wiskott-Aldrich syndrome protein family (WASP), which causes release of the intramolecular inhibitory interaction of the Arp2/3 complex, consequently allowing it to engage in an active state and promote F-actin formation (Millard et al., 2004). Another direct target linking Arp2/3 and Cdc42 was recently identified and is referred to as Toca-1 (Transducer of

Cdc42-dependent actin assembly-1). Toca-1 was proven to be required for the activation of WASP (Ho et al., 2004). However, the existence of two direct targets within this pathway opened many questions about their cooperation. Recently, Cdc42 interaction with Toca-1-WASP complexes was implicated in many biological functions, like endocytosis, cell motility and invasiveness (Bu et al., 2010; Chander et al., 2012; Hu et al., 2011). Moreover, the direct binding of Cdc42 and phosphatidylinositol (4,5) bisphosphate (PtdIns (4,5) $P_2$) simultaneously activates neural WASP (N-WASP), which leads to the activation of the Arp2/3 complex (Badour et al., 2004; Vartiainen and Machesky, 2004).

Arp2/3 complex can also be activated by regulator of lamellipodia formation – Rac, through NPFs called verprolin-homologous proteins (WAVEs). WAVE functions in Rac-induced membrane ruffling, but Rac does not bind directly to WAVE, which raised questions about its regulation (Miki et al., 1998). A substrate for insulin receptor, IRSp53, was found to activate Arp2/3 (Miki et al., 2000). Activated Rac was found to bind the N-terminus of IRSp53 and synergistically IRSp53 C-terminal domain was shown to bind to WAVE. Consequently, a trimolecular complex was formed to promote Arp2/3-mediated actin polymerisation, which caused membrane ruffling. The Scar/WAVE regulatory complex (WRC) was shown to be a component of a pentameric complex containing direct Rac targets, like Sra1 (Steroid receptor RNA activator 1)/PIR121 (p53-inducible messenger RNA), Nap1 (Nck-associated protein 1), Hem-1 (hematopoietic protein 1), HSPC300 and Abi1 (Abl-interactor 1) (Eden et al., 2002; Gautreau et al., 2004; Innocenti et al., 2004; Kunda et al., 2003; Steffen et al., 2004; Weiner et al., 2006). WRC exists in an autoinhibited state and is activated by negatively charged phospholipid membranes or the small GTPase Rac1 (Koronakis et al., 2011).

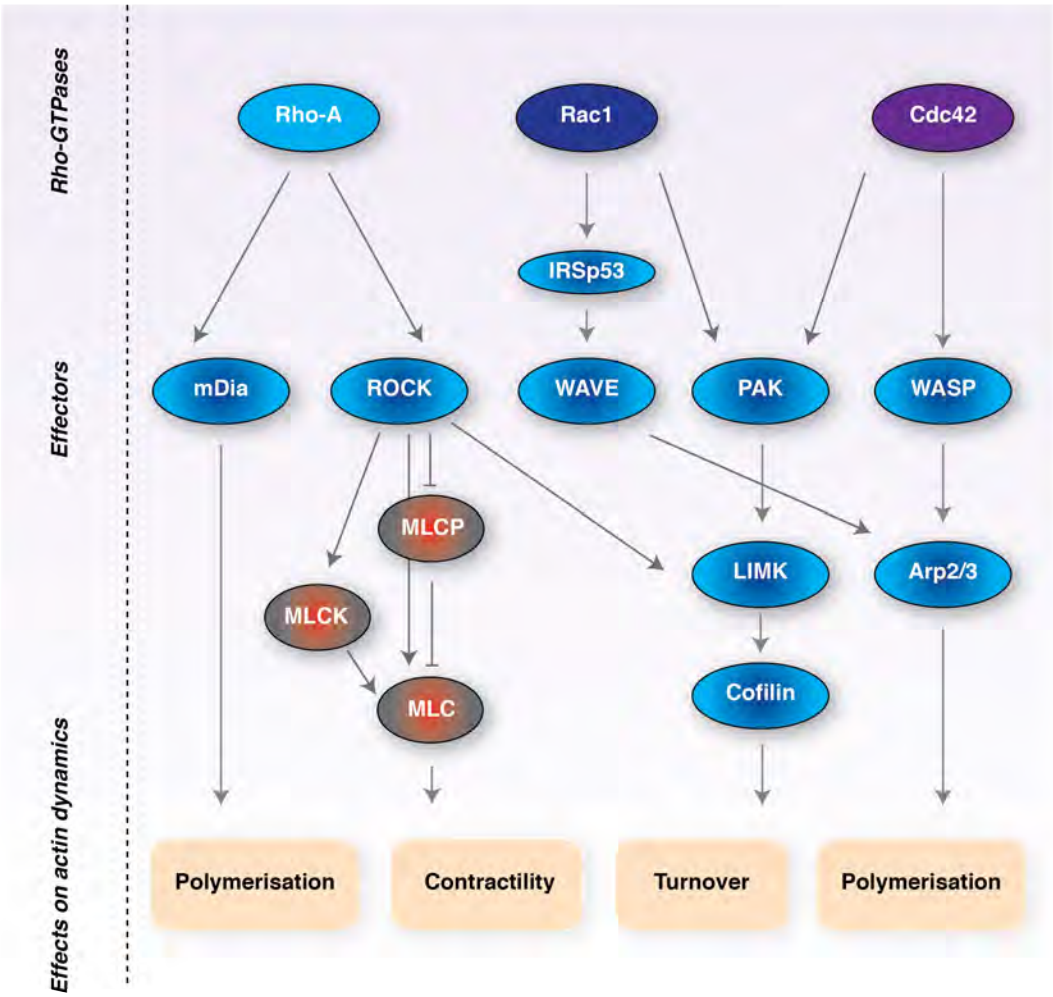


**Figure 1.3 Rho-GTPases in actin dynamics.**

The downstream targets of active Rho-GTPases (Rho-A, Rac1 and Cdc42) include variety of effectors (not all are shown), like kinases: PAK and ROCK and nucleation promoting factors: mDia, WASP, WAVE. mDia stimulates polymerisation of actin by producing unbranched actin filaments. WASP and IRSp53/WAVE interact with Arp2/3 complex to generate branched actin filaments. PAK phosphorylates LIMK, which in turn phosphorylates and inhibits cofilin thereby regulating actin filament turnover. ROCK contributes to actin turnover by phosphorylating LIMK. ROCK also directly phosphorylates MLC and MLCK and promotes inhibitory phosphorylation of MLCP, therefore regulating actomyosin contractility.

#### *1.1.2.2 Rho-GTPases in gene expression*

Rho-GTPases also regulate signal transduction pathways that regulate gene expression. Those functions can be either actin-related or actin-independent. The best-known Rho-dependent mechanism of transcription regulation is the Serum Response Factor (SRF)-myocardin related transcription factor (MRTF) pathway (described in detail in section: 'Actin in transcription regulation – regulation of SRF cofactors MRTFs') (Miralles et al., 2003). In this pathway transcriptional activity responds directly to changes in G-actin concentration induced by Rho activation. Rho signalling stimulates changes in actin cytoskeleton, through the activation of formins, Arp2/3 complex or actomyosin formation, depending on the cell type. Activation of those pathways leads to overall decrease of the cellular G-actin pool. MRTF, a G-actin binding protein, senses the decrease in G-actin concentration, which causes its detachment from G-actin and subsequent nuclear accumulation. In the nucleus, MRTF co-activates SRF-dependent transcription. Interestingly, SRF is responsible for mediating expression of many cytoskeletal genes, including actin itself. Therefore, this circuit might serve as an example of signal-induced, actin-dependent cellular homeostasis.

Not all gene expression events mediated by Rho-GTPases are actin-dependent. Rho, Rac and Cdc42 can all activate c-Jun N-terminal kinase (JNK) and mitogen-activated protein kinase (MAPKs) (Coso et al., 1995; Minden et al., 1995; Puls et al., 1999). JNK/MAPK signalling pathway is involved in integrating extracellular signals into such physiological responses like differentiation, development, inflammatory response and apoptosis. JNK signalling is activating components of transcription machinery, e.g. activator protein-1 (AP-1), which becomes active through phosphorylation (for review, see (Weston and Davis, 2007)). Rho GTPases were reported to target four different MAP kinase kinase kinases (MAPKKKs). Rac and Cdc42 interact with MLK2, MLK3 and MEKK4, while MEKK1 is a target for all three GTPases (Burbelo et al., 1995; Gallagher et al., 2004; Teramoto et al., 1996).

Additionally, Rho-GTPases target different scaffold proteins, which regulate the specificity of MAP kinase signalling pathways (Morrison and Davis, 2003). For example, a scaffold protein CNK1 was identified as a Rho target, because it interacts with Rho-specific GEFs, Net1 and p115RhoGEF (Jaffe et al., 2005). CNK1, a protein controlling activation and specificity of MAP kinase signalling cascade, was shown to specifically promote Rho-dependent JNK activation in HeLa cells.

Moreover, in response to extracellular stimulus, Rho, Rac and Cdc42 can activate nuclear factor κ-light-chain-enhancer of activated B cells (NFκB) (Perona et al., 1997). NFκB proteins are abundant transcription factors (Sen and Baltimore, 1986), found in all cell types, regulating variety of cellular processes like development, cellular growth or apoptosis and are critically responsible for immune response during inflammation (for review, see (Gilmore, 2006)). It was suggested that Rho-GTPases might induce transcriptional activity of NFκB through a mechanism that involves phosphorylation of inhibitory subunits IκBs at serines S32 and S36 (Perona et al., 1997). However, this finding was disputed due to the fact that Rac and Cdc42 can stimulate production of reactive oxygen species (ROS) and cytokines, which are powerful activators of NFκB (Kheradmand et al., 1998; Tapon et al., 1998). Therefore, it is unlikely that Rho-GTPases act directly on NFκB.

### 1.1.3 Actin binding proteins and their roles

Actin can bind a number of proteins, commonly called ABPs (actin-binding proteins). They have diverse functions and can be divided into G-actin sequestering, filament capping, crosslinking and filament severing. They belong to different structural families and can bind actin in a variety of ways. Proteins that interact with F-actin are involved in the regulation of actin dynamics or they are recruited to the cytoskeleton to perform specific functions. Proteins that interact with G-actin can either regulate actin assembly (e.g. profilin, cofilin) (for review, see (dos Remedios et al., 2003)) or they can be themselves regulated by G-actin (e.g. RPEL proteins: MRTFs and Phactr family) (Huet et al., 2012; Miralles et al., 2003; Wiezlak et al., 2012).

Altogether, ten years ago there were over 160 identified ABPs (dos Remedios et al., 2003) but this number is still growing. Most of ABPs bind to the same element in G-actin, and therefore compete with each other. ABPs can include membrane-associated proteins, receptors or ion transporters. At least thirteen can cross-link filaments of actin and other can bind other cytoskeletal elements. Recent classification divides cytoskeletal ABPs into seven main groups, including monomer-binding proteins (e.g. DNaseI), filament depolymerising (e.g. CapZ and cofilin), pointed-end-binding (e.g. tropomodulin) and severing (e.g. gelsolin). Proteins that have two actin-binding sites belong are actin nucleators (e.g. Arp2/3) and those that prevent polymerisation (e.g. tropomyosin) are called stabilising proteins. Finally, there is a group of motor proteins that can rapidly move on actin filaments (i.e. myosin family) (dos Remedios et al., 2003). Therefore, actin filaments together with big group of cytoskeletal actin binding proteins provide molecular basis for cell movement and mechanical structure of the cell (Figure 1.4).

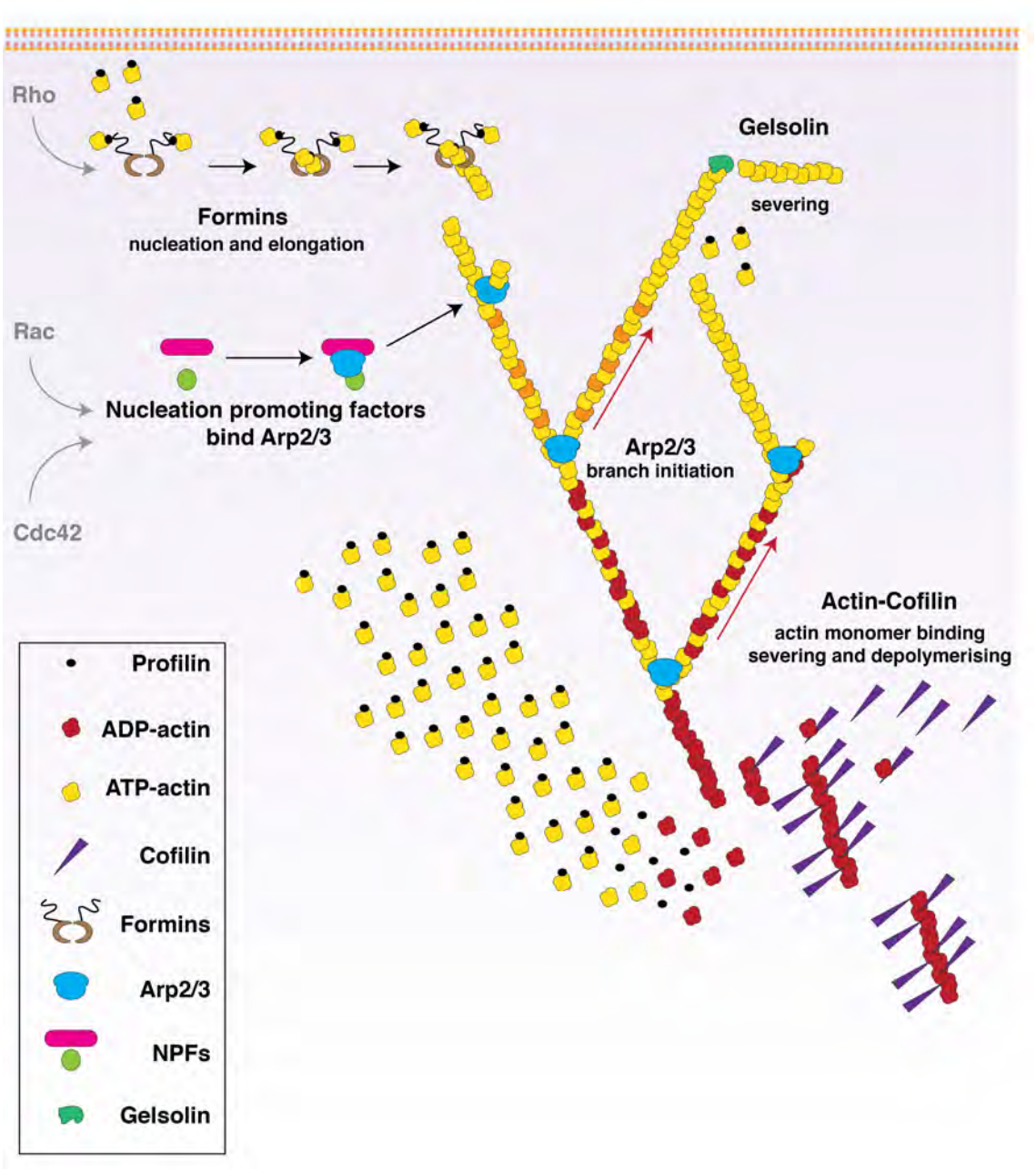


**Figure 1.4 Cytoskeletal roles of actin binding proteins.**

Overview of actin-binding proteins functions in actin dynamics. Rho-GTPases (Rho, Rac and Cdc42) regulate actin filament formation through different mechanism. Formins are mediating *do novo* filament nucleation and filament elongation (top left); NPFs activate Arp2/3 to mediate actin branching (left and middle); profilin promotes F-actin assembly (middle); cofilin promotes depolymerisation of F-actin and maintains G-actin pool (below, right); gelsolin severs and cap actin filaments (top, right); adapted from (Pollard and Cooper, 2009).

However, not all ABPs are involved in filament dynamics. There are many other biological functions that depend on actin dynamics, like endocytosis or cytokinesis. Endocytosis is a process that begins at many independent sites in the cell and involves variety of membrane proteins, clathrin and some adaptor proteins. The forces, which are contributing to the deformation of plasma membrane and into executing the fission itself, come from actin polymerisation and from actin motors action on the filaments. ABPs involved in this process include actin nucleators such as formins, Arp2/3, WH2 domain and other groups like profilin, WASP of cofilin (for review see (Mooren et al., 2012)). During cytokinesis, separation of two daughter cells occurs when myosin II generates contraction on polymerising actin filaments by pulling them together (for review see (Pollard, 2010)). Actin and nucleation-promoting factors are also crucial elements involved in the formation of bacterial comet tail after eukaryotic cell invasion, and myosin motors can transport organelles along actin filaments (Pollard and Cooper, 2009).

Moreover, actin is component of nuclear structure and function, a regulator of chromosome organisation and gene activity. Actin and multiple actin binding factors, even those normally mediating cytoskeletal processes, are also involved in multiple tasks that control transcription (for review, see (Olson and Nordheim, 2010; Percipalle, 2012)).

This discussion will be focused on actin dynamics and regulation. In the section below, I will first summarise crucial cytoskeletal actin binding partners and then focus on the non-cytoskeletal roles of actin and ABPs. I will provide insights into actin binding mechanisms and later explain why G-actin binding is a critical aspect of RPEL (RPxxxEL motif) proteins regulation.

### 1.1.4 Actin-binding proteins involved in actin filament nucleation and dynamics.

#### *1.1.4.1 ADF/Cofilin*

ADF/Cofilin family members are small (15-19kDa), ubiquitously expressed proteins involved in actin filament depolymerisation. They act mainly in such processes as cytokinesis or membrane ruffling (for review, see (Bernstein and Bamburg, 2010)). ADF and cofilin are expressed at different levels in adult tissues. ADF is highly expressed in kidney, testes, intestine and nerve tissue (Bamburg et al., 1980) and high cofilin levels are found mainly in fibroblasts, osteoclasts and hematopoetic cells (Yonezawa et al., 1990). The ADF/cofilin family of proteins contains actin-depolymerising factor (ADF), cofilin-1 expressed in non-muscle cells, cofilin-2 found in muscle cells and twinfilin. Twinfilin is made of two ADF-homology (ADF-H) domains separated by a linker and its role is to prevent filament assembly by binding to the barbed end of the growing actin filament (Ojala et al., 2002). Because twinfilin has a slightly different mechanism of action than other family members, it has recently been classified separately (Bernstein and Bamburg, 2010).

Cofilin is mainly localised in the cytoplasm and upon activation it relocates to cortical regions to drive cell motility though membrane ruffling (Bamburg and Bray, 1987). It is also found at cleavage furrow of cells under division (Nagaoka et al., 1995) or at the neuronal growth cones (Nagaoka et al., 1996). Interestingly, the function of cofilin depends largely on how its concentration relates to overall actin concentration. At low cofilin/actin concentrations *in vitro,* filament severing will occur, while high concentrations will promote stabilisation of actin filament. At saturating concentrations cofilin can even nucleate actin and form complexes with actin monomers. It still remains to be elucidated how exactly this concentration dependence coordinates actin dynamics at the molecular level (Bernstein and Bamburg, 2010).

Recent studies revealed the interplay between cofilin and Arp2/3, a complex involved in basic processes such as forward movement of cells, crucial for embryonic development. Cofilin binding to actin was shown to reduce both the affinity of actin filaments for Arp2/3 complex and the stability of F-actin branches (Chan et al., 2009). There is no nuclear localisation signal in actin, but several studies found that cofilin can facilitate actin nuclear functions such as chromatin remodelling or regulation of gene expression by chaperoning actin to the nucleus (Pederson, 2008; Zheng et al., 2009). Recent study showed that dephosphorylated cofilin is required for nuclear localisation of actin, mediated by Importin 9 (Dopie et al., 2012). Importin 9 interacts with both actin and cofilin to promote active import of actin, therefore regulating actin-dependent transcription.

Some recently characterised functions of cofilin are not related to cytoskeleton dynamics. Cofilin was found in mitochondria of apoptotic neuroblastoma cells. The presence of cofilin in the mitochondria seems to be required for mitochondrial pore permeability and cytochrome *c* release during apoptosis. There is no requirement for actin binding to cofilin during this process, but mutation of actin binding domain can in turn block apoptosis (Chua et al., 2003; Klamt et al., 2009). Previously described as an inactive form, phospho-cofilin emerging function is to activate phospholipase D1 (PLD1) (Han et al., 2007). This function is largely relevant during such processes as cancer cell migration or neuronal development (Bernstein and Bamburg, 2010).

The structure of actin binding to ADF was recently reported, in the form of a complex with the C-terminal ADF part of twinfilin (Paavilainen et al., 2008). This structural study revealed how ADF-H domain inhibits G-actin nucleotide exchange, a mechanism occurring during gelsolin and WH2 proteins interaction with actin. The proposed model of inhibition explains in molecular detail how weakening intrafilament interactions can induce depolymerisation of actin filament (Paavilainen et al., 2008).

#### *1.1.4.2 Profilin*

Profilin facilitates nucleotide exchange and acts as an important chaperone during F-actin assembly. The family of profilins consists of small (around 19kDa) (Ampe et al., 1988) proteins found in all eukaryotes, with four profilin genes found in humans (for review, see (Polet et al., 2007)). There are several isoforms of profilin and they all have highly conserved N-terminus with the C-terminal part resembling gelsolin.

The main function of profilin is to bind actin subdomains 1 and 3 close to the hinge and to modulate nucleotide cleft opening. Essentially, profilin together with cofilin enhance the filament turnover (Didry et al., 1998). Profilin binding to actin allows for a quick growth of the barbed-end of actin filament (Ampe et al., 1988). Cofilin phosphorylation facilitates its dissociation from ADP-actin while profilin promotes the exchange of ADP for ATP and allows for profilin-ATP-actin addition. Profilin binds actin in a specific way, which leaves the front of actin cleft unoccupied. This allows for simultaneous binding of other proteins, especially WH2 domains (for review, see (Dominguez and Holmes, 2011)).

The crystal structure of profilin bound to actin pointed out two molecular states of the complex, an “open” and a “closed” state (Chik et al., 1996). It was shown that profilin-actin assembled into a high-order structure and actin-actin contacts resembled an oligomeric protein. This was the first step towards understanding the interactions within the actin filament. Crystallographic data also demonstrated that profilin could bind proline-rich ligands (Mahoney et al., 1999). The interaction with proline-rich motifs enables targeting of profilin to specific sites to perform regulatory functions. Moreover, active export of actin from the nucleus, mediated by Exportin 6 depends on actin-profilin interaction (Stuven et al., 2003).

### *1.1.4.3 Gelsolin*

Gelsolin is the founding member of a gelsolin superfamily of proteins. It is localised to the cytoplasm of variety of eukaryotic cells and can bind, sever and cap filaments of actin (Sun et al., 1999). One isoform of gelsolin can also be found in plasma, where its levels largely increase after trauma (Christofidou-Solomidou et al., 2002; Rothenbach et al., 2004). All members of gelsolin superfamily contain three to six gelsolin-like repeats. One of the main functions of this 84kDa protein is to control polymerisation of barbed ends, but gelsolin was also described as an actin filament initiator, due to its capability to bind two actin molecules. $Ca^{2+}$ levels, phosphorylation of tyrosine, phosphoinositides and pH can all regulate activity of gelsolin (for review, see (Silacci et al., 2004)). Structural studies revealed that the C-terminal tail of gelsolin could modify its conformation by sensing $Ca^{2+}$ levels. When $Ca^{2+}$ levels are low, gelsolin remains in a globular conformation. High $Ca^{2+}$ levels induce structural change in gelsolin, which results in the release of its C-terminal tail and exposes actin-binding sites (for review, see (McGough et al., 2003)).

There are two actin-binding sites in gelsolin, one at the N- and one at the C-terminus, which allows severing of two actin filaments while remaining bound to the newly formed one. The uncapping of actin requires binding to phosphatidylinositol lipids by gelsolin, exposing the barbed end of actin for polymerisation (Liepina et al., 2003). Actin filament remodelling by gelsolin is linked to its role in cell motility. The first indication of this role was provided by experiments on fibroblasts that were transfected with gelsolin (Cunningham et al., 1991). Overexpression of gelsolin resulted in more motile cell behaviour and phospholipase C inhibition (Sun et al., 1997). Later, gelsolin was also linked to the regulation of hematopoetic stem cell motility, podosome formation and neuronal growth cones regulation (for review, see (Silacci et al., 2004)).

#### *1.1.4.4 Thymosin*

Thymosin β4 (Tβ4) is an actin-buffering agent. Tβ4, the best-known member of the thymosin family is an important G-actin-sequestering molecule in mammalian cells. This small (around 5kDa) protein is unstructured in solution due to hydrophobic amino acid composition (Low et al., 1981). Interestingly, when Tβ4 binds to actin, it increases its helical content, but still remains unstructured. Tβ4 was first isolated from the thymus, but it is widely distributed in different tissues (Erickson-Viitanen et al., 1983). Tβ4 is mainly found in neural tissue, in leukocytes and macrophages (for review, see (dos Remedios et al., 2003)). Its main function is to inhibit polymerisation of actin filaments by sequestering actin. Hence, the function of Tβ4 is to maintain the pool of unpolymerised actin, which can be used to promote robust assembly of F-actin. Tβ4 is overexpressed in many tumours, it promotes wound healing and was recently found to be a potent therapeutic tool for myocardial infarction (Husson et al., 2010). Moreover, studies of the unique property of Tβ4 to promote wound healing has revealed that it can be used to reprogram adult cardiac fibroblasts into cardiomyocyte-like cells, what can have potential regenerative purposes (Qian et al., 2012). However, it is not known if the effects of Tβ4 expression are directly linked to its actin binding capability or to interactions with other partners. Understanding roles of this small peptide requires detailed analysis of its structural properties.

Tβ4 serves as a model for actin-binding WH2 (WASP Homology 2) motifs. WH2 motifs were first recognised in WASP (Wiskott-Aldrich Syndrome Proteins) family of proteins and later in variety of other proteins. These proteins consists of one, two or more WH2 motifs and, in spite their homology, there are some that promote profilin-like, F-actin assembly. Crystallographic and mutagenetic studies revealed that if the motifs are in cluster of three, only the first one has very high affinity to actin. Consequently, the weaker interaction of the C-terminal region of Tβ4/WH2 with actin accounts for the rapid change between inhibition and promotion of F-actin assembly (Hertzog et al., 2004). It was later confirmed that mulifunctionality of Tβ4/WH2 is gained when WH2 motifs are in tandem (Husson et al., 2010). This structural feature can generate new functions, like actin filament nucleation or severing. Current work on

Tβ4 includes designing single or repeated WH2 motifs, that have a potential of modulating their own function and could be used as therapeutics.

#### *1.1.4.5 Formins*

The ability to form actin filaments *de novo* from monomers requires actin-nucleating proteins. Formins are major actin nucleating factors. They are large proteins (120-220 kDa), containing several protein-interacting domains and binding to variety of partners (Chesarone et al., 2010). They are defined by a presence of the highly conserved formin homology 1 and 2 (FH1 and FH2) domains. The mechanism of nucleation by formins depends on stabilisation of the actin dimer through FH2 domain interaction. The FH1 domain contains a proline-rich region, which increases the local concentration of profilin-bound actin monomers, therefore driving filament elongation (Paul and Pollard, 2009).

The ability of the formin family to drive actin elongation and nucleate actin makes them very important building components of the cytoskeleton. Because they are important for the formation of F-actin filaments, formins play multiple roles in cell migration. They mediate the growth of filopodia, support lamellipodial sheets and drive stress fibres assembly. They are also required for endosome formation and efficient phagocytosis. Moreover, they support membrane transport and assembly of the cytokinetic ring in yeast (for review, see (Chesarone et al., 2010)).

Regulation of the activity of formins can depend on allosteric autoinhibition or might be mediated by other proteins (Firat-Karalar and Welch, 2011). For example, it is not clear how formins can be released from certain autoinhibitory interactions, but there is evidence that Rho-GTPases have crucial roles in activating formins at various levels (Heasman and Ridley, 2008). It was recently shown that binding of actin monomers by formins is mediated by their autoinhibitory C-terminal DAD domains, which cooperate with FH2 to enhance nucleation without affecting the rate of filament elongation (Gould

et al., 2011). The DAD domain therefore has dual function as it mediates autoinhibition and nucleation.

#### *1.1.4.6 The Arp2/3 complex*

The second major actin nucleating factor is the actin related protein (Arp2/3) complex. Arp2/3, together with nucleation promoting factors (NPFs) have the ability to nucleate the formation of new filaments extending from the sides of existing filaments. As a consequence, a Y-branched network of filaments can be formed. The actin nucleation mechanism mediated by Apr2/3 is essentially different from the formins-driven mechanism, because Arp2/3 binds to the existing filament and recruits actin monomers. The exact mechanism of Arp2/3-mediated nucleation is still not well understood, but several models have been proposed (for review, see (Firat-Karalar and Welch, 2011)).

Arp2/3 complex contains Arp2, Arp3 and additional subunits ARPC1-5 (Goley and Welch, 2006). Moreover, to be able to nucleate actin, Arp2/3 requires the cooperation of NPFs, which contain multiple WH2 domains and Arp2/3-binding central/acidic sites (CA), called WCA domains. A recent model of Arp2/3 complex Y-branching mechanism suggests that Arp2 and Arp3 interact with the new filament while ARPC2 and ARPC4 contact the mother filament in the same time (Rouiller et al., 2008). It is believed that all seven subunits of Arp2/3 coordinate to anchor the pointed end of the new filament to the existing network. NPFs then deliver actin subunits to the Arp2/3 complex at the barbed end, through WH2 domain interaction (Pollard and Borisy, 2003; Rouiller et al., 2008). More mutational analysis is required to better understand the mechanism of Y-branching by Arp2/3.

The activity of NPFs is required for the efficient nucleation of actin by Arp2/3. Therefore, understanding the function of NPFs is crucial to elucidate how these complexes act. There are several well-characterised NPFs in mammalian cells, like Wiskott-Aldrich Syndrome Protein (WASP), neuronal WASP (N-WASP) or verprolin-

homologous protein (WAVE), which are all Rho-GTPase effectors (Firat-Karalar and Welch, 2011). The mechanism of actin nucleation by NPFs could be mediated through allosteric regulation of their WCA domains, for example by autoinhibition (e.g. WASP and N-WASP) (Derivery and Gautreau, 2010). Another mode of regulation includes simultaneous interaction with signalling molecules, like Rac-GTPase and phospholipids (e.g. WAVE) (Lebensohn and Kirschner, 2009). Some studies also suggest that regulation of nucleation can be driven by oligomerisation mechanism, as dimerization of WCA domains can increase Arp2/3 binding affinity of NPFs (Padrick et al., 2008).

Some actin-binding proteins compete with Arp2/3 for F-actin binding, which leads to debranching of F-actin filament. Recently, actin-cofilin interaction was found to change actin conformation and prevent it from binding to Arp2/3, therefore inhibiting actin nucleation (Bernstein and Bamburg, 2010). Another, recently discovered protein, glia maturation factor (GMF) targets Arp2/3 at branch points and prevents actin binding at those sites (Gandhi et al., 2010). Those, and other mechanisms are coordinated in the migrating cell to efficiently nucleate F-actin and promote branching in different cellular locations.

Rho-driven nucleation of actin filaments by the Arp2/3 complex and formins promotes cell migration. Cell movement also depends on force generation that is created by the assembly of F-actin with myosin II. The details of this association are presented in the section below.

### 1.1.5 Actomyosin contractility

Studies of cell movement have been pursued for decades and questions about how muscle contraction drives movement resulted in many theories (for review, see (Vale and Milligan, 2000)). Over forty years ago, electron microscopy of muscle tissue revealed that F-actin filaments are bridged by myosin and it was proposed that this association could generate force (Huxley, 1969). This concept was soon coupled to the discovery that the tight actomyosin complex dissociates in the presence of ATP, and the

power stroke is a result of the phosphate release after the hydrolytic step of this reaction (Lymn and Taylor, 1971). The power generated during this hydrolysis is basic to cell movement. Given the profound effects that the actomyosin-generated force can have on a cell, it is not surprising that this process must very tightly regulated.

#### *1.1.5.1 Myosin II*

Myosin II (also known as conventional myosin) is a crucial motor molecule in both muscle and non-muscle cells. Myosin II is an important component of stress fibres, contractile structures containing actin filaments, crosslinking proteins and arrays of myosin. Stress fibres are found in non-muscle cells, where they are involved in adhesion and motility. Bundles of actomyosin in stress fibres are major mediators of cell contraction and resemble highly organised actomyosin structures present in muscle cells (for review, see (Pellegrin and Mellor, 2007)).

Myosin II belongs to a large family of myosins and is known to be involved in cell migration, cell adhesion and cell polarity. Other subfamilies of myosin are called unconventional myosins and are involved in variety of processes ranging from membrane transport, mRNA transport to cytokinesis and signal transduction (Vale and Milligan, 2000). Muscle myosin II is mainly involved in muscle contraction and is expressed in muscle cells. Non-muscle myosin II is expressed in all eukaryotic cells and mediates variety of processes including cytokinesis and cell movement (Ma et al., 2012).

Non-muscle myosin II is a multi-subunit protein, a product of MYH9, MYH10 and MYH14 genes encoding three different isoforms of the 230 kDa myosin heavy chains and MYL6, MYL9, MYL12 genes encoding 20 kDa ‘regulatory’ light chains (Conti and Adelstein, 2008). All isoforms of non-muscle myosin II are hexamers, consisting of two heavy chains and two pairs of light chains. There is no evidence that the light chains have specificity towards certain isoforms of the heavy chains (Ma et al., 2012), therefore for simplicity they will be referred to here as non-muscle myosin II. The important property of myosin II is the ability of actin binding in an ATP-dependent

manner. ATP dissociates from the actin-myosin complex in $Mg^{2+}$-dependent process, which results in power stroke-driven tension or translocation of myosin on actin filaments. Structurally, the helical coiled coil domain located at the C-terminus of myosin is responsible for filament formation and the N-terminal globular motor domain contains ATP-binding and actin-binding sites. Thus, the N-terminal part of non-muscle myosin II and smooth muscle myosin is responsible for its ability to create tension (Kovacs et al., 2003; Wang et al., 2003a). Although structurally similar, isoforms of non-muscle myosin exhibit differences in their motor activities, resulting from alterations in ATP hydrolysis rate and the actin-myosin association period (Kovacs et al., 2003; Wang et al., 2003a).

Importantly, the activation of ATPase activity of myosin II strictly depends on the phosphorylation of S19 and sometimes additionally T18 of the 20 kDa myosin light chain. Therefore, myosin light chain is often referred to as regulatory myosin light chain (RMLC/ RLC/ MLC).

#### *1.1.5.2 Regulation of actomyosin crosslinking*

Both non-muscle and smooth muscle myosin II are regulated by phosphorylation of their MLC. This phosphorylation plays an essential role in smooth muscle contraction in muscle cells and in actin-myosin interaction during stress fibres and contractile ring formation in non-muscle cells (Adelstein and Sellers, 1987; Huttenlocher et al., 1995). MLC phosphorylation allows the heavy chain of myosin II to be released, which facilitates the association of myosin globular head with actin filaments. Subsequently, the force generated by ATP release is used by myosin to translocate ("walk") on F-actin. When multiple myosins associate with actin filaments, contractile force is generated (Olson and Sahai, 2009).

There are multiple kinases involved in MLC phosphorylation (Figure 1.5). Initially, $Ca^{2+}$-calmodulin-dependent myosin light chain kinase (MLCK) was found to mediate phosphorylation of MLC at S19 (Adelstein et al., 1975). However, it was

already known that $Ca^{2+}$-independent mechanisms could regulate smooth muscle myosin II (for review, see (Somlyo et al., 2000)). This led to the discovery of primary pathway involved in this phosphorylation, involving Rho and Rho-associated kinase ROCK (Amano et al., 1996). ROCK, which phosphorylates MLC at S19 and T18, is now established as a major $Ca^{2+}$ -independent MLC kinase.

Additionally, other kinases have been shown to mediate MLC phosphorylation at those two sites, like zipper-interacting protein kinase (ZIPK), which is primarily involved in apoptosis (Murata-Hori et al., 1999). Recently, myotonic dystrophy kinase-related Cdc42-binding kinase (MRCK) and Rho-ROCK pathway were reported to cooperate to phosphorylate MLC during cell invasion. Interestingly, the involvement of those pathways was dependent on cell morphology and the type of cell movement (Wilkinson et al., 2005). Another, recently found kinase associated with MLC diphosphorylation is integrin-linked kinase (ILK), which most likely mediates this process in vascular smooth muscle cells and tissues (Wilson et al., 2005). During endothelial cell retraction, MLC phosphorylation might be mediated by p21-activated kinase (PAK) (Zeng et al., 2000). Additional kinases were also implicated in facilitating this process (for review, see (Olson and Sahai, 2009)). Nevertheless, two critical kinases mediating this phosphorylation are MLCK and ROCK, acting in $Ca^{2+}$-dependent and $Ca^{2+}$-independent manner respectively. To effectively control the phosphorylation level of MLC, a specific MLC phosphatase (MLCP) must act on myosin (Figure 1.5).

MLC phosphorylation level is therefore determined by the balanced activities of MLC kinases and MLCP. At a given $Ca^{2+}$ concentration, MLCP can alter MLC phosphorylation levels hence regulating the contractile behaviour of the cell (Ito et al., 2004).

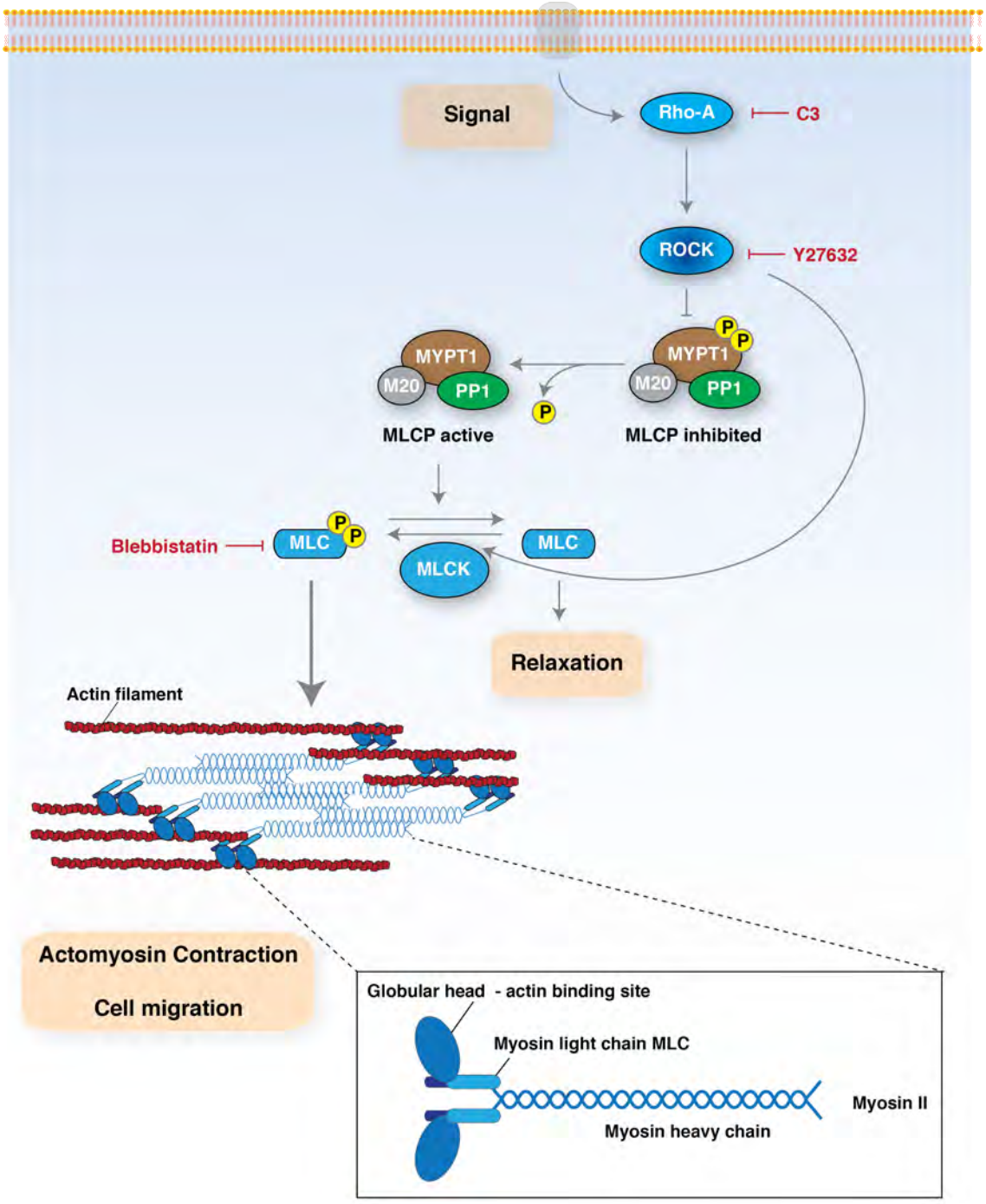
Signal
Rho-A
C3
ROCK
Y27632
MYPT1
M20
PP1
MLCP active
MLCP inhibited
Blebbistatin
MLC
MLCK
Relaxation
Actin filament
Actomyosin Contraction
Cell migration
Globular head - actin binding site
Myosin light chain MLC
Myosin heavy chain
Myosin II

**Figure 1.5 Regulation of actomyosin contractility.**

Phosphorylated MLC promotes actomyosin crosslinking, cell contraction and migration. Myosin II binds actin filaments through its globular heads and forms multimers through interaction of its heavy chains (indicated in the box on the bottom). The major, $Ca^{2+}$-independent mechanism that regulates actomyosin contraction is driven by signal-regulated Rho-kinase activity through direct phosphorylation of myosin light chain (MLC) of myosin II at S19 and T18 (location of MLC within myosin II is schematically indicated in the box on the bottom). Rho-kinase also directly phosphorylates regulatory subunit of MLCP, MYPT1 at T853 and T696, which leads to inhibition of MLCP. Inhibitors of this pathway include Rho inhibitor C3 transferase (C3), ROCK inhibitor (Y-27632) and Myosin II ATPase inhibitor Blebbistatin.

#### 1.1.5.2.1 Regulation of MLC phosphorylation by MLCK

MLCK is a ubiquitous, $Ca^{2+}$-calmodulin-activated kinase, found in many tissues. It is specifically implicated in regulating phosphorylation of MLC in smooth muscle, therefore mediating muscle contraction. Smooth muscle MLCK is encoded by a single MYLK1 gene, but its expression is not restricted to muscle tissues. MYLK2 encodes the skeletal muscle isoform and MYLK3 is a cardiac specific gene (Hong et al., 2011). Studies of the MLCK-mediated enzymatic reaction suggest that MLCK can bind MLC and ATP and than convert bound substrates to MLC-P and ADP. There are differences in the relative amounts of two MLC forms (MLC/ MLC-P) in smooth muscle and non-muscle cells and this can be evaluated by measuring the ADP concentration in those cells. Consequently, the kinetics of this reaction can differ depending on the cell type and is rather isoform-specific. Nevertheless, both skeletal and smooth muscle isoforms show strong reaction inhibition upon phosphorylated MLC (Geuss et al., 1985).

Structurally, MLCK contains a calmodulin and actin-binding site at the N-terminus followed by the unstructured proline-rich region. Interestingly, it also contains additional two F-actin binding sites called Ig1 and Ig2. The kinase domain of MLCK is located in the middle of the protein and it can mediate binding to MLC and to ATP. This catalytic domain of MLCK phosphorylates MLC at S19. At the C-terminus, MLCK contains smooth muscle myosin binding site and can bind both smooth muscle myosin monomers and filaments (Hong et al., 2009). No crystal structure of full length MLCK is available, but structures of several domains of MLCK suggest that it is a flexible molecule. Electron microscopy studies suggest that it can adopt either elongated or compact conformation (Mabuchi et al., 2010). It has been an intriguing question how MLCK phosphorylates MLC in the environment of the muscle. MLCK is understood to be tightly bound to the contractile apparatus therefore it is puzzling how it mediates the phosphorylation. Supposedly, its flexibility can explain now MLCK can simultaneously bind actin, myosin and initiate phosphorylation of MLC to stimulate muscle contraction (Hong et al., 2011).

In contrast to ROCK, MLCK has only two known substrates in vivo: MLC of smooth muscle myosin and non-muscle myosin. MLCK can only phosphorylate S19 and not T18 like some other MLC kinases. However, phosphorylation of MLC S19 is sufficient to promote muscle contraction. Additionally, knockout mice studies reveal that MLCK-mediated phosphorylation is essential in tracheal, bronchial and gastrointestinal smooth muscle (He et al., 2008; Zhang et al., 2010). It was only shown recently that MLCK can phosphorylate non-muscle myosin in addition to smooth muscle myosin, but no kinetic evidence was shown (Yuen et al., 2009). An *in vitro* study shows that non-muscle myosin is not as good substrate for MLCK as the smooth muscle myosin (Hong et al., 2011).

#### 1.1.5.2.2 Regulation of MLC phosphorylation by ROCK

ROCK phosphorylates multiple cellular substrates and is involved in essential processes like cell migration, cell polarity, cytokinesis, stress fibre and focal adhesion formation and smooth muscle contraction (for review, see (Amano et al., 2010)). Interestingly, to control MLC phosphorylation during these processes it acts in two different ways. The first mechanism involves phosphorylation of MLC S19 and T18 by ROCK (Amano et al., 1996). The second mechanism is less direct. MLC phosphorylation is controlled by MLCP complex (described in section: 'MLC dephosphorylation by MLCP'), which consists of catalytic subunit (PP1), and two regulatory subunits. One of those subunits is myosin phosphatase targeting subunit (MYPT1). ROCK phosphorylates MYTP1 at T853 and T696, which results in MLCP inhibition and consequent increase of the MLC phosphorylation (Kimura et al., 1996).

The formation of stress fibres and focal adhesions is regulated by the Rho-ROCK signalling pathway (Amano et al., 1997). Again, a crucial regulatory mechanism in this process is the specific phosphorylation of MLC, which can be mediated by direct kinase activity of ROCK in cooperation with actin nucleating factor, formin mDia. It was proposed that different ratios of the mDia and ROCK activities could result in various F-actin morphologies, like diverse thickness and densities of actin fibres

(Watanabe et al., 1999). Another mechanism involved in stress fibre formation is the phosphorylation of LIMK by ROCK, which results in the increased cofilin phosphorylation at serine S3. Cofilin depolymerizing activity towards F-actin becomes inhibited by this phosphorylation, resulting in F-actin stabilization. ROCK emerges here as a crucial molecule involved in maintaining stress fibre assembly, by balancing phosphorylation of MLC and LIMK. Indeed, purified stress fibres from fibroblasts contain Rho, ROCK and MYPT1 and treatment with specific inhibitors of ROCK but not MLCK results in the loss of stress fibres and tension (Katoh et al., 2001).

#### 1.1.5.2.3 MLC dephosphorylation by MLCP

MLCP was originally purified from chicken gizzard myofibrils as a heterotrimer (Alessi et al., 1992). The catalytic part was a 37kDa protein and the two regulatory subunits were described as 110kDa large subunit and 20kDa small subunit. The catalytic component was found to be the β isoform of protein phosphatase 1 catalytic subunit (PP1C β), also known as PP1Cδ. The larger regulatory subunit was later described as myosin phosphatase targeting subunit (MYPT) also known as myosin binding subunit (MBS) and the smaller subunit was called small regulatory subunit (M20) (Hartshorne et al., 1998).

To form an active MLCP holoenzyme, MYPT binds PP1 through its N-terminal region and M20 through the C-terminal part. MYTP is a critical component of this complex, as it brings together the phosphatase catalytic subunit and the phosphorylated myosin. The association of PP1 with MYPT1 also contributes to substrate specificity (Terrak et al., 2004). The MYPT gene encodes for many isoforms, but the best known is MYPT1 as it is expressed in many tissues with dominant expression levels in smooth muscle. The N-terminal region of MYPT1 contains seven ankyrin repeats and a PP1-binding motif defined by a specific consensus (R/K)$x_{0\text{-}1}$(V/I)$x$(F/W). At the very C-terminus, MYPT binds to M20 regulatory subunit. Importantly, MYPT1 can be a platform for interaction with multiple ligands. Firstly, MYPT1 binds myosin at two different sites: it interacts with phosphorylated MLC at the N-terminus and binds

myosin through its C-terminal domain. Moreover, it was reported to interact with GTP-bound RhoA and with phospholipids (for review, see (Ito et al., 2004)).

The M20 subunit is a non-catalytical part of the MLCP holoenzyme of unknown function. Interestingly, the C-terminal region of M20 shares 91% amino acid identity with an isoform of MYPT, MYPT2. This finding may suggest that M20 can be in fact produced the same gene as MYPT2. Binding of M20 to MYPT1 does not interfere with the phosphatase activity of the complex, and it was proposed that M20 might bind myosin dimers or microtubules (for review, see (Ito et al., 2004)).

There are several mechanisms that regulate the activity of MLCP. The inhibitory phosphorylation sites in MYPT1 (T853 and T696) can be targeted by multiple kinases, including ROCK. ZIPK (also referred to as MYPT1 kinase) increases phosphorylation of another inhibitory phospho-site, T654. ILK is implicated in phosphorylating MYPT1 at T696. ROCK, ZIPK and ILK can all directly phosphorylate S19 and T18 of MLC and are all implicated in $Ca^{2+}$-independent regulation of smooth muscle (Ito et al., 2004). Other inhibitory mechanisms were also proposed, like phosphorylation by the Cdc42 effector PAK or the Rac1 effector DMPK (Ito et al., 2004). Taken together, these findings show that variety of kinases are involved in the regulation of MLCP activity.

The mechanism by which phosphorylation of MYPT1 inhibits MLCP is not understood. Possibly, MYPT1 phosphorylated at T696 induces conformational change of the holoenzyme, which affects the active site of PP1 and inhibits its activity. Alternatively, the inhibitory phosphorylation at T696 could affect the binding of PP1 to the substrate. Nevertheless, this issue needs to be investigated further through structural and biochemical analysis.

Since MYTP1 contributes to substrate recognition, dissociation of MYPT from PP1 promotes MLC phosphorylation (Gong et al., 1992). Subcellular localisation of the complex can have a role in modulating its function. It was shown that stimulation of smooth muscle cells with a specific agonist, prostaglandin, induced translocation of the MLCP complex from the cytoplasm to the plasma membrane, which resulted in the

dissociation of the subunits (Shin et al., 2002). This translocation was effectively inhibited by the ROCK inhibitor, Y-27632, but no direct role of T853 or T696 phosphorylation in this process was shown. Instead, it was proposed that the lipid environment in the plasma membrane could promote dissociation of the holoenzyme. This shows that the activity of MLCP can be regulated by complex dissociation or targeting to specific subcellular compartments.

MLCP activity can also be regulated by CPI-17, a small (17kDa), inhibitory protein expressed mainly in muscle and nervous tissues. CPI-17 is a specific inhibitor of MLCP holoenzyme, which and can also inhibit dissociated PP1. The centrally located domain of CPI-17 is essential for the specific recognition of MLCP. Within this region, CPI-17 is phosphorylated at T38 primarily by PKC, which leads to its activation. Interestingly, ROCK, ILK and PAK were also implicated in mediating this phosphorylation (for review, see (Ito et al., 2004)). Some studies suggest a potential role of CPI-17 in $Ca^{2+}$ sensitization as phosphorylation of CPI-17 correlates with MLC phosphorylation during stimulation with agonists in smooth muscle (Kitazawa et al., 2003; Niiro et al., 2003).

Lastly, MLCP can be regulated through activation. The most important mechanism that mediates MLCP activation is the interaction of MYPT1 with the cyclic guanosine monophosphate (cGMP)-dependent protein kinase Iα (cGKIα). A structural study recently showed that MYPT1 binds to cGKIα through its C-terminal leucine zipper site (Zhou, 2011). Another described mechanism is related to the cyclic nucleotide signalling and involves RhoA inhibition by cGKIα or PKA. Several studies indicate that phosphorylation of RhoA at S188 can influence its interaction with RhoGDI, which results in reduction of the active GTP-bound RhoA. Consequently, this inhibition decreases ROCK activity therefore promoting MLCP activation (Ellerbroek et al., 2003).

## 1.2 Actin in transcription regulation – regulation of SRF cofactors MRTFs

It has now been established that besides its cytoskeletal roles, actin can also mediate non-cytoskeletal processes in the cell. Years of research now show that actin is involved in chromatin remodelling, histone modification and gene transcription by all three RNA polymerases in eukaryotes. Actin also binds several ribonucleoprotein (RNP) complexes in cell nuclei. Moreover, actin can regulate the activity of some transcription factors and determine their subcellular localisation (for review, see (Olson and Nordheim, 2010; Percipalle, 2012)). G-actin can enter and exit cell nuclei by diffusion; however, it has now been established that actin can also be actively imported to the nucleus through Importin 9 and cofilin association, and exported through interaction with Exportin 6 and profilin (for review, see (Olson and Nordheim, 2010). It is puzzling how actin mediates functions in the nucleus and why it is crucial for variety of aspects during gene expression.

The ability of actin to polymerise in the cytoplasm is well characterised and was introduced in previous sections. It is not well understood however, if actin can form filaments in the nucleus, as many components of the machinery that drives F-actin formation are absent from the cell nuclei. Some effectors of Rho-GTPases were found to shuttle between the nucleus and the cytoplasm, like mDia2 (Miki et al., 2009) or N-WASP (Suetsugu and Takenawa, 2003), but the significance of these events is not clear. Some studies revealed that the conformation of actin in the nucleus is different than in the cytoplasm. This was achieved by the generation of specific antibodies that only recognised a conformation of native actin, present in the nucleus and not in actin filaments in the cytoplasm (Gonsior et al., 1999). Some studies indeed show by photobleaching that F-actin is present in the nucleus (McDonald et al., 2006). There is now evidence that actin is involved in transcription initiation, elongation and at gene level (for review, see (Olson and Nordheim, 2010; Percipalle, 2012)). Recent evidence demonstrates presence of nuclear actin targets, like pluripotency gene *Oct4* in *Xenopus*. Nuclear actin polymerisation is necessary for transcriptional reprogramming of *Oct4*

through *Toca1* (Miyamoto et al., 2011) and for retinoic acid-induced *HoxB* transcription (Ferrai et al., 2009). These observations suggest that polymerised actin is functional in cell nuclei.

G-actin is also involved in transcriptional activities. Identification of G-actin regulated nucleocytoplasmic shuttling of Serum Response Factor (SRF) coactivators, MRTFs, revealed for the first time a direct mechanism enabling cytoplasmic G-actin to control nuclear transcriptional activity (Miralles et al., 2003). It was later shown that nuclear G-actin regulates the activity of nuclear MRTFs towards SRF-dependent transcription (Vartiainen et al., 2007).

In the following section I will focus on the specific function of G-actin in controlling nucleocytoplasmic shuttling and the activity of transcription cofactors of the MRTF family. I will discuss how G-actin binding through regulatory RPEL motifs in MRTFs confers their subcellular localisation and SRF-dependent transcription (for review, see (Olson and Nordheim, 2010; Posern and Treisman, 2006)).

### 1.2.1 SRF transcription factor

SRF is a ubiquitous transcription factor, encoded by a single gene, whose homologs are found across metazoans (Norman et al., 1988). It belongs to a larger group of MADS-box (name is derived from the founding members of the family: MCM-1, AG, DEFA and SRF) transcription factors, which have been defined on the basis of their primary sequence homology between proteins in yeast, plants, insects, amphibians and mammals (Shore and Sharrocks, 1995). MADS-box transcription factors have significant biological roles in the yeast pheromone response, cell cycle regulation, metabolism and flower development in plants. The MADS-box is a sequence of 56 amino acids, with nine identical residues in all described proteins. The deletion studies of the 90 amino acid sequence encompassing this region in SRF showed that this region and its C-terminal extension are sufficient for DNA binding

(Norman et al., 1988). Most of the MADS-box proteins have the MADS-box located N-terminally, but in SRF it is located in the central part of the protein.

To bind DNA, SRF homodimerises and specifically targets a palindromic DNA sequence $CC(A/T)_6GG$ called the CArG-box, found upstream SRF-dependent genes (Pellegrini et al., 1995). This sequence is called a serum response element (SRE) and is a genomic sequence first identified as a c-*fos* promoter (Treisman, 1986). The crystal structure of SRF bound to DNA revealed that the homodimeric SRF-DNA complex is organised in three structural layers, which contain the coiled coil (bottom) layer, the β-sheet (middle) layer and the C-terminal region (top layer). The DNA is tightly bound around SRF, which causes DNA bending (Figure 1.6) (Pellegrini et al., 1995). SRF has the ability to select a narrow minor groove, a structural feature of the AT-rich DNA sequences, flanked by a GG or CC sequences, which promote bending onto the minor grove (Pellegrini et al., 1995).

**Figure 1.6 Serum response factor (SRF) bound to DNA.**

The X-ray crystal structure of human serum response factor core bound to DNA reveals DNA bending (for details, see text). Figure according to 3.2 Å structure by Pellegrini and Richmond (Pellegrini et al., 1995).

SRF is localised in the nucleus and is often found to bind DNA constitutively, but it remains inactive in the absence of stimulus (Herrera et al., 1989). Various studies, including genome-wide expression profiling analyses, identified many SRF candidate genes with the estimated number of around 300 (Descot et al., 2009; Hill et al., 1995; Medjkane et al., 2009; Philippar et al., 2004; Posern et al., 2004; Schratt et al., 2002). SRF plays a dominant role in the activation of genes, which encode for example proteins involved in the cell cycle G0 – G1 transition. (Descot et al., 2009; Selvaraj and Prywes, 2004). Above all however, SRF target genes encode for protein products that control and build the actin cytoskeleton. Within these, are proteins controlling cell contractility, microfilament dynamics and cell motility. Interestingly, the activation of specific genes (immediate early and/or cytoskeletal) is largely dependent on the SRF interaction with its cofactors. Consequently, to achieve transcriptional activity from binding the SRE of selected genes, SRF requires cofactors (Herrera et al., 1989; Shaw et al., 1989). Genome-wide ChiP-Seq analysis is underway to elucidate how the expression of different SRF target genes depends on binding events of specific SRF cofactors. This analysis reveals that there are nearly 850 genes that specifically interact with SRF (Esnault and Treisman, unpublished observations). The signal-regulated, tissue-specific cofactors of SRF can be divided into two main groups and are described below (Figure 1.7).

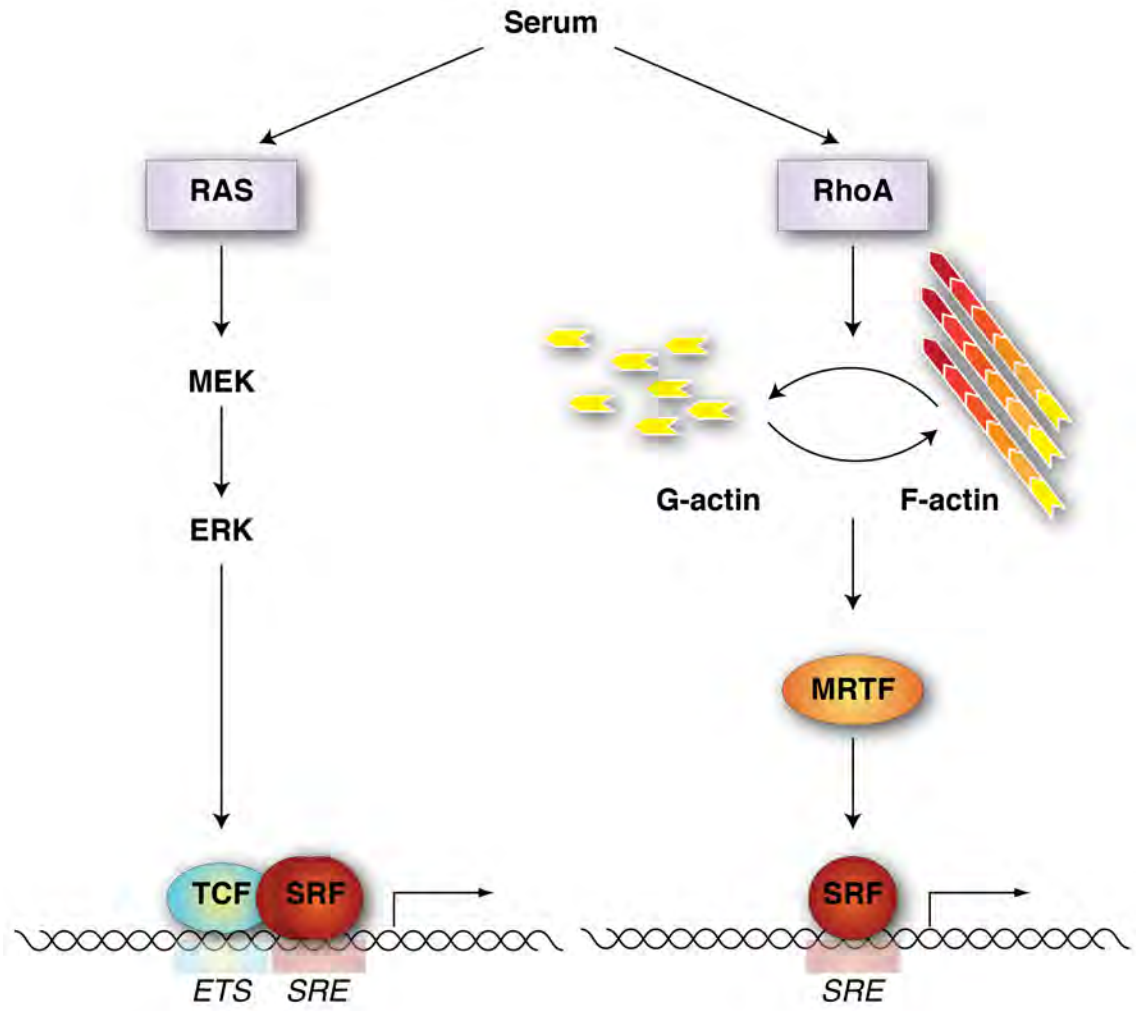


**Figure 1.7 Two pathways regulating SRF activity.**

To activate transcription, SRF requires additional binding partners. SRF cofactors respond to two different signal transduction pathways. TCFs bind SRF at a subset of genes where SRE is located close to ETS site (left). TCFs respond to MAPK pathway activation by phosphorylation. The second set of SRF target genes is controlled via MRTFs (right), which respond to changes in actin dynamics induced by Rho-actin signalling. When actin polymerisation occurs, MRTFs accumulate in the nucleus and activate SRF-dependent transcription.

The initially discovered group of SRF cofactors are the ternary complex factor (TCF) family of proteins (Dalton and Treisman, 1992), which were found to be activated by mitogen activated protein kinase (MAPK) phosphorylation (Gille et al., 1992; Janknecht et al., 1993; Marais et al., 1993; Shaw et al., 1989), (for review, see (Treisman, 1994)). TCFs possess an N-terminal ETS domain, a site though which they form ternary nucleoprotein complexes with SRF over the SRE site (Figure 1.7) (Buchwalter et al., 2004). Other described ETS proteins were found to be fundamental for development, differentiation, cellular proliferation and transformation (Oikawa and Yamada, 2003). There are three TCFs that were found to specifically form ternary complexes with SRF: Elk1, Net and Sap1. Structurally, they share four similar regions (Dalton and Treisman, 1992). Elk1, Net and Sap1 are recruited to the SRE through protein-protein and protein-DNA interaction, but all of them interact with the DNA through an ETS (Buchwalter et al., 2004). Interestingly, the expression of SRF target genes, which are activated through the activation of MAPK signalling and subsequent TCF binding, are unaffected by the changes in actin dynamics in the cell (Sotiropoulos et al., 1999).

More recently, members of myocardin family of proteins were found to be SRF cofactors. This finding was driven by the fact that the formation of TCF complexes could not fully explain SRF-dependent transcription activities that result from serum induction (Hill et al., 1994). The answer to this puzzling issue came from the discovery that signalling to SRF requires activation of another signalling pathway, acting independently from MAPK pathway, the Rho-GTPase signalling (Hill et al., 1995). Indeed, it was shown that serum-regulated activation of SRF is mediated by changes in Rho-dependent actin dynamics (Sotiropoulos et al., 1999). It was later shown that cofactors that mediate the SRF-dependent expression of cytoskeletal genes belong to myocardin family.

The discovery of a new SRF cofactor, myocardin, was firstly restricted to muscle cells (Wang et al., 2001). Not much later, a ubiquitously expressed megakaryocytic acute leukaemia (MAL or megakaryoblastic leukaemia 1, MKL1) protein was found together with one twenty-two MAL (OTT-MAL). They were

identified as fusion products of t(1;22)(p13,q13) chromosomal translocation present in megakaryoblastic leukaemia (AML) patients (Ma et al., 2001; Mercher et al., 2001). It was then established that a related protein, MAL 16, encoded by a gene in chromosome 16 is also able to interact with SRF. Mouse homologs of MAL and MAL16 are referred to as myocardin-related transcription factors A and B (MRTF-A and MRTF-B) (Wang et al., 2002).

Miralles and co-workers found that MRTF-A interacts with G-actin, but not with F-actin, therefore being a sensor of the monomeric actin concentration in the cell (Miralles et al., 2003). MRTF-A remains cytoplasmic in serum-starved NIH3T3 cells and accumulates in the nucleus upon serum-driven RhoA activation. Recent years yielded detailed analysis of the molecular mechanism underlying MRTF-SRF signalling to actin cytoskeleton (Guettler et al., 2008; Mouilleron et al., 2008; Mouilleron et al., 2011; Pawlowski et al., 2010; Vartiainen et al., 2007; Zaromytidou et al., 2006). Below, I will introduce an actin-dependent regulatory mechanism that drives MRTF-SRF activity.

### 1.2.2 MRTF family of SRF cofactors

The founding member of the MRTF family of proteins is the initially characterised myocardin found in cardiac and smooth muscle cells. Myocardin can be found in two distinct isoforms, which result from alternative splicing reactions. Consequently, two different in size proteins can be found in either cardiac tissues or smooth muscle cells (myocardin-935 and myocardin-856). Myocardin was shown to be a potent transcription cofactor of SRF and to be required for myocardial cell differentiation *in vivo* (Wang et al., 2001). Myocardin was described as a SAP (SAF-A/B, Acinus, PIAS) domain protein, which relates to a group of nuclear regulators of transcription and chromatin remodelling factors (Aravind and Koonin, 2000). Indeed, myocardin was later shown to regulate many SRF-dependent genes. In 10T1/2 fibroblasts, myocardin expression stimulates expression of smooth muscle actin, calponin or smooth muscle MLCK, proteins normally restricted to myocytes (Wang et

al., 2003b). In contrast to myocardin, two other family members MRTF-A and MRTF-B have more widespread expression patterns (Wang et al., 2002).

Loss-of-function studies of both myocardin and MRTF genes show that these SRF cofactors are required *in vivo* in distinct cell types and at various developmental stages. Mouse embryos that are homozygous for a myocardin loss-of-function mutation die during the embryonic development and show no differentiation of smooth muscle vasculature. Given the fact that expression of myocardin in fibroblasts can trigger smooth muscle gene expression, this shows that myocardin is regarded as necessary and sufficient for smooth muscle cells vasculature differentiation (Li et al., 2003). However, no defect in heart development is present, which is somewhat surprising given that mice carrying the null mutation of the myocardin gene in their cardiomyocytes suffer from heart failure, preceded by reorganization or sarcomeres and loss or cardiomyocytes through apoptosis (Huang et al., 2009). This shows that the expression of myocardin is required for cardiomyocyte survival. This report was in agreement with the finding that knockdown of myocardin in *Xenopus* embryos inhibits cardiac development and leads to downregulation of cardiac differentiation markers (Small et al., 2005). The fact that myocardin knockout mice embryos showed no defect in the development of the heart might be explained by the substitution of this function by MRTFs, therefore implicating possible functional redundancy of the family members.

The loss-of-function study of MRTF-B in mice shows lethality during gestation stage resulting from multiple defects in the development of cardiovasculature. These included abnormalities in bronchial arch arteries, formation of right ventricle and thin-walled myocardium. The defects were accompanied by a failure of smooth muscle cells differentiation within the arteries. Interestingly, these phenotypes were distinct from those observed in the myocardin loss-of-function study suggesting different roles of myocardin and MRTFs in the development of smooth muscle cells (Oh et al., 2005). Studies of MRTF-A knockout mice show no defects in the muscle cells development but exhibit abnormal differentiation of mammary myoepithelial cells. This results in defects in mammary gland formation and defective milk ejection, hence the inability of these mice to effectively nurse their offspring. Myoepithelial cells are derived from a

lineage distinct to smooth muscle cells, but the apparatus required for contraction of myoepithelial cells is strikingly similar to the smooth muscle cell contractile machinery. Myoepithelial cells from these mice exhibit downregulation of SRF target genes required for the effective contraction of these cells (Li et al., 2006). Therefore, MRTF-A function might exhibit gene dose redundancy.

### 1.2.3 Protein interaction and domain organisation of MRTFs

The domain organization of MRTFs and myocardin is similar (Figure 1.8 A). All family members are around 100 kDa in size. The highly conserved C-terminal sequences mediate the transcriptional activity of myocardin family members (Miralles et al., 2003; Selvaraj and Prywes, 2004; Wang et al., 2001).

The SRF binding site is located more N-terminally and is referred to as the B1 box (Miralles et al., 2003; Zaromytidou et al., 2006). The analysis of the SRF-binding region by gel mobility shift assays identified a 'LKYHQYI' sequence, which is required for the formation of the MRTF-SRF ternary complex (Miralles et al., 2003; Zaromytidou et al., 2006). Immediately after the B1 box, a conserved Q-rich region is located (referred to as the Q-box). Analysis of the Q-box shows that it contributes to SRF binding, but is not essential (Miralles et al., 2003; Zaromytidou et al., 2006). The function of the SAP domain is not well understood, but reporter gene studies suggest that it plays a role in determining promoter specificity (Wang et al., 2003b).

Myocardin family of proteins possess the ability to homo- and hetero-dimerise through their leucine-zipper (LZ) motifs, located C-terminally to the SAP domain (Miralles et al., 2003). Interestingly, dimerization might also occur between the family members and it was reported that SRF activity could be enhanced due to this dimerization (Miralles et al., 2003; Selvaraj and Prywes, 2004; Wang et al., 2003b).

At the N-terminus, MRTF-A, MRTF-B and in myocardin-935 contain an RPEL domain, which is only partially present in myocardin-856 (Figure 1.8 A). The RPEL

domain consists of three RPEL motifs (Pfam 02755) (Figure 1.8 B), which are separated by linker sequences. The motif is described by the presence of the RP-$(x)_3$-EL consensus at its core, but some variability within the sequence of the motif can occur between different species and family members. There are only two known families of RPEL proteins, myocardin and Phactr (Phosphatase and actin regulator) families (Figure 1.10). In both families RPEL domain acts as G-actin sensor and is critical for their Rho-dependent regulation (Miralles et al., 2003; Wiezlak et al., 2012). Interestingly, only MRTFs and not myocardin respond to the regulation by G-actin due to the lower affinity of the myocardin RPEL domain for G-actin (Guettler et al., 2008).

Within the RPEL domain in MRTF-A, there is an extended bipartite nuclear localisation signal (NLS), containing two elements, referred to as B3 and B2 regions, separated by 30-residue linkers (Figure 1.8 A) (Pawlowski et al., 2010). Both are required for the nuclear import of MRTF-A, which is mediated by a classical Importin α (Imp α)-Importin β (Imp β) pathway. Moreover, binding of actin to the RPEL motifs inhibits the interaction of Impα-Impβ with the NLS in MRTF-A (Pawlowski et al., 2010). Below, I will describe how actin binding to the RPEL domain in MRTFs regulates its subcellular localisation and activity.

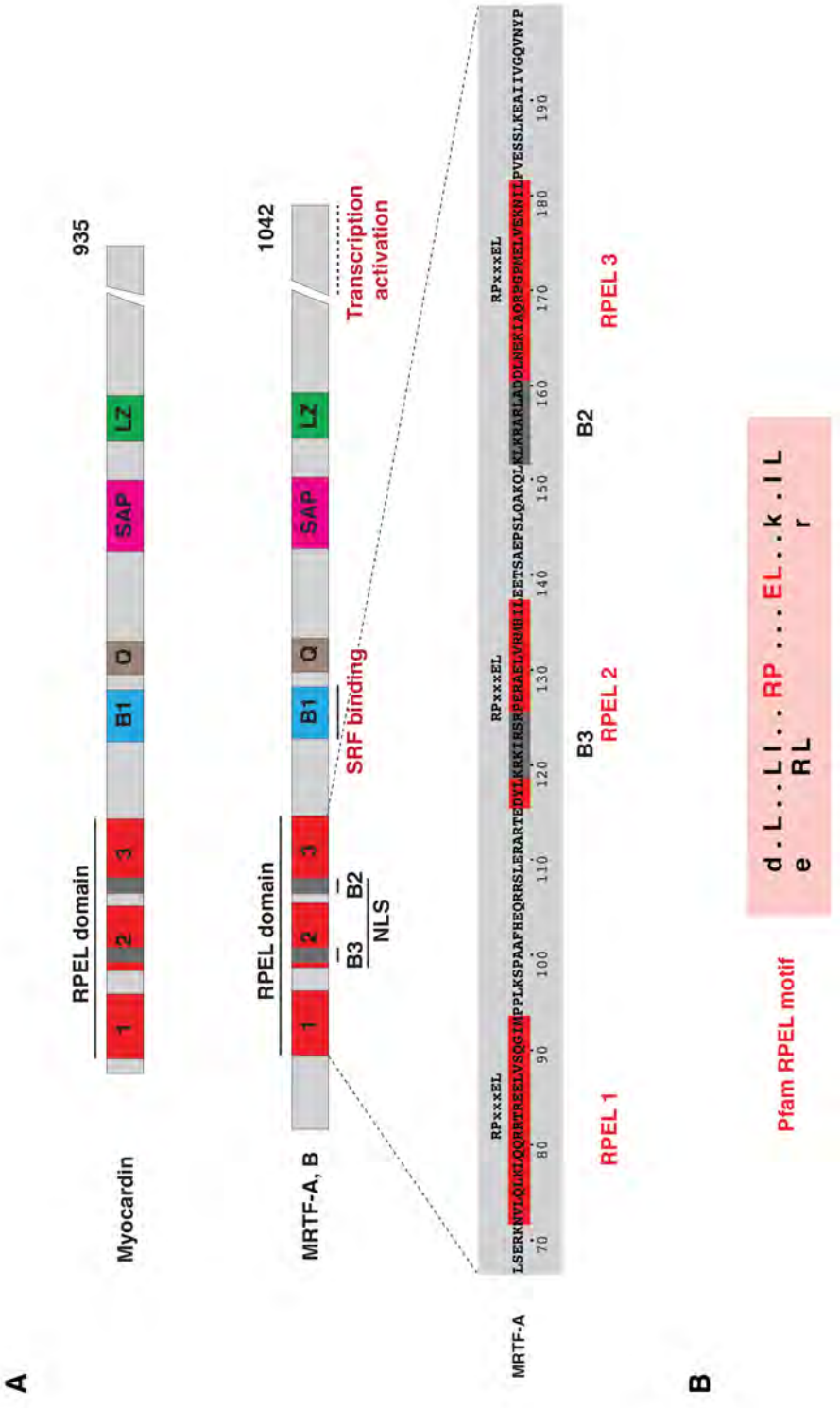
A
935
RPEL domain
1
2
3
B1
Q
SAP
LZ
Myocardin
1042
RPEL domain
1
2
3
B3
B2
NLS
B1
Q
SAP
LZ
MRTF-A, B
SRF binding
Transcription activation
MRTF-A
RPxxxEL
RPxxxEL
RPxxxEL
B3
B2
RPEL 1
RPEL 2
RPEL 3
B
Pfam RPEL motif
d . L . . L l . . RP . . . EL . . k . l L
e RL r

**Figure 1.8 Domain organisation of myocardin and MRTFs.**

**(A)** Similar domain organisation of myocardin and MRTFs (details in text). The RPEL domain consisting of three RPEL motifs (red) and B3-B2 NLS sequences (dark grey) are indicated. SRF binding site B1 box (B1, blue), Q-rich region (Q, brown), SAP domain (SAP, pink) and leucine zipper dimerization site (LZ, green) are schematically shown. **(B)** Pfam RPEL motif (02755) with RPEL core residues shown in red.

### 1.2.4 Actin-dependent regulation of MRTF localisation and activity

The role of actin in the regulation of transcription was initially reported before the discovery of MRTFs. It was reported that the stabilisation of actin dimers by cytochalasin D, an actin-binding compound, enhances transcription of *c-fos* (Zambetti et al., 1991). Only later, it was shown that changes in actin concentration could influence expression of some SRF-target genes, like *vinculin*, *β-actin* or *srf* itself (Sotiropoulos et al., 1999). Interestingly, the treatment of cells with agents that promote F-actin formation, like jaspakinolide or overexpression of actin nucleating factors, like formins could stimulate the activity of SRF. In contrast, the treatment of cells with actin depolymerising agents like Latrunculin B, blocked the serum-induced activation of SRF target genes. These studies suggested that SRF responds to the depletion of monomeric actin levels in the cell. It was additionally shown that actin overexpression inhibits SRF activity, but profilin-induced F-actin assembly has the opposite effect on SRF. Taken together, these observations led to the proposal that SRF senses the depletion of G-actin pool through an additional, actin-interacting cofactor (Sotiropoulos et al., 1999). It was later shown that the G-actin sensing by SRF is communicated through its association with MRTF (Miralles et al., 2003).

Miralles and colleagues showed that MRTF-A is retained in the cytoplasm of NIH3T3 fibroblasts in serum starved cells and upon serum stimulation it relocates to the nucleus (Figure 1.9). The nuclear accumulation of MRTF-A was triggered upon activation of Rho-actin signalling pathway (Miralles et al., 2003), which stimulates the formation of F-actin filaments and decreases the G-actin pool in the cytoplasm (Ridley et al., 1992). G-actin was found to be associated with the RPEL domain in MRTF-A in co-immunoprecipitation studies, which suggested that this interaction could dictate the cytoplasmic localisation of MRTF-A (Miralles et al., 2003; Posern et al., 2004). Interestingly, the RPEL domain from MRTF-A was shown to directly interact with G-actin with very high affinity in actin polymerisation assays (Posern et al., 2004). Moreover, the N-terminal sequence containing the RPEL domain is sufficient for regulated translocation to the nucleus upon serum stimulation (Guettler et al., 2008).

These studies clearly showed that the RPEL domain in MRTF-A acts as an actin sensor and mediates its localisation and activity (Figure 1.9).

G-actin influences the function of MRTF-A in multiple ways. Studies of the dynamics of MRTF-A GFP fusions showed that MRTF-A is continuously imported into the nucleus in the absence of stimuli and serum stimulation induces depletion of the G-actin pool, which results in reduced binding of MRTF-A to G-actin. This mechanism was shown to reduce the nuclear export of MRTF-A, which is mediated by the exportin Crm1 (Vartiainen et al., 2007). Moreover, the inhibition of nuclear export by leptomycin B (LMB) causes MRTF-A nuclear accumulation but is not sufficient to activate SRF. Only additional actin removal (from MRTF-A) by cytochalasin D, which competes with MRTF-A for G-actin binding, can activate SRF (Posern et al., 2002; Vartiainen et al., 2007). This shows that actin is directly involved in the inhibition of transcriptional activity. On the other hand, the artificial increase of the G-actin pool in unstimulated cells effectively inhibits the (Impα-Impβ)-mediated nuclear import of MRTF-A, as the B2-B3 NLS overlaps the G-actin binding sites (Pawlowski et al., 2010). As indicated earlier, Guettler and colleagues showed that myocardin is not regulated by the Rho-actin signalling owing to the low affinity of RPEL1 and RPEL2 for G-actin. It was recently suggested that two leucine-rich sequences in myocardin and MRTFs mediate Crm1 binding, but in myocardin those sites can be inhibited autonomously and by SRF binding, which impairs the export of myocardin (Hayashi and Morita, 2013). However, the export mechanism of MRTFs is not yet fully understood. Myocardin or actin-defective MRTFs mutants are available for binding Impα-Impβ but are not effectively exported and thus localise constitutively to the nucleus (Guettler et al., 2008). Therefore, regulation of MRTFs depends on the specific Rho-signalling-mediated changes in actin interactions with the single RPEL motifs, which can individually bind G-actin with different affinities.

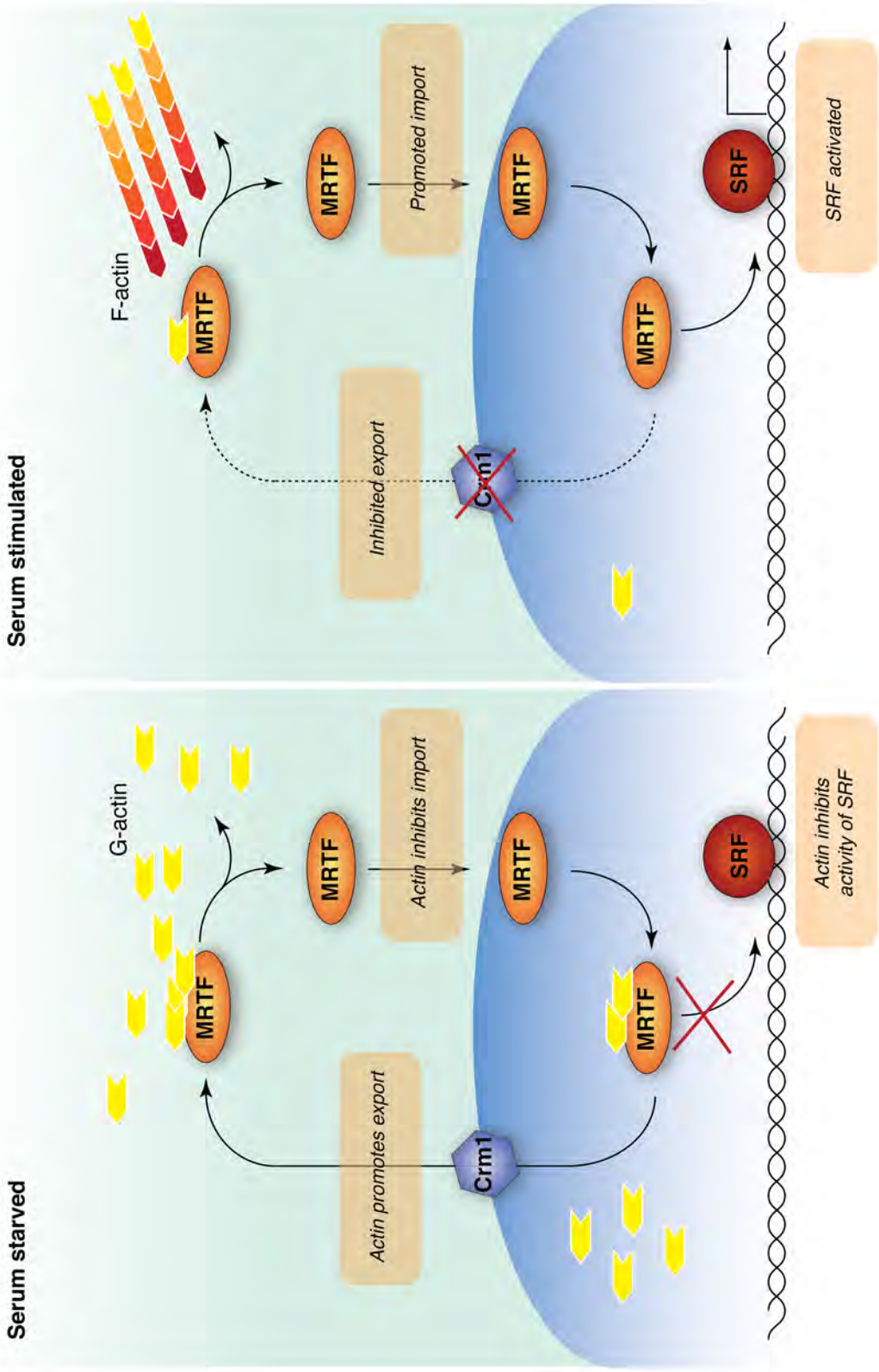
Serum stimulated
F-actin
MRTF
Promoted import
MRTF
MRTF
SRF
SRF activated
Inhibited export
Crm1
MRTF
Serum starved
G-actin
MRTF
Actin inhibits import
MRTF
SRF
Actin inhibits activity of SRF
MRTF
Actin promotes export
Crm1

**Figure 1.9 Regulation of MRTFs by actin.**

Interaction between actin and MRTFs regulates localisation and activity of MRTFs. In serum-starved cells, MRTFs shuttle continuously between the nucleus and the cytoplasm. Actin inhibits import of MRTFs, promotes its export and inhibits transcriptional activity of SRF. Upon serum-induced actin polymerisation and G-actin depletion, MRTFs are no longer exported to the cytoplasm, but accumulate in the nucleus. Disruption of actin interaction with MRTFs leads to SRF activation.

### 1.2.5 The RPEL motif defines a G-actin binding element.

The molecular basis for the RPEL domain interaction with G-actin and the significance of the RPEL motif sequence conservation were initially elucidated through structural analysis of single RPEL motifs bound to LatB-G-actin (Mouilleron et al., 2008). This study showed that RPEL motifs (RPEL1 and RPEL2 from the triple RPEL domain), normally unstructured in solution, gain their secondary structure upon interaction with a single G-actin molecule. Mouilleron and colleagues showed that actin binding to a single RPEL motif induces the formation of two helices, helix-α1 and helix-α2 joined by an R-loop with an α2-C-cap at the C-terminus (Figure 1.10 A). Helix-α1 binds within the hydrophobic cleft between subdomain 1 and 3 of actin molecule and helix-α2 binds the hydrophobic ledge of the subdomain 3 (Figure 1.10 B). The structural and mutational analysis of RPEL motifs interacting with G-actin showed that sequence conservation occurs at positions that make direct contacts with G-actin or form intramolecular RPEL interactions induced upon actin binding (Mouilleron et al., 2008).

Crucial RPEL motif G-actin contacts within subdomain 3 ledge are predominantly hydrophobic and in RPEL2 involve L131, I136 and L137 in helix-α2 (Figure 1.10 C). Helix-α1 also makes hydrophobic contacts through residues L118 and I122. The conserved proline P126 stabilises the angle between the two helices. The invariant R-loop arginine $R125^{RPEL2}$, critical for G-actin binding, forms a cation interaction and a salt bridge with the C-terminus of G-actin (Figure 1.10 C) (Mouilleron et al., 2008).

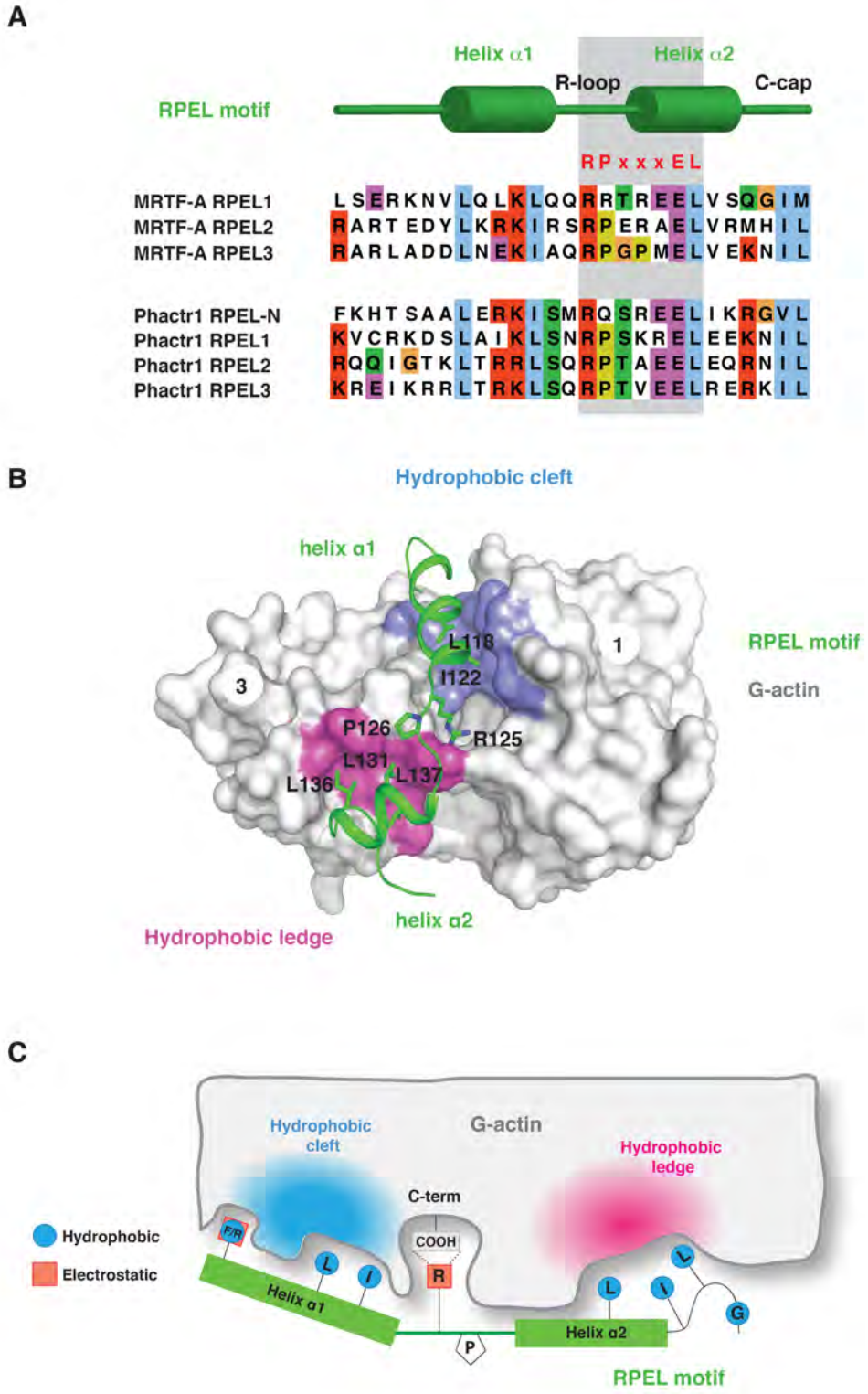
A
Helix α1
Helix α2
R-loop
C-cap
RPEL motif
R P x x x E L
MRTF-A RPEL1
MRTF-A RPEL2
MRTF-A RPEL3
Phactr1 RPEL-N
Phactr1 RPEL1
Phactr1 RPEL2
Phactr1 RPEL3
B
Hydrophobic cleft
helix α1
L118
I122
P126
R125
L131
L136
L137
1
3
RPEL motif
G-actin
helix α2
Hydrophobic ledge
C
Hydrophobic cleft
G-actin
Hydrophobic ledge
C-term
COOH
F/R
R
L
I
V
G
P
Helix α1
Helix α2
Hydrophobic
Electrostatic
RPEL motif

**Figure 1.10 The RPEL motif interaction with G-actin.**

**(A)** Sequence alignment of individual RPEL motifs from MRTF-A and a member of Phactr family, Phactr1; secondary structure features of the RPEL motif (green) are schematically indicated; core of the motif is shaded (grey box). **(B)** Structure of the RPEL2 motif from MRTF-A bound to G-actin between subdomains 1 and 3; RPEL motif is drawn in green (cartoon) and highly conserved residues are indicated as sticks; adapted from (Mouilleron et al., 2008). **(C)** Critical RPEL motif G-actin contacts; hydrophobic and electrostatic interactions are indicated (for details, see text).

Both RPEL1 and RPEL2 bind G-actin with high affinities (1.0 μM and 1.9 μM), but RPEL3 binds with significantly lower affinity (28.9 μM) (Guettler et al., 2008; Mouilleron et al., 2008). The differences in affinities were explained by the distinct contacts that those motifs make with actin. Even though the structure of RPEL3 with G-actin was not available, the mutational analysis and fluorescence anisotropy revealed the molecular basis of RPEL3 low affinity binding to actin. Most importantly, structural analysis showed crucial differences between the RPEL motifs binding to actin, which are reflected in a distinct amino acid content of the three RPEL peptides. The conserved RPEL arginine, located within the R-loop, was shown to be a crucial actin contact in RPEL2 and RPEL3, making an ion pair with the actin C-terminal carbonyl moiety, but the mutation of this arginine into alanine in RPEL1 did not decrease G-actin binding affinity as significantly. Consistently, the introduction of this mutation into the context of the full-length protein had a minor effect on the localisation of MRTF-A in unstimulated cells. In contrast, the R/A mutation of the RPEL3 had a very pronounced effect. Similar mutational analysis was performed for the actin-contact residues within helix-α1 and helix-α2 and showed a similar pattern. Taken together, these results suggested that the weakly interacting RPEL3 of MRTF-A is an important element that mediates localisation of MRTF-A, but the integrity of the whole domain is necessary to confer MRTF-A nucleocytoplasmic shuttling (Mouilleron et al., 2008).

Within RPEL1 and RPEL2 motifs, conservation of most residues was explained, apart from the highly conserved RPEL glutamate, as this residue showed no direct contact with G-actin. The role of the RPEL glutamate was therefore not known. We recently explained the conservation of this residue through structural analysis of Phactr1 interaction with G-actin, and showed that it is involved in the formation of higher-order actin assemblies on tandem RPEL motifs (Mouilleron et al., 2012)(see section 'Structural analysis of Phactr1 interaction with actin').

Recently, structure of the RPEL domain from MRTF-A bound to G-actin molecules was reported at 3.5Å resolution (Mouilleron et al., 2011). Surprisingly, this study revealed a pentavalent G-actin•MRTF-A$^{\text{RPEL domain}}$ complex, with three G-actin molecules binding to each RPEL motif (actins R1, R2 and R3) and two additional actins

binding to the spacers between the motifs (actins S1 and S2) (Figure 1.11). Mutational analysis showed that binding of the spacer actins is required for MRTF-A cytoplasmic localisation in resting cells. Within the pentavalent complex, the RPEL domain is shown to possess a crank-shaped conformation with a superhelical twist of 150° within the crank. The conformation of a single RPEL motif within the helix is similar to the previously observed conformation in the single RPEL structures. The spacers joining RPEL motifs make similar contacts to the N-terminal RPEL contacts within the pentavalent assembly. Interestingly, this study also identified a trivalent G-actin complex (shown at 3.15Å resolution). Within the complex, the trivalent assembly was virtually identical to the RPEL domain binding actin R1, S1 and R2 within the pentavalent complex, but the two C-terminally located actins (R3 and S2) were missing from the structure. Both the pentavalent (5:1, actin:RPEL) and trivalent (3:1, actin:RPEL) complexes existed in solution when examined by gel filtration, but the pentavalent complex was only formed upon addition of G-actin to the running buffer. Consistent with the idea that RPEL3 motif in MRTF-A plays a crucial role in the regulation of its shuttling, the mutation of the crucial actin contact in RPEL3 caused the switch between the pentavalent and the trivalent complex in gel filtration.

Shuttling of MRTF-A is dependent on the formation of the described above complexes. Depletion of the G-actin pool causes reduced formation of the pentavalent complex, therefore allowing for the Impα-Impβ heterodimers to associate with MRTF-A and leading to the reduction of export rates. This is possible due to lower affinities of G-actin binding to RPEL3 and linker2 within the RPEL domain (Mouilleron et al., 2011). Upon the artificial increase of G-actin concentration, all actin-binding sites would become saturated and NLS sequences become occluded. This would lead to the retention of MRTF-A in the cytoplasm (Figure 1.11). Taken together, studies of MRTF-A RPEL domain complexes with G-actin show how actin can operate a molecular partner to dictate its function as a transcriptional coactivator.

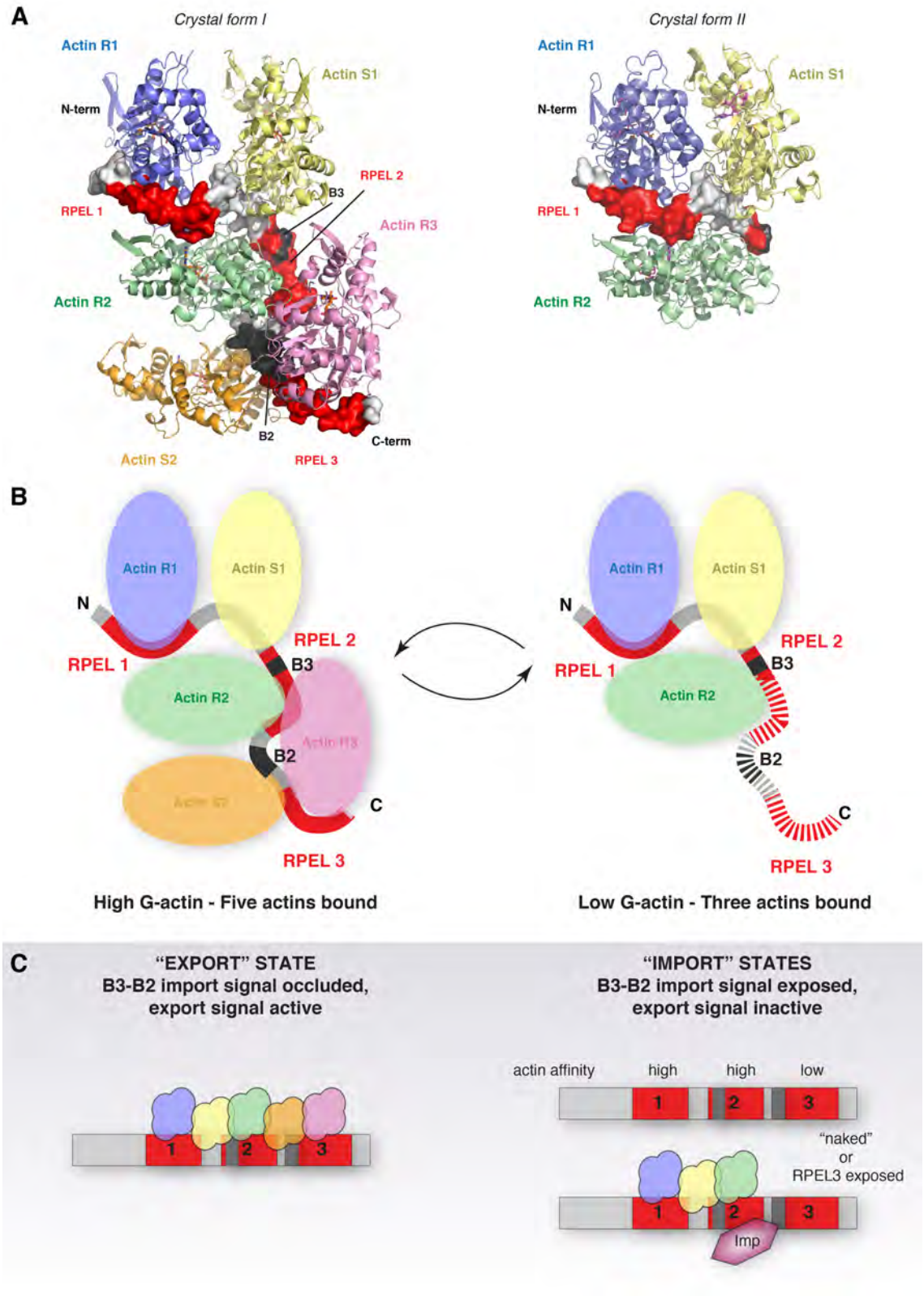
A
Crystal form I
Actin R1
Actin S1
N-term
RPEL 2
B3
RPEL 1
Actin R3
Actin R2
B2
C-term
Actin S2
RPEL 3
Crystal form II
Actin R1
Actin S1
N-term
RPEL 1
Actin R2
B
Actin R1
Actin S1
N
RPEL 2
RPEL 1
B3
Actin R2
B2
C
RPEL 3
High G-actin - Five actins bound
Actin R1
Actin S1
N
RPEL 2
RPEL 1
B3
Actin R2
B2
C
RPEL 3
Low G-actin - Three actins bound
C
"EXPORT" STATE
B3-B2 import signal occluded,
export signal active
1
2
3
"IMPORT" STATES
B3-B2 import signal exposed,
export signal inactive
actin affinity
high
high
low
1
2
3
"naked"
or
RPEL3 exposed
1
2
3
Imp

**Figure 1.11 Two crystal forms of the RPEL domain bound to actin reveal a model of MRTF-A regulation.**

**(A)** Two distinct complexes of MRTF-A RPEL domain bound to G-actins. Crystal form I reveals five G-actin molecules bound to RPEL motifs (red) and intervening spacers (left side); crystal form II contains three G-actin molecules bound to RPEL1, Spacer1 and RPEL2 (right side). **(B)** Schematic representation of the pentavalent and trivalent G-actin•RPEL domain complexes (each G-actin is colour-labelled as in A). Within the pentavalent complex B2-B3 NLS sequences (dark grey) are occluded, in the trivalent complex B2-B3 NLS sequences are available (dotted line). Five G-actin molecules bind in high actin concentration and the trivalent complex exists in a low G-actin concentration. **(C)** Proposed mechanism of MRTF-A regulation by G-actin. The 5:1 G-actin•RPEL domain assembly (left) represents the export state of the complex, the 3:1 or 'naked' RPEL domain represents the import state (G-actin, RPEL motifs and NLS sequences are colour-labelled as in A and B).

Because the RPEL motif allows MRTF to respond to change in actin dynamics, MRTFs emerge as major players in cytoskeletal homeostasis by linking cytoskeletal gene expression to G-actin. It is therefore intriguing to understand if the function of RPEL motifs is restricted to MRTFs or if they regulate activity of other RPEL protein families. This thesis will focus on the role of RPEL motifs in Phosphatase and actin regulator (Phactr) family. Before discussing Phactr family, I will introduce PP1, the other binding partner of Phactr proteins.

## 1.3 Protein Phosphatase 1 (PP1)

Activity of more than a half of proteins is regulated by phosphorylation of their serine, threonine or tyrosine residues. To be effective in activating a big range of proteins, phosphorylation events are dynamic and reversible. In eukaryotic cells, there is a wide range of enzymes that control these reactions. All protein kinases and phosphatases have their own substrate specificities, subcellular localisation and regulatory factors. Interestingly, mammalian genomes encode around 100 protein tyrosine kinases, 400 serine/threonine kinases, but only around 40 serine/threonine phosphatases (Ceulemans and Bollen, 2004). This is because the full functional diversity of protein phosphatases is only visible when the enzyme and its regulatory partner are both considered. Often, these associations are referred to as protein phosphatase holoenzymes.

Most protein serine/threonine phosphatases are classified in the phosphoprotein phosphatase (PPP) family, which consists of several subfamilies. PP1 and PP2A subfamilies are the two most abundant and account for more 90% of de-phosphorylation events in the eukaryotic cell. The PP2B subfamily (also called Ca2+-calmodulin-regulated phosphatase calcineurin) together with PP5 also mediate a variety of processes, but are less abundant. Other subfamilies include PP4, PP6, and PP7. All subfamilies of PPP family of phosphatases have structurally related catalytical domains, but the composition of their holoenzymes differs significantly. Recent studies suggests that there are around 650 complexes containing PP1 protein phosphatase in mammals,

compared to 70 containing PP2A, placing PP1 in the forefront of all other phosphatases (for review, see (Bollen et al., 2010)).

### 1.3.1 The structure of PP1 catalytic subunit

PP1, also referred to as PP1 catalytic subunit (PP1c), is a very highly conserved eukaryotic protein. Eukaryotic genomes contain from one to eight genes encoding this abundant 37kDa protein. The differences between PP1 proteins among species are mainly due to the variability of the amino acid content of the C-terminal and N-terminal regions. Most of the middle region of the protein is highly conserved and 70% of the residues in the central part are virtually identical. There are three PP1 genes in mammals, encoding isoforms PP1α, PP1γ and PP1β (also referred to as PP1δ). Additionally, gene encoding PP1γ isoform can be alternatively spliced, which results in the formation of two splice variants, $PP1\gamma_1$ and $PP1\gamma_2$. All isoforms of PP1 are ubiquitously expressed, apart from the less abundant $PP1\gamma_2$ (Ceulemans and Bollen, 2004; Cohen, 2002). All isoforms of PP1 were reported both in the nucleus and the cytoplasm of the interphase HeLa cells, human lymphocytes and CHO fibroblasts, but more enhanced nuclear staining was always noted (Andreassen et al., 1998). PP1 does not contain a nuclear localisation signal, but is targeted to the nucleus through multiple regulatory proteins.

Goldberg and colleagues reported three-dimensional structure of a PP1 catalytic subunit complexed with toxin microcystin (from marine cyanobacteria, *Microcystis* sp. and *Nodularia* sp.) (Goldberg et al., 1995). The structure of PP1 showed a compact ellipsoidal structure with dimensions 50 Å × 35 Å × 35 Å (Figure 1.12). The molecular analysis reveals requirement of PP1 catalytic subunit to bind metal ions $Fe^{2+}$ and $Zn^{2+}$ (Ceulemans and Bollen, 2004). The activity of PP1 was shown to be severely impaired when the metal-interacting residues were mutated, suggesting the critical role of those ions for PP1 function.

The PP1 catalytic subunit consists of 10 α-helices and 3 β-sheets comprised of 14 β-strands. Overall, the structural features of PP1 can be grouped into two sub-structures, the N-terminal region and the C-terminal region (also called N-subdomain and C-subdomain); this division of PP1 structure is only conceptual and does not indicate separate structures, though. Metal ions are embedded within the N-terminal part of PP1, which is mainly represented by α-helices and β-strands and forms a secondary arrangement containing a β-α-β-α-β metal-coordinating unit. This metal-coordinating site is specifically formed into a regular, compact pocket (Figure 1.12). The existence of a di-nuclear ion-binding pocket is also presented in a structure of PP1 catalytic subunit complexed with tungstate (Egloff et al., 1995). This study showed, that the enzymatic activity of PP1 is based on a single-step reaction involving a di-nuclear metal-activated water molecule. The central residue within the catalytic site, H125, plays a vital role in substrate immobilisation. Three longer and more exposed loops, which connect β-strands and α-helices in the β-α-β-α-β motif, provide a core of the catalytic site of the enzyme (Egloff et al., 1997). The C-terminal domain of the structure reveals a more irregular conformation, containing more β-strands than α-helices, providing a binding surface for many PP1 regulatory proteins. Catalytic Y-shaped cleft of PP1 contains three main substrate-interacting sites, referred to as C-terminal groove, hydrophobic groove and acidic groove (Figure 1.12) (Goldberg et al., 1995).

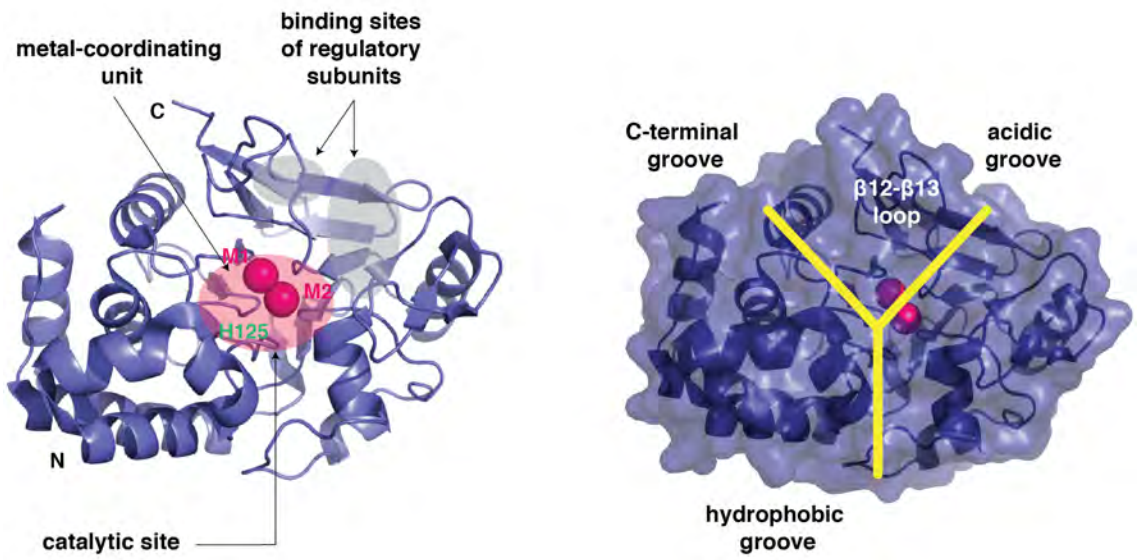


**Figure 1.12 Structure of PP1 catalytic subunit.**

Structural representation of PP1 catalytic subunit shown as a cartoon (left) and as a surface model (right). The catalytic site of PP1 contains two metals (pink spheres) at metal coordinating unit (shaded in pink) with H125 (green) at its core. The Y-shaped catalytic cleft (yellow) of PP1 is composed of three substrate-binding groves: C-terminal, acidic and hydrophobic. Major binding sites for regulatory subunits are located in the C-terminal part (shaded in grey) and often include the surface of β12-β13 loop (shown on the surface model on the right). Structure is based on a model from Goldberg (Goldberg et al., 1995) and was created using PYMOL.

The structural studies of PP1 revealed a mechanism for PP1 inhibition by toxins, such as microcystin, okadaic acid and others, which have been extensively used to dissect the molecular functions of phosphatases. PP1 inhibitors are also being exploited therapeutically, for example in cancer therapies (Kelker et al., 2009).

Microcystin was shown to interact with two metal-bound water molecules, which results in the inhibition of enzyme activity through substrate displacement. It also interacts with the hydrophobic groove, located closely to the to the catalytic site, thus interfering with the catalysis (Goldberg et al., 1995). Okadaic acid (OA, polyether fatty acid from the marine dinoflagellates *Prorocentrum* sp. and *Dinophysis* sp.) also binds directly to the hydrophobic groove, and to some basic residues at the catalytic site itself, thereby inhibiting the catalytic reaction (Dounay and Forsyth, 2002). Calyculin A (octamethyl polyhydroxylated fatty acid from marine sponges) binds within the hydrophobic groove and the acidic groove, with its phosphate group occupying the metal-binding pocket (Kita et al., 2002). Structural study of PP1 bound to nodularin-R (cyclic penta-peptides occurring in marine cyanobacteria (Cheng et al., 1987)) and tautomycin (derived from bacteria *Streptomyces* sp. (Honkanen et al., 1991)) showed that hydrophobic groove interaction induces conformational changes of PP1 upon toxin binding, through removal of stabilising interactions in the active site (Kelker et al., 2009).

### 1.3.2 Substrate specificity, recognition and inhibition mechanisms

The catalytic mechanism of all phosphatases from the PPP family is similar, as they share structurally comparable catalytic core. The differences between subfamilies of these enzymes reside in the conformation of their solvent-exposed loops. The secondary structure of those loops effectively determines the shape of the PP1 surface, and this contributes to substrate recognition. The specific feature of PP1 is the composition of the active site, which is surrounded by a cluster of acidic amino acids. This specific characteristic of PP1 contributes to the speed of catalytic reaction towards β-subunit of phosphorylase a, which is mediated much faster than dephosphorylation of

more acidic α-subunit. Other Ser/Thr phosphatases catalyse these reactions with virtually the same kinetics (Bollen and Stalmans, 1992). PP1 has another unique feature in its substrate recognition. Unlike other phosphatases, it poorly recognises short sequences surrounding the phosphorylated residue. In contrast, substrate recognition depends on docking motifs interactions with PP1 surface grooves, located distantly from the active site (for review, see (Bollen et al., 2010)).

For efficient substrate recognition, PP1 almost always requires PP1 interacting proteins (PIPs), which contribute to substrate specificity and affinity. Some PP1 substrates bind to PP1 with low affinities and cannot form stable complexes with PP1, such as glycogen phosphorylase, which contains weakly interacting docking site (Hubbard and Cohen, 1989). Therefore, to increase concentration of some substrates, PP1 requires PIPs, called also regulatory subunits. One of the best examples of PP1 regulatory subunit that mediates substrate specificity is the binding of MYPT1 to PP1. MYTP1 is not only a targeting subunit but also enhances the specificity of PP1 towards MLC (for review, see (Bollen, 2001)).

The mechanism of PP1 inhibition by physiological PP1 inhibitors is based on blocking the access to the active site, thus preventing dephosphorylation of all the substrates. Inhibitor-1 and CPI-17 have inhibitory functions only when phosphorylated, operating as pseudo substrates, but Inhibitor-2 and Inhibitor-3 function without prior phosphorylation. Although structural analysis is not available, the mechanism of PP1 inhibition by Inhibitor-1 seems to rely on its phosphorylated residue being pushed to the active site of PP1 (for review, see (Roy and Cyert, 2009)). The structure of PP1 bound to inhibitor-2 indicated three crucial interaction points, involving two docking sites: RVxF motif and a SILK motif, and a long α-helix covering the active site by interacting with the acidic and hydrophobic grooves of PP1. Inhibitor-2 binding does not induce conformational change, but triggers the release of two metals, which are essential for catalysis (Hurley et al., 2007).

### 1.3.3 PP1 holoenzymes

PP1 forms a variety of different multimeric holoenzymes, containing substrates of PP1 and its regulators, which can be either activators, inhibitors or substrate targeting subunits. A decade of studies on PP1 showed that classification of PP1 interactors is somewhat difficult, due to the complexity of interactions. For example MYTP1, is a targeting subunit, a substrate specificity enhancer and can have an inhibitory effect once phosphorylated (Bollen, 2001). Another example is neurabin, both a substrate-specifier and an inhibitor (Carmody et al., 2008). Phosphatase interacting proteins are often referred to as regulatory subunits, and can be classified as direct or indirect partners, according to whether binding is direct or through an additional interactor. Sometimes, it is even difficult to classify a PP1 binding partner as a regulator or a substrate, as it is not yet clear how certain interactors regulate PP1 activity (for review, see (Ceulemans and Bollen, 2004)).

Nevertheless, some classify PP1 interactors as primary and secondary regulators, depending on the point of which PP1 binding was acquired during eukaryotic evolution (Ceulemans et al., 2002a). Primary regulators typically contain specific PP1-binding sites throughout different species, where they occur (e.g. Inhibitor-2, NIPP1). This characteristic enables to describe PP1 regulators, whose PP1-binding capability is their primary function. In contrast, secondary regulators have acquired the ability to regulate PP1 recently during evolution, and their primary function is unrelated to PP1 (e.g. AKAP149, Nek2) (for review, see (Ceulemans and Bollen, 2004)).

Another way of classifying PP1 interactors can be based simply on their function, if this function is known (Bollen, 2001). Proteins that bind PP1 can be grouped as substrate-independent activity regulators (e.g., Inhibitor-1, Inhibitor-2, dopamine and cAMP-regulated phosphoprotein of 32 kDa (DARPP-32)), substrate-specific targeting subunits (e.g., MYTP1, Neurabin I) or just substrates (e.g., Aurora kinase, Retinoblastoma protein, phosphofruktokinase). This classification is limited by the fact that functions of many known PP1 interactors are still not known. Moreover, some proteins can act as both substrates and inhibitors, such as Inhibitor-2 or CPI-17, or

targeting subunits as well as substrates (e.g. NEK2, TIMAP), which adds another level of complexity to their categorisation (Eto, 2009; Helps et al., 2000; Hurley et al., 2007; Li et al., 2007).

### 1.3.4 Regulatory binding sites

The discovery of common binding sequences within the regulatory subunits of PP1 suggested that interaction of many PP1 interactors is based on competition. Moreover, some proteins possess a variety of PP1 interaction sites and bind PP1 through several short motifs (for review, see (Ceulemans and Bollen, 2004)). Studies of different PP1 holoenzymes revealed that the activity of PP1 could be modified by an allosteric regulation or reversible phosphorylation of its regulatory subunits. These discoveries led to the proposal of a combinatorial control model of PP1, where a limited number of interaction sites for regulatory subunits combine with PP1 in many different ways to form a large variety of holoenzymes with distinct activities and substrate specificities (Bollen, 2001; Ceulemans and Bollen, 2004).

Structural and mutational studies of PP1 complexes revealed some regulatory binding sites of PP1, which are conserved within many PP1-binding proteins. The best characterised site on PP1 in the "RVxF" binding channel, located in a hydrophobic groove, away from the catalytic pocket, formed by the top edges of the two central β-sheets (Egloff et al., 1997). The consensus sequence recognised by this channel is present in most PP1 regulatory subunits and can be described as (R/K)$x_{0\text{-}1}$(V/I)$x$(F/W), where $x$ refers to any residue. This consensus is commonly denoted as simply RVxF motif and was first identified in studies of the glycogen-targeting subunits ($G_M$ and $G_{L)}$ as well as in the myosin targeting subunits (MYPTs) (for review, see (Cohen, 2002)). Mutation of valine or phenylalanine within the conserved motif can prevent PP1 binding completely or significantly weaken the interaction of such important PP1 interactors as NIPP1, AKAP220 or neurabin II (Hsieh-Wilson et al., 1999; Schillace et al., 2001; Trinkle-Mulcahy et al., 1999). Moreover, peptides containing RVxF motif can effectively block the interaction of some PP1 targeting subunits, like PNUTs or Nek2

(Helps et al., 2000; Kreivi et al., 1997). Several, highly conserved variations of the RVxF motif have been identified, which led to the final characterisation of the consensus. Screening of the catalytic subunit of PP1 with a peptide library revealed that peptides containing VxF and VxW motifs, following a basic residue, could bind PP1 equally well (Zhao and Lee, 1997). Additionally, some PP1-binding mammalian proteins, like PNUTS, did not contain the basic residue, preceding the Vx(F/W) motif (Kreivi et al., 1997). Nevertheless, several lines of evidence now show, that RVxF motif is essential *in vivo* (for review, see (Cohen, 2002)). Recent bioinformatic efforts showed that the (R/K)$x_{0\text{-}1}$(V/I)$x$(F/W) consensus could be found in more than 90% of PP1 interacting proteins. Nevertheless, this motif can be randomly found in around 25% of proteins, therefore serves as a poor tool in new PP1 partners discovery (Roy and Cyert, 2009). However, combining this strategy with searches containing stricter RVxF consensus could yield more comprehensive identification. When candidates found in one study were validated in vitro and in vivo, this resulted in almost doubling the amount of PP1 regulators in mammalian PP1 interactome (Hendrickx et al., 2009).

Binding of the RVxF motif to PP1 is not associated with significant changes in the conformation of PP1 or its catalytic activity. However, because RVxF motifs are not independent units, but parts of often large regulatory proteins, the initial binding of PP1 to this motif presumably anchors the primary interaction facilitating secondary interaction, which is frequently less strong, but can modulate the activity of PP1 (Bollen, 2001; Ceulemans and Bollen, 2004).

Other major regulatory binding site on PP1 includes the loop joining β-strands β12 and β13 (Figure 1.12). This loop is a flexible part of PP1, essential for the interaction with some inhibitors (Inhibitor-1, Inhibitor-2 and DARPP-32) and several inhibitory toxins (Connor et al., 1999). Another common interaction site includes the triangle of α-helices, precisely α4, α5 and α6, which have been shown to interact with Sds22, a specific regulator of Aurora-related protein kinases (Ceulemans et al., 2002b). Additionally, interaction of PP1 with Sds22 does not involve the RVxF channel in PP1. Lastly, some regulatory subunits of PP1, like MYPTs or neurabins interact with PP1 in an isoform-specific manner, indicating isoform-specific interaction sites on PP1.

Apart from the abundant RVxF motif, two other PP1-interacting consensus sequences were described in PP1-binding proteins. Crystallographic studies of PP1 in complex with the N-terminal domain of myosin phosphatase targeting subunit 1 (MYPT1) showed, that besides interacting through the conserved RVxF motif, and ankyrin repeats, MYPT1 also contains a myosin phosphatase N-terminal element (MyPhoNE) (Terrak et al., 2004). This element was shown to direct binding of the N-terminus of MYPT1 to PP1, consequently acting as a second docking site (Figure 1.13). It was then shown, that this motif is present in many PP1-interacting proteins. Bioinformatic analysis in the ENSEMBL database shows that MyPhoNE consensus RxxQ(V/I/L)(K/R)x(Y/W) occurs at increased frequency in proteins that interact with PP1 in comparison to other human proteins (Hendrickx et al., 2009). Similar analysis showed another conserved PP1-interacting sequence, identified initially in Inhibitor-2 and referred to as SILK motif, with consensus (G/S)IL(R/K). The SILK motif was found in 7 out of 143 PP1-interacting proteins analyzed (Hendrickx et al., 2009; Hurley et al., 2007).

Taken together, these analyses show that firstly, PP1 is structurally designed to interact with different regulatory sites of various proteins and that many proteins compete for PP1 binding. Secondly, specific interaction of regulatory subunits with PP1 can be achieved by combination of several binding sites.

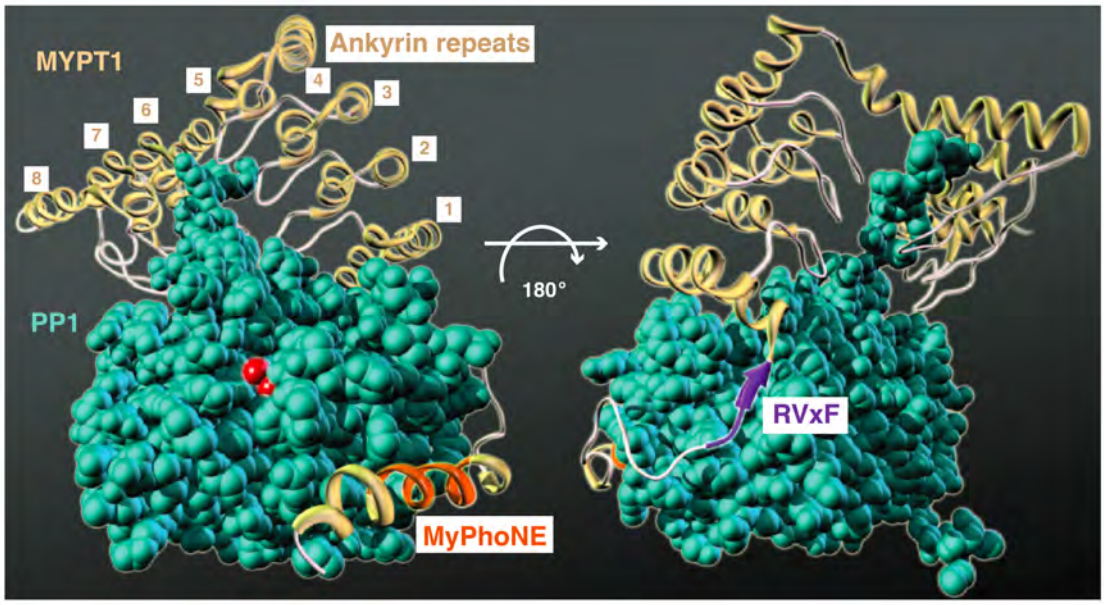


**Figure 1.13 Structure of PP1 bound to MYPT1 indicating multiple docking sites.**
Major interaction sites between MYTP1 (yellow) and PP1 (green). The RVxF motif (purple) interacts within the 'RVxF channel' in PP1; the N-terminal MyPhoNE motif (orange) interacts with the base of PP1 catalytic cleft. Third contact consists of multiple ankyrin repeats (1-8, top of the figure). Figure was adapted from Roy and Cyert (Roy and Cyert, 2009), based on the PP1-MYPT1 structure from Terrak and Dominguez (Terrak et al., 2004).

### 1.3.5 Functions of PP1 regulatory subunits

Thorough classification of mammalian PP1 regulatory subunits was performed by Patricia Cohen over ten years ago (Cohen, 2002). This study presents 54 well-established PP1 regulators and classifies them into groups according to their physiological function, tissue distribution and, importantly, the cellular compartment targeted. Later, PP1 interactors were classified according to their cellular function, specifically showing diverse mechanisms that can be regulated by PP1 complexes (Ceulemans and Bollen, 2004). PP1 holoenzymes can regulate variety of unrelated mechanisms in the cell such as cell cycle, apoptosis, metabolism, new protein synthesis, ion channels, actomyosin organisation and others, but some picture its overall function in the cell as energy-conserving (Ceulemans and Bollen, 2004) (Figure 1.14). Furthermore, the function of many regulatory subunits is to specifically target PP1 to various compartments, therefore enabling its distinct roles. For example, PP1 can be targeted to glycogen and have roles in its metabolism or it can be targeted to actomyosin and act in muscle relaxation. PP1 can also be targeted to the nucleus, to the plasma membrane, mitochondrium, endoplasmic reticulum or to the proteasome (Cohen, 2002).

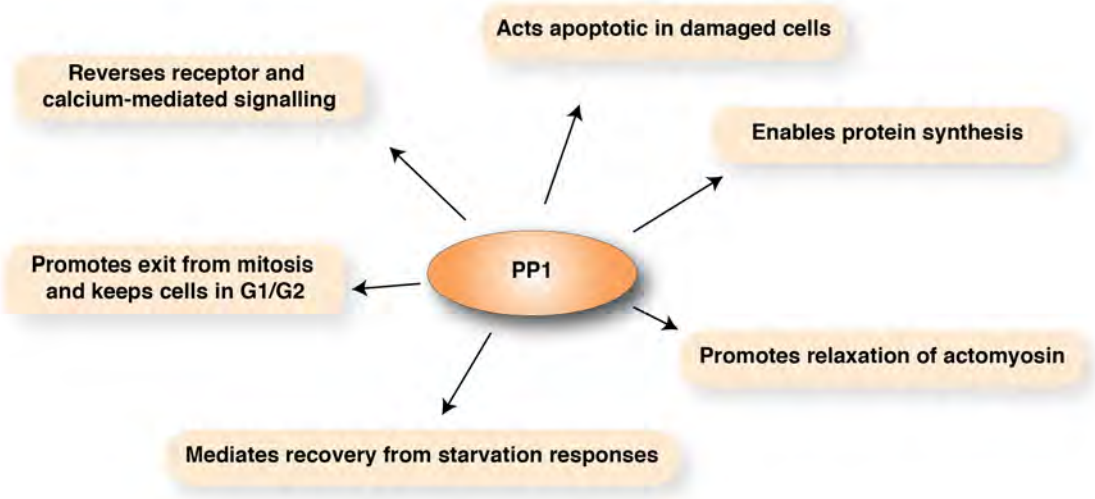


**Figure 1.14 Functional diversity of PP1.**

Overview of PP1 activity pictures it as a 'green' enzyme (Ceulemans and Bollen, 2004), which reduces energy and stockpiles it in the form of glycogen, promotes protein synthesis and returns cell to its basal state after stress, starvation or upregulation of some signalling pathways. PP1 reverses translational mechanisms induced by stress, inactivates several transcription factors and promotes recycling of transcription factors; PP1 resets neural tissue to energy-conserving state, promotes muscle relaxation and actomyosin relaxation in non-muscle cells. After cell damage, PP1 induces apoptosis. PP1 is thus often referred to as an energy-conserving 'reset' enzyme (for an overview of PP1 functions, refer to (Ceulemans and Bollen, 2004)).

Here, I will present examples of PP1 functions and show how structural and mutational analysis of some PP1 holoenzymes helps to explain its diversity.

#### *1.3.5.1 Cell cycle*

One of the best-described roles of PP1 is the regulation of cell division, through variety of targets like Aurora B and crucially Retinoblastoma (Rb). Early mutagenesis and microinjection studies show that cells which contain defective PP1 stop dividing (for review, see (Ceulemans and Bollen, 2004)). Interestingly, studies in yeast show big phenotypical variability suggesting many different targets of PP1. PP1 was shown to have pleiotropic effects in mitosis in mammals as it was observed to target variety of structures involved in mitosis regulation, like centrosomes, the mitotic spindle or chromosomes (Andreassen et al., 1998; Bloecher and Tatchell, 2000). One of the best-studied mitotic mechanisms controlled by PP1 is spindle checkpoint, which involves protein kinase Aurora B. Aurora B is an activator of spindle checkpoint and allows phosphorylation of various checkpoint proteins thus allowing them to prevent activation of degradation mechanisms (for review, see (Lesage et al., 2011)). In vertebrates, six different PP1 holoenzymes have been found to counteract Aurora B signalling at the kinetochores, therefore enabling effective spindle checkpoint exit and cell division (Lesage et al., 2011).

An important cell cycle PP1 interactor is Retinoblastoma protein (Rb), introduced here because of its reported link to Phactr4-PP1 interaction (Kim et al., 2007) (described in section: 'The Phactr family of G-actin binding PP1 cofactors'). Initially identified as tumour suppressor, Rb is one of the main players in cell cycle (Friend et al., 1986; Weinberg, 1995). Rb possesses a bipartite pocket structure, which mediates its association with variety of cellular proteins, mainly transcription factors and components of transcription machinery. The best known partners of Rb are E2F transcription factors, which control activity of vital cell cycle genes, like cyclinE, cyclinA or Cdc25. Interestingly, some E2F family members can act as cell cycle activators (E2F1-3) and some as repressors (E2F4-5). Rb is a crucial component of this

machinery as it differentially associates with E2F transcription factors and prevents cell cycle progression (for review, see (Kolupaeva and Janssens, 2013)).

The interaction of Rb with E2F transcription factors depends on the phosphorylation state of Rb. Best known phosphatases responsible for regulating Rb phosphorylation are cyclin-dependent kinases (CDKs). CDKs phosphorylate Rb at various sites throughout cell cycle to inactivate its activity and allow cell cycle progression. During early G1-phase, Rb has a low phosphorylation state and becomes phosphorylated by cyclinD/CDK4 in the middle of G1-phase. Later, Rb undergoes phosphorylation at the G1/S boundary by cyclinE/CDK2 and then in S phase by cyclinA/CDK2 (Grana et al., 1998; Kitagawa et al., 1996; Mayol et al., 1995; Xiao et al., 1996). Therefore, the Rb phosphorylation state is high at S-phase and it becomes low during the exit from mitosis. Highly phosphorylated Rb releases E2F transcription factors, which activates cell cycle progression. Many phosphorylation sites on Rb have been identified and are well established *in vivo* (Zarkowska and Mittnacht, 1997). PP1 was shown to be the major Rb phosphatase at mitotic exit. Studies of PP1 indicate that PP1 dephosphorylates Rb in mitotic cell lysates and that it directly interacts with Rb in yeast two-hybrid screens (Durfee et al., 1993; Nelson et al., 1997).

Interestingly, the control of Rb by CDKs occurs not only by direct phosphorylation of Rb, but also by phosphorylating and inactivating PP1. This mechanism depends on phosphorylation of PP1 on T320 by CDKs. This regulatory mechanism was shown by the expression of constitutively active PP1 T320A mutant, which prevented Rb phosphorylation and caused cell cycle arrest (Berndt et al., 1997). The interaction between PP1 and Rb was shown to occur at the C-terminus of Rb, but several studies suggest that this interaction is very complex and involves more than one interaction surface (for review, see (Kolupaeva and Janssens, 2013)). Many studies also suggest that all PP1 isoforms bind to Rb equally well (Flores-Delgado et al., 2007; Vietri et al., 2006). Recent structural study of PP1α isoform bound to short Rb peptide elucidated many molecular details of this interaction (Hirschi et al., 2010). Firstly, the C-terminus of Rb was shown to be an enzyme docking site, required for the activity of PP1 towards Rb. Secondly, it was suggested that CDKs bind competitively to the same

surface on Rb and the competition between Rb and CDKs is sufficient to block cell cycle progression. Moreover, Rb interacts with PP1 at a site that is distinct from the catalytic site and the motif required for this interaction, a KLRF motif, similar to a KVxF consensus (Hirschi et al., 2010).

#### *1.3.5.2 Gene expression*

Transcription by RNA polymerase II relies on dynamic phosphorylation of the heptapeptide repeats in the C-terminal domain (CTD) of the polymerase. Phosphorylation of CTD is maintained by the activity of CDK7 and CDK9, while dephosphorylation depends on PP1 activity. Although one of the main phosphatases involved in this process was initially found to be the phosphoserine phosphatase FCP1, PP1 was found to play a dominant role in this process (Washington et al., 2002).

One of the major regulators of PP1 in the nucleus is nuclear inhibitor of PP1 (NIPP1), which inhibits dephosphorylation of a large amount of nuclear PP1 substrates (for review, see (Bollen and Beullens, 2002)). Both PP1 and NIPP1 have been found as components of Tat (Transactivator of transcription)-associated RNA polymerase II complex regulating transcription of human immunodeficiency virus type 1 (HIV-1). The expression of HIV-1 is blocked by NIPP1 addition, which can be reversed by the expression of PP1. Tat was found to contain a PP1-binding motif and act as PP1 regulatory subunit (Ammosova et al., 2005). Mutations of the PP1-binding motif in Tat prevent Tat from activating HIV-1 transcription and PP1 nuclear translocation. Moreover, it was recently shown that the expression of NIPP1 suppresses HIV-1 replication (Ammosova et al., 2011).

PP1 was also implicated in the regulation of chromatin remodelling. Although one of the main nuclear regulators of PP1 is NIPP1, many other were also found (Ceulemans and Bollen, 2004). Nuclear PP1 also binds embryonic ectoderm development protein (EED), a member of the Polycomb family, which maintain transcription repression by epigenetic marks of histone deacetylation and methylation.

Interestingly, NIPP1, EED and PP1 can form a ternary complex, suggesting mutual targeting for dephosphorylation. Another trimeric complex consisting of PP1 and proteins involved in chromatin remodelling contains GADD34 (growth arrest and DNA damage protein) and SNF5 (component of the chromatin remodeling complex SWI/SNF). PP1 associates with GADD43 through canonical RVxF motif and also requires binding of SNF5. Both proteins bind PP1 simultaneously, but do not compete with each other. GADD34 seems to be involved in targeting PP1 to SNF5 therefore promoting dephosphorylation of SWI/SNF by PP1 (Wu et al., 2002).

Eukaryotic translation initiation factor (eIF2α) is a key integrator of translational repression and stress-responsive genes during stress conditions. The phosphorylated form of eIF2α disables translation initiation complexes by sequestering some of their components. During stress, phosphorylated eIF2α acts as an activator of transcription factors involved in the stress response. Specific, stress-activated kinases stimulate eIF2α. One of them, protein kinase R (PKR), was found to be directly targeted and dephosphorylated by PP1 (Tan et al., 2002). Moreover, some studies indicate that PP1 also contributes to recovery from stress by dephosphorylation of eIF2α. Consistently, experiments in reticulocyte lysates identified PP1 as eIF2α phosphatase. Targeting of PP1 to eIF2α was found to be mediated by GADD34, as GADD34/PP1 complexes dephosphorylate eIF2α *in vitro* (Connor et al., 2001). Moreover, the complex comprising PP1 and GADD34 also contained Inhibitor-1, one of the main PP1 inhibitors. The analysis of these interactions suggested that direct cooperation of the three proteins mediated function of eIF2α through activating phosphorylation of Inhibitor-1 by PKA (Connor et al., 2001).

#### *1.3.5.3 Cytoskeleton*

Because several studies and our findings suggest that Phactr proteins associate with PP1 to induce cytoskeletal rearrangements (Allain et al., 2011; Huet et al., 2012; Jarray et al., 2011; Sagara et al., 2009; Wiezlak et al., 2012; Zhang et al., 2012), I will now introduce roles of PP1 in cytoskeleton regulation.

Dynamic reorganisation of actin cytoskeleton is controlled by phosphorylation of its components. PP1 emerged as an important regulator of cytoskeletal reorganisation as many of its regulatory subunits are targeting it to cytoskeleton (Cohen, 2002; Fernandez et al., 1990). Phylogenic analysis indicates that the role of PP1 in the regulation of cytoskeleton became evolutionally significant during a switch to multicellular organisation (Ceulemans et al., 2002a). Well-studied families of cytoskeletal regulatory subunits of PP1 include MYTPs, which control actomyosin phosphorylation and neurabins (neuronal actin binding proteins), which are targeted to F-actin to regulate synaptic plasticity.

As described earlier, in smooth muscle and non-muscle cells, phosphorylation of MLC activates the ATPase activity of myosin and enables actomyosin crosslinking and muscle contraction. Several kinases and one major myosin light chain phosphatase (MLCP) regulates the phosphorylation state of MLC. PP1 and MYPT1 are crucial components of the MLCP complex and their association is vital for MLC dephosphorylation. The role of PP1 association with MYPT1 was described in previous section (see section: 'Regulation of actomyosin crosslinking'). A structural insight into the regulation of PP1 by MYPT1 was gained through crystallisation of MYTP1 with PP1δ isoform (Figure 1.13) (Terrak et al., 2004). The most intriguing outcome of this study is the formation of extended catalytic cleft, which is specifically adapted to sense myosin as a substrate and is not compatible with other substrates. Moreover, the complex clearly shows multiple interaction sites of MYPT1 and PP1, with N-terminal part of MYPT1 tightly wrapping around PP1 (Figure 1.13). It is also shown that the overall charge of sequences surrounding the RVxF motif plays a role in PP1 binding and that weak interactions within the complex play important roles in modulating PP1 activity (Terrak et al., 2004).

The second group of actin-related PP1 regulators is the family of neurabins. They are large, membrane-associated proteins expressed at postsynaptic densities, growth cones and in the cytoplasm (Oliver et al., 2002; Sakisaka et al., 1999). There are two isoforms of neurabins in vertebrates, neurabin I and neurabin II (also called

spinophilin (Satoh et al., 1998)) and both of them contain an N-terminal F-actin binding domain. The middle part of neurabins contains a PP1-binding RVxF motif and a PDZ domain, which recruits the C-terminus of p70S6 kinase. Interestingly, the central domain of neurabins is selective towards PP1 isoforms and prefers the α-isoform to others. Furthermore, the central part of neurabins contains an oligomerisation domain, which enables them to homodimerise.

Functionally, neurabins act as scaffolds for PP1 and other proteins at the synaptic cytoskeleton and enable them to regulate signals of neurotransmitters (Oliver et al., 2002). The link between regulation of synaptic plasticity and PP1 was previously shown (Malenka and Bear, 2004) (for review, see (Munton et al., 2004)). Recently, Both F-actin and PP1 binding was shown to be required for the regulation of synaptic transmission and hippocampal plasticity (Hu et al., 2006). PP1 inhibition coincides with long-term potentiation (LTP), a long-lasting enhancement of neurons enabling them to be stimulated simultaneously. LTP is a mechanism responsible for the ability of synapses to modulate their strength and is therefore considered vital during learning and memory (Bliss and Collingridge, 1993). The opposite mechanism, long-term depression (LTD), was consequently linked to PP1 activity (Malenka and Bear, 2004). Postsynaptic PP1 substrates include Ca2+/calmodulin-dependent protein kinase II (CaMKII) (Strack et al., 1997), α-amino-3-hydroxy-5-methyl-4-isoxazolepropionic acid (AMPA) (Kameyama et al., 1998) and N-Methyl-D-aspartate (NMDA) receptors (Westphal et al., 1999), all crucial for synaptic plasticity. It was established that the N-terminal F-actin binding domain of neurabins could modulate actin dynamics and stimulate growth of dendritic filopodia, which consist of actin-associated cytoskeletal proteins. Moreover, both PP1 and F-actin binding to neurabin is required for dendritic filopodia maturation and transition into dendritic spines (Terry-Lorenzo et al., 2005).

## 1.4 The Phactr family of G-actin binding PP1 cofactors

The Phactr (Phosphatase and actin regulator) family of proteins is a recently discovered group of proteins, which like MRTFs and myocardin contain RPEL motifs and bind G-actin. However, whether Phactr protein function is regulated by G-actin has been unexplained until recently. Here, I will introduce Phactr protein family, discuss their domain organisation, reported functions and implication in human disease.

### 1.4.1 Early studies of Phactr family

Phactr family has four members: Phactr1, Phactr2, Phactr3 (also referred to as Scapinin) and Phactr4 (Figure 1.15). The founding family member, Phactr1, was discovered by the Greengard group in yeast-two-hybrid screen, which was designed to detect proteins interacting with the catalytic subunit of PP1α (Allen et al., 2004). Expression of the Phactr1 cDNA in mammalian cells revealed a protein with an apparent molecular weight of 75 kDa. By homology, three other members of the family were found. The examination of amino acid sequence revealed conserved RPEL motifs in the newly discovered proteins. Immunoprecipitation experiments with Phactr1 confirmed that it binds both PP1 and actin (Allen et al., 2004).

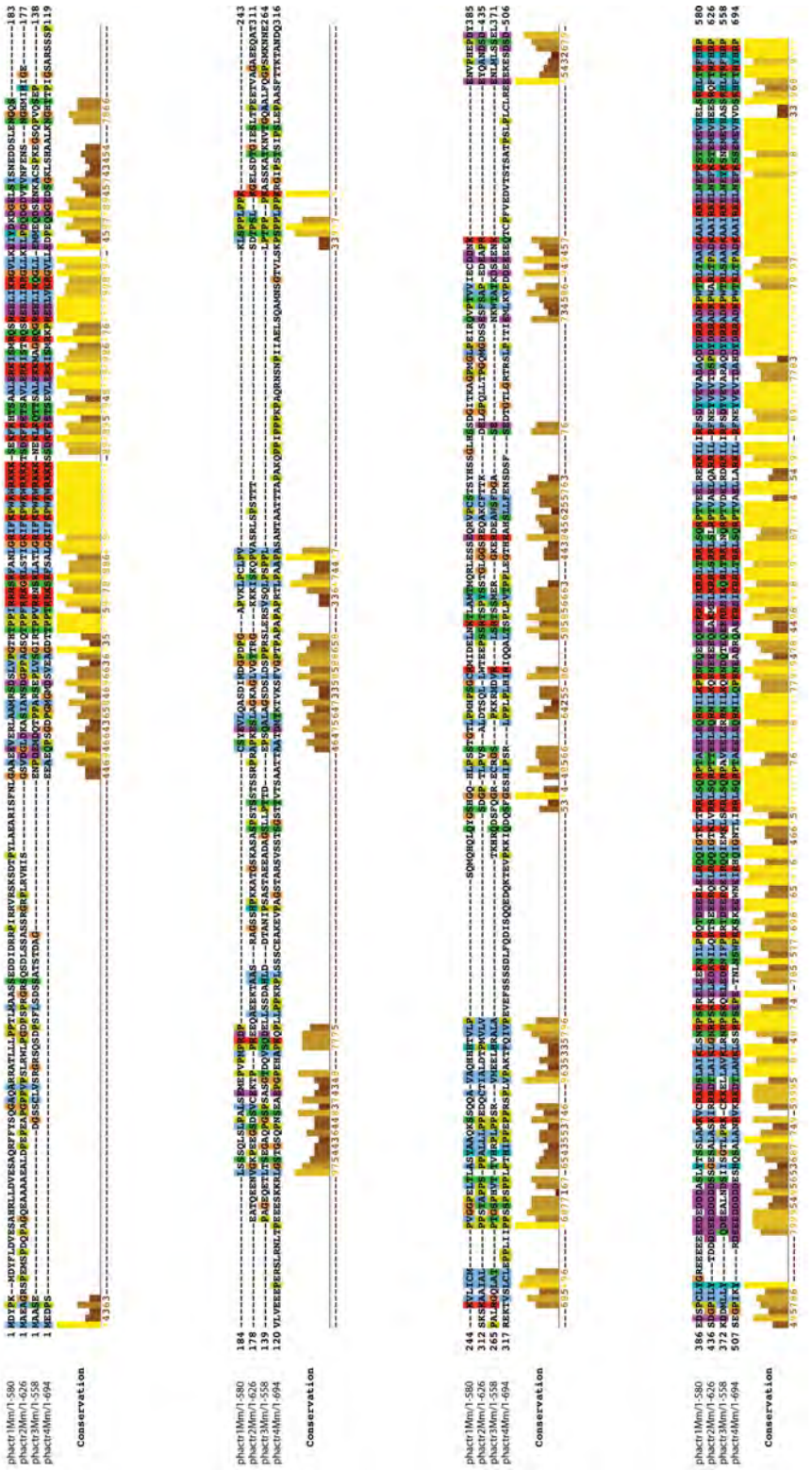

**Figure 1.15 Phosphatase and actin regulator family of proteins.**

Alignment of four Phactr family members form *Mus musculus* performed using Muscle Multiple Protein Sequence Alignment (Edgar, 2004) in Jalview software.

Another study of PP1 also led to the discovery of a member of Phactr family, Phactr3/Scapinin (Sagara et al., 2003). PP1α was previously shown to be associated with the nuclear matrix and nuclear lamina, structures implicated in the segregation of chromatin and regulation of other nuclear processes (Berezney and Coffey, 1975; Ma et al., 1999; Mirkovitch et al., 1984). To investigate novel proteins of the chromatin-depleted nuclear structure (referred to as nuclear matrix intermediate filament scaffold, NM-IF) monoclonal antibodies against the HL-60 NM-IF were developed in mice leading to the discovery of Phactr3/Scapinin (scaffold-associated PP1 inhibiting protein) (Sagara et al., 2003). There are three Scapinin splice variants encoding proteins of 559 amino acids, 518 amino acids and 448 amino acids. Isoform 2 (518 amino acids), found by Sagara and colleagues was predominant in the human brain (Sagara et al., 2009). Scapinin was reported to co-immunoprecipitate with PP1 and to bind PP1 in yeast two hybrid assays (Sagara et al., 2003).

Finally, Favot and colleagues identified Phactr proteins by screening the ENSEMBL database in order to find novel genes containing RPEL motifs, referring to them as 'RPELs' (Favot et al., 2005).

### 1.4.2 Phactr family domain organisation and reported interactions

Phactr proteins contain several highly conserved regions (Figure 1.16). Conservation of Phactr family of proteins is high throughout species, with domain conservation ranging from *Caenorhabditis elegans* to *Homo sapiens.* Most vertebrates contain four Phactr proteins and in *Caenorhabditis elegans* and *Drosophila melanogaster* there is only one. There is no exact homolog of a Phactr family member in yeast *Saccharomyces cerevisiae*, but one report describes a protein called Bni4, which contains a region 32% identical to the C-terminal domain of Phactr proteins (around 70 amino acids) (Larson et al., 2008). This region in Bni7 is responsible for binding PP1 in yeast (Glc7). A protein called Afr1 was also reported, containing a similar Glc7-binding region (Bharucha et al., 2008). By similarity, Afr1 resembles the C-terminus of mammalian Phactr4.

The most conserved part within the family is the C-terminal region, which contains three RPEL motifs (Pfam 02755) separated by short spacers forming an RPEL domain (around 110 amino acids long), highly homological to the RPEL domain in the MRTFs and myocardin. The very C-terminal region contains a sequence of 55 highly conserved amino acids, shown to be required for PP1 binding (Wiezlak et al., 2012). The RPEL domain and the PP1-binding sites overlap. The N-terminal region of Phactr family is also conserved and contains a basic region and one unusual RPEL motif (RPEL-N) (Figure 1.16). In Phactr1-3 the N-terminal RPEL motif contains glutamine instead of proline within the consensus, and in Phactr4 this proline is substituted by a lysine. Located N-terminally to RPEL-N and RPEL3 in Phactr1 and are two Importin α-β binding nuclear localisation signals (Wiezlak et al., 2012), also reported to be present at the C-terminus of Phactr4 (Huet et al., 2012). The middle region of Phactr proteins is not highly conserved and contains multiple prolines and glycines (Figure 1.15).

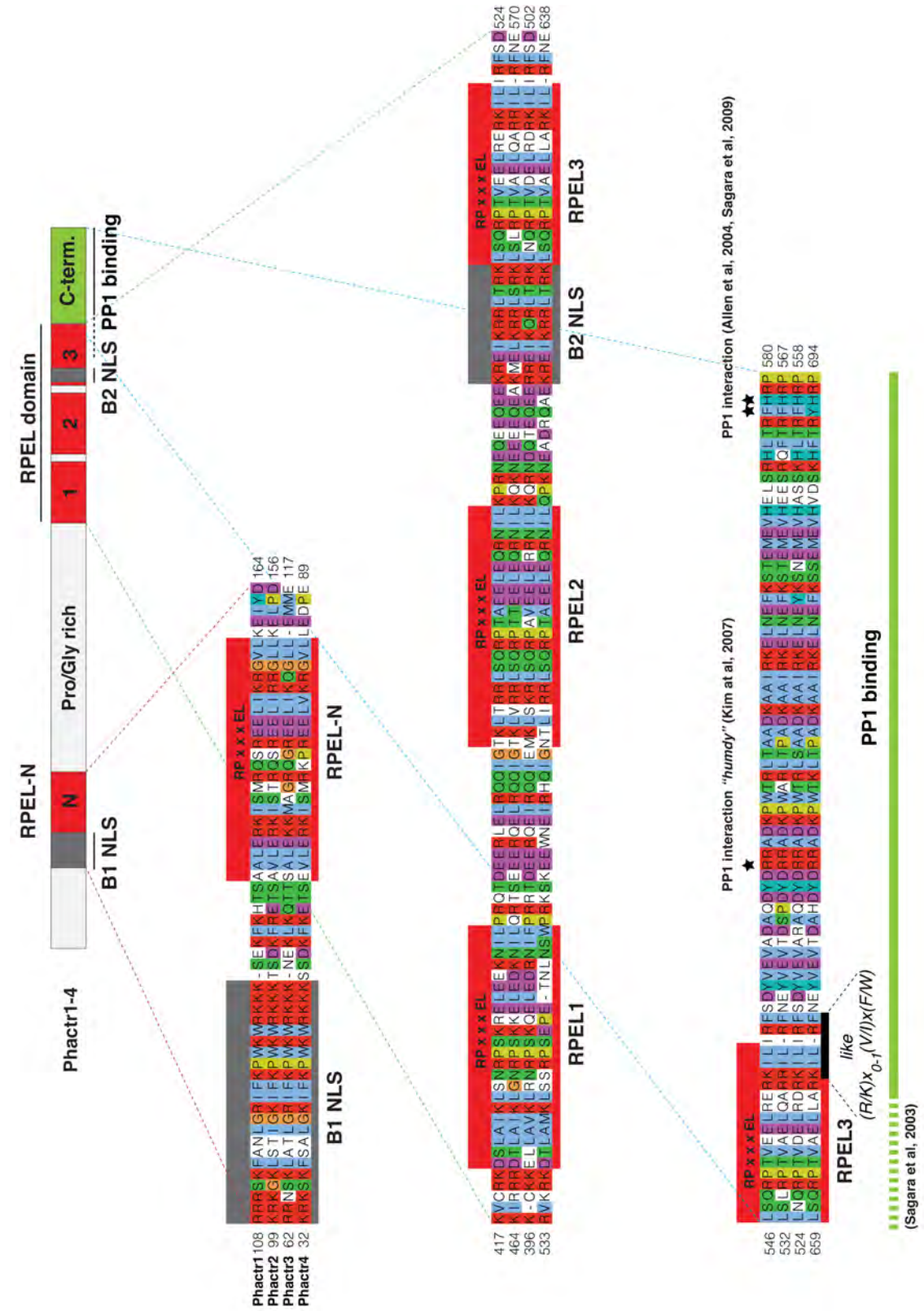
RPEL domain
RPEL-N
Pro/Gly rich
C-term.
1
2
3
N
B1 NLS
B2 NLS
PP1 binding
Phactr1-4
RPEL-N
B1 NLS
RPEL-N
RPEL1
RPEL2
RPEL3
B2 NLS
RPEL3
PP1 binding
PP1 interaction "humdy" (Kim at al, 2007)
PP1 interaction (Allen et al, 2004, Sagara et al, 2009)
like
(R/K)x0-1(V/I)x(F/W)
(Sagara et al, 2003)
Phactr1 108
Phactr2 99
Phactr3 62
Phactr4 32
164
156
117
89
417
464
396
533
546
532
524
659
524
570
502
638
580
567
558
694

**Figure 1.16 Conserved sequences in Phactr family of proteins**

Highly conserved Phactr family sequences from *Mus musculus* are shown as alignments (performed using Muscle Multiple Protein Sequence Alignment (Edgar, 2004) in Jalview software). Four RPEL motifs (red boxes) and two NLS sequences, B1 and B2 (grey boxes) and PP1 binding region (green box on the top and green line on the bottom) are schematically indicated. Localisation of potential RVxF-like motif is indicated on the right and reported interaction points of PP1 are shown (black stars). Note that sequences overlap.

Several reports describe interactions of the conserved regions in Phactr family with PP1, actin and other proteins.

#### *1.4.2.1 Interaction with PP1*

Early studies of Phactr proteins examined the PP1 binding property of their conserved C-terminal region. Allen and colleagues report the requirement of last ten amino acids from Phactr1 to efficiently co-immunoprecipitate with the α-isoform of PP1 catalytic subunit and alanine substitutions of the last five amino acids of Phactr1 ($^{576}$RFHRP$^{580}$) suggest a role of F577 and H578 in PP1 binding (Allen et al., 2004). Studies of the brain-specific isoform of Phactr3/Scapinin showed loss of PP1 interaction in co-immunoprecipitation assay when F515 (equivalent of F577 in Phactr1) was substituted by an alanine (Sagara et al., 2009). Sagara and colleagues also showed that last 70 amino acids of Phactr3/Scapinin can inhibit the activity of PP1 as efficiently as a Inhibitor-2, but a peptide containing last 54 amino acids cannot. A construct containing the last 59 amino acids was also able to inhibit PP1 but to a lesser extent. We recently showed that the deletion of the whole RPEL domain also abolished the PP1 interaction (Wiezlak et al., 2012).

Additionally, deletion of the last 10 amino acids from the C-terminus of Phactr3/Scapinin reduced PP1 inhibition activity towards phosphorylase *a* (Sagara et al., 2003). Consistent with this finding, Allen and colleagues also reported inhibition of PP1 activity towards phosphorylase *a* using full-length Phactr1 construct (Allen et al., 2004). In both of these studies, a established previously method for *in vitro* PP1 activity measurement was used (Shirato et al., 2000), but no *in vivo* activity of PP1 or its potential substrates were examined. In contrast, Huet and colleagues performed a colorimetric PP1 activity assay and showed that Phactr4 is a potent activator of PP1 (Huet et al., 2012). These inconsistent results might reflect diverse functions of Phactr family members.

Additionally, it was shown that the mouse *humdy* mutant has a missense mutation within the PP1-binding conserved C-terminal region of Phactr4, substituting the conserved R650 (equivalent of R536 in Phactr1) with a proline, and is unable to bind PP1 in co-immunoprecipitation assays (Figure 1.15)(Kim et al., 2007).

It was assumed that the PP1 binding consensus (R/K)$x_{0\text{-}1}$(V/I)$x$(F/W) is not present in Phactr proteins. However, the analysis of the alignment between Bni4, a protein in yeast *Saccharomyces cerevisiae* containing PP1 binding site (~70 amino acids) that is similar to the one in the Phactr family, reveals a $^{828}$DQGVRF$^{833}$ motif in Bni4 similar to $^{517}$KILIRF$^{522}$ in Phactr1 (Larson et al., 2008) (Figure 1.16). Interestingly, the mutation of V831A F833A within this motif in Bni4 disrupts binding to Glc7 (yeast homolog of PP1). Moreover, the substitution of the Glc7 binding domain with the PP1 binding domain from Phactr1 containing last 80 amino acids can functionally replace its function, which is targeting Glc7 and yeast chitin synthase III (CSIII) to the bud neck allowing it to act on a yet undefined substrate. Another yeast protein, Afr1, also contains similar sequence $^{543}$KKDVRF$^{548}$ and similarly to Bni4, the mutation of V546A and F548A inhibit its binding to Glc7 (Bharucha et al., 2008). When Afr1 cannot bind Glc7, it is defective in regulating septin architecture during mating. Considering a huge variability of the KVxF motifs in PP1 binding proteins, it is probable that a similar motif is indeed present in Phactr family (by homology KILIRF in Phactr2, KILRF in Phactr3 and RILRF in Phactr4), but more mutational analysis in needed to address this issue (Figure 1.15).

Taken together, those reports show that the C-terminal region in Phactr proteins is required for the interaction with PP1. The binding of PP1 seems to encompass multiple interaction points, which is consistent with the binding modes of many PP1 regulatory subunits (Roy and Cyert, 2009). The function of PP1 binding to Phactr proteins is not clear, but some reports suggest a molecular role of this interaction (see section: ‘Proposed functions of Phactr proteins’).

#### *1.4.2.2 Interaction with actin*

Allen and colleagues were the first to report an interaction between Phactr1 and actin. Yeast two-hybrid screen with a fragment of Phactr1 containing amino acids 161-580 identified independent isolates of the cDNA encoding β-actin. Actin binding was abolished when a fragment containing last 80 amino acids of Phactr1 was used. Immunoprecipitation experiments from rat brain lysate also showed actin in complex with full length Phactr1 and with several Phactr1 C-terminal truncations, apart from Phactr1 1-490 (truncation of the last RPEL motif within the RPEL domain), where no actin binding was detected (Allen et al., 2004).

Sagara and colleagues suggest that fragments containing GST-tagged RPEL1 and RPEL2 (amino acids 350-422) or the whole RPEL domain (amino acids 350-468) of Phactr3/Scapinin bind actin in pull-down assays. In contrast, GST-tagged RPEL1 (amino acids 350-385) or a RPEL domain containing a RP/AA mutation (Guettler et al., 2008) within the second RPEL motif was unable to bind actin in pull-down assays. The authors also report severe degradation problems during the performance of their pull-down assays, especially when using full length RPEL domain of Phactr3/Scapinin. Due to the degradation issues authors later used a construct containing RPEL1 and RPEL2 (amino acids 350-422) and not the full length RPEL domain. They show that this fragment directly interacts with purified actin and inhibits actin polymerisation in ultracentrifugation experiments (Sagara et al., 2009). We recently showed by fluorescence polarization assays that all four RPEL motifs from Phactr1 interact directly with G-actin (Wiezlak et al., 2012).

The actin binding ability of the full length RPEL domain was not tested until recently. We and Huet and colleagues respectively showed that Phactr1 and Phactr4 bind G-actin directly through the C-terminal RPEL domain and that PP1 competes with actin for Phactr1 and Phactr4 binding (Huet et al., 2012; Wiezlak et al., 2012). We also showed by X-ray crystallography that the full length RPEL domain from Phactr1 interacts with three G-actins and each RPEL motif interacts with one G-actin molecule. Our structural analysis shows that RPEL-N also interacts with G-actin (Mouilleron et al.,

2012). Our study describes several similarities and differences between the Phactr1 and MRTF-A interactions with G-actin (details of these findings will be presented in section: 'Structural analysis of Phactr1 interaction with actin').

### 1.4.3 Expression and tissue distribution

Several reports suggest that members of Phactr family might be differentially expressed, showing high expression levels in neuronal tissues and cancer cell lines (Allen et al., 2004; Kim et al., 2012; Kim et al., 2007; Sagara et al., 2003; Solimini et al., 2013). Additionally, Phactr1 was highly expressed in malignant melanomas (Koh et al., 2009; Trufant, 2010; Wiezlak et al., 2012).

Allen and colleagues performed Northern blot analysis to find location of Phactr1 cDNA. The transcript was most abundant in brain, but also present in heart, lung, kidney and testis (Allen et al., 2004). Small amounts were also reported in skeletal muscle, but Phactr1 cDNA was absent from spleen and liver. More detailed analysis of Phactr1 expression pattern within the brain revealed enhanced protein expression in cortex, hippocampus, olfactory tubercle and particularly striatum. Allen and colleagues also examined the expression of other Phactr family members in rat brain by *in situ* hybridisation. They picture the expression of Phactr1 and Phactr2 as complementary, with Phactr2 enhanced in cerebellum, choroid plexus and thalamus. Expression of Phactr3 was diffuse throughout the brain section and Phactr4 expression was reported in the hippocampus and cerebellum.

Recent study of Phactr proteins expression pattern in the brain supports those observations (Kim et al., 2012). The mRNA expression patterns of Phactr family members were examined in developing, adult and injured mouse brains. Each member of the family was expressed in different brain regions. The mRNA level of Phactr2 was particularly high in regions associated with learning and memory and Phactr4 mRNA was enhanced in regions where neural stem cells and progenitors are localised. Authors also suggest that mRNA of Phactr1 and Phactr3 is mainly expressed in neurons and

Phactr2 and Phacr4 in astrocytes (Kim et al., 2012). Phactr4 is also highly expressed during the development of the neural tube and retina (Kim et al., 2007). Interestingly, Phactr4 RNA is expressed in a dynamic pattern during neurulation. Early in the development Phactr4 is expressed in the ventral region of the cranial tube and later its expression becomes uniform throughout the dorsal and ventral parts. Additionally, Phactr4 was recently shown as highly expressed in the enteric nervous system (Zhang et al., 2012).

Recent report shows that Phactr4 gene is deleted in breast, colorectal, lung, neural, ovarian and renal cancer, with only 2.6% of all genes deleted as significantly as Phactr4. Furthermore, whole-genome and exome sequencing databases analysis from around 2500 solid tumours and found 11 loss-of-function and 16 missense mutations in Phactr4 (Solimini et al., 2013). Sagara and colleagues described Scapinin/Phactr3 expression patterns in some tumour human cell lines and normal tissues (Sagara et al., 2003). Northern blot analysis showed enhanced expression in the brain, in HL-60 leukemia, U937 leukemia, and in GOTO neuroblastoma cells.

Two independent studies found high expression levels of Phactr1 in malignant melanomas. Koh and colleagues employed gene expression microarray to increase the accuracy of discrimination between benign lesion and a malignant melanocytic tumour (Koh et al., 2009). Cells used in this study were isolated by microdissection from large numbers of formalin-fixed and paraffin-embedded tissues. This study found 14 genes, which were either significantly upregulated or downregulated in melanomas. Compared to nevi, melanoma had increased expression of Phactr1 and other, previously reported genes. A second study was based on immunohistochemical analysis of tissue arrays containing different malignant melanomas and nevi with several antibodies and markers of malignant melanoma. This work shows that Phactr1 staining is a highly sensitive tool in the clinical diagnosis of primary cutaneous melanoma (Trufant, 2010). We also show that Phactr1 is highly expressed in malignant melanoma cell line CHL-1 (Wiezlak et al., 2012).

### 1.4.4 Subcellular localisation

Analyses of reported Phactr family subcellular localisation suggest that they might be localised differentially depending on their expression level, the molecular tag they are linked to, cell type and isoform examined.

In N2a neuroblastoma cells, HA-tagged Phactr1 was found in the cytoplasm, unlike its binding partner PP1α, which was enhanced in the cell nuclei (Allen et al., 2004). Immunocytochemical analysis of brain sections showed endogenous Phactr1 localisation in cell bodies and proximal dendrites, but not in nuclei. In cultured hippocampal neurons, GFP-tagged Phactr1 localised in cell bodies, dendrites and dendritic spines. Fractionation experiments suggested the enrichment of Phactr1 at postsynaptic densities (Allen et al., 2004). Immunohistochemical staining of paraffin-embedded malignant melanoma tissues with Phactr1 antibody showed that it is predominantly cytoplasmic (Trufant, 2010).

In proliferating HL-60 cells, endogenous Phactr3/Scapinin was reported in nuclei (Sagara et al., 2003), but in HeLa cells enhanced expression of exogenous Phactr3/Scapinin was reported in both the cytoplasm and nucleus with the enrichment at the cell edge (Sagara et al., 2009). Additionally, Phactr3/Scapinin did not translocate to the nucleus upon serum stimulation of HeLa cells. In Cos7 kidney carcinoma cells, GFP-tagged Phactr3/Scapinin was also localised throughout the cell with enrichment at the cell periphery (Sagara et al., 2009). Kim and colleagues report subcellular localisation of endogenous Phactr4 in the cytoplasm of neural tube cells in mouse embryos. However, the same study shows that in HeLa cells, Myc-tagged Phactr4 was found throughout the cell (Kim et al., 2007).

Recent analysis shows that in starved NIH3T3 cells all GFP-tagged Phactr proteins are found in the cytoplasm (Huet et al., 2012). Phactr4 additionally exhibits enhanced localisation at the plasma membrane and the deletion of Phactr4 N-terminal region potentially triggers its nuclear accumulation (Huet et al., 2012). Huet and colleagues show that Phactr4 subcellular localisation is independent from G-actin

binding to the RPEL domain. Using FRAP assays they also showed that Phactr4 is imported to the nucleus *in vivo* and suggest that Phactr4 might actually shuttle between the plasma membrane and the nucleus. However, no mutational analysis showing the potential membrane localisation and/or nuclear localisation sites was performed.

Our analysis of Phactr proteins shows that in serum starved NIH3T3 cells FLAG-tagged Phactr1 and Phactr2 are predominantly cytoplasmic and Phactr3 and Phactr4 are expressed throughout the cell. Phactr1 is the only member of the family that accumulates in the nucleus upon serum stimulation, both in fibroblasts and in melanoma cells (Wiezlak et al., 2012). Details of these findings will be presented in section: 'Molecular mechanisms of Phactr1 regulation'.

### 1.4.5 Proposed functions of Phactr proteins

Given that all Phactr proteins bind PP1, it is intriguing to understand whether they all perform the same biological function and what is the significance of the existence of four family members. Different functions of Phactr family members were suggested, but not many reports propose roles for Phactr proteins in *in vivo* models. First two reports suggest that they might have cytoskeletal roles due to their actin binding ability or could control neuronal functions due to their high expression levels in the neural tissues (Allen et al., 2004; Favot et al., 2005). One study suggests a role of Phactr1 in angiogenesis and few studies link Phactr3/Scapinin to neuroplasticity and actin dynamics (Allain et al., 2011; Farghaian et al., 2011; Jarray et al., 2011; Sagara et al., 2009; Sagara et al., 2003). Phactr4 is probably the best-studied member of the family as its function was examined in a mutant mouse model and linked to cell cycle regulation (Kim et al., 2007). Very recent report also suggests Phactr4 regulatory roles in cell cycle by revealing that Phactr4 is a tumour suppressor (Solimini et al., 2013). Two studies also link Phactr4 function to cofilin regulation, which have effects in actin pool maintenance and cell migration (Huet et al., 2012; Solimini et al., 2013). We uncover a role of Phactr1 in the regulation of actomyosin assembly (Wiezlak et al., 2012). Below, I will review recent discoveries in Phactr family biology.

#### *1.4.5.1 Neuroplasticity*

A recent study of Phactr3/Scapinin explored its roles in neural tissues using transient transfection with GFP-tagged Scapinin, to examine morphological changes of cultured neurons (Farghaian et al., 2011). The expression of Phactr3/Scapinin caused inhibition of axon elongation in neurons and this effect required actin binding, but not PP1 binding. This study showed that S277 phosphorylation is required for Phactr3/Scapinin inhibition of axon elongation and suggested that S277 phosphorylation directs localisation of Phactr3/Scapinin from the axon to the cytoplasm. Because treatment of cells with Latrunculin A or Cytochalasin D had no effect on Scapinin localisation, authors also suggested that, unlike MRTFs, Scapinin localisation is independent from actin polymerisation. Farghaian and colleagues conclude that Scapinin might play a role in the regulation of neurite outgrowth and neuroplasticity. However, the relevance of this study is hard to assess as the phenotype might be caused by titrating G-actin through RPEL motifs in Phactr3/Scapinin.

#### *1.4.5.2 Cell cycle*

The function of only one Phactr family member, Phactr4 was studied in a mouse model (Kim et al., 2007). Kim and colleagues performed ethyl nitrosourea (ENU) mutagenesis screens for mutations in mice causing neural tube closure defects. *Humdy* (Phactr4 R650P) embryos were characterised by the failure to close the neural tube, exhibited exencephaly, shortened body axis, optic fissure defects and most died at embryonic day E14.5. Interestingly, *humdy* neural tube and retina cells displayed increased proliferation and decreased differentiation. Further analysis revealed, that the *humdy* mutation critically affects cell cycle exit and its overall length.

Kim and colleagues propose that, due to PP1 binding defect, *humdy* mutation induces inhibitory phosphorylation of PP1 at T320 leading to hyper-phosphorylation of Rb, upregulation of E2F-dependent transcription and cell cycle progression (for details,

see section 'Functions of PP1 regulatory subunits'). Indeed, one of the targets of E2F transcription factor, a protein called MCM2 was overexpressed in *humdy* mutants. To ultimately demonstrate that defects in *humdy* mutants are a result of increased E2F activity, the rescue of the *humdy* phenotype with the loss of *E2F1* was shown. Thus, it was suggested that Phactr4 is involved in the control of cell cycle progression by regulating Rb and E2F1 function, but other targets of Phactr4-PP1 complex were not excluded. Surprisingly, it was recently shown that *humdy* enteric neural crest cells exhibit a perfectly well functioning cell cycle (Zhang et al., 2012), suggesting that their migratory defects are not related to the Rb-E2F1 pathway. This implies that disruption of cell cycle in the developing nervous system of *humdy* mouse (Kim et al., 2007) might not be directly related to Phactr4.

Interestingly, a recent report also links Phactr4 function to cell cycle control (Solimini et al., 2013). Because cancer progression depends on a cell's ability to continuously proliferate, authors employed genetic tools to identify suppressors of tumorigenesis and/or proliferation (STOP) genes, whose loss of function promotes cell proliferation and cancer development (Solimini et al., 2012). Solimini and colleagues analysed loss-of-function shRNA screens, which target the whole genome (Paddison et al., 2004; Schlabach et al., 2008; Silva et al., 2005) to find a set of uncharacterised tumour suppressors. They uncovered a tumour-suppressive role for *Phactr4*, as a STOP gene, with cell proliferation phenotypes linked to *Phactr4* gene disruption. Interestingly, analysed tumours contained frameshift mutations at the N-terminus of Phactr4 resulting in the generation of short peptides. The ratio of nonsynonymous to synonymous mutations was significantly higher than that in the entire genome, showing that those mutations are functionally relevant to tumorigenesis. Phactr4 shRNA indeed increased proliferation in human mammary epithelial cells (HMECs). Cell cycle and tumorigenic phenotypes associated with Phactr4 deletion could be supressed by re-expression of wild-type protein. Because Phactr4 was previously shown to regulate the cell cycle through PP1-Rb-E2F pathway (Kim et al., 2007), Solimini and colleagues hypothesised that this pathway might be defective in Phactr4-depleted cells. Consistent with the findings of Kim and colleagues, Phactr4 depletion maintained Rb phosphorylation, while wild-type cells exhibited significant decrease of Rb phosphorylation. However,

HMECs express large T-antigen, which is a potent inhibitor of Rb, meaning that its activity in those cells is independent of Phactr4. Phactr4 must therefore interact with the cell cycle machinery using additional mechanisms.

Nevertheless, Solimini and colleagues further characterised a role of Phactr4 in tumorigenesis. They subsequently showed that cancer cells in which Phactr4 is deleted are sensitive to Phactr4 complementation. The authors also determined if Phactr4 could act as a tumour suppressor *in vivo*. The injection of Phactr4-expressing breast cancer cells into the flanks of nude mice using a Doxycycline-inducible system showed significant decrease in tumour size upon Phactr4 expression.

Although the mechanism of tumour suppression by Phactr4 must still be better explained, it is conceivable that it is linked to actin cytoskeleton regulation by Phactr4 though G-actin binding. The anchorage-independent growth of Phactr4-depleted cells may suggest cytoskeletal rearrangements in these cells. Finally, Solimini and colleagues refrain to comment if other Phactr family members have roles in cell cycle, but genetic screen approach suggests that this function is specific to Phactr4.

#### *1.4.5.3 Actin dynamics*

##### 1.4.5.3.1 Cell morphology and motility

Recent study describing the regulation of angiogenesis, a process where new vessels are formed from the existing vasculature, identified Phactr1 as a potential Vascular Endothelial Growth Factor (VEGF)-dependent gene (Allain et al., 2011). VEGF is a cell-specific mitogen *in vitro* and a pro-angiogenic factor *in vivo* (Ferrara, 2004; Senger et al., 1983). VEGF binds to specific receptors on the cell surface, called VEGFRs, which are transmembrane proteins containing receptor tyrosine kinase (RTK) domains. Additionally, VEGF can also bind other co-receptors, called neuropilins,

previously implicated in neuronal guidance (Harper and Bates, 2008) (for review, see (Neufeld et al., 2002)).

To find new genes, which respond to $VEGF_{165}$ stimulation, cross analysis of two suppression subtractive hybridizations (SSH) was performed (Rebrikov et al., 2004). One SSH was between cDNA libraries from human umbilical vein endothelial cells (HUVECs) and some non-endothelial cell lines (including tumour cells and lymphobasts) and the second SSH between $VEGF_{165}$-stimulated and unstimulated HUVECs (Jarray et al., 2011). Phactr1 emerged as a new endothelial factor candidate, as significant upregulation of Phactr1 mRNA upon $VEGF_{165}$ stimulation in endothelial cells was observed. To examine the role of Phactr1 in angiogenesis, the authors analysed the formation of new vessels *in vitro* upon Phactr1 depletion. Phactr1-silenced HUVECs failed to form tubular structures suggesting a role of Phactr1 in this process. The knock-down of both VEGF-R1 and neuropilin-1 inhibited the mRNA expression of Phactr1, highlighting the potential role of these two receptors in Phactr1 expression. To evaluate roles of PP1 and actin binding to Phactr1 in these processes (Allen et al., 2004), actin polymerisation assays and measurement of PP1 activity by colorimetric assay were performed. The depletion of Phactr1 interfered with $VEGF_{165}$-induced actin polymerisation and significantly decreased the activity of PP1 in HUVECs. Moreover, the amount of actin filaments in Phactr1-depleted cells seemed to be reduced and the lamellipodium formation was disrupted. Allain and colleagues therefore suggest a role for Phactr1 in angiogenesis and propose that this function of Phactr1 is related to actin and PP1 binding capability (Allain et al., 2011).

Because expression of Phactr3/Scapinin in Cos7 cells induced cell spreading and some morphological changes, the relevance of both PP1 and actin binding in the context of this phenotype were examined (Sagara et al., 2009). The disruption of PP1 binding to Phactr3/Scapinin induced cell rounding or shrinkage, but it did not promote cell spreading. Further deletion of actin binding sites together with PP1-interacting regions abolished all morphological changes in Cos7 cells. Abolishing actin-binding ability also reversed the phenotype completely. In HeLa cells, exogenously expressed Phactr3/Scapinin was shown to co-localise with F-actin at the cell edge. It was therefore

suggested that Phactr3/Scapinin might play roles in the regulation of actin dynamics, but the mechanism underling this process needs to be investigated. However, this study is reliant on phenotypes induced by overexpression of Phactr3/Scapinin, therefore effects linked to G-actin titration cannot be excluded.

We recently showed that Phactr1 depletion in malignant melanoma cells leads to stress fibre and motility defects. Conversely, Phactr1 overexpression in NIH3T3 cells enhances actomyosin crosslinking and stress fibre assembly, a phenotype caused by Phactr1 binding to PP1 (Wiezlak et al., 2012)). We reveal a novel role of the Phactr1-PP1 interaction in the regulation of actomyosin, cell motility and melanoma cell invasiveness (for details, see sections: 'Molecular mechanisms of Phactr1 regulation' and 'Functional studies of Phactr1').

#### 1.4.5.3.2 Cofilin regulation and maintenance of actin pool

Recent report describes a role of Phactr4 in the genesis of Hirschsprung disease (HSCR) (Zhang et al., 2012). Gastrointestinal system has its own nervous system, called the enteric nervous system (ENS), which is composed of neural crest-derived neurons and glial cells (Heanue and Pachnis, 2007). Disruption of the ENS during development causes HSCR, a common congenital disorder. Many mutations of HSCR have been mapped, like defects in *c-Ret* gene encoding receptor tyrosine kinase (RET) or *EdnrB* encoding a ligand for RET (McCallion et al., 2003). One of the key mechanisms responsible for the accurate formation of the ENS during embryogenesis is the directed migration of neural crest cells to the gut (Druckenbrod and Epstein, 2005; Young et al., 2004). To efficiently migrate to the ENS, enteric neural crest cells (ENCCs) must become polarised and form lamellipodial protrusions.

Analysis of the previously described Phactr4 mutant *humdy* mouse embryos (Kim et al., 2007) revealed abnormal accumulation of the material in the gut, common for HSCR patients. Further analysis showed reduced number of ENCCs in the hindgut and their disorganisation. Because the differentiation of those cells was unaffected, cell

migration was investigated. Zhang and colleagues showed that Phactr4 is required for the directional migration of those cells. It is important to emphasise here that only the *humdy* mutant was analysed, and no phenotype resulting from the full knock-out of the gene is shown. Further analysis of the *humdy* ENCCs showed extensive defects in the migration along the gut and the regulation of cell directionality, suggesting the requirement of Phactr4 interaction with PP1 for proper regulation of these processes.

The *Humdy* mutation seemed to affect the directionality and speed of mouse embryonic fibroblasts (MEFs) (Zhang et al., 2012). Moreover, the size and number of lamellipodia in these cells were also significantly decreased. The *Humdy* mutation did not affect Phactr4 subcellular localisation, as a *humdy* construct was concentrated at the tip of the lamellipodium, like in the cells transfected with wild-type Phactr4. Therefore, authors suggest that the *humdy* mutation does not affect actin binding ability of Phactr4, however no biochemical analysis was shown.

Because *humdy* MEFs exhibited migratory defects and disrupted lamellipodia formation, a process regulated by Rho-GTPases and the activity of multiple actin binding proteins (Etienne-Manneville and Hall, 2002), Zhang and colleagues sought to analyse the activity of one of the most important cytoskeletal regulators, cofilin. They found that, indeed, the level of phosphorylated cofilin was increased in mutant MEFs in comparison with the wild-type cells. The inhibition of PP1 activity by okadaic acid also resulted in cofilin hyper-phosphorylation, which suggests that the Phactr4-PP1 complex might directly dephosphorylate cofilin. Phactr4 was also shown to co-localise with β1-intergrin at the tips of the lamellipodia, and the phosphorylation of FAK was increased in the mutant MEFs, suggesting that Phactr4 might be a negative regulator of integrin signalling. Moreover, analysis with specific inhibitors showed that the increase in phospho-cofilin levels might be due to the activity of ROCK. To directly show that defects in integrin and cofilin signalling are caused by the disruption of Phactr4-PP1 interaction, the *humdy* phenotype was rescued with integrin and ROCK inhibitors respectively. However, those inhibitors might also downregulate the basal level of phospho-cofilin, which complicates the interpretation. Zhang and colleagues suggest a role for Phactr4 in the control of directional migration of ENCCs through regulation of

integrin signalling and ROCK-cofilin pathway. How these observations relate to the studies of Phactr1 and Phactr3 remains unclear.

Huet and colleagues examined the effect of Phactr4 expression on phospho-cofilin (Huet et al., 2012). Consistent with previous results that the *humdy* mutation increases phospho-cofilin levels, expression of Phactr4 *humdy* in NIH3T3 cells increased phospho-cofilin level while wild-type Phactr4 expression resulted in decreased phospho-cofilin levels. This effect was abolished by addition of actin monomers in the context of wild-type Phactr4, but not when actin-binding-defective mutant of Phactr4 was expressed. In contrast, depletion of Phactr4 resulted in increased phospho-cofilin levels and the addition of actin monomers to Phactr4-depleted cells had no effect on cofilin phosphorylation. Additionally, the levels of G-actin in cells expressing Phactr4 or an actin-binding-defective mutant of Phactr4 were increased, suggesting that PP1 binding to Phactr4 affects cofilin phosphorylation. Okadaic acid was used to abolish this effect, suggesting that the increase of G-actin level was a result of PP1 activity. To show that G-actin levels in those cells are controlled by cofilin activity, cofilin was then depleted by siRNA and Phactr4 constructs failed to increase actin monomer levels upon this depletion. Lastly, Huet and colleagues showed by quantifying F-actin staining in NIH3T3 cells that expression of wild-type Phactr4 decreases the F-actin signal, while the expression of the *humdy* mutant increases F-actin levels. Huet and colleagues conclude that Phactr4 responds to G-actin binding through RPEL domain to guide PP1 to dephosphorylate cofilin, a crucial actin disassembly factor. Therefore, Phactr4 might be involved in the maintenance of the G-actin pool in the cell.

It is difficult to dissect the role of G-actin and PP1 binding in Phactr4 and Huet and colleagues attempt to address this issue by employing actin-binding-defective and PP1-binding-defective mutants of Phactr4. However, it is still unclear why the authors claim that exogenous expression of the *humdy* mutant in NIH3T3 cells affects cofilin levels. It is conceivable that the endogenous pool of PP1 will not be affected by the ectopic expression of the *humdy* mutant at all. One may hypothesise that this effect is

rather caused by the actin binding ability of the *humdy* mutant and not by the defective PP1 interaction. More biochemical analysis is required to better understand this issue.

### 1.4.6 Implications in human disease

Members of Phactr family were implicated in human diseases through genome-wide association studies (GWAS) focused on analysing links between single-nucleotide polymorphisms (SNPs) and major disorders. Expression level studies and genetic models also suggest potential roles in human diseases. How these disorders relate to Phactr proteins biochemical and cellular functions in general remains unresolved.

Several GWAS reports strongly associate the *Phactr1* gene with myocardial infarction (Kathiresan et al., 2009; Patel et al., 2012). Other studies showed strong association of the *Phactr1* gene and coronary artery disease and coronary artery calcification, an underlying cause of coronary artery disease (Hager et al., 2012; Lu et al., 2012; O'Donnell et al., 2011; Pechlivanis et al., 2013; Qi et al., 2011). These studies show the association of several SNPs in *Phactr1* with myocardial infarction and related disorders, but Phactr1 function in this disease is not discussed. Two GWAS studies describe the association of *Phactr2* with Parkinson's disease (Maraganore et al., 2005; Wider et al., 2009). A recent GWAS study shows that the genetic locus of *Phactr2* gene is associated with DNA repair capacity (DRC), linked to enhanced lung cancer risk (Wang et al., 2013).

DNA fingerprinting analysis of genomic instability in 30 patients with non-small lung cancer suggest that *Phactr3* and two other unrelated genes might play important roles in the genesis of this disease (Bankovic et al., 2010). *Phactr3* was also identified as a novel hyper-methylated gene, showing significant increase in DNA methylation levels in advanced colorectal cancers (Bosch et al., 2012).

Expression studies strongly implicate Phactr1 in melanoma progression (Koh et al., 2009; Trufant, 2010; Wiezlak et al., 2012). Expression studies of Phactr4 in mice

show that it could be involved in neural tube birth defects and in the genesis of Hirschprung disease (Kim et al., 2007; Zhang et al., 2012).

## 1.5 Aims

In this thesis I ask whether Phactr proteins are regulated by G-actin and how. To study a role of the RPEL motifs in Phactr proteins I compare their regulation to the previously established molecular mechanism of the MRTF's nucleocytoplasmic shuttling. I also address a role of PP1 binding to Phactr1 and study a function of Phactr1 in two systems: NIH3T3 fibroblasts and CHL-1 melanoma cells.

# Chapter 2. Materials and Methods

## 2.1 Chemicals and reagents

Chemicals and reagents described in this chapter were obtained from Invitrogen, Sigma or Roche unless stated otherwise. The most commonly used chemicals are listed below. Subsequent sections contain descriptions of all method-specific reagents.

| **Reagent** | **Supplier** |
|---|---|
| 4',6'-diamidino-2-phenylindole (DAPI) | Molecular Probes |
| AEBSF | Sigma |
| Agarose | Invitrogen |
| Ampicillin | Sigma |
| Anti-Flag M1 agarose affinity gel | Sigma |
| Anti-HA-agarose | Sigma |
| ATP (disodium salt) | Sigma |
| Blebbistatin | Sigma |
| Bromophenol Blue | BioRad |
| BSA | Sigma |
| Chloramphenicol | Boehringer Mannheim |
| Complete protease inhibitor cocktail tablets | Roche |

| | |
|---|---|
| Coomassie Brilliant Blue | BioRad |
| Cytochalasin D | Calbiochem |
| Dimethyl sulfoxide (DMSO) | Fisher Scientific |
| Dithiothreitol (DTT) | Calbiochem |
| DMEM | Invitrogen |
| Ethanol | Sigma |
| Ethidium Bromide | Boehringer Mannheim |
| FCS | Invitrogen |
| Fish skin gelatin | Sigma |
| Formaldehyde | Fisher Scientific |
| Glutathione sepharose 4B | GE Healthcare |
| Isopropanol | Sigma |
| Isopropyl-β-D-thiogalactopyranoside (IPTG) | MP Biomedicals |
| Kanamycin | Sigma |
| Latrunculin B | Calbiochem |
| Leptomycin B | Calbiochem |
| LipofectamineTM2000 | Invitrogen |
| Methanol | Sigma |
| Milk powder | Marvel |

| | |
|---|---|
| Nonidet P-40 | Sigma |
| Optimem | Invitrogen |
| PMSF | Sigma |
| Protease inhibitors | Roche |
| PROTRAN transfer membranes | Whatman |
| RPMI | Invitrogen |
| Triton X-100 | Sigma |
| Trizma-base | Sigma |
| Tween 20 | Sigma |
| Xylene cyanol | Biorad |
| Y-27632 | Sigma |
| Y27632 | Calbiochem |
| β-mercaptoethanol | Sigma |

**Table 2.1 General chemicals and reagents.**

## 2.2 General buffers and solutions

The most commonly used buffers are listed below. Specific buffers are described in the relevant chapters. Deionised Milli-Q water was used to prepare all buffers. Where necessary, vacuum-driven filtration system was used (0.2 μm sterile-filter from Milipore).

**Phosphate Buffered Saline A (PBSA)**

137 mM NaCl

2.7 mM KCl

10 mM $Na_2HPO_4$

1.8 mM $KH_2PO_4$ pH 7.4

**Tris-Buffered Saline (TBS)**

50 mM Tris-HCl pH 7.5

150 mM NaCl

**Tris/Borate/EDTA (TBE)**

80 mM Tris base

89 mM Boric acid

2 mM EDTA

**Luria-Bertani (LB) medium**

1% w/v Bacto-tryptone

0.5% w/v Bacto-yeast extract

1% w/v NaCl

**SOC medium**

2% w/v Bacto-tryptone

0.5% w/v Bacto-yeast extract

10 mM NaCl

2.5 mM KCl

10 mM $MgCl_2$

20 mM glucose

**Mowiol**
6 ml glycerol
2.4 g Mowiol (Calbiochem)
12 ml Tris-HCl pH 8.5
add 6 ml water and mix at 50°C, 0.45 µm filter
add 2.5 w/v 1,2-diazabucyclo-[2.2.2]octane (Dabco, Sigma) and store at -20°C

## 2.3 Molecular cloning

### 2.3.1 Bacterial techniques

#### *2.3.1.1 Strains of bacteria*

For all cloning One Shot Top10 *E.coli* chemically competent cells were used (genotype: F- *mcr*A Δ(*mrr-hsd*RMS-*mcr*BC) Φ80*lac*ZΔM15 Δ*lac*X74 *rec*A1 *ara*D139 Δ(*ara leu*) 7697 *gal*U *gal*K *rps*L ($Str^R$) *end*A1 *nup*G; Invitrogen). For protein expression BL 21 (genotype: F- *omp*T *hsd*SB(rB – mB-) *gal dcm* (DE3); Invitrogen) or Rosetta (genotype: F- *omp*T *hsd*SB(rB – mB-) *gal dcm* (DE3) pLysSRARE2 (CamR); Novagen) strains were used.

#### *2.3.1.2 Electrocompetent cells*

For the preparation of electrocompetent bacterial strains, relevant cells were plated on LB agar (LB medium supplemented with 1.5% w/v Bacto-agar) without antibiotics and cultured overnight. On the next day, a single colony was transferred to 50 ml LB and cultured overnight at 37°C and 190 rpm. Subsequently, 10 ml of pre-culture was used to inoculate 1 litre of LB medium and incubated at 37°C and 190 rpm

until OD reached 0.6. The culture was then spun down at 3000 x g for 15 min at 4°C. After spinning, the pellet was resuspended in 1 litre of ice-cold 10% glycerol. The wash was repeated several times, until the volume was reduced to 0.5 litre, 250 ml, 100 ml. Finally, bacteria were resuspended in 2 ml of 10% glycerol, aliquoted, frozen on dry ice and stored at -80°C until use was necessary.

#### *2.3.1.3 Transformation of competent cells*

The transformation of competent bacteria was initiated either through heat shock of electroporation. Transformation by heat shock was performed on chemically competent Top10 cells. 50 µl of Top 10 cells was thawed on ice and incubated with relevant plasmid DNA for 10 minutes. Subsequently, the mix was transferred to a thermoblock, which was heated up to 42°C for 40 seconds. The mix was then incubated on ice for 2 minutes. If the transformation of competent cells with a plasmid encoding ampicillin resistance was performed, bacteria were directly plated on LB agar supplemented with the antibiotic (100 µg/ml). If plasmid contained kanamycin resistance, bacteria were incubated with 500 µl of SOC medium without the antibiotic for 1 hour before plating on LB agar supplemented with kanamycin (30 µg/ml).

Transformation by electroporation was performed using 50 µl of electrocompetent bacteria. Cells were firstly thawed on ice and then incubated with the relevant plasmid DNA for 10 minutes. In order to deliver the electric pulse, the mix was transferred to an electroporation cuvette (0.2 cm gap, Geneflow) and subjected to BioRad Gene pulser, which generated 2.5 kV, capacitance 25 µF and resistance 200 Ω. The bacterial solution was then mixed and cells were seeded on plates. If the transformation of competent cells with a plasmid encoding ampicillin resistance was performed, bacteria were directly plated on LB agar supplemented with the antibiotic (100 µg/ml). If plasmid contained kanamycin resistance, bacteria were incubated with 500 µl of SOC medium without the antibiotic for 1 hour before plating on LB agar supplemented with kanamycin (30 µg/ml).

### 2.3.2 Expression vectors

#### *2.3.2.1 Protein expression in mammalian cells*

All Phactr1, Phactr2, Phactr3 and Phactr4 constructs used in the mammalian cell culture were cloned into pEF-Flag, a plasmid derived from previously described EF.plink vector (Hill and Treisman, 1995); produces an N-terminal FLAG epitope.

Phactr1 cDNA sequence encodes protein of 580 aa, 'phosphatase and actin regulator 1, isoform 4' from *Mus musculus,* NCBI accession number AAY42814.1. This transcript variant encodes an isoform, which differs from the longest transcript variant encoding protein of 649 aa ('phosphatase and actin regulator 1, isoform 1' from *Mus musculus,* NCBI accession number NP_940811.2) by the deletion of aa 222-290 within the non-conserved proline-rich region of the protein. Of all Phactr1 isoforms, isoform 4 from *Mus musculus* is the most similar to the longest Phactr1 isoform from *Homo sapiens* (97.59% similarity). Phactr2 cDNA sequence encodes protein of 626 aa, 'phosphatase and actin regulator 2, isoform A' from *Mus musculus,* NCBI accession number NP_001181994.1. Phactr3 cDNA sequence encodes protein of 558 aa, 'phosphatase and actin regulator 3, isoform 1' from *Mus musculus,* NCBI accession number NP_083082.1. Phactr4 cDNA sequence encodes protein of 694 aa, 'phosphatase and actin regulator 4, isoform 1' from *Mus musculus,* NCBI accession number NP_780515.2. Phactr2, 3 and 4 transcript variants encode their longest isoforms.

To insert Phactr1 cDNA *BamHI* and *SpeI* sites were used. To insert Phactr2 cDNA *EcoRI* and *SpeI* sites were used. Phactr3 and Phactr4 cDNA were inserted using *BamHI* and *XbaI* sites. Relevant cDNA was obtained by PCR with the use of specific primers, described in the sections below.

PP1cα cDNA was inserted into the pEF-HA vector, derived form previously described EF.plink plasmid (Hill et al., 1995) using sites *BamHI* and *XbaI*. Mammalian

expression plasmids for C3 transferase, wild-type actin and R62D actin were previously described (Miralles et al., 2003; Posern et al., 2002). The MLC-GFP plasmid obtained from Eric Sahai was previously described (Wyckoff et al., 2006). MRTF-A plasmid was described previously (Miralles et al., 2003).

#### *2.3.2.2 Protein expression in bacteria*

Phactr1 constructs were expressed in pGEX-6P-2, a bacterial expression vector designed for expressing N-terminally tagged, GST-fusion proteins, containing a PreScission protease site (GE Healthcare). Phactr1 cDNA sequences were inserted between *EcoRI* and *XhoI* sites. PP1cα was expressed from a previously described plasmid containing an N-terminal His-tag (Kelker et al., 2009) (Addgene). Plasmids containing GST-tagged Importinα and Importinβ were previously described (Pawlowski et al., 2010).

### 2.3.3 Purification of plasmid DNA

LB medium (5 ml for a miniprep and 100 ml for a maxiprep) was inoculated with a single bacterial colony grown on an LB agar plate with the relevant antibiotic. The culture was grown overnight at 37°C, shaking with 190 rpm. The isolation of the DNA was performed by the CRUK Equipment Park service (minipreps) or using Plasmid Maxi Kit (Qiagen, maxipereps) according to the manufacturer's instructions. To calculate DNA quantity, a ND-1000 UV/Vis spectrophotometer was used (NanoDrop Technologies) to read DNA absorption at 260 nm. Plasmid DNA was dissolved in deionised Milli-Q water, and stored at -20°C.

### 2.3.4 Polymerase chain reaction

To amplify DNA, standard polymerase chain reaction (PCR) was implemented. Each PCR reaction was performed using appropriate primers, described below. PCR was carried out using KOD Hot Start Polymerase kit (Novagen) using a specific program (see below).

**Reaction components**

10 ng DNA

1.5 µl forward primer (0.3 mM)

1.5 µl reverse primer (0.3 mM)

5 µl 10x PCR buffer

5 µl 25 mM $MgSO_4$

6 µl dNTPs (2mM)

1 µl KOD polymerase

add water up to 50 µl

**PCR program cycles**

1. 95°C for 2 minutes
2. 95°C for 30 seconds
3. 50 - 55°C for 30 seconds
4. 68°C for 0.5-3 minutes, back to step 2., repeat 35 times
5. 68°C for 10 minutes
6. 4°C pause

### 2.3.5 Site directed mutagenesis

#### *2.3.5.1 Substitutions of amino acids*

To substitute single or clusters of amino acids, a 'quick change' technique was implemented. Primers were designed to contain the relevant mutation in the middle, if possible (see below). Total length of primers was 33-37 bp, where at least 13-17 bp were not modified to achieve efficient annealing. PCR was carried out using the *PfuTurbo* DNA polymerase (Agilent Technologies). The reaction components and PCR program used for amino acid substitutions is described below. After the PCR reaction 1 µl of *DpnI* restriction enzyme was added to the mix in order to digest the methylated DNA template and incubated for 2 hours at 37°C. Subsequently, the DNA was precipitated by the addition of 1.25 µl 0.5 M EDTA, 5 µl 3M NaOAc pH 5.2 and 125 µl 96% ethanol. The precipitated DNA was pelleted by centrifugation at 13 000 x g at 4°C for 20 minutes and washed with 175 µl of 70% ethanol, before final centrifugation. The pellet was then dried at 37°C for 20 minutes and re-suspended in 10 µl of deionised Milli-Q water. Before transformation, the DNA solution was chilled on ice for 2 minutes and 5 µl of the mix were added onto competent bacteria. The transformation was carried out as described above and the following day single colonies were harvested for sequence analysis.

**Reaction components – amino acid substitutions**

10 ng DNA

1.5 µl forward primer (0.3 mM)

1.5 µl reverse primer (0.3 mM)

5 µl 10x *PfuTurbo* buffer

6 µl dNTPs (2mM)

1 µl *PfuTurbo* polymerase

add water up to 50 µl

| **PCR program cycles – amino acid substitutions** |
|---|
| 1. 95°C for 30 seconds |
| 2. 95°C for 30 seconds |
| 3. 50 - 55°C for 1 minute |
| 4. 68°C for 6 minutes, back to step 2., repeat 17 times |
| 5. 68°C for 7 minutes |
| 6. 4°C pause |

| *Mutation* | *Primers* |
|---|---|
| **Plasmid pEF-FLAG-Phactr1** | |
| Nx: R147A | Forward: aggaagatttcgatg**GC**gcagagcagagaggag<br>Reverse: ctcctctctgctctgc**GC**catcgaaatcttcct |
| x23: R431A | Forward: catcaaactcagcaac**GCG**ccctctaagcgagagc<br>Reverse: gctctcgcttagaggg**CGC**gttgctgagtttgatg |
| 1x3: R469A | Forward: caggcggctgagccag**GCA**ccaactgcagaggaac<br>Reverse: gttcctctgcagttgg**TGC**ctggctcagccgcctg |
| 12x: R507A | Forward: tcgcaagctcagccaa**GCG**cccacagtggaagaac<br>Reverse: gttcttccactgtggg**CGC**ttggctgagcttgcga |
| R3A:<br>RRR 108-110 AAA | Forward: caccccgcccatc**GC**g**GC**g**GC**gagtaagtttgcc<br>Reverse: ggcaaacttactc**GC**c**GC**c**GC**gatgggcggggtg |
| K3A:<br>KKK 127-129 AAA | Forward: cctggaaatggagg**GC**g**GC**g**GC**aagtgaaaagttcaa<br>Reverse: ttgaacttttcactt**GC**c**GC**c**GC**cctccatttccagg |
| KRE/3A:<br>KRE 493-495 AAA<br>(Cloned by J. Diring) | Forward: gaagaacaggaggag**GC**g**GC**g**GC**aatcaagaggaggc<br>Reverse: gcctcctcttgatt**GC**c**GC**c**GC**ctcctcctgttcttc |

| | |
|---|---|
| KRR/3A:<br>KRR 497-499AAA<br>(Cloned by J. Diring) | Forward: gagaagcgggaaatc**GC**g**GC**g**GC**gctgactcgcaagc<br>Reverse: gcttgcgagtcagc**GC**c**GC**c**GC**gatttcccgcttctc |
| M146A | Forward: gaaaggaagatttcga**GC**aggcagagcagagagga<br>Reverse: tcctctctgctctgcct**GC**tcgaaatcttcctttc |
| E152A | Forward: ggcagagcagagagg**C**gctgatcaagagaggggtc<br>Reverse: gacccctctcttgatcagc**G**cctctctgctctgcc |
| R156A | Forward: agaggagctgatcaag**GC**aggggtcttgaaggaga<br>Reverse: tctccttcaagacccct**GC**cttgatcagctcctct |
| G157N | Forward: ggagctgatcaagaga**AAC**gtcttgaaggagatct<br>Reverse: agatctccttcaagac**GTT**tctcttgatcagctcc |
| G157H | Forward: ggagctgatcaagaga**CAC**gtcttgaaggagatct<br>Reverse: agatctccttcaagac**GTG**tctcttgatcagctcc |
| **Plasmid pGEX-6P-2** | |
| Phactr1 (414-528)<br>R431A | Forward: catcaaactcagcaac**GCG**ccctctaagcgagagc<br>Reverse: gctctcgcttagaggg**CGC**gttgctgagtttgatg |
| Phactr1 (414-528)<br>R469A | Forward: caggcggctgagccag**GCA**ccaactgcagaggaac<br>Reverse: gttcctctgcagttgg**TGC**ctggctcagccgcctg |
| Phactr1 (414-528)<br>R507A | Forward: tcgcaagctcagccaa**GCG**cccacagtggaagaac<br>Reverse: gttcttccactgtggg**CGC**ttggctgagcttgcga |
| Phactr1 (414-528)<br>E436A/K440A | Forward: ctctaagcgag**C**gctagaagaa**GC**gaacatcctcc<br>Reverse: ggaggatgttc**GC**ttcttctagc**G**ctcgcttagag |

| | |
|---|---|
| Phactr1 (414-528)<br>E474A/R478A | Forward: caactgcagagg**C**actggaacag**GC**gaacattttgaa<br>Reverse: ttcaaaatgttc**GC**ctgttccagt**G**cctctgcagttg |
| Phactr1 N171 (1-171)<br>stop codon introduced<br>(Cloned by J. Diring) | Forward: gagaactctctatat**G**a**T**aatgaagatgactcc<br>Reverse: ggagtcatcttcatt**A**t**C**atatagagagttctc |

**Table 2.2 Site-directed mutagenesis – primers designed for amino acid substitutions.**

### *2.3.5.2 Deletions of DNA fragments*

In order to delete desired fragments of DNA from plasmids, we used *Phusion Hot Start* high fidelity DNA polymerase (Finnzymes). 21 bp-long primers engineered for DNA deletions were 5'-phosphorylated and flanked the deletion (sequences are listed below). The PCR reaction components and PCR reaction cycles are summarised below. After the PCR reaction 1 µl of *DpnI* restriction enzyme was added to the mix in order to digest the methylated DNA template and incubated for 2 hours at 37°C. Subsequently, 5µl of the digestion reaction was mixed with Quick Ligation buffer and 0.5 µl of Quick T4 DNA ligase (New England Biolabs). The ligation reaction was carried out at room temperature for 20 minutes. Before transformation, the ligation mix was chilled on ice for 2 minutes and 5 µl of the mix were added onto competent bacteria. The transformation was carried out as described above and the following day single colonies were harvested for sequence analysis.

**Reaction components – DNA fragment deletions**

10 ng DNA

2.5 µl forward primer (0.3 mM)

2.5 µl reverse primer (0.3 mM)

10 µl 5x *Phusion Hot Start* buffer

1 µl dNTPs (2 mM)

0.5 µl *Phusion Hot Start* polymerase

add water up to 50 µl

**PCR program cycles – DNA fragment deletions**

1. 95°C for 30 seconds
2. 95°C for 15 seconds
3. 55°C for 30 seconds
4. 72°C for 4 minutes, back to step 2., repeat 25 times
5. 72°C for 5 minutes
6. 4°C pause

| *Deletion* | *Primers* |
|---|---|
| **Plasmid pEF-FLAG-Phactr1** | |
| ΔN: Δ139-159 | Forward: `tgctgacgtgtgcttgaactt`<br>Reverse: `aaggagatctacgataaagat` |
| Δm: Δ171-413 | Forward: `ctggccatgaaggtgtgcagg`<br>Reverse: `agagagttctccatctttatc` |
| ΔRPEL123: Δ414-522 | Forward: `agtgactacgtggaagtggca`<br>Reverse: `tgagctggtgtacaaagaggc` |

| | |
|---|---|
| ΔC: Δ529-580 | Forward: `taaactagtctagaaattcac`<br>Reverse: `cacttccacgtagtcactgaa` |
| ΔB1: Δ108-129 | Forward: `agtgaaaagttcaagcacacg`<br>Reverse: `gatgggcggggtgtgcgtacc` |
| **Plasmid pGEX-6P-2 –Phactr1** | |
| Phactr1 392C (Δ2-392) | Forward: `ggccgggaggaggaggaagag`<br>Reverse: `catggatcccaggggcccctg` |

**Table 2.3 Site-directed mutagenesis – primers designed for DNA fragments deletions.**

#### *2.3.5.3 Insertions of DNA fragments*

Standard molecular cloning techniques were used for inserting DNA fragments into desired vectors. Fragments were firstly amplified using a PCR program described in the section "Polymerase chain reaction". Digestion with relevant restriction enzymes was performed according to the manufacturers instructions (New England Biolabs). To prevent re-ligation of vectors by removal of 5' phosphate groups, calf intestinal phosphatase (CIP, NEB) was included to reaction mix. Subsequently, DNA was separated with agarose gel electrophoresis and purified with MinElute PCR Purification Kit or MinElute Gel Extraction Kit (Qiagen). Ligation of DNA fragments was performed using T4 DNA ligase (New England Biolabs) according to the manufacturer's instructions at 16°C overnight. Before transformation, the ligation mix was chilled on ice for 2 minutes and 5 µl of the mix were added onto competent bacteria. The transformation was carried out as described above and the following day single colonies were harvested for sequence analysis.

| *Construct description* | *Primers* |
|---|---|
| **pEF-FLAG constructs** | |
| Phactr1 (1-580) cloned with *BamHI* and *SpeI* | Forward: gcg**GGATCC**atggattatcccaaaatggat<br>Reverse: gcg**ACTAGT**ttaaggtcgatgaaacctggt |
| Phactr2 (1-626) cloned with *EcoRI* and *SpeI* | Forward: gcta**GAATTC**atgggccagacctcggtgtcc<br>Reverse: gcta**ACTAGT**ttatggacgatgaaaccttgt |
| Phactr3 (1-558) cloned with *BamHI* and *XbaI* | Forward: gcta**GGATCC**atggccgcatccgaggacggc<br>Reverse: gcta**TCTAGA**ctatggcctgtggaatcttgt |
| Phactr4 (1-694) cloned with *BamHI* and *XbaI* | Forward: gcta**GGATCC**atggaagacccatcggaagaa<br>Reverse: gcta**TCTAGA**tcatgggcgatggtagcgtgt |
| **pEF-HA construct** | |
| PP1cα cloned with *BamHI* and *XbaI* | Forward: ggcc**GGATCC**gacagcgagaagctcaac<br>Reverse: ggcc**TCTAGA**ctatttcttggctttggcaga |
| **pGEX-6P-2 construct** | |
| Phactr1 (414-528) cloned with *BamHI* and *XhoI* | Forward: tat**GGATCC**ctggccatgaaggtgtgcagg<br>Reverse: tat**CTCGAG**ttacacttccacgtagtcactgaa |

**Table 2.4 Primers designed through standard DNA insertions.**

#### *2.3.5.4 Sequences generated through consecutive cloning steps*

Some sequences were obtained through multiplication of the techniques described above or through their combination. All constructs derived this way (listed below) were always sequenced before introducing a new substitution of deletion.

| *Construct description* | *Obtained through consecutive substitutions or/and deletions* |
|---|---|
| **pEF-FLAG-Phactr1 constructs** | |
| xxx | R431A, R469A, R507A |
| x2x | R431A, R507A |
| xx3 | R431A, R469A |
| 1xx | R469A, R507A |
| xx23 | R147A*, R431A |
| x1x3 | R147A*, R469A |
| x12x | R147A*, R507A |
| xxxΔC | R431A, R469A, R507A, Δ529-580 |
| R3A,K3A | RRR 108-110 AAA, KKK 127-129 AAA |
| xxx K3A | R431A, R469A, R507A, KKK127-129AAA |

| | |
|---|---|
| xxx K3A KRE/3A | R431A, R469A, R507A, KKK127-129AAA, KRE493-495AAA |
| **pGEX-6P-2 Phactr1 constructs** | |
| E436A/K440A, E474A/R478A | Substitutions: E436A/K440A, E474A/R478A in pGEX-6P-2 Phactr1(414-528) |
| E436A/K440A, E474A/R478A R469A | Substitutions: E436A/K440A, E474A/R478A, R469A in pGEX-6P-2 Phactr1(414-528) |

**Table 2.5 Mutants generated through consecutive cloning steps.**
(*) Substitution performed by J. Diring.

#### *2.3.5.5 Generation of chimeric constructs*

In order to generate 'MRTF-A-Phactr1 RPEL domain' construct, I combined standard cloning methods and overlap extension technique (Bryksin and Matsumura, 2010). This technique allows cloning an insert of choice into a destination of choice without restriction endonucleases or DNA ligase. Overlap extension involves the design of chimeric primers containing the destination sequence at the 5' ends and the insert sequence at the 3'ends. To substitute the RPEL domain from MRTF-A into the RPEL domain from Phactr1 I generated a chimeric fragment using overlap extension technique and inserted it into pEF-HA-MRTF-A plasmid with *BamHI* sites (using one internal *BamHI* site in MRTF-A cDNA sequence at position $777^{bp}$). To obtain chimeric fragment, six consecutive PCR reactions were performed, using standard PCR program described in section 'Polymerase chain reaction'. Cloning steps are summarised in a table below.

| *PCR* | *Primer sequence and reaction description* |
|---|---|
| I. | PCR using pEF - MRTF-A as a template<br><br>*BamHI*<br>Forward `tat`*`ggatcc`*`CCCCCTTCCGTCATTGCTGTG`<br>Reverse `CCTGCACACCTTCATGGCCAG ATTGGGGTTCCTCCCAGGATG`<br>*Phactr1RPEL* *MRTF-A (2-63)*<br><br>Generates fragment of 207bp including 21 bp extension (MRTF-A 2-62) |
| II. | PCR using pEF - Phactr1 as a template<br><br>*MRTF-A (2-63)* *Phactr1RPEL*<br>Forward `CATCCTGGGAGGAACCCCAAT CTGGCCATGAAGGTGTGCAGG`<br>Reverse `ATTTACCTGGCCCACAATGAT CACTTCCACGTAGTCACTGAA`<br>*MRTF-A (191-260)* *Phactr1RPEL*<br><br>Generates fragment of 387 bp including 2x21 bp extension (Phactr1 RPEL domain) |
| III. | PCR using pEF - MRTF-A as a template<br><br>*Phactr1RPEL* *MRTF-A (191-260)*<br>Forward `TTCAGTGACTACGTGGAAGTG ATCATTGTGGGCCAGGTAAAT`<br>Reverse `CTCTCCA`*`ggatcc`*`GGAGCCATTGGGAG`<br>*BamHI*<br><br>Generates fragment of 231 bp including 21 bp extension (MRTF-A 191-260) |
| IV. | PCR using products of PCR I and II as a template<br><br>*BamHI*<br>Forward `tat`*`ggatcc`*`CCCCCTTCCGTCATTGCTGTG`<br>Reverse `ATTTACCTGGCCCACAATGAT CACTTCCACGTAGTCACTGAA`<br>*MRTF-A (191-260)* *Phactr1RPEL*<br><br>Generates intermediate fragment of 552 bp |

| | |
|---|---|
| V. | PCR using products of PCR II and III as a template<br><br>*MRTF-A (2-63)* *Phactr1RPEL*<br>Forward CATCCTGGGAGGAACCCCAAT CTGGCCATGAAGGTGTGCAGG<br>Reverse CTCTCCA*ggatcc*GGAGCCATTGGGAG<br>*BamHI*<br><br>Generates intermediate fragment of 576 bp |
| VI. | PCR using products of PCR IV and V as a template<br><br>*BamHI*<br>Forward tat*ggatcc*CCCCCTTCCGTCATTGCTGTG<br>Reverse CTCTCCA*ggatcc*GGAGCCATTGGGAG<br>*BamHI*<br><br>Generates final chimeric fragment of 741 bp |

**Table 2.6 Generation of chimeric fragment for 'MRTF-A-Phactr1 RPEL domain' cloning.**

In order to generate 'MRTF-A-RPEL 3-Phactr1' construct, I used 'quick-change' technique using primers listed below. Magaprimer generated in Step I was used to replace DNA sequence encoding RPEL3 in MRTF-A into DNA sequence encoding RPEL3 from Phactr1.

| *PCR* | *Primer sequence and reaction description* |
|---|---|
| Megaprimer generation (Step I) | **Reaction components**<br>2 µl forward primer (10 mM)<br>2 µl reverse primer (10 mM)<br><br>Forward<br>AAGAGAGCCAGGCTGGCTagaagacttacccgtaagctcagc caacgtcccacagttgaa<br>Reverse<br>CAGGCTGGACTCCACAGGtaagatcttcctctcccggagttc ttcaactgtgggacgttggct<br><br>**PCR program cycles**<br>1. 95°C for 60 seconds (denaturation)<br>2. 60°C for 60 seconds (annealing)<br>3. 72°C for 30 seconds (extension) |
| MRTF-A-RPEL 3-Phactr1 chimera generation (Step II) | Standard PCR using pEF - MRTF-A as a template and megaprimer generated in step I followed by a Dpn1 digestion (for chimeric sequence see Figure 7.3). |

**Table 2.7 Generation of 'MRTF-A- RPEL3-Phactr1 chimera.**

### 2.3.6 DNA Sequencing

All constructs generated in the presented above sections were confirmed by DNA sequencing. 20 µl or sequencing reactions contained 150-200 ng of plasmid DNA, 3.2 pmol of the relevant sequencing primer, 8 µl of dirhodamine BigDye Terminator mix (BDT v3.1, Applied Biosystems) and deionised Milli-Q water. The PCR program cycles are described below. Subsequently, the DNA was precipitated by the addition of 1.25 µl 0.5 M EDTA, 5 µl 3M NaOAc pH 5.2 and 125 µl 96% ethanol. The precipitated DNA was pelleted by centrifugation at 13 000 x g at 4°C for 20 minutes and washed

with 175 µl of 70% ethanol before final centrifugation. The pellet was then dried at 37°C for 20 minutes and resuspended in deionised Milli-Q water. The sequences were analysed by sequencing service in Cancer Research UK Equipment Park.

**PCR program cycles – DNA sequencing**

1. 96°C for 5 minutes
2. 96°C for 30 seconds
3. 50°C for 15 seconds
4. 72°C for 4 minutes, back to phase 2., repeat 25 times
5. 4°C pause

### 2.3.7 Agarose gel electrophoresis

Where necessary, DNA fragments were separated by electrophoresis for analysis or purification purposes. Agarose gel was prepared with 1-2% w/v agarose in TBE buffer. The solution was heated up until agarose dissolved completely. Subsequently, ethidium bromide was added to the solution (0.5 µg/ml). Loading buffer (30% glycerol, 0.25% bromophenol blue, 0.25% xylene cyanol FF) was added to the DNA samples before loading onto the gel. Agarose gels were run in TBE buffer at 100V until the desired separation of DNA fragments was obtained. For separation analysis, 100bp or 1kb DNA ladders (New England Biolabs) were used. DNA was visualised with a UV transilluminator.

## 2.4 Oligonucleotides

Sigma Genosys performed synthesis of primers listed in the sections above. Lyophilised oligonucleotides were dissolved in deionised Milli-Q water. The final concentration of oligonucleotides was adjusted to 100 µM and they were stored at -20°C.

Depletion of Phactr1 was performed using Phactr1 siRNA ON-TARGETplus SMARTpool purchased from Dharmacon (sequences blow). siRNA was dissolved in siRNA buffer (Dharmacon) to final concentration of 75 μM. Depletion was performed with 20nM siRNA. Depletion of Importin β was performed using Importin β siRNA ON-TARGET SMARTpool (Dharmcon). For negative controls, AllStars siRNA was used (Qiagen).

| **Gene** | **Target siRNA sequence** | **Cat No. (Dharmacon)** |
|---|---|---|
| PHACTR1 | 5'-ccacauuaauggcggcauc-3' | J-025063-17 |
| | 5'-gcagaaugauagacgagcu-3' | J-025063-18 |
| | 5'-agaggaggcuaacccgaaa-3' | J-025063-19 |
| | 5'-acaaagcugccauccgaaa-3' | J-025063-20 |
| KPNB1 (Importin β) | 5'-ggaggagccuaguaacaau-3' | J-058740-05 |
| | 5'-gguuacauuugccaagaua-3' | J-058740-06 |
| | 5'-ucacacagacacugacuaa-3' | J-058740-07 |
| | 5'-ggauagaguucugguccaa-3' | J-058740-08 |

**Table 2.8 si-RNA sequences.**

## 2.5 Peptides

All peptides and N-terminally FAM (fluorescein maleimide)-conjugated peptides used in this study were synthesised and HPLC (high-performance liquid chromatography)-purified by Protein and Peptide Chemistry Laboratory in Cancer Research UK (sequences below). Synthesis was accomplished by coupling the 5-carboxylic acid group of 5-carboxy fluorescein maleimide (5-FAM) to the N-terminus of the protected peptide. Peptides were obtained in lyophilised form and stored in -20°C. When required, lyophilised FAM-conjugated peptides were dissolved in peptide stock buffer (see below) and centrifuged. Peptide solutions were kept in -80°C.

| **Peptide stock buffer** |
|---|
| 20 mM Tris-HCl pH 8.0 |
| 100 mM NaCl |
| 3 mM $MgCl_2$ |
| 0.2 mM EGTA |
| 0.7mM ATP |
| 2 mM DTT |

| *Peptide name* | *Peptide sequence* |
|---|---|
| **FAM-conjugated peptides for Fluorescence Polarisation assays** | |
| Phactr1 RPEL-N | FKHTSAALERKISMRQSREELIKRGVLKEIYD |
| Phactr1 RPEL1 | KVCRKDSLAIKLSNRPSKRELEEKNILPRQTD |
| Phactr1 RPEL2 | RQQIGTKLTRRLSQRPTAEELEQRNILKPRNE |
| Phactr1 RPEL3 | KREIKRRLTRKLSQRPTVEELRERKILIRFSD |

| | |
|---|---|
| Phactr1 RPEL-Nx | FKHTSAALERKISM**A**QSREELIKRGVLKEIYD |
| Phactr1 RPEL1x | KVCRKDSLAIKLSN**A**PSKRELEEKNILPRQTD |
| Phactr1 RPEL2x | RQQIGTKLTRRLSQ**A**PTAEELEQRNILKPRNE |
| Phactr1 RPEL3x | KREIKRRLTRKLSQ**A**PTVEELRERKILIRFSD |
| Phactr1 RPEL-N F133A | **A**KHTSAALERKISMRQSREELIKRGVLKEIYD |
| Phactr1 RPEL-N E141A | FKHTSAAL**A**RKISMRQSREELIKRGVLKEIYD |
| Phactr1 RPEL2 G459K | RQQI**K**TKLTRRLSQRPTAEELEQRNILKPRNE |
| Phactr1 RPEL3 I496A | KRE**A**KRRLTRKLSQRPTVEELRERKILIRFSD |
| Phactr1 RPEL3 R516A | KREIKRRLTRKLSQRPTVEELRE**A**KILIRFSD |
| Phactr1 RPEL1 E436A | KVCRKDSLAIKLSNRPSKR**A**LEEKNILPRQTD |
| Phactr1 RPEL2 E474A | RQQIGTKLTRRLSQRPTAE**A**LEQRNILKPRNE |
| Phactr1 RPEL3 E512A | KREIKRRLTRKLSQRPTVE**A**LRERKILIRFSD |
| Phactr1 RPEL1 E436A/K440A | KVCRKDSLAIKLSNRPSKR**A**LEE**A**NILPRQTD |
| Phactr1 RPEL2 E474A/R478A | RQQIGTKLTRRLSQRPTAE**A**LEQ**A**NILKPRNE |
| Phactr1 RPEL3 E512A/R507A | KREIKRRLTRKLSQRPTVE**A**LRE**A**KILIRFSD |

| | |
|---|---|
| Phactr1 RPEL-N M146A | FKHTSAALERKIS**A**RQSREELIKRGVLKEIYD |
| Phactr1 RPEL-N E152A | FKHTSAALERKISMRQSRE**A**LIKRGVLKEIYD |
| Phactr1 RPEL-N R156A | FKHTSAALERKISMRQSREELIK**A**GVLKEIYD |
| Phactr1 RPEL-N G157N | FKHTSAALERKISMRQSREELIKR**N**VLKEIYD |
| Phactr1 RPEL-N G157H | FKHTSAALERKISMRQSREELIKR**H**VLKEIYD |
| Phactr2 RPEL-N | FRETSAVLERKISTRQSREELIRRGLLKELPD |
| Phactr2 RPEL1 | KIRRRDTLAIKLGNRPSKKELEDKNILQRTSE |
| Phactr2 RPEL2 | RQQIGTKLVRRLSQRPTTEELEQRNILKQKNE |
| Phactr2 RPEL3 | KMELKRRLSRKLSLRPTVAELQARRILRFNEY |
| Phactr3 RPEL-N | LKQTTSALEKKMAGRQGREELIKQGLLEMMEQ |
| Phactr3 RPEL1 | RKCKKELLAVKLRNRPSKQELEDRNIFPRRTD |
| Phactr3 RPEL2 | RQQIEMKLSKRLSQRPAVEELERRNILKQRND |
| Phactr3 RPEL3 | RREIKQRLTRKLNQRPTVDELRDRKILIRFSD |
| Phactr4 RPEL-N | FKETSEVLERKISMRKPREELVKRGVLLEDPE |
| Phactr4 RPEL1 | RVKRKDTLAMKLSSRPSEPETNLNSWPRKSKE |

| | |
|---|---|
| Phactr4 RPEL3 | RHQIGNTLIRRLSQRPTAEELEQRNILQPKNE |
| Phactr4 RPEL4 | KREIKRRLTRKLSQRPTVAELLARKILRFNEY |
| Chimeric peptide A1<br>**MRTF-A**-Phactr1 | **RARL**KRRLTRKLSQRPTVEELRERKIL**PVESS** |
| Chimeric peptide B1<br>**MRTF-A**-Phactr1 | **RARLA**RRLTRKLSQRPTVEELRERKIL**PVESS** |
| Chimeric peptide C1<br>**MRTF-A**-Phactr1 | **RARLAD**RLTRKLSQRPTVEELRERKIL**PVESS** |
| Chimeric peptide A<br>**MRTF-A**-Phactr1 | **RARL**KRRLTRKLSQRPTVEELRERKILIRFSD |
| Chimeric peptide B<br>**MRTF-A**-Phactr1 | **RARLA**RRLTRKLSQRPTVEELRERKILIRFSD |
| Chimeric peptide C<br>**MRTF-A**-Phactr1 | **RARLAD**RLTRKLSQRPTVEELRERKILIRFSD |
| **Peptides for Crystallisation** | |
| Phactr1 RPEL-N | FKHTSAALERKISMRQSREELIKRGVLKEIYD |
| Phactr1 RPEL1 | KVCRKDSLAIKLSNRPSKRELEEKNILPRQTD |
| Phactr1 RPEL2 | RQQIGTKLTRRLSQRPTAEELEQRNILKPRNE |
| Phactr1 RPEL3 | KREIKRRLTRKLSQRPTVEELRERKILIRFSD |

**Table 2.9 Peptides used in the study.**

## 2.6 Mammalian cell culture

### 2.6.1 Cell culture maintenance

Mammalian cell lines used in this study are summarised below. All cell lines were maintained in 15cm$^2$ cell culture dishes. Cell lines were cultured in DMEM or RPMI (Invitrogen) supplemented with 10% foetal calf serum (FCS) (Invitrogen) and Pen/Strep (100 units/ml penicillin, 100 µg/ml streptomycin from 100x stock) (Cancer Research UK media production facility) at 37°C in incubators, supplemented with 10% $CO_2$ (Wolf Laboratories).

Once thawed, cells were grown until confluent and either sub-cultured for propagation or seeded for relevant experiment. For sub-culturing, cells were washed with PBS, incubated with trypsin/Versene (0.25% (w/v) trypsin in 5x Versene) (Cancer Research UK media production facility) until they detached (around 3 min.) and suspended in relevant FCS-supplemented media (typical sub-culturing ratio was 1:10 – 1:15). Cells suspension was then distributed into new cell culture dishes. For starvation, cells were kept in relevant cell culture media supplemented with 0.3% FCS overnight.

| Cell line | Species | Media |
|---|---|---|
| NIH3T3 fibroblasts | Mouse | DMEM |
| MDA-MB-231 breast carcinoma | Human | DMEM |
| CHL-1 melanoma | Human | RPMI |

**Table 2.10 Cell lines used in the study.**

In order to freeze cells in liquid nitrogen, cells were incubated with trypsin/Versene solution as described above, re-suspended in culture media and centrifuged at 120g for 5 min. at room temperature. The cell pellet was re-suspended in FCS supplemented with 5% DMSO and aliquoted into cryo-vials (typically one 10cm$^2$

dish into one cryo-vial) and transferred into -80°C. One week later cells were transferred into liquid nitrogen for a long-term storage.

### 2.6.2 Transfection

#### *2.6.2.1 Transient transfection with plasmid DNA*

The method of transfection with plasmid DNA varied depending on the experimental format (see below). Cells were firstly sub-cultured into desired size cell culture dishes and grown until 80% confluent. The next day cells were either starved with 0.3% FCS or transfection with plasmid DNA was initiated. Cells were transfected with Lipofectamine2000 (Invitrogen) according to manufacturer's instructions. Plasmid DNA was added to the indicated volume of Opti-MEM (Invitrogen) and Lipofectamine was suspended in the same volume of Opti-MEM (see below for specific volumes). DNA/Opti-MEM and Lipofectamine2000/Opti-MEM solutions were incubated separately for 5 min., then mixed together by vortexing and incubated at room temperature for 30 min. Prior to transfection, cells were washed with Opti-MEM and indicated volumes of the transfection mix were added onto the cells. Cells were incubated with the transfection mix and indicated volumes of Opti-MEM for 2h. Afterwards, the transfection mix was removed by vacuum pump and relevant media was added onto the cells. Cells were normally grown overnight before proceeding to relevant experiment.

| **Format** | **Total amount of DNA** | **Vol. Lipofectamine 2000** | **Vol. Opti-MEM in transf. mix** | **Vol. Opti-MEM on cells** |
|---|---|---|---|---|
| *Immunofluorescence microscopy* | | | | |
| 6-well plates | 1 µg | 3µl | 200µl | 1ml |

| *Co-immunoprecipitation* | | | | |
|---|---|---|---|---|
| 10-cm dishes | 4 μg | 17μl | 1ml | 4ml |

**Table 2.11 Amounts of reagents required for transient transfection with plasmid DNA.**

### *2.6.2.2 Transfection with siRNA*

Transfection with siRNA was performed in order to deplete Phactr1 in CHL-1 cells. Transfection volumes were adjusted according to the format of relevant experiment (see below). Transfections were carried out using Lipofectamine RNAiMAX reagent (Invitrogen) according to manufacturer's instructions protocol for reverse transfection. Cells were washed with PBS, incubated with trypsin/Versene until they detached (as described above) and suspended in FCS-supplemented RPMI media. siRNA (from 20μM stock) was added to the indicated volume of Opti-MEM (Invitrogen) and Lipofectamine RNAiMAX was suspended in the same volume of Opti-MEM (see below for specific volumes). siRNA/ Opti-MEM and Lipofectamine RNAiMAX/ Opti-MEM solutions were incubated separately for 5 min., then mixed together by vortexing and incubated at room temperature for 20 min. The transfection mix was re-suspended in the media containing cells (volumes indicated below) in the well and mixed by gentle manual shaking. To obtain efficient knock-down, cells were grown for 72h without change of media.

| Format | siRNA (from 20 µM) | Vol. Lipofectamine RNAiMAX | Vol. Opti-MEM in transf. mix | Vol. cells |
|---|---|---|---|---|
| *Western blotting/ Immunofluorescence/ Matrigel invasion assays* | | | | |
| 6-well plates ($10^4$ cells/well) | 2.4 µl | 4µl | 200µl | 2.2ml |
| *Scratch-wound assays* | | | | |
| 96-well plate (5000 cells/well) | 0.1 µl | 0.16µl | 20µl | 80µl |

**Table 2.12 Amounts of reagents required for transient transfection with siRNA**

### 2.6.3 Scratch-wound assays

#### *2.6.3.1 Evaluation of wound closure*

In order to investigate cell motility defects in Phactr1-depleted CHL-1 melanoma cells, scratch-wound assays were performed using IncuCyte Live-Cell Imaging System (Essen BioScience). 5000 cells per well was seeded in 96-well Essen ImageLock plates (Essen BioScience). Cells transfected with relevant siRNA were grown in media supplemented with 10% FCS were transfected with siRNA (see above for siRNA transfection details). 72 hours post-transfection, confluent cells were scratch-wounded using Woundmaker 96 (Essen BioScience) according to manufacturer's instructions. Cell migration in the wound was monitored using IncuCyte (Essen BioScience) video microscope residing inside 37°C tissue culture incubator (LEEC) every 30 min for 45 hours after the scratch was applied.

#### *2.6.3.2 Cell tracking*

Cells at the leading edge of the wound were tracked using Tracker software, designed by Daniel Zicha in London Research Institute. To visualise tracks, each cell was tracked over the recording time and tracks were plotted on the graph. Mean speeds were calculated over the recording time for each cell. Persistence was measured during successive 50-minute windows for each cell. To evaluate the speed and persistence of cell migration, a previously described algorithm was implemented in Mathematica software (Wolfram Research), with ANOVA (analysis of variance) analysis (Medjkane et al., 2009). ANOVA provides a statistical test of whether or not the means of several groups are all equal, and therefore generalizes t-test to more than two groups. Here, only two groups are analysed, therefore the implemented test is equivalent to a t-test.

### 2.6.4 Matrigel invasion assays

Matrigel invasion assays were performed in collaboration with Cell Motility Laboratory at London Research Institute (Cancer Research UK) by Jasmine Abella.

After siRNA transfection (see above for siRNA transfection details) cells were transferred to duplicate wells (2 x$10^4$ cells/well) of a BD Matrigel Invasion Chamber (24-well plate, 8.0 micron; BD biosciences) is serum free medium. Cells were allowed to migrate through the matrigel-coated filter towards the medium for 22 hours at 37°C. Afterwards, cells on both sides of the wells were fixed for 20 min with 4% paraformaldehyde (Sigma) in PBS, then stained with Phalloidin Alexa-488 (Invitrogen) and DAPI for 1 hour. Cells, which had migrated through the filter were visualised by microscopy and imaged using a LSM 510 Zeiss confocal microscope (20x lens, 16 images per well). Invasion of Phactr1 depleted cells was assessed by evaluating the DAPI staining of cells that migrated through the filter and compared to the invasion of control cells. Subsequently, the evaluated percentage of invasion/control cells was plotted on the graph and analysed using two unpaired t-tests. The unpaired t-test tests

the hypothesis that the population means related to two independent, random samples from an approximately normal distribution are equal (Armitage P, 1994).

## 2.7 Immunofluorescence microscopy

For immunofluorescence, relevant cells were grown in 6-well plates containing coverslips (2 coverslips per well) until they were 80% confluent. If starvation was required, 10% FCS/media was replaced with 0.3% FCS/media and cells were starved overnight. If required, cells were transfected with plasmid DNA or with siRNA (see above for transfection details). The following day cells were treated with specific inhibitors for indicated times (30 nM leptomycin B, 1 μM latrunculin B, 10 μM Y27632, 10 μM cytochalasin D or 20 μM blebbistatin) and/or stimulated with 15% FCS for appropriate time. Afterwards, cells were fixed with 4% formaldehyde in PBS for 15 minutes and washed with PBS. Fixed cells were stored at 4°C for up to 7 days, if necessary. After fixation, cells were permeabilised with 0.2% TritonX-100 in PBS for 10 minutes at room temperature. Non-specific binding sites were then blocked with blocking solution (10%FCS, 1% fish skin gelatin in PBS) for 1 hour. Staining with primary antibodies (listed below) was performed by placing coverslips (cell-side down) on a 50 μl drop of blocking solution with an antibody (for specific dilutions see below). Staining was performed at room temperature for 1h on Parafilm (Pechiney), in closed plastic dishes containing moist wipers (Wypall) to prevent samples from drying out. To wash cells, coverslips were dipped in PBS twice. Staining with secondary antibodies was performed in blocking solution for 1h using the same technique. If staining with phalloidin and DAPI was required, they were added to the secondary antibody solution. Next, cells were washed in PBS and water and mounted on microscopy slides using Mowiol. Slides were kept in the dark until analysed by microscopy.

In order to investigate Phactr1 localisation in either NIH3T3 cells of CHL-1 cells, Zeiss Axioplan 2 microscope (Plan-NEOFLUAR 40x/1.3 Oil or 63x/1.25 Oil lenses) equipped with a digital camera (Hamamatsu) was used. Imaging was carried out using Smart Capture software. Localisation of Phactr1 was scored as nuclear, pan-cellular or

cytoplasmic using specific antibodies (listed below) in indicated number of cells per experiment.

Images of Phactr1-depleted /control CHL-1 cells were collected using a Zeiss Axioplan 2 microscope (Apochromat 63x/1.40 NA Oil or Plan-NEOFLUAR 25x lenses) controlled by Metamorph (Molecular Devices Corporation) using a monochromatic CoolSNAP HQ camera (Photometrics).

| **Primary antibodies** | | |
|---|---|---|
| *antibody* | *species* | *concentration* |
| Flag (F7425, Sigma) | rabbit | 1:500 |
| c-Myc (9E10, Abcam) | mouse | 1:500 |
| Phactr1 (HPA029756, Sigma) | rabbit | 1:200 |
| PP1α (C-19, Santa Cruz) | goat | 1:200 |
| Paxilin (BD Bioscience) | mouse | 1:200 |

| **Secondary antibodies** | | |
|---|---|---|
| *antibody* | *species* | *concentration* |
| Rabbit Cy3 (Molecular Probes) | donkey | 1:500 |
| Mouse Cy3 (Molecular Probes) | donkey | 1:500 |
| Rabbit Cy2 (Molecular Probes) | donkey | 1:200 |
| Rabbit Alexa Fluor 350 (Molecular Probes) | donkey | 1:200 |
| Goat Cy2 (Jackson Laboratories) | donkey | 1:200 |

| **Staining reagents** |
|---|

| *reagent* | *specificity* | *concentration* |
|---|---|---|
| FITC-Phalloidin (Molecular Probes) | F-actin | 1:200 |
| Texas Red -Phalloidin (Molecular Probes) | F-actin | 1:200 |
| DAPI (Molecular Probes) | DNA | 300nM |

**Table 2.13 Antibodies and staining reagents used for immunofluorescence microscopy.**

## 2.8 Fluorescence polarisation assays

Fluorescence anisotropy assays were performed essentially as described previously (Guettler et al., 2008; Mouilleron et al., 2008). The reactions were set up at room temperature in a total volume of 75µl in 96-well plates and incubated for 2h in FP binding buffer (see below). FAM-conjugated peptides (for sequences see section "Peptides") were used at a concentration of 0.5 µM. LatB-actin was added at a concentration range of 1nM up to 60 µM. The preparation of LatB-actin was described previously (Mouilleron et al., 2008). In order to perform readouts, reactions were transferred into 384-well flat-bottom plates with a non-binding surface (3654, Corning) and Safire2 microplate reader was used (Tecan). Magellan software was used to read anisotropies. Dissociation constants ($K_D$) were calculated by nonlinear regression in Prism software using the equation: $Y=((A_b-A_f)*(X/(K_D+X))) +A_f$, where X is protein concentration; Y is total anisotropy; $A_b$ is anisotropy from bound ligand; $A_f$ is anisotropy from free ligand (Heyduk and Lee, 1990). $K_D$ values were derived from duplicate samples in three independent experiments.

| **FP binding buffer** |
| --- |
| 2 mM Tris-HCl pH 8.0 |
| 100 mM NaCl |
| 3 mM $MgCl_2$ |
| 0.2 mM EGTA |
| 0.7mM ATP |
| 2 mM DTT |

## 2.9 Protein expression and purification

In order to express proteins in bacteria, we used *E.coli* BL21 or Rosetta (DE3) pLysS strains. Firstly, bacteria were transformed with the expression plasmid of interest and plated on an agar plate containing relevant antibiotic. The next day, a single colony was harvested and transferred into 1/200 of the final volume LB media with the relevant antibiotic. The pre-culture was grown overnight at 37°C with 190 rpm agitation. The following day, the expression culture was inoculated with the pre-culture. The bacterial culture growth was monitored by OD measurement and expression was induced when the $OD_{600}$ =0.6 by the addition of 0.5mM IPTG. The expression was carried out at appropriate, optimised temperature for relevant period of time.

For the purpose of pull-down assays, GST-tagged Phactr1 constructs were expressed for 3h at 37°C. Importin α and Importin β were expressed as previously described (Pawlowski et al., 2010). PP1 was directly co-expressed with the GST-tagged Phactr1 392C construct. For the purpose of structural analysis, GST-tagged Phactr1(414-528) was expressed at 30°C.

After protein expression, cells were harvested by centrifugation for 15 minutes at 7000 rpm and the pellet was resuspended in the bacterial lysis buffer (see below for details). The suspension was then sonicated on ice with the maximum energy at the Soniprep 150 (MSE) using 9.5mm/19mm probe. The obtained cell lysates were then centrifuged for 40 minutes at 20 000 rpm at 4°C. Supernatants were incubated with the

appropriate volume (1 ml resin per 1 litre culture) of glutathione sepharose (GE Healthcare), which has been prewashed in the lysis buffer for equilibration. The incubation was performed for 3 hours at 4°C with continuous rotation. Afterwards, the resin was subsequently washed with "wash buffer 1" and "wash buffer 2" and with an "ATP wash buffer" (see below for details). Next, the resin was equilibrated in the "equilibration buffer" and the GST tag was cleaved by overnight incubation with GST-3C protease (obtained from Structural Biology Laboratory at the London Research Institute). The following day, cleaved proteins were eluted from the resin and protein was concentrated to desired volume in Vivaspin concentrators (Vivascience) at 4°C according to manufacturers instructions.

For the purpose of structural analysis Phactr1(414-528) and derivatives were purified by size exclusion chromatography using Superdex 200 column on ÄKTA FPLC (Fast Protein Liquid Chromatography) system (GE Healthcare).

| **Lysis buffer** | **Wash buffer 1** | **Wash buffer 2** |
|---|---|---|
| 50 mM Tris-HCl pH8.0<br>300 mM NaCl<br>1% Triton X-100<br>0.5 mM AEBSF<br>1 mM EDTA<br>15 µg benzamidine | 50 mM Tris-HCl pH8.0<br>300 mM NaCl<br>1 mM DTT<br>0.5 mM AEBSF<br>1 mM EDTA<br>15 µg benzamidine | 50 mM Tris-HCl pH8.0<br>500 mM NaCl<br>1 mM DTT<br>1 mM EDTA |

| **ATP wash buffer** | **Equilibration buffer** |
|---|---|
| 50 mM Tris-HCl pH7.5<br>50 mM KCl<br>1 mM DTT<br>20 mM $MgCl_2$<br>5 mM ATP | 50 mM Tris-HCl pH8.0<br>100 mM NaCl<br>1 mM DTT |

**Table 2.14 Buffers used for protein purification.**

## 2.10 Protein analysis

### 2.10.1 Co-immunoprecipitation

In order to co-immunoprecipitate FLAG-Phactr1 or derivatives and/or HA-PP1, NIH3T3 cells were transfected with relevant plasmids in 10 $cm^2$ dishes (for details see section "Transfection"). Cells were lysed in 0.5% Nonidet P-40, 1 mM EDTA, 50 mM Tris pH 8.0, 120 mM NaCl, 0.1 mM sodium vanadate, 1 tablet/50ml protease inhibitors cocktail (Roche) ice. Lysates were centrifuged at 13000 rpm for 30 minutes and supernatants processed further. For immunoprecipitation, anti-HA-agarose or anti-FLAG agarose affinity gels were incubated with a total of 1 mg protein for 2h at 4°C. Four consecutive washes in lysis buffer were performed before separation of proteins by SDS-PAGE. Proteins were detected by immunoblotting with specific antibodies (see section "Protein detection").

To co-immunoprecipitate endogenous proteins in CHL-1 cells, lysis was performed in 20 mM Tris-HCl pH 7.4, 150 mM NaCl, 0.1% (w/v) SDS, 0.5% (w/v) Na-deoxycholate, 1% (v/v) Triton X-100, 1 tablet per 50ml Roche Complete, 1.0 mM PMSF. Lysates were centrifuged at 13000 rpm for 30 minutes and supernatants processed further. To immunoprecipitate, 1μg PP1α (C-19, Santa-Cruz), antibody was used per 500 mg lysate. Subsequently, three consecutive washes in lysis buffer were performed before separation of proteins by SDS-PAGE. Proteins were detected by immunoblotting with specific antibodies (see section "Protein detection").

### 2.10.2 GST-affinity pull down assay

In order to perform GST-affinity pull down assays, appropriate GST-tagged Phactr1 constructs were expressed in bacteria. Glutathione-sepharose was saturated with GST-tagged proteins from *E.coli* lysates and the beads were washed once with 20mM

Tris-HCl pH7.8, 150 mM NaCl, 10mM $MgCl_2$, 1 mM PMSF, 1mM DTT and once with 20mM Tris-HCl pH7.8, 500 mM NaCl, 10mM $MgCl_2$, 1 mM PMSF, 1mM DTT. Lastly, the beads were washed with the binding buffer (50 mM Tris-HCl pH 7.8, 50 mM NaCl, 5 mM $MgCl_2$). The beads were then incubated with purified recombinant Importin α3 and Importin β1. The pulldown was performed for 1h at 4°C in binding buffer. Afterwards, the resin was washed four times with binding buffer and resuspended in SDS loading buffer for further analysis by SDS-PAGE.

PP1 protein was co-expressed with GST-Phactr1-C in *E.coli* (for details see above). To purify the resulting complex, a previously described method for PP1 purification was used (Kelker et al., 2009). The pulldown was performed for 1h at 4°C in binding buffer (20 mM Tris pH8.0, 100 mM NaCl, 0.5% Triton X-100, 5 mM $MgCl_2$, 0.5 mM $MnCl_2$, 0.2 mM EGTA, 0.2 mM ATP, 1 mM DTT). Again, the resin was washed four times with binding buffer and resuspended in SDS loading buffer for protein separation by SDS-PAGE. Proteins were stained with Coomassie Brilliant Blue or detected by immunoblotting with specific antibodies (see section "Protein detection").

### 2.10.3 SDS-PAGE

In order to fractionate proteins according to their size, sodium dodecyl sulfate-polyacrylamide gel electrophoresis (SDS-PAGE) was performed. Prior to loading on the gel, samples were resuspended in 6x SDS-loading buffer (375 mM Tri-HCl pH6.8, 12%SDS, 60% glycerol, trace bromophenol blue, 600 mM DTT), sonicated if necessary and boiled for 5 minutes in thermoblock. Usually for electrophoresis, pre-cast NuPAGE Novex Bis-Tris 4-12% gradient gels were used (Invitrogen). For the separation of smaller proteins (Phactr1 truncations, MLC2) NuPAGE Novex Tricine 10-20% gels were used (Invitrogen). Buffers used for electrophoresis differed according to the size of proteins (MOPS, MES, Tricine SDS running buffers; Invitrogen) and separation was carried out for 45min-2h at 120-200 volts according to the specific gel/buffer requirements. SeeBlue Pre-Stained standard was used as a protein molecular weight marker (Invitrogen).

### 2.10.4 Protein detection

#### *2.10.4.1 Coomassie staining*

If immunoblotting was not required, proteins fractionated by SDS-PAGE were detected by Coomassie brilliant blue staining. Coomassie staining was achieved by incubating gels in staining solution (2% Coomassie R250, 3% acetic acid in methanol) for 20 minutes with agitation. To visualize proteins, de-staining was performed in de-staining solution (10% acetic acid, 40% methanol) for 1h-3h.

#### *2.10.4.2 Immunoblotting*

If detection of proteins with specific antibodies was required, immunoblotting was performed. After SDS-PAGE, gels were transferred onto activated in methanol PVDF membranes or onto nitrocellulose (Whatman). Proteins on the gels were transferred onto membranes using Mini Trans-Blot Electrophoretic Transfer Cell (Biorad). Gels were assembled in between foam pads and filter paper (Whatman 3MM). The transfer was carried out at 400 mA for 90 minutes in transfer buffer (192 mM glycine, 25 mM Tris base, 10% methanol). Afterwards, membranes were immersed for 1h in blocking solution containing 5% milk powder, 0.1% Tween 20 in PBS for M2 FLAG-HRP and HA-HRP or in 2% BSA, 0.1% Tween 20 in TBS for all other antibodies (see below for details). Membranes were then incubated with appropriate primary antibodies diluted to optimal concentration (see below) in relevant blocking solution overnight. The following day, membranes were washed in wash buffers (0.1% Tween 20 in PBS or 0.1% Tween 20 in TBS) four times for 5 minutes and incubated with secondary antibodies for 2h (this step was omitted if primary antibodies were coupled to HRP). Then, membranes were washed three times and developed with enhanced chemiluminescence (ECL) reagents (GE Healthcare) according to

manufacturers instructions. Subsequently, membranes were exposed to ECL Hyperfilm (GE Healthcare) or chemiluminescent readout was performed in ImageQuant LAS 4000 biomolecular imager (GE Healthcare).

| **Primary antibodies** | | |
|---|---|---|
| *antibody* | *species* | *concentration* |
| M2 FLAG-HRP (Sigma) | mouse | 1:1000 |
| HA-HRP (3F10, Roche) | rat | 1:1000 |
| Phactr1 (HPA029756, Sigma) | rabbit | 1:200 |
| MLC2 (3672, Cell Signalling) | rabbit | 1:1000 |
| P-MLC2 T18/S19 (3674, Cell Signalling), | rabbit | 1:1000 |
| PP1α (C-19, Santa-Cruz) | goat | 1:1000 |
| Importin α (612654, BD Transduction Laboratories) | mouse | 1:1000 |
| Importin β (ab45938, Abcam). | rabbit | 1:1000 |
| α-Tubulin (T5168, Sigma), | mouse | 1:1000 |
| Actin (C-4, Santa-Cruz) | mouse | 1:1000 |
| **Secondary antibodies were obtained from DAKO (used at dilution 1:1000)** | | |

**Table 2.15 Antibodies used for immunoblotting.**

## 2.11 Complex stoichiometry analysis

### 2.11.1 Size exclusion chromatography

In order to perform analysis of G-actin•RPEL$^{Phactr1}$domain complexes, size exclusion chromatography was used. Calibrated Superdex 200 column was linked to ÄKTA FPLC (Fast Protein Liquid Chromatography) system (GE Healthcare) and previously obtained proteins were injected onto the system (see "Protein expression" for Phactr1 constructs and (Mouilleron et al., 2008) for the preparation of LatB-actin). Stoichiometry analysis was performed in the presence or absence of 4μM LatB-actin in the running buffer: 20 mM Tris, pH 8, 100 mM NaCl, 3 mM $MgCl_2$, 0.2 mM EGTA, 0.2 mM ATP, 0.3 mM TCEP and 5 % glycerol (v/v). The stoichiometry of the complex was then calculated from obtained molecular weight of the complex, where one molecule of Phactr1(414-528) is 14kDa and one molecule of G-actin is 42kDa.

### 2.11.2 SEC-MALLS

Where more precise analysis of the molecular weight was necessary (analysis of Phactr1(414-528) mutants interaction with G-actin), we used multi-angle laser light scattering coupled with size exclusion chromatography using a SEC-MALLS/UV/RI Wyatt system (Mouilleron et al., 2012). For size exclusion chromatography ÄKTA FPLC system linked to Superose 6 column was used (GE Healthcare). After injecting proteins onto the system, the isocratic elution was performed at a flow rate of 0.5 ml/min in running buffer (20 mM Tris pH 8, 100 mM NaCl, 3mM MgCl2, 0.2 mM EGTA, 0.2 mM ATP, 0.3 mM TCEP at 25 °C). The light scattering analysis of the complexes was monitored using a Mini Dawn–Treos instrument and an Optilab TrEX differential refractometer (Wyatt technology, Santa Barbara, CA). The concentration of the molecule in solution was evaluated by a specific refractive index increment (*dn/dc*) of 0.185. In order to measure the absolute refractive index of the solution, the refractive

index detector was implemented. To calibrate the light scattering detector we used toluene. ASTRA 6 software was used to analyse the data (Wyatt technology, version 6.0.2). SEC-MALLS was performed by Stephane Mouilleron from Structural Biology Laboratory in London Research Institute.

## 2.12 Crystallisation

### 2.12.1 Complex preparation

#### *2.12.1.1 G-actin• RPEL$^{Phactr1}$ domain complex*

To obtain a complex of Phactr1(414-528) with G-actin, size exclusion chromatography was used (see above). Phactr1(414-528) is sensitive to proteolysis during purification (see Chapter 4). This results in heterogeneous distribution of G-actin•RPEL$^{Phactr1}$ complexes, when complexes are formed upon actin excess. A heterogeneous G-actin•RPEL$^{Phactr1}$ complex is a mix of different complexes containing G-actin bound to full length RPEL$^{Phactr1}$ as well as G-actin bound to smaller products of protease cleavage. A homogenous complex was obtained by mixing purified Phactr1(414-528) and LatB-actin at a 3:1 molar ratio. Afterwards, the complex was purified by size exclusion chromatography in running buffer (20 mM Tris pH 8, 100 mM NaCl, 3 mM MgCl2, 0.2 mM EGTA, 0.2 mM ATP, 0.3 mM TCEP and 5% glycerol) and stoichiometry was evaluated by SEC-MALLS as 3:1 (G-actin:Phactr1(414-528)) (see above and Chapter 4 for details). Purified complexes were processed further for crystallization.

G-actin•RPEL$^{Phactr1}$ complex Small Angle X-ray scattering data (SAXS) was collected at the SWING beamline of the Soleil synchrotron by Stephane Mouilleron (Mouilleron et al., 2012).

#### *2.12.1.2 G-actin• RPEL$^{Phactr1}$ peptide complexes*

To obtain complexes of individual RPEL motifs with G-actin, the molar ratio of 1:2 (G-actin:RPEL motif) was established for each motif (RPEL-N, RPEL1, RPEL2 and RPEL3) before injection onto Superdex 200 column linked to ÄKTA FPLC system. The column was equilibrated in 20 mM Tris pH 8, 50 mM NaCl, 3 mM MgCl2, 0.2 mM EGTA, 0.2 mM ATP, 0.3 mM TCEP and 5% glycerol). Purified complexes were processed further for crystallization.

### 2.12.2 Crystallisation and structure determination

Crystallisation and structure determination was performed by Stephane Mouilleron from Neil McDonald's Laboratory (Structural Biology Laboratory in London Research Institute).

#### *2.12.2.1 Crystallisation of G-actin•RPEL$^{Phactr1}$ domain complex*

After complex preparation, the obtained sample was concentrated to 20 mg/ml and crystallised at 20°C using the sitting-drop vapour diffusion method. Each sitting drop contained 6µl of 1:1 (v:v) mixture of protein and a well solution containing 0.1 M TRIS pH 7, 14 % PEG 6000, 0.2 M sodium chloride. The appearance of the crystals was seen after three days and after 10 days they reached their maximum size of 0.2 mm x 0.2 mm. To cryoprotect crystals, 0.1M TRIS pH 7, 20% PEG 6000, 0.2 M sodium chloride and 20% glycerol was used. Then, crystals were frozen in liquid nitrogen and X-ray data sets collected at 100 K at the 104 beamline of the Diamond Light Source Synchrotron (Oxford, UK). Data collection, refinement with molecular replacement, model building, model validation was performed by Stephane Mouilleron. Figures representing structural data were prepared in PYMOL graphics program by Stephane

Mouilleron (Mouilleron et al., 2012). For data collection and refinement statistics see Table 7.3.

#### *2.12.2.2 Crystallisation of G-actin•RPEL$^{Phactr1}$ peptides complexes*

Complexes of G-actin•RPEL$^{Phactr1}$ peptides were crystallized at 20°C using the sitting-drop diffusion method after obtaining a desired concentration of 10 mg/ml. Each sitting drop contained 1µl of 1:1 (v:v) mixture of concentrated protein and a well solution. Crystals appeared after two days, and after 14 days they reached their maximum size. Crystals were frozen in liquid nitrogen and X-ray data sets collected at 100 K at the ID23-1 beamline (ID29 for G-actin•RPEL3$^{Phactr1}$) of the European Synchrotron Radiation Facility (ESRF, Grenoble, France). Data collection, refinement with molecular replacement, model building and model validation was performed by Stephane Mouilleron (Mouilleron et al., 2012). Figures representing structural data were prepared in PYMOL graphics program by Stephane Mouilleron, where indicated. For data collection and refinement statistics see Table 7.3.

# Chapter 3. Molecular mechanisms of Phactr1 regulation

## 3.1 Aims

We previously observed that MRTFs accumulate in the nucleus upon serum stimulation (Miralles et al., 2003; Vartiainen et al., 2007). Rho-actin signal induces actin filaments formation causing depletion of the G-actin pool, which leads to translocation of MRTF-A to the nucleus and activation of SRF-dependent transcription. The availability of G-actin is detected by the regulatory RPEL domain of MRTF-A, which contains three G-actin binding RPEL motifs (Mouilleron et al., 2008).

Because the Phactr family of PP1 binding proteins contain four RPEL motifs, with RPEL domain at the C-terminus and single RPEL motif at the N-terminus, we hypothesised that the activity of Phactr proteins might also be regulated by G-actin levels. Considering, that the relevance of G-actin binding to Phactr was unclear and the potential possibility that G-actin might influence Phactr behaviour towards PP1 activity, we firstly tested whether Phactr proteins exhibit nucleocytoplasmic shuttling in NIH3T3 fibroblasts and sought to determine the signalling pathway responsible for this regulation.

## 3.2 Cellular localisation of Phactr1

### 3.2.1 Phactr1, but not Phactr2, 3 or 4 accumulate in the nucleus upon serum stimulation

To determine the subcellular localisation of Phactr family of proteins, we transiently transfected NIH3T3 fibroblasts with FLAG-tagged Phactr1, 2, 3 and 4 cDNA and monitored protein localisation using immunofluorescence (Figure 3.1). In the unstimulated condition Phactr1 localised in the cytoplasm and upon one hour of serum stimulation it accumulated in the nucleus. Phactr2 was cytoplasmic in unstimulated cells and did not respond to serum stimulation. Both Phactr3 and Phactr4 were pan-cellular and their localisation remained unaffected by the addition of serum.

The translocation of Phactr1 to the nucleus upon serum stimulation exhibits somewhat slower dynamics in comparison to MRTF-A in this system, with MRTF-A fully accumulating in the nucleus after 5 minutes of serum treatment (Vartiainen et al., 2007). Nevertheless, Phactr1 responded to the concentration of the G-actin pool, like MRTF-A and therefore was a good candidate for further analysis.

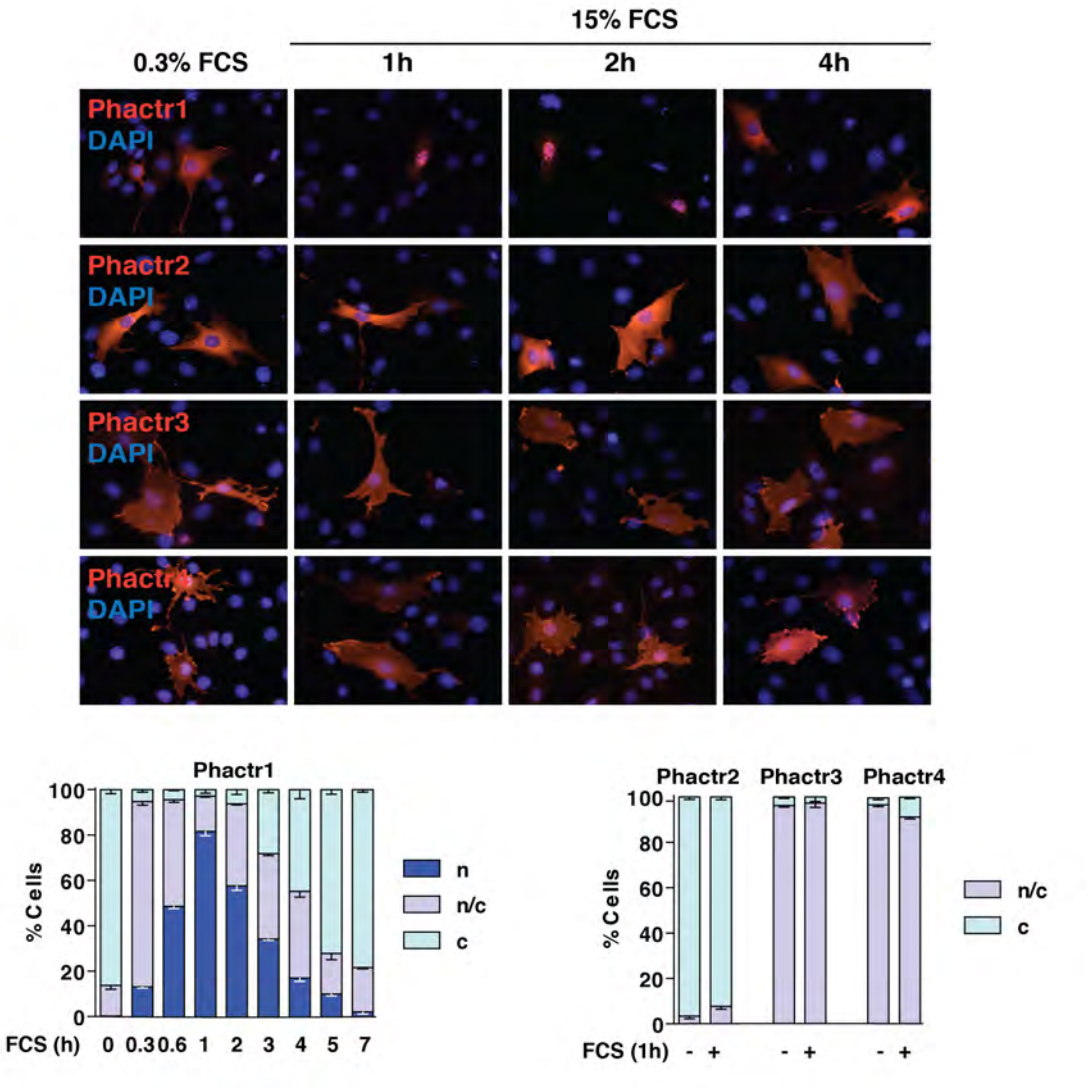


**Figure 3.1 Phactr1, but not Phactr2, 3 or 4, accumulates in the nucleus upon serum stimulation.**

(Top) NIH3T3 cells expressing FLAG-tagged Phactr proteins were maintained in media containing 0.3% FCS for 24 hours, then stimulated with 15% FCS for indicated period of time; localisation of the proteins was visualised by fluorescence microscopy. (Bottom) Quantification of Phcatr1 (left) and Phactr2, 3 and 4 (right) subcellular localisation as indicated in A (C, cytoplasmic; N/C, pan-cellular; N, nuclear; at least 75 cells were counted per point, error bars represent the s.e.m. of three independent experiments).

### 3.2.2 Rho-actin signalling controls subcellular localisation of Phactr1

It was previously shown that expression of C3 transferase, which ADP-ribosylates and inactivates Rho, inhibits nuclear accumulation and reporter activation of MRTF-A. We co-expressed Phactr1 with C3 transferase in NIH3T3 fibroblasts and monitored localisation of Phactr1 by immunofluorescence (Figure 3.2 B and C). In cells expressing C3 transferase, serum stimulated Phactr1 nuclear accumulation was blocked, suggesting that the dynamic change of Phactr1 localisation in the cell depends on Rho signal.

To further analyse the signalling pathway responsible for Phactr1 behaviour, we used specific inhibitors that act during different steps of the Rho pathway (Figure 3.2 A). Y-27632 is a selective, ATP-competitive inhibitor of Rho-associated protein kinase (ROCK), including ROCK-II and p160ROCK. We used Y-27632 to investigate whether Phactr1 nuclear accumulation is dependent on ROCK kinase. Pre-treatment of cells with Y-27632 caused significant, but not complete inhibition of Phactr1 nuclear accumulation suggesting that another branch of the pathway might also be involved in Phactr1 dynamics (see: Discussion).

Because the critical downstream effect of Rho-actin signalling is the G- to F-actin turnover, we tested whether preventing actin polymerisation inhibits Phactr1 nuclear localisation. We pre-treated cells with latrunculin B, toxin that has the ability to modulate actin filaments (Spector et al., 1983). Latrunculin B binds to G-actin and inhibits F-actin formation (Coue et al., 1987). Phactr1 localisation was constitutively cytoplasmic in cells treated with latrunculin B suggesting that nuclear accumulation of Phactr1 critically depends on interaction with G-actin.

Previous studies of MRTF-A showed that actin associates with MRTF-A via RPEL motifs and that disruption of this association is caused by Rho-actin pathway and subsequent depletion of the G-actin pool (Miralles et al., 2003; Sotiropoulos et al., 1999). Cytochalasin D, an actin polymerisation inhibitor, was found to inhibit actin-RPEL interaction causing constitutive nuclear localisation of MRTF-A and promoting

the activity of SRF (Miralles et al., 2003; Sotiropoulos et al., 1999). We found that similarly to MRTF-A, Phactr1 was also constitutively nuclear in cells that were pre-treated with cytochalasin D. This finding suggests that RPEL motifs in Phactr1 are also responsible for the interaction with actin.

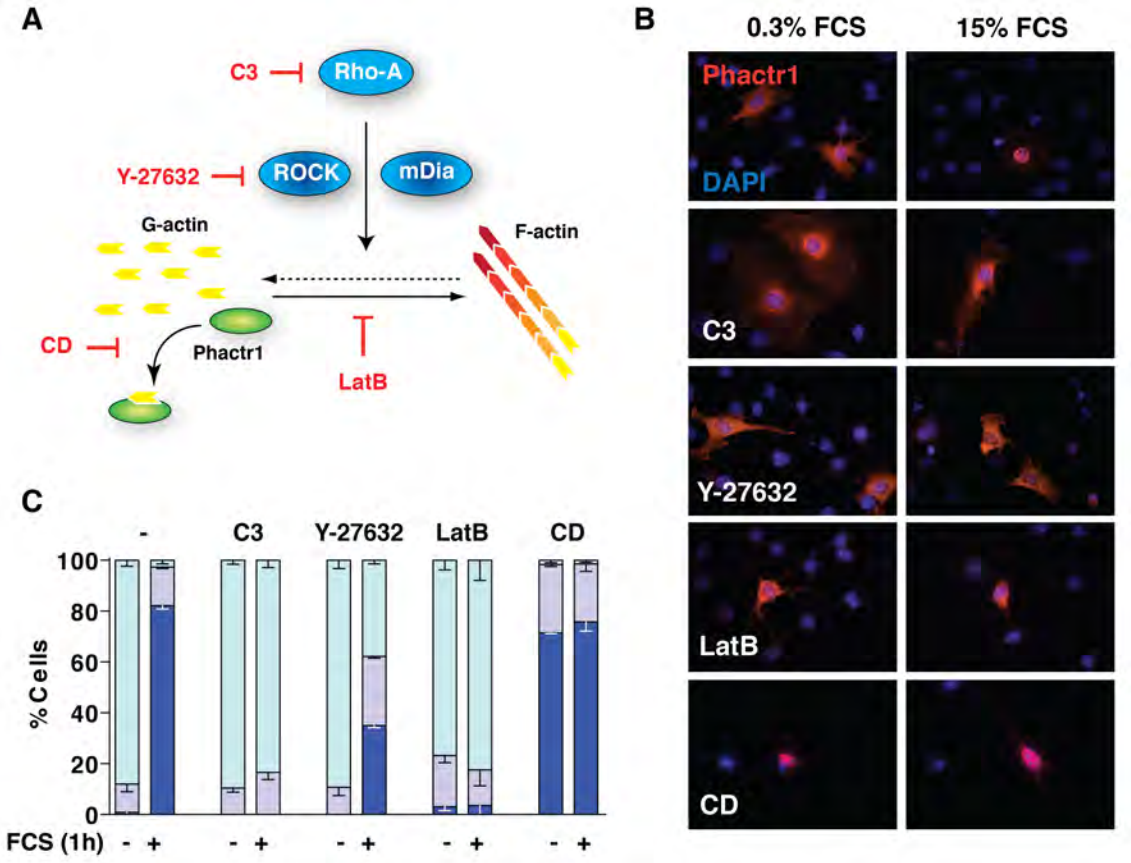


**Figure 3.2 Phactr1 nuclear accumulation is controlled by Rho-actin signalling pathway.** Effects of inhibitors on serum-induced nuclear accumulation of Phactr1. **(A)** Schematic of the Rho-actin signal pathway, indicating points of action of the inhibitors used. **(B)** Immunofluorescence microscopy images showing effects on nuclear accumulation of FLAG-tagged Phactr1, by co-expression with C3 transferase (C3), or following pre-treatment with 10 µM Y-27632, 1 µM latrunculin B (LatB) or 10 µM cytochalasin D (CD), 1 hr after FCS addition. **(C)** Summary of the data, scored as in Figure 3.1.

Another study of MRTFs showed that in contrast to NIH3T3 fibroblasts, in MDA-MB-231 breast cancer cells localisation of MRTFs is predominantly nuclear in the unstimulated condition (Medjkane et al., 2009). *In vitro*, the MDA-MB-231 cell line has an invasive phenotype and exhibits abundant activity in both the chemoinvasion and chemotaxis assays. Those cells also form tumours in nude mice. Because Rho signalling is upregulated in some cancer cells, the basal level of Rho is higher in MDA-MB-231 in comparison with NIH3T3 cells (Medjkane et al., 2009). We found that Phactr1 is also predominantly nuclear in MDA-MB-231 cells indicating that both proteins react similarly to various basal levels of Rho-actin signalling (Figure 3.3). Taken together this data indicates that the subcellular localisation of Phactr1 is controlled by Rho-actin signalling pathway.

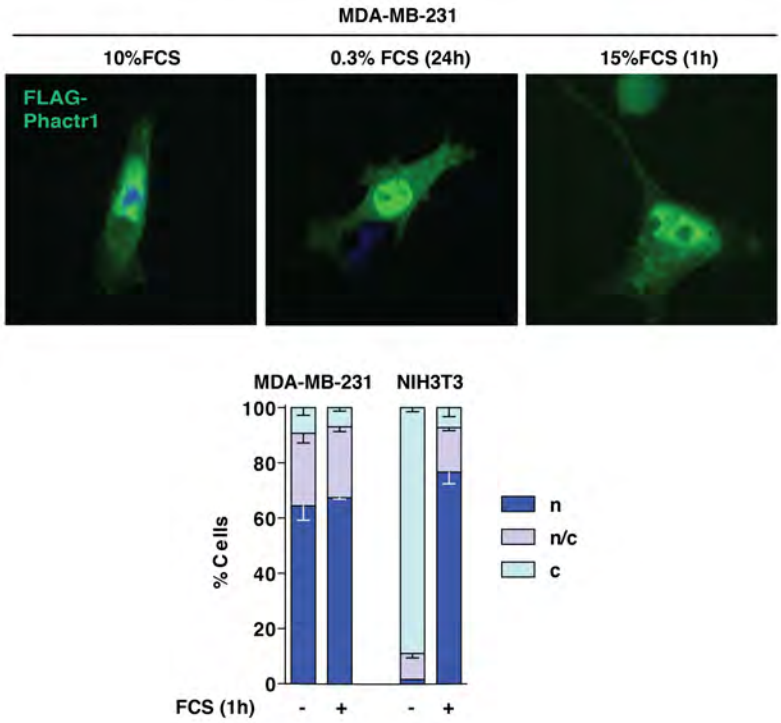


**Figure 3.3 Phactr1 is predominantly nuclear in MDA-MB-231 cells.**

Cells expressing FLAG-tagged Phactr1 were either grown in 10% serum (FCS) or maintained in 0.3% serum for 20h with or without subsequent 1h stimulation with 15% serum. Localisation of Phactr1 was visualised by immunofluorescence microscopy. Comparison of Phactr1 localisation between MDA-MB-231 and NIH3T3 cells is summarized on the bottom (cells quantified as in Figure 3.1).

### 3.2.3 Phactr1 nuclear export is not Crm1-dependent

Nuclear export of MRTFs depends on Crm1 (Vartiainen et al., 2007). Because MRTF-A and Phactr1 are both regulated by the Rho-actin signalling pathway and exhibit high homology of their RPEL domains, we sought to compare the export machinery of those two proteins. Treatment with the Crm1 inhibitor leptomycinB (LMB) did not induce nuclear accumulation of Phactr1 in unstimulated cells, which indicates that Crm1 exportin does not mediate nuclear export of Phactr1 (Figure 3.4), (see: 'Discussion').

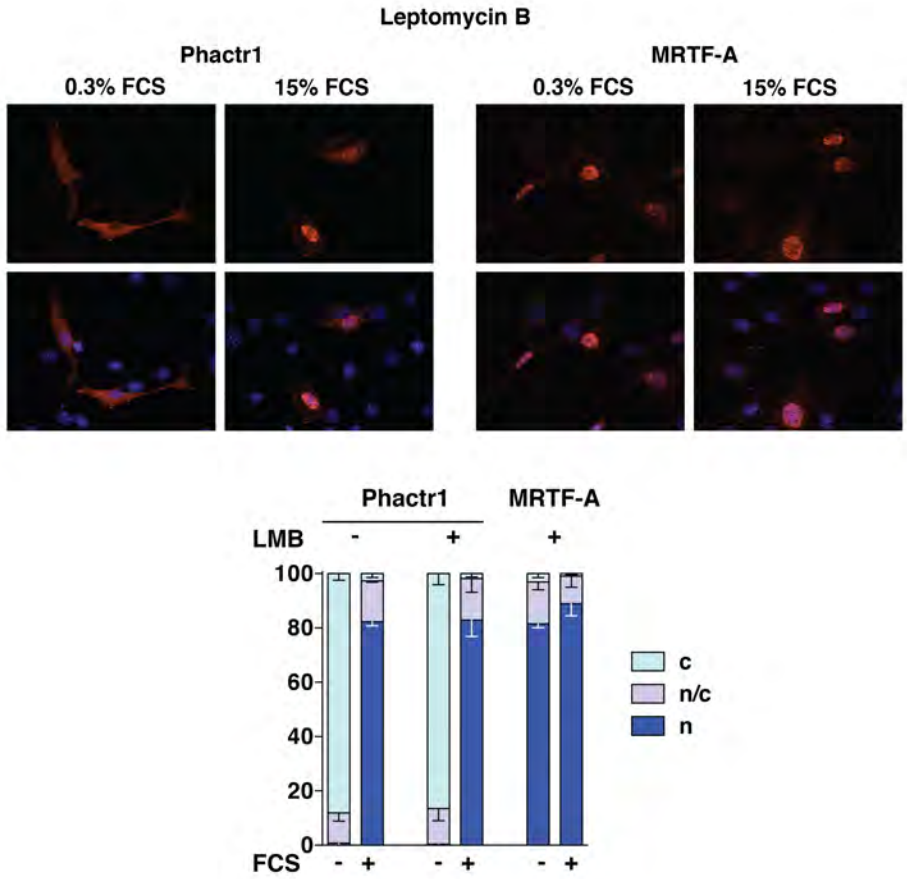


**Figure 3.4 Phactr1 export is not Crm1-dependent.**

NIH 3T3 cells were transfected with FLAG-tagged Phactr1 or HA-tagged MRTF-A. Cells were pre-treated with 30 nM (LMB) and stimulated with serum. (Top) Protein localisation before and after serum stimulation was monitored using immunofluorescence microscopy. (Bottom) Summary of the data, assessed as in Figure 3.1.

### 3.2.4 Phactr1 RPEL motifs are G-actin binding elements

To define the interactions between actin and RPEL motifs in Phactr1, we employed fluorescence anisotropy assays. This approach was previously used to measure the affinity of MRTF-A RPEL motifs to actin (Guettler et al., 2008). We titrated increasing amounts of non-polymerisable latrunculinB-actin into steady amounts of fluorescently labelled Phactr1 RPEL peptides and measured the anisotropy. The binding affinity of RPEL motifs in Phactr1 to actin was higher than the affinity previously observed for MRTF-A. In MRTF-A, RPEL1 and RPEL2 bound G-actin with affinities of 5.4 ± 0.5 μM and 2.3 ± 0.2 μM, respectively (Figure 3.5 A), whereas MRTF-A RPEL3 bound much weaker, with $K_D$ of only 18.8 ± 1 μM (Guettler et al., 2008). In Phactr1, affinities for RPEL motifs within the RPEL domain were 0.9 ± 0.1 μM for RPEL1, 4.34 ± 0.86 μM for RPEL2 and 0.27 ± 0.02 μM for RPEL3. The N-terminal RPEL motif, RPEL-N bound actin with high affinity of 0.32 ± 0.05 μM. Taken together, this data shows that similarly to MRTF-A, Phactr1 binds G-actin through its RPEL motifs. However, RPEL motifs (N, 1 and 3) bind actin with higher affinities than in MRTF-A. Because MRTF-A regulation depends on the weak affinity of RPEL3 (Guettler et al., 2008; Mouilleron et al., 2008; Mouilleron et al., 2011), our study suggests that the molecular mechanism of G-actin sensing by Phactr1 might be different.

Having demonstrated that RPEL motifs in Phactr1 are G-actin binding elements, we determined how R->A substitution in each RPEL motif affected actin binding affinity. Similarly to MRTF-A, this mutation significantly reduced actin binding affinity of RPEL motifs. Affinities for RPEL1 and RPEL2 were reduced to non-detectable anisotropies, while RPEL3 was reduced almost 70 fold, and RPEL-N almost 30 fold (Figure 3.5 A).

### 3.2.5 RPEL motifs in Phactr2, 3 and 4 bind actin less efficiently

Puzzled by the fact that Phactr2, 3 and 4 do not shuttle into the nucleus in NIH3T3 cells, we examined their distinct behaviour by investigating their affinity to G-actin. Again, we employed fluorescence anisotropy assays to test the affinity of G-actin to the RPEL motifs in Phactr2, 3 and 4. Surprisingly, although the homology between the motifs across Phactr family is quite high (Figure 4.9 A), their binding affinities differed significantly. Between all four RPEL motifs in Phactr2, 3 and 4 there was always one RPEL motif that had either very low affinity or showed no affinity for G-actin at all (Figure 3.5 B).

RPEL motifs in Phactr2 show high affinity to G-actin, apart from RPEL2, where the $K_D$ is only 28.1 ± 4.02 μM. In Phactr3, RPEL motifs within the C-terminal RPEL domain bind G-actin with high affinities, but RPEL-N seems not to bind actin at all. Phactr4 has quite low affinity to actin overall, with RPEL-N and RPEL3 binding strongly, but RPEL2 with $K_D$ of 6.35 ± 0.61 and RPEL1 showing no binding.

The above results suggest that the homology between RPEL motifs in the Phactr family is not sustaining the similarities in actin binding affinity. The differences in the manner of actin binding might explain the alternative behaviour of Phactr1 in comparison to other family members (see: ‘Discussion’).

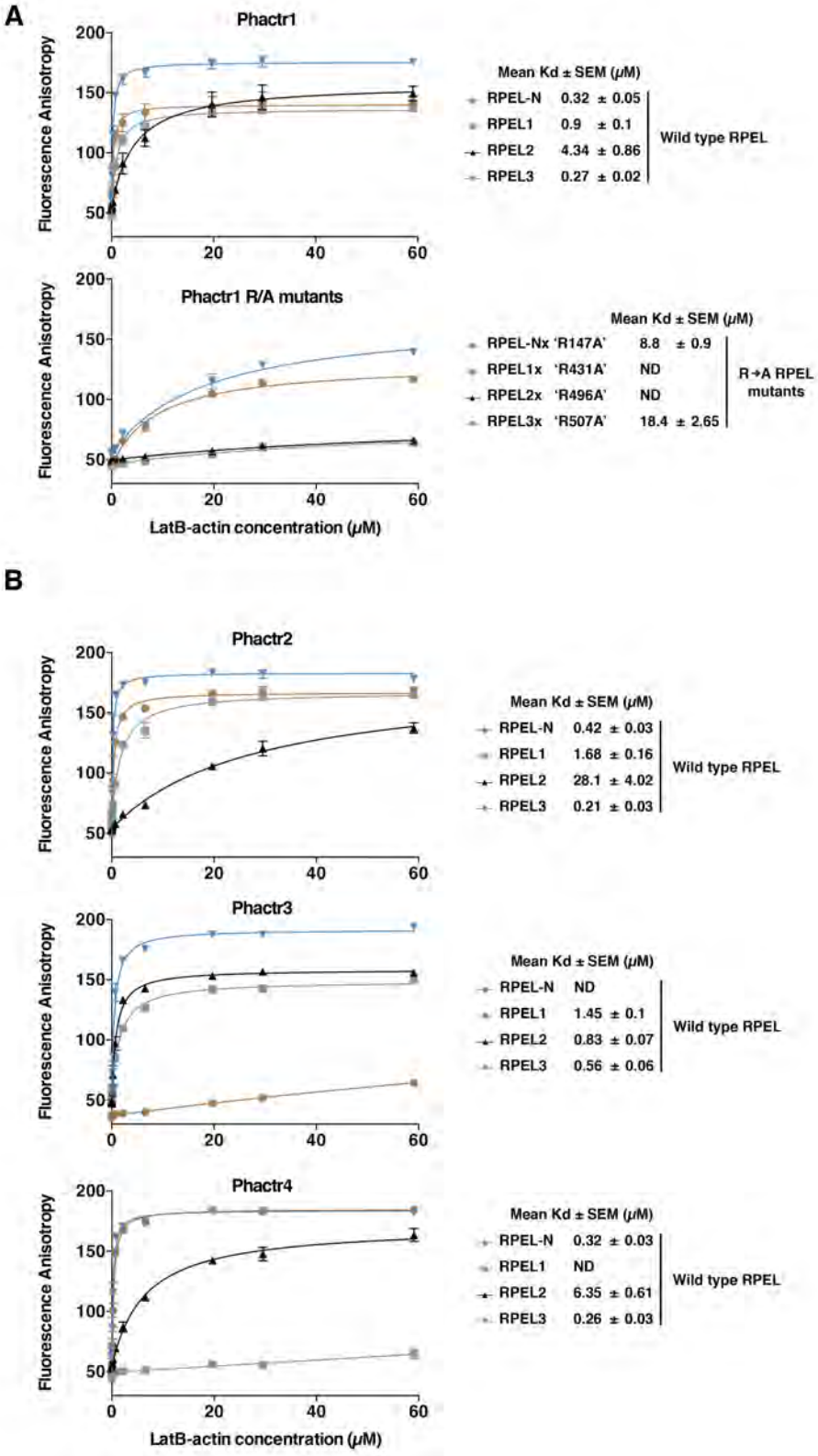
A
Phactr1
Fluorescence Anisotropy
200
150
100
50
0
20
40
60
Mean Kd ± SEM (μM)
RPEL-N 0.32 ± 0.05
RPEL1 0.9 ± 0.1
RPEL2 4.34 ± 0.86
RPEL3 0.27 ± 0.02
Wild type RPEL
Phactr1 R/A mutants
Mean Kd ± SEM (μM)
RPEL-Nx 'R147A' 8.8 ± 0.9
RPEL1x 'R431A' ND
RPEL2x 'R496A' ND
RPEL3x 'R507A' 18.4 ± 2.65
R→A RPEL mutants
LatB-actin concentration (μM)
B
Phactr2
Mean Kd ± SEM (μM)
RPEL-N 0.42 ± 0.03
RPEL1 1.68 ± 0.16
RPEL2 28.1 ± 4.02
RPEL3 0.21 ± 0.03
Wild type RPEL
Phactr3
Mean Kd ± SEM (μM)
RPEL-N ND
RPEL1 1.45 ± 0.1
RPEL2 0.83 ± 0.07
RPEL3 0.56 ± 0.06
Wild type RPEL
Phactr4
Mean Kd ± SEM (μM)
RPEL-N 0.32 ± 0.03
RPEL1 ND
RPEL2 6.35 ± 0.61
RPEL3 0.26 ± 0.03
Wild type RPEL
LatB-actin concentration (μM)

**Figure 3.5 Affinities of Phactr family RPEL motifs to G-actin.**

**(A)** Fluorescence anisotropy measurement of G-actin binding by the four wild-type Phactr1 RPEL motifs and Phactr1 RPEL R/A (x) mutant motifs. **(B)** Fluorescence anisotropy measurement of G-actin binding by RPEL motifs in Phactr2, Phactr3 and Phactr4. Anisotropies of FITC-conjugated 32-amino acid RPEL peptides (0.5 mM) were measured over a range of LatB–actin concentrations. Graphs correspond to one of three experiments performed in duplicate. Dissociation constants ($K_D$) are means of three independent experiments ± s.e.m. ND, binding not detectable.

### 3.2.6 RPEL domain is required for Phactr1 nuclear accumulation upon serum stimulation.

To test the functional significance of actin binding to Phactr1 we sought to determine which domains in Phactr1 are required for Phactr1 nuclear accumulation. We transiently transfected NIH3T3 cells with various FLAG-tagged Phactr1 truncations and mutants (Figure 3.6). Firstly we demonstrated that neither deletion of RPEL-N (Phactr1ΔN) or R->A substitution at the conserved RPEL arginine in RPEL-N had an affect on the localisation of Phactr1, in unstimulated or serum-induced cells. Similarly, the deletion of proline-rich, middle region from Phactr1 (Phactr1Δm) had no significant effect on Phactr1 accumulation. In contrast, both deletion of RPEL domain (Phactr1Δ123) and triple R->A substitution (Phactr1-xxx) resulted in constitutive Phactr1 nuclear accumulation. However, deleting the C-terminal conserved PP1-interacting sequence (Phactr1ΔC) had no effect. These data show that C-terminal RPEL domain is required for Phactr1 nuclear accumulation upon serum stimulation, but the N-terminal RPEL motif is not required.

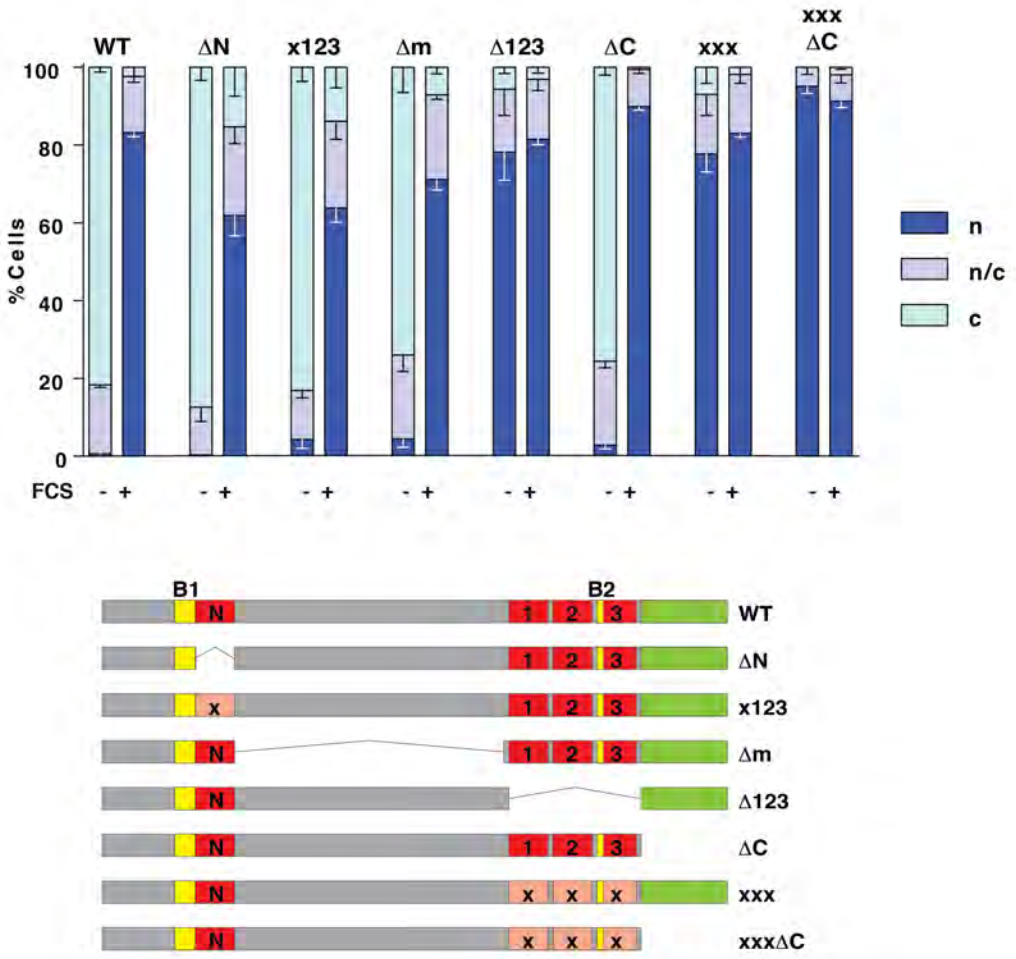


**Figure 3.6 Domains required for Phactr1 nuclear accumulation.**

Localisation of Phactr1 deletion and point mutants in resting and serum-stimulated cells visualised by fluorescence microscopy and scored as in Figure 3.1 (c, cytoplasmic; n/c, pan-cellular; n, nuclear). The Phactr1 derivatives are shown schematically below; RPEL motifs are shown in red or pale red, NLS sequences are shown in yellow, PP1 binding site is in green; WT, wild-type. R->A mutations in the RPEL motifs are indicated by 'x'.

### 3.2.7 All three C-terminal RPEL motifs are required to maintain Phactr1 in the cytoplasm.

It was previously shown that RPEL motifs in MRTF-A functionally cooperate in regulating MRTF-A activity (Guettler et al., 2008). Therefore, we investigated the role of individual RPEL motifs in the regulation of Phactr1. Because R->A mutations of the conserved arginine in RPEL motifs efficiently reduced G-actin binding, we introduced those mutations into the full-length Phactr1 (Figure 3.7 A).

Within the C-terminal RPEL repeat, R->A mutation of RPEL1 (Phactr1-x23) or RPEL2 (Phactr1-1x3) had small effect on the localisation of Phactr1 in resting cells. In contrast, when introduced into RPEL3 (Phactr1-12x), R->A mutations caused nuclear accumulation of Phactr1. We next introduced pairwise combinations of RPEL1 and RPEL2 mutations (Phactr1-xx3), these exhibited a lower effect in comparison with pairwise combinations of RPEL3 and RPEL1 (Phactr1-x2x) and RPEL3 and RPEL2 (Phactr1-1xx). To investigate the role of RPEL-N in this assay, we introduced an RPEL-N R->A mutation into all three single C-terminal RPEL R->A mutants. We found that this change had a small, additional effect on Phactr1 nuclear accumulation. Taken together these results demonstrate that RPEL motifs at the C-terminal cluster of Phactr1 are all required to maintain Phactr1 in the cytoplasm in unstimulated cells. Additionally, RPEL3 has a dominant role in this regulation while the N-terminal RPEL-N seems to have minor function in this localisation assay.

Studies of RPEL R->A mutations revealed that as the number of C-terminal R->A mutations increased, the number of NIH3T3 cells expressing Phactr1 mutants decreased (Figure 3.7 B). This result suggests that abolishing actin binding in Phactr1 leads to toxicity. In comparison with WT Phactr1, Phactr1-xxx had the most toxic effect, together with RPEL3 pairwise mutants of RPEL1 (x2x) and RPEL2 (1xx). This data is consistent with our finding, that RPEL3 is the major contributor to actin-dependent Phactr1 regulation. This result suggests that the toxicity is caused by the loss of G-actin contacts within Phactr1 RPEL domain.

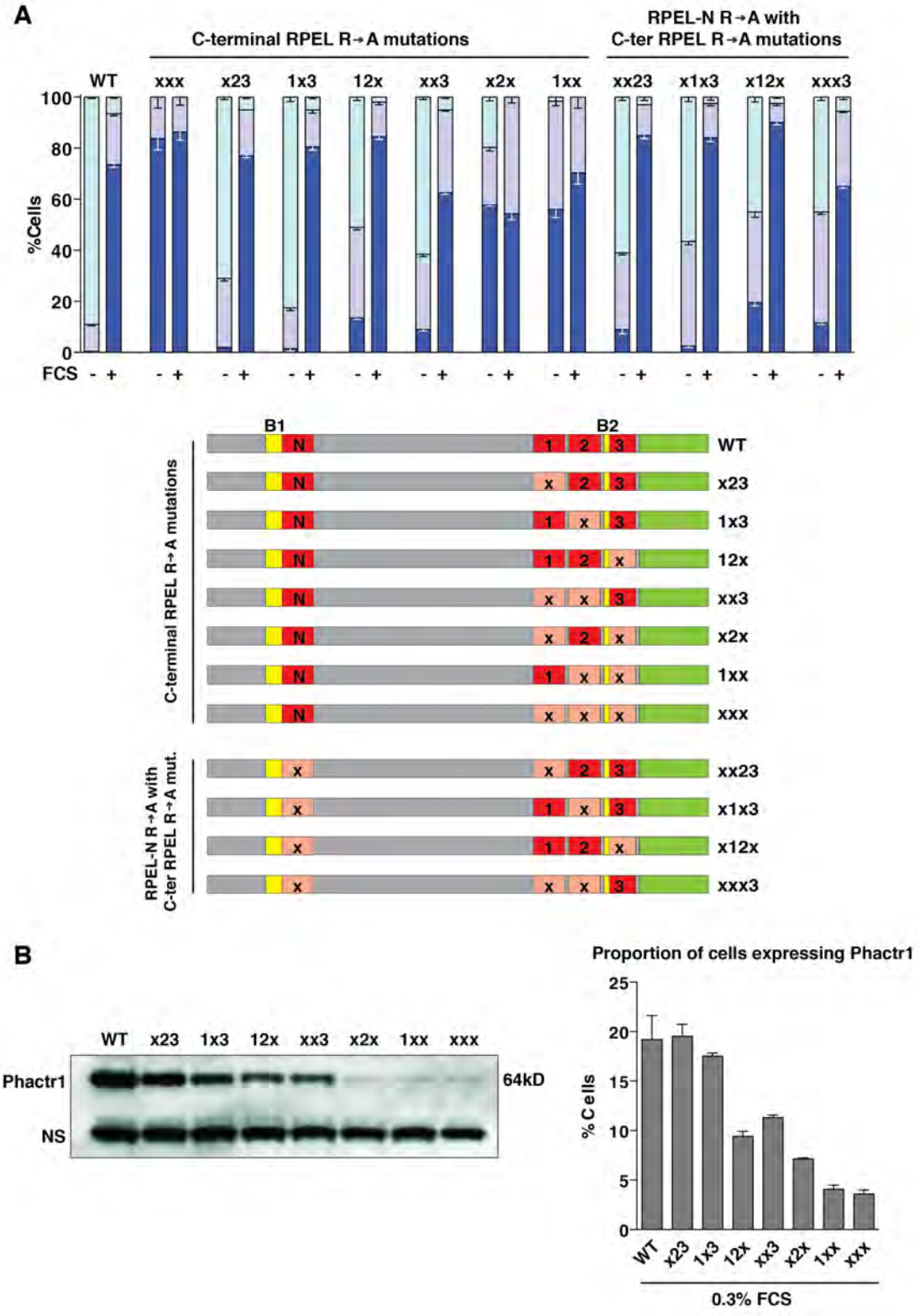
A
C-terminal RPEL R→A mutations
RPEL-N R→A with C-ter RPEL R→A mutations
WT
xxx
x23
1x3
12x
xx3
x2x
1xx
xx23
x1x3
x12x
xxx3
%Cells
FCS
B1
B2
C-terminal RPEL R→A mutations
RPEL-N R→A with C-ter RPEL R→A mut.
B
Phactr1
NS
64kD
Proportion of cells expressing Phactr1
% Cells
0.3% FCS

**Figure 3.7 C-terminal RPEL motifs are required to maintain Phactr1 in the cytoplasm.**
**(A)** Localisation in starved and serum-stimulated cells of Phactr1 derivatives carrying RPEL motif R->A mutations, singly and in combination, scored as in Figure 3.1; The Phactr1 derivatives are shown schematically below. **(B)** Expression levels of Phactr1 C-terminal RPEL R->A mutants. NIH3T3 cells were transfected with FLAG-tagged Phactr1 derivatives (shown in A) and expression levels assessed. Left, immunoblotting; nonspecific band (NS) allows comparison of relative Phactr1 expression level. Right, number of transfected cells detected per field for the different mutants. At least 75 cells were counted per point; error bars represent the s.e.m. of three independent experiments.

### 3.2.8 RPEL domain from Phactr1 cannot functionally replace the RPEL domain from MRTF-A.

MRTF-A and Phactr1 contain three highly homologous tandem RPEL motifs. In MRTF-A, the RPEL domain confers nucleo-cytoplasmic shuttling. Because the Phactr1 RPEL domain is required for the nuclear accumulation of Phactr1, I asked if it could functionally replace the RPEL domain in MRTF-A (Figure 3.8).

I therefore replaced the RPEL domain in MRTF-A with the RPEL domain from Phactr1 (Figure 3.8 A) and assessed subcellular localisation of the 'MRTF-A-Phactr1 RPEL domain chimera' in comparison with MRTF-A. Surprisingly, the domains are not replaceable, as the chimera did not accumulate in the nucleus upon serum stimulation, Leptomycin B (LMB) or Cytochalasin D (CD) treatment (Figure 3.8 B). This suggests that Phactr1 RPEL domain utilises a distinct mechanism to confer nuclear accumulation of Phactr1 than the RPEL domain in MRTF-A. Most probably, Importin α-β cannot efficiently bind to the RPEL domain from Phactr1 to confer MRTF-A import (see: 'Discussion').

When only RPEL3 in MRTF-A was replaced by the high-actin-affinity Phactr1 RPEL3 ('MRTF-A RPEL3-Phactr1 chimera'), and the NLS of MRTF-A was not changed, the behaviour of MRTF-A was not affected in the localisation assay (preliminary observation, Figure 7.3). Taken together, these results suggest that the molecular mechanism of Phactr1 import might be different. To test this hypothesis we next examined Phactr1 nuclear import machinery.

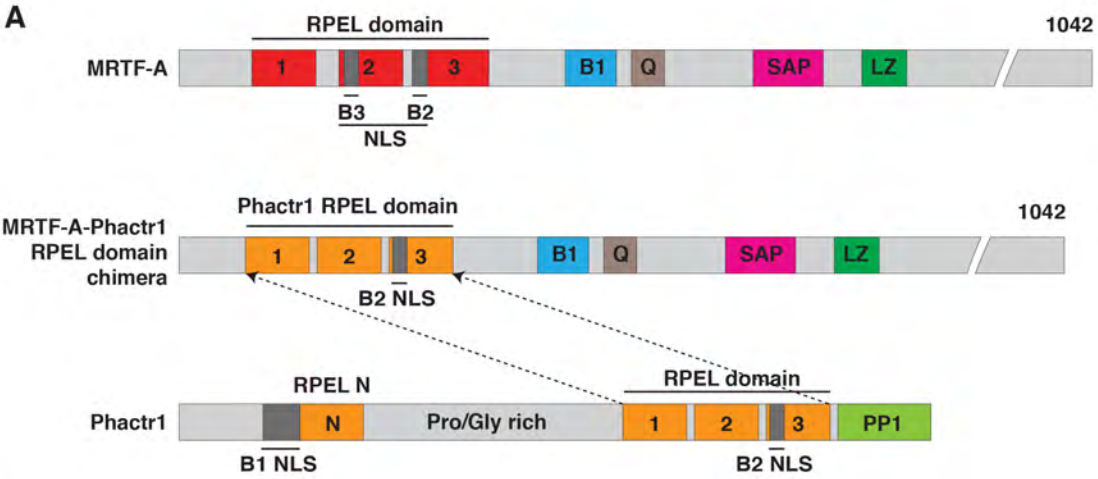
A
RPEL domain
1042
MRTF-A
1
2
3
B1
Q
SAP
LZ
B3
B2
NLS
Phactr1 RPEL domain
1042
MRTF-A-Phactr1
RPEL domain
chimera
1
2
3
B1
Q
SAP
LZ
B2 NLS
RPEL N
RPEL domain
Phactr1
N
Pro/Gly rich
1
2
3
PP1
B1 NLS
B2 NLS

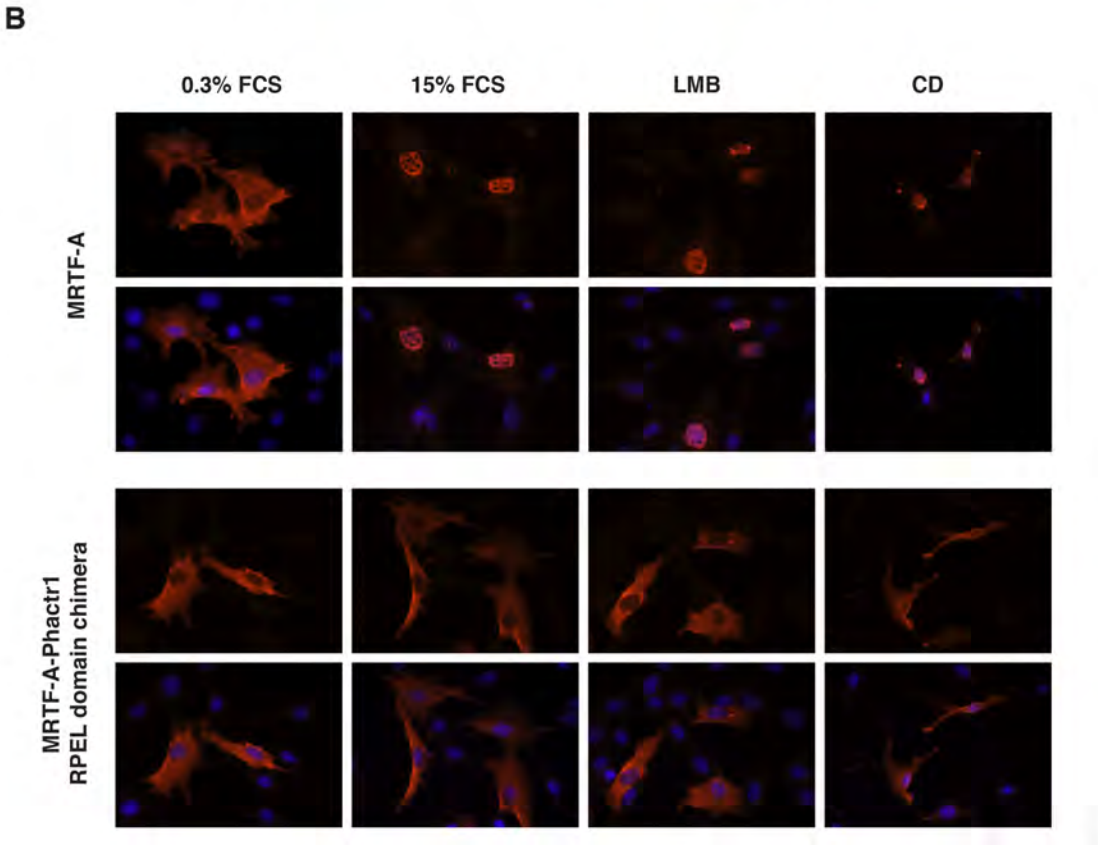
B
0.3% FCS
15% FCS
LMB
CD
MRTF-A
MRTF-A-Phactr1
RPEL domain chimera

**Figure 3.8 Phactr1 RPEL domain is not functionally replaceable.**

**(A)** Schematic representation of the constructs used to perform the assay. As a control, HA-tagged MRTF-A construct was used; 'MRTF-A-Phactr1 RPEL domain chimera' was also HA-tagged (for construct generation, see; 'Materials and methods'); RPEL motifs from Phactr1 are shown in orange and MRTF-A RPEL motifs are coloured in red (junctions are: N-terminal **(MRTF-A) …HRGRNPN**//*LAMKVCR… (Phactr1)*, C-terminal *(Phactr1) …FSDYVEV*// **IIVGQVN… (MRTF-A)**; other domains are labeled as in Figure 1.8 (MRTF-A) and Figure 1.16 (Phactr1). **(B)** Subcellular localisation of MRTF-A and 'MRTF-A-Phactr1 RPEL domain chimera' in starved and stimulated cells and upon 10 μM Cytochalasin D (CD) and 30 nM Leptomycin B (LMB) treatment visualised by immunofluorescence.

## 3.3 Phactr1 nuclear import

### 3.3.1 Two nuclear localisation signals in Phactr1 are recognised by the PredictProtein algorithm

#### *3.3.1.1 The PredictProtein server*

PredictProtein is a widely used online tool, designated for protein sequence analysis (Rost et al., 2004). Since 1999, it has been the standard protein structure and function prediction server. Currently, PredictProtein deals with multiple protein alignments, predicting protein domains and unusual regions, evaluating secondary structure of the protein with high accuracy and, most importantly, assessing protein domains function. It has been reported that PredictProtein server is very accurate in finding NLS sequences (Rost et al., 2004). To investigate the mechanism of Phactr1 nuclear import, we therefore employed PredictProtein to find potential NLSs within Phactr1 sequence.

#### *3.3.1.2 NLS sequences found with PredictProtein algorithm.*

Having found a reliable tool to investigate presence of NLS sequences in Phactr1, we analysed Phactr1 sequence using PredictProtein algorithm. Within full-length Phactr1 we were able to characterise two separate basic sequences as potential NLSs. The first sequence, B1 ($^{108}$RRRSKFANLGRIFKPWKWRKKK$^{129}$) is located at the N-terminus of Phactr1 and the second one, B2 ($^{493}$KREIKRRL$^{500}$) is close to the C-terminus (Figure 1.16). Previous studies have shown that there are two types of common nuclear localisation signals: (1) monopartite, which contain one sequence of basic residues and (2) bipartite, which contain two short basic sequences separated by a linker (Dingwall and Laskey, 1991; Robbins et al., 1991). We therefore speculated that

the B1 sequence represents a bipartite NLS with two basic sequences ($^{108}$RRR$^{110}$) and ($^{126}$RKKK$^{129}$) flanking a linker. In contrast, B2 sequence would represent a monopartite NLS. In order to test this hypothesis, we performed mutagenesis of these sequences and examined the nuclear accumulation of Phactr1.

### 3.3.2 Nuclear accumulation of Phactr1 is mediated by two RPEL-associated nuclear localisation signals.

We firstly deleted the B1 region in Phactr1 (Phactr1ΔB1) to test the effect on nuclear accumulation of Phactr1. In serum-stimulated cells, Phactr1ΔB1 was almost completely cytoplasmic, which suggests that the B1 region is required to promote nuclear import of Phactr1. Within the B1 sequence, the highest level of homology is seen at the basic flanking sequences. The B1 N-terminal flanking sequence: $^{108}$RRR$^{110}$ in Phactr1 is represented in both Phactr2 and Phactr4 by "KRK" and in Phactr3 by "RRN". The C-terminal basic region of B1: $^{126}$RKKK$^{129}$ is identical in all Phactr family. We therefore sought to substitute basic residues in those regions with clusters of alanines (Figure 3.9). The N-terminal B1 mutant RRR108-110AAA (R3A) was constitutively cytoplasmic as was the KKK127-129AAA (K3A) C-terminal B1 basic cluster mutant. When the mutations were combined, the R3A,K3A mutant also exhibited constitutive cytoplasmic localisation (Figure 3.9). This result suggests that two clusters of basic residues in B1 sequence are responsible for the maintenance of Phactr1 import.

To examine the presence of the C-terminal NLS, we performed mutagenesis of the B2 region (Figure 3.9). We mutated the three first amino acids of the predicted sequence into an alanine cluster: KRE493-495AAA (KRE/3A) and found that this mutant did not accumulate in the nucleus as efficiently as WT Phactr1. Mutation of subsequent three amino acids in B2: KRR497-499AAA caused even more significant inhibition of Phactr1 nuclear accumulation (Figure 3.9).

Interestingly, the B1 sequence is in high proximity to RPEL-N, a G-actin interaction site. Similarly, the B2 region overlaps with RPEL3. It was previously shown that the nuclear localisation signal in MRTF-A is also located within the RPEL motifs (Pawlowski et al., 2010). We therefore sought to test how the actin-free, constitutively nuclear Phactr1 mutant (Phactr-xxx) behaves in the context of NLS mutations. We combined the cytoplasmic B1 mutant K3A with the xxx mutation (Figure 3.9) and found that Phactr1-xxxK3A was predominantly nuclear in unstimulated cells. This suggests that abolishing acting binding uncovers the B2 region. We then combined xxxK3A mutations with the B2 mutation KRE/3A to achieve complete inhibition of Phactr1 import. In this case, Phactr1-xxxK3A,KRE/3A was indeed much more cytoplasmic, but the inhibition of nuclear import was not complete. However, we noted that this mutant did not respond to signal, suggesting that its import signals are severely impaired. The fact that we were not able to inhibit import completely in this context might suggest that further, weak import signals are present in Phactr1 (see: 'Discussion').

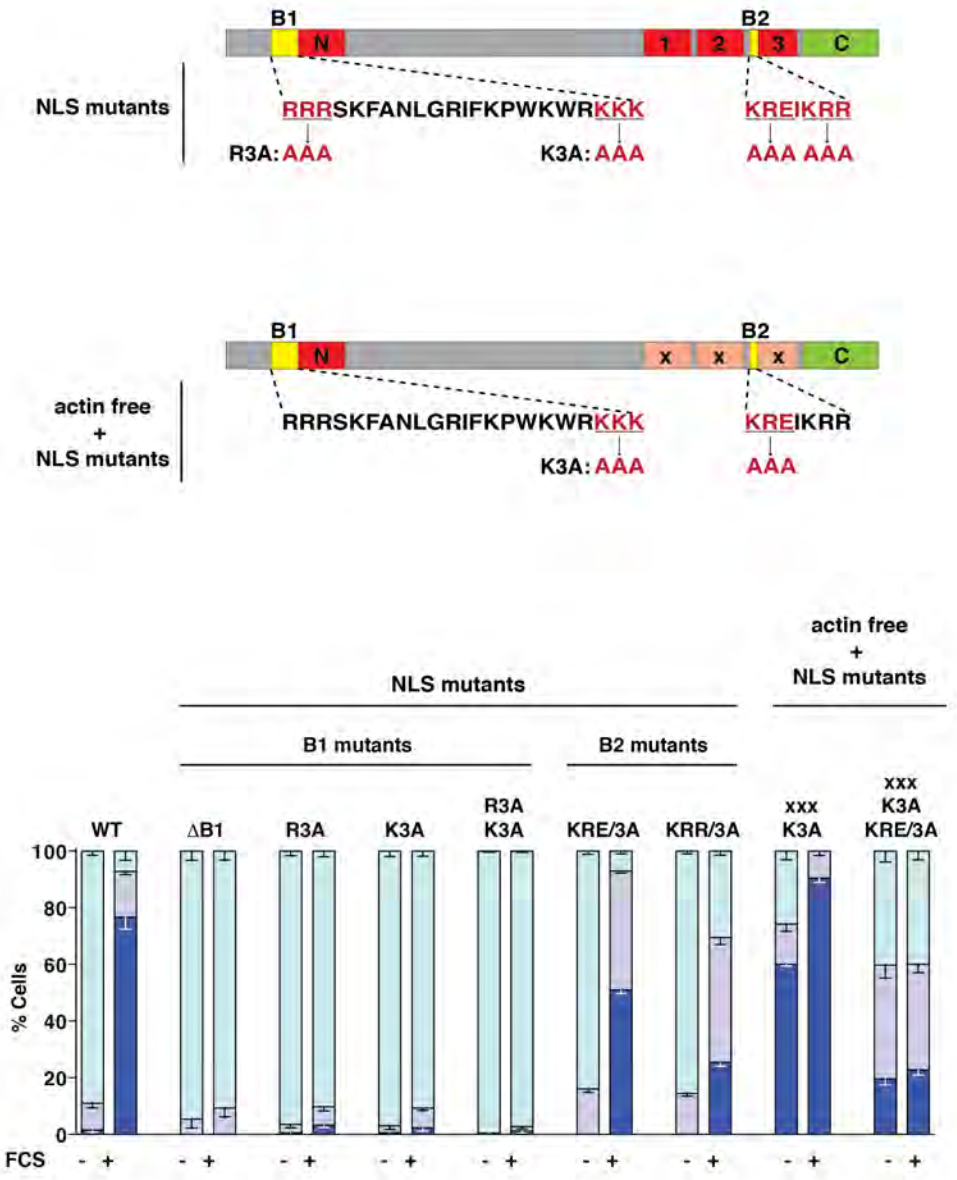


**Figure 3.9 Nuclear localisation signals in Phactr1.**

(Top) Schematic representation of Phactr1 mutants, showing wild-type and mutant Phactr1 nuclear localisation signals B1 and B2. (Bottom) Localisation of different Phactr1 NLS mutants in resting and serum-stimulated cells, assessed as in Figure 3.1; WT, wild-type; mutants are described in the text.

### 3.3.3 Importin β is required for serum induced Phactr1 nuclear accumulation.

Having identified sequences responsible for mediating Phactr1 import, we next sought to determine the nuclear import pathway, which is utilised by Phactr1. The most common nuclear import pathway involves a heterodimer of Importinα (Impα) and Importinβ (Impβ) with up to 50% of receptor-mediated protein import events in the cell utilising this machinery (Lange et al., 2007). It was previously demonstrated that Impα –Impβ heterodimers are required and sufficient for MRTF-A nuclear import. Because both Phactr1 and MRTF-A accumulate in the nucleus in response to Rho-actin signalling and cellular G-actin levels, we hypothesised that they might also exploit similar nuclear import machinery. To test this hypothesis we used the RNA interference approach to knockdown endogenous Impβ in NIH3T3 fibroblasts and monitored Phactr1 nuclear accumulation (Figure 3.10 A and B). Depletion of Impβ1 completely abolished serum-induced Phactr1 nuclear accumulation, suggesting that the nuclear import of Phactr1 is Importin α–β dependent (Figure 3.10 B) (depletion of Impβ1 was performed by Jessica Diring).

To directly test the interaction between Phactr1 and Impα –Impβ heterodimer, we employed an Impα–β pull-down assay. We expressed GST-fusion Phactr1 derivatives containing two truncated constructs of Phactr1 (Figure 3.10 C). GST-Phactr1-N171 contained the B1 region together with RPEL-N while GST-Phactr1-392C consisted of the triple RPEL domain and the C-terminal PP1-binding region. Because we previously found that the middle region of Phactr1 is not required for Phactr1 import, we did not include it is the assay. Consistent with the Impβ1 knockdown experiment, in pulldown assay, Phactr1 derivatives efficiently recovered recombinant Impα–β from solution (Figure 3.10 C) (Impα–β pulldown assay was performed by Jessica Diring).

### 3.3.4 Importin α-β and actin compete for binding to the Phactr1 N- and C-terminal regions.

During previous studies of MRTF-A we learned that G-actin binding RPEL motifs and Impα–β binding sites overlap. Pawlowski and colleagues showed a molecular mechanism for MRTF-A nuclear import, where monomeric actin competes with Impα-Impβ complex for binding the RPEL domain of MRTF-A (Pawlowski et al., 2010).

We reasoned that due to the overlap of the B2 region and the RPEL3 motif as well as close proximity of RPEL-N and the B1 region, G-actin might be in direct competition with Impα-Impβ heterodimer. Therefore, we titrated latrunculinB-actin (G-actin) against constant amounts of N-terminal (GST-Phactr1-N171) and C-terminal (GST-Phactr1-392C) Phactr1 in the Impα/Impβ pulldown assays. The addition of G-actin to the binding reaction effectively competed for binding with both Impα and Impβ (Figure 3.10 C).

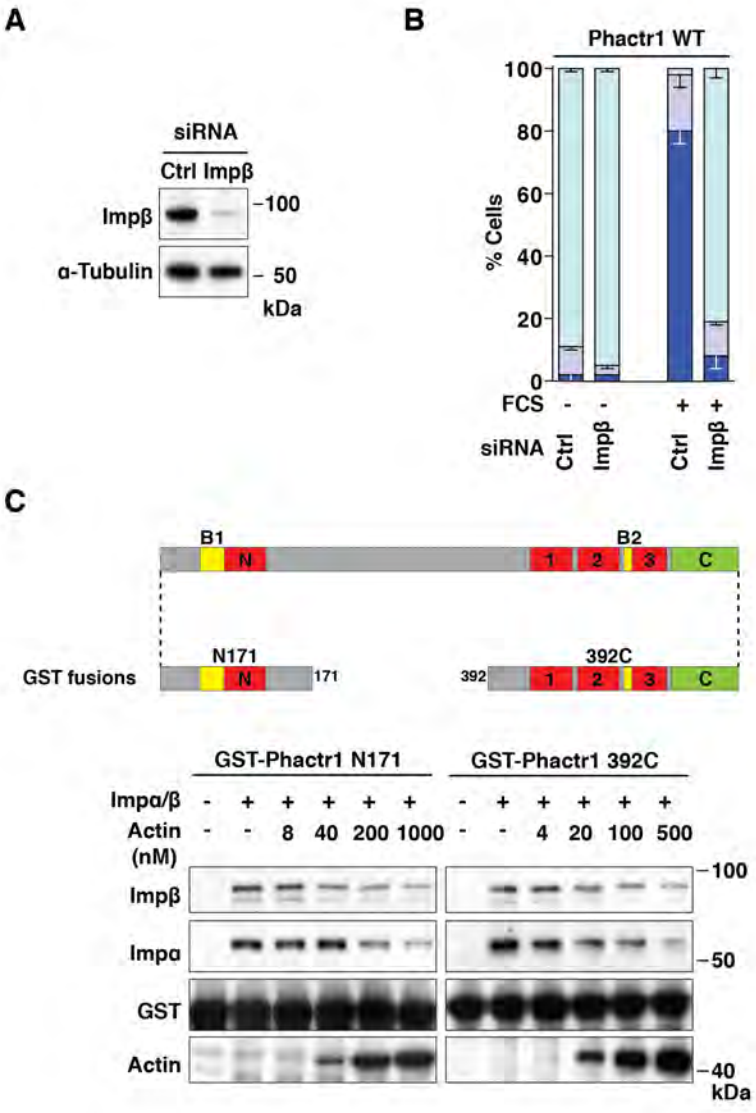


**Figure 3.10 Impα–β-dependent import signals in Phactr1 are actin dependent.**

**(A)** Depletion of Imp-β shown by western blotting. **(B)** Localisation of wild-type Phactr1 in resting and serum-stimulated cells with or without Imp-β depletion showing requirement of Imp-β activity for Phactr1 nuclear accumulation in NIH3T3 cells; localisation was assessed as in Figure 3.1. **(C)** Actin competes with Impα–Impβ for binding to the Phactr1 N- and C-termini. GST-Phactr1 fusion derivatives containing either the N- or C-terminal NLS elements (schematic representation of Phactr1 showing wild-type Phactr1, GST-Phactr1 N171 and GST-Phactr1 392C is shown on top) were used for pulldown of recombinant Impα or Impβ in the presence of increasing amounts of LatB–actin. Bound proteins were analysed by immunoblotting. Performed by Jessica Diring.

Taken together, these data elucidate the presence of two Impα-β-dependent nuclear import signals (B1 and B2) in Phactr1 and shows that Impα-β heterodimer competes with actin for Phactr1 binding similarly to MRTFs (Hirano and Matsuura, 2011; Pawlowski et al., 2010). Because NLSs in Phactr1 are associated with the N- and C-terminal RPEL motifs, we hypothesised that the integrity of both RPEL-N and the RPEL domain might be required for Phactr1 regulation.

### 3.3.5 Inhibition of Phactr1 accumulation by elevated actin requires both RPEL-N and the RPEL domain.

Studies of MRTF-A interaction with actin allowed us to understand how actin regulates nuclear accumulation of MRTF-A and activity of SRF. When the concentration of cellular G-actin was artificially elevated by the expression of a R62D non-polymerising actin mutant, the nuclear accumulation of MRTF-A was blocked (Miralles et al., 2003; Posern et al., 2002; Sotiropoulos et al., 1999). The organisation of actin binding sites in Phactr1 is fundamentally different from that in MRFT-A, as the single RPEL-N motif is separated from the RPEL domain by the relatively long middle region of the protein, containing around 250 amino acids. We have already shown that subtle R->A mutation of RPEL-N or deletion of the whole RPEL-N sequence has no effect on Phactr1 nuclear accumulation in serum-induced cells (Figure 3.6). Because we found that both the N-terminal and the C-terminal regions mediate Phactr1 import and Impα-β compete with actin binding for those sites, we tested the behaviour of RPEL domain and RPEL-N deletions during artificial actin elevation (Figure 3.11).

Firstly, we tested the localisation of Phactr1 upon overexpression of wild-type actin. We found that elevating actin levels in cells leads to inhibition of Phactr1 nuclear accumulation. Similarly, when the G-actin level was elevated through addition of R62D actin, Phactr1 import was blocked. Deletion of the entire RPEL domain in Phactr1 (Δ123) led to constitutive nuclear localisation and elevating actin levels had no inhibitory effect in this context. When we deleted RPEL-N (ΔN), this mutant was much less susceptible to actin overexpression in comparison with wild-type Phactr1 (Figure

3.11 B and C). This result shows that overexpression of actin inhibits Phactr1 nuclear accumulation and that this inhibition requires the integrity of both RPEL-N and the C-terminal RPEL domain. We therefore suggest that saturation of all the G-actin binding sites in Phactr1 is required for efficient inhibition of its nuclear accumulation in the context of actin overexpression. Moreover, this finding is consistent the view that actin binding to the RPEL domain in essential for maintaining Phactr1 in the cytoplasm.

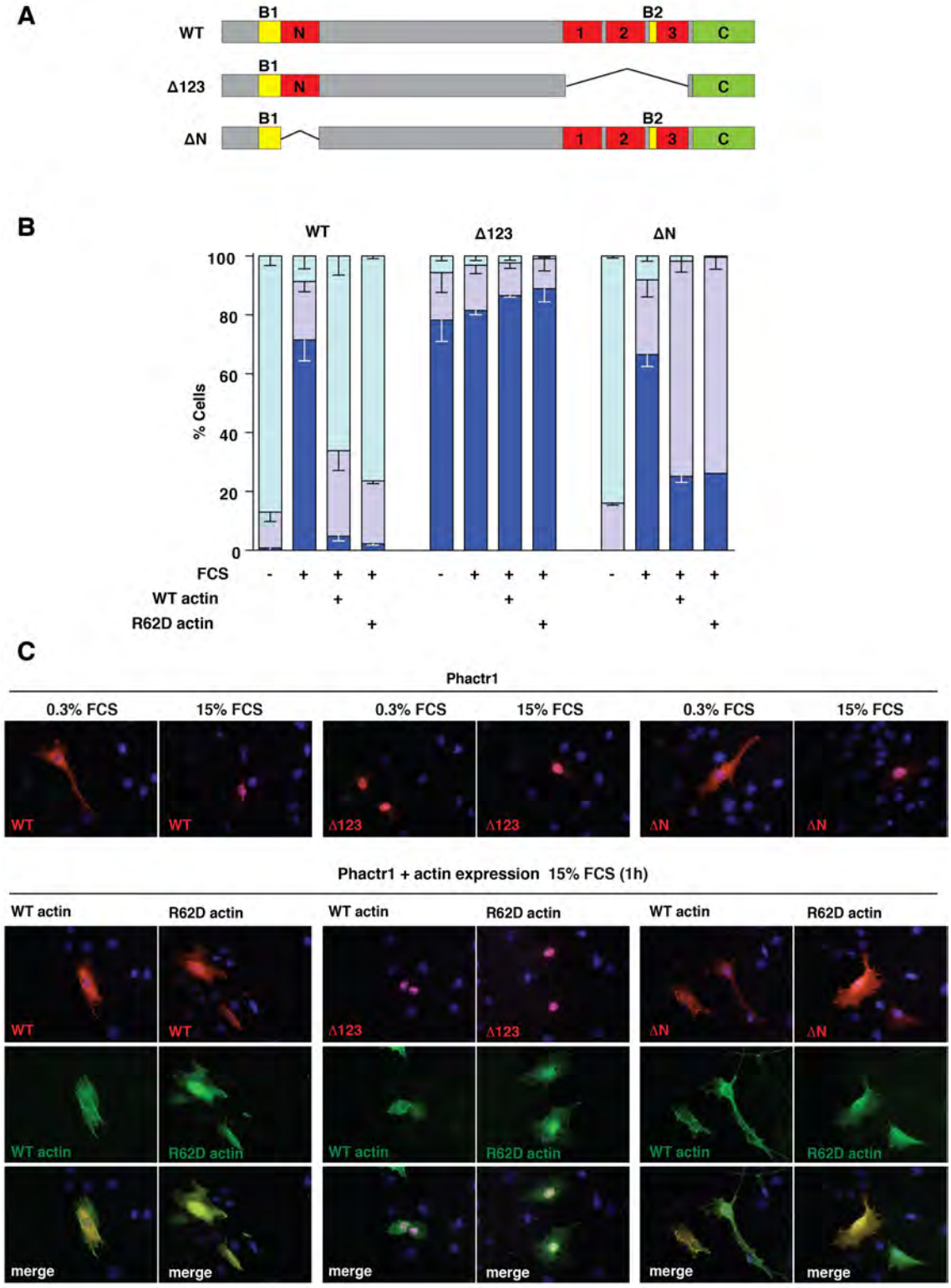
A
B1
B2
WT
N
1
2
3
C
Δ123
ΔN
B
WT
Δ123
ΔN
100
80
60
40
20
0
% Cells
FCS
WT actin
R62D actin
C
Phactr1
0.3% FCS
15% FCS
WT
Δ123
ΔN
Phactr1 + actin expression 15% FCS (1h)
WT actin
R62D actin
merge

**Figure 3.11 Actin-mediated inhibition of Phactr1 nuclear accumulation.**

Integrity of both RPEL-N and the C-terminal RPEL domain is required for the inhibition of Phactr1 nuclear accumulation by actin overexpression. **(A)** Schematic representation of constructs used in the localisation assay; deletion of RPEL domain (Δ123); deletion of RPEL-N (ΔN). **(B)** Phactr1 derivatives were co-expressed with wild-type actin or non-polymerisable actin R62D and their localisation before and after serum stimulation was scored as in Figure 3.1. **(C)** Immunofluorescence microscopy images representing cells scored in part B.

## 3.4 Phactr1 interaction with PP1

### 3.4.1 Activated Phactr1 interacts with PP1

It was previously shown that Phactr family of proteins interact with Protein Phosphatase 1 (PP1), but the relevance of this interaction and the mechanism of PP1 binding was not well understood (Allen et al., 2004; Sagara et al., 2009; Sagara et al., 2003). Because Phactr proteins bind actin through RPEL motifs, with the C-terminal RPEL domain playing a dominant role, we were intrigued that the PP1 binding site overlapped with the RPEL domain (Sagara et al., 2003). Consequently, we undertook a biochemical analysis of the PP1 binding region in Phactr1, to determine its role and mechanism of PP1 interaction.

We have previously learned that Phactr1 responds to stimulus by accumulating in the nucleus in NIH3T3 cells. Therefore, we first attempted to investigate the localisation of PP1 in this cell line. Because PP1 is a protein ubiquitously expressed in all tissues, we characterised the localisation of endogenous PP1. Using immunofluorescence microscopy, we visualised PP1 in the cells that were transiently expressing wild-type and constitutively nuclear Phactr1-xxx, before and after serum stimulation. We found that the localisation of endogenous PP1 was not altered in response to serum and PP1 was primarily nuclear with some diffuse cytoplasmic staining (Figure 3.12 A). However, when Phactr1 was localised in the nucleus, the nuclear staining of PP1 was much more defined. We could observe strong co-localisation of Phactr1 and PP1 in the nucleus of NIH3T3 cells.

This finding suggests that Phactr1 and PP1 might interact in the nucleus. To test this hypothesis we used a co-immunoprecipitation assay, where we expressed Phactr1 and PP1 and determined the recovery of wild-type and Phactr1-xxx before and after serum stimulation. Adding serum, which induces nuclear accumulation of wild-type Phactr1, significantly increased recovery of Phactr1 in PP1 immunoprecipitates. In

contrast, the interaction between constitutively nuclear Phactr1-xxx and PP1 was considerably stronger than between wild-type Phactr1 and PP1, and it did not increase upon stimulus (Figure 3.12 B).

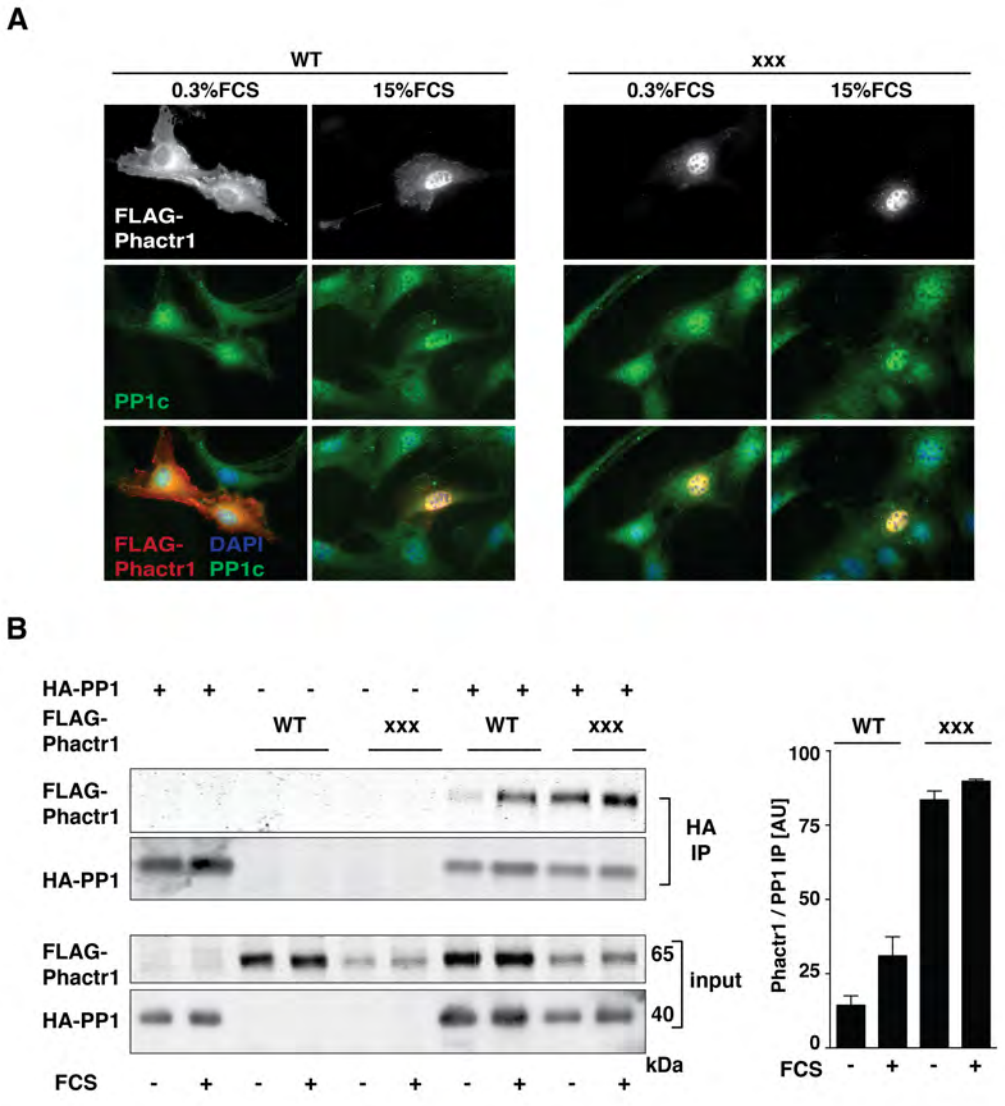


**Figure 3.12 Activated Phactr1 interacts with PP1.**

**(A)** Subcellular localisation of PP1. PP1 was visualised by fluorescence microscopy in cells transfected with FLAG-tagged wild-type Phactr1 (WT) or Phactr1-xxx before and after serum stimulation. **(B)** Nuclear accumulation of Phactr1 correlates with increased PP1 binding. Cells were transfected with wild-type Phactr1 or Phactr1-xxx and HA-tagged PP1; interaction between PP1 and Phactr1 before and after serum stimulation was monitored by quantitative immunoblotting of immunoprecipitates with FLAG and HA antibodies using ImageQuant Analysis Software (AU, arbitrary units).

### 3.4.2 The RPEL domain in Phactr1 is required for PP1 binding

Since the PP1-binding C-terminal sequence is located immediately next to the actin-binding site, we attempted to investigate the requirement of the RPEL domain for PP1 binding. To address this issue, we performed co-immunoprecipitation assays in resting NIH3T3 fibroblasts, where we co-expressed PP1 with the four mutants and/or truncations of Phactr1 (Figure 3.13 A). Consistent with our previous result, when Phactr1-xxx was expressed we could observe protein interaction, but no interaction was detected when Phactr1-xxx lacked the C-terminal region (xxxΔC). Deletion of the RPEL domain from Phactr1 (Δ123) was also sufficient to abolish the recovery of Phactr1 in PP1 immunoprecipitates. This result shows that Phactr1 lacking its RPEL domain, even though it is constitutively nuclear, is not able to bind PP1. Furthermore, the C-terminal deletion is sufficient to abolish binding of PP1 to both wild-type and Phactr1-xxx (Figure 3.13 B).

### 3.4.3 Actin and PP1 bind competitively to Phactr1

The results presented above show that the RPEL repeat and the conserved C-terminal region are both required for the interaction with PP1. This finding is consistent with previous study of Phactr3 (Sagara et al., 2003) and suggests that actin might compete with PP1 for Phactr1 binding. To verify that possibility, we tested the PP1-Phactr1 interaction directly. We co-expressed the GST-Phactr1 C-terminal fusion and PP1 in bacteria (Figure 3.13 B), and added increasing amounts of LatB-actin to the GST-Phactr1-PP1 complex. As a result, LatB-actin efficiently competed with PP1 for binding. To control the specificity of the interaction, we utilized cytochalasin D, whose binding site on actin overlaps that of the RPEL motif (Mouilleron et al., 2008; Nair et al., 2008; Vartiainen et al., 2007). Cytochalasin D was able to substantially impair the competition between actin and PP1. Previous co-immunoprecipitation assays showed that the PP1-Phactr1 interaction is less efficient than PP1-Phactr1-xxx interaction,

which suggests that even lower G-actin concentrations are sufficient to effectively compete with PP1 for Phactr1 binding.

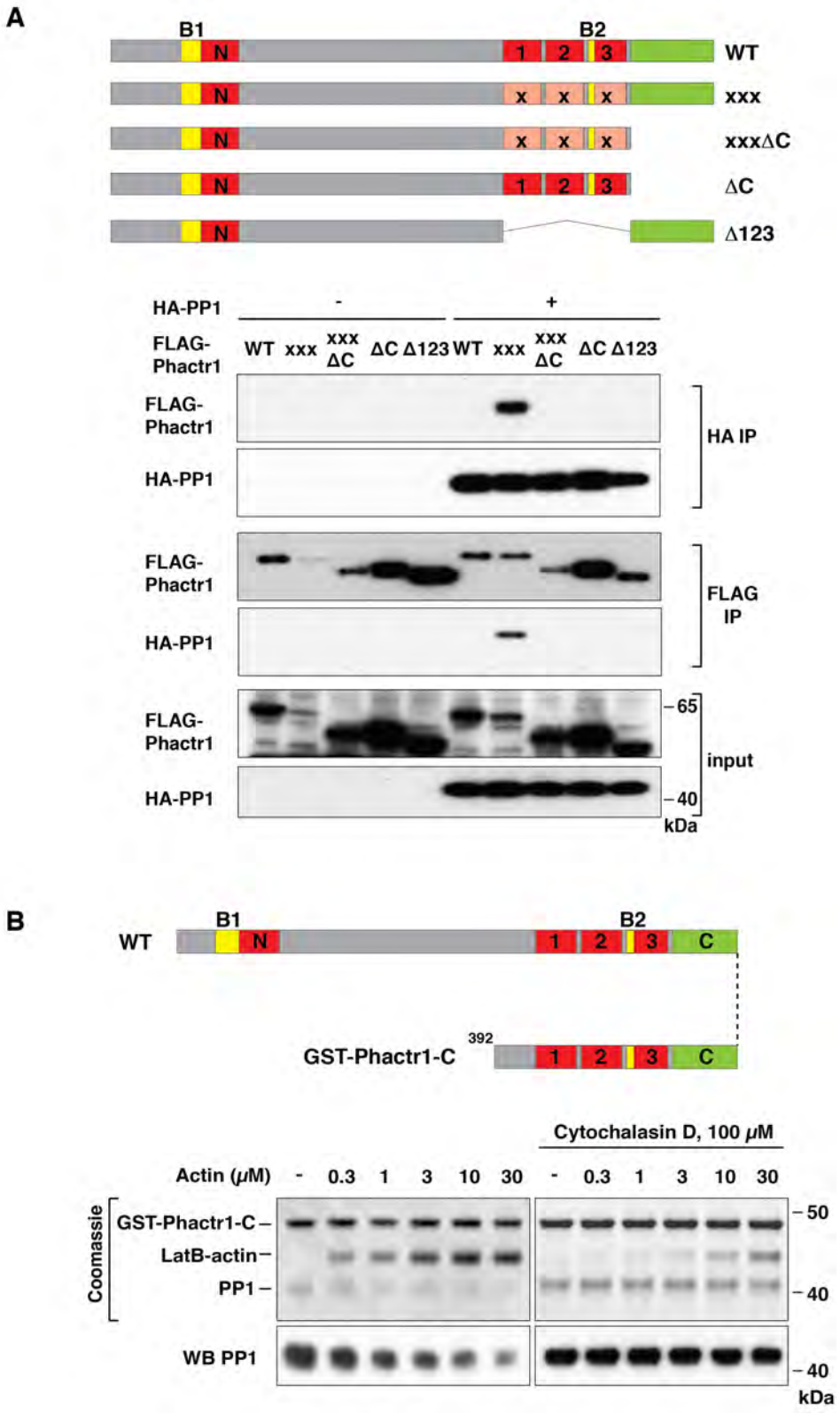

**Figure 3.13 Actin and PP1 bind competitively to Phactr1.**

**(A)** Phactr1 interaction with PP1 requires both the RPEL domain sequences and the conserved C-terminal sequences. Interaction between the indicated Phactr1 mutants (top) and PP1 in serum-starved cells was monitored by co-immunoprecipitation assay as in Figure 3.12 B. (**B**) G-actin competes directly with PP1 for Phactr1 binding. GST-Phactr1 392C and PP1 were co-expressed in bacteria (GST fusion is schematically shown on the top). The resulting complex was purified and incubated with increasing amounts of LatB–actin in the presence or absence of 100 mM cytochalasin D. GST-Phactr1 392C-bound proteins were recovered by pulldown and analysed by Coomassie blue staining or immunoblotting (WB). GST pulldown performed by Jessica Diring.

### 3.4.4 Phactr1-PP1 interaction induces actomyosin rearrangements in NIH3T3 fibroblasts.

Abolishing actin binding in Phactr1 has a toxic consequence in NIH3T3 fibroblasts (Figure 3.7 B). Because loss of actin binding enhances the interaction between Phactr and PP1, this effect might be linked to Phactr1-dependent PP1 behaviour. Consistent with this idea, we observed striking actomyosin rearrangement in the cytoplasm of cells expressing constitutively nuclear Phactr1-xxx. We analysed the appearance of the phenotype in the context of Phactr1-PP1 interaction and examined the connection between the observed phenotype and nuclear localisation of Phactr1.

#### *3.4.4.1 Phactr1-xxx expression induces actomyosin foci and thickened fibres*

Analysis of F-actin localisation in cells expressing Phactr1-xxx led to the discovery of actin rearrangements in the cytoplasm of NIH3T3 cells. Deletion of the PP1-binding C-terminal region (xxxΔC) abolished the formation of F-actin rearrangement (Figure 3.14 A). Interestingly, we observed two similar types of rearrangements in cells expressing Phactr-xxx, 'foci' and 'thick fibres' (Figure 3.14 A). Presumably, this is the appearance of the same phenotype, but one shows much more punctate staining (foci) and the other appears as bright lines of phalloidin staining (thick fibres).

Similar F-actin phenotypes were previously observed when the N-terminal catalytic domain of ROCK was expressed (Sahai et al., 1998). In addition, overexpression of ROCK in HeLa cells promoted formation of stress fibres and adhesion complexes (Leung et al., 1996). Phalloidin staining of those HeLa cells showed actin rearrangements that were analogous to those observed upon activated Phactr1 expression. Because ROCK is a potent kinase of MLC (Amano et al., 1996), we co-transfected cells with Phactr1-xxx and MLC-GFP and stained cells with an antibody

against MLC. This staining revealed that the F-actin rearrangements induced by Phactr1-xxx expression contained MLC (Figure 3.14 E and F). Taken together these data indicate that the presence of aberrant fibres in the cytoplasm of cells expressing Phactr1-xxx contain both F-actin and myosin, and that their formation is dependent on PP1 binding to Phactr1.

Analysis of the phenotype caused by Phactr1-xxx expression led us to notice the appearance of a similar, but less pronounced phenotype in stimulated cells expressing wild-type Phactr1 (Figure 3.14 C). This phenotype was observed in only low frequency of untransfected cells (Figure 3.14 D). Because this phenotype differed from the one induced by Phactr-xxx, it was referred to as ‘bright fibre’. Confirming the requirement of PP1-Phactr1 interaction, deletion of the PP1 binding site abolished the formation of actomyosin rearrangements (Figure 3.14 D).

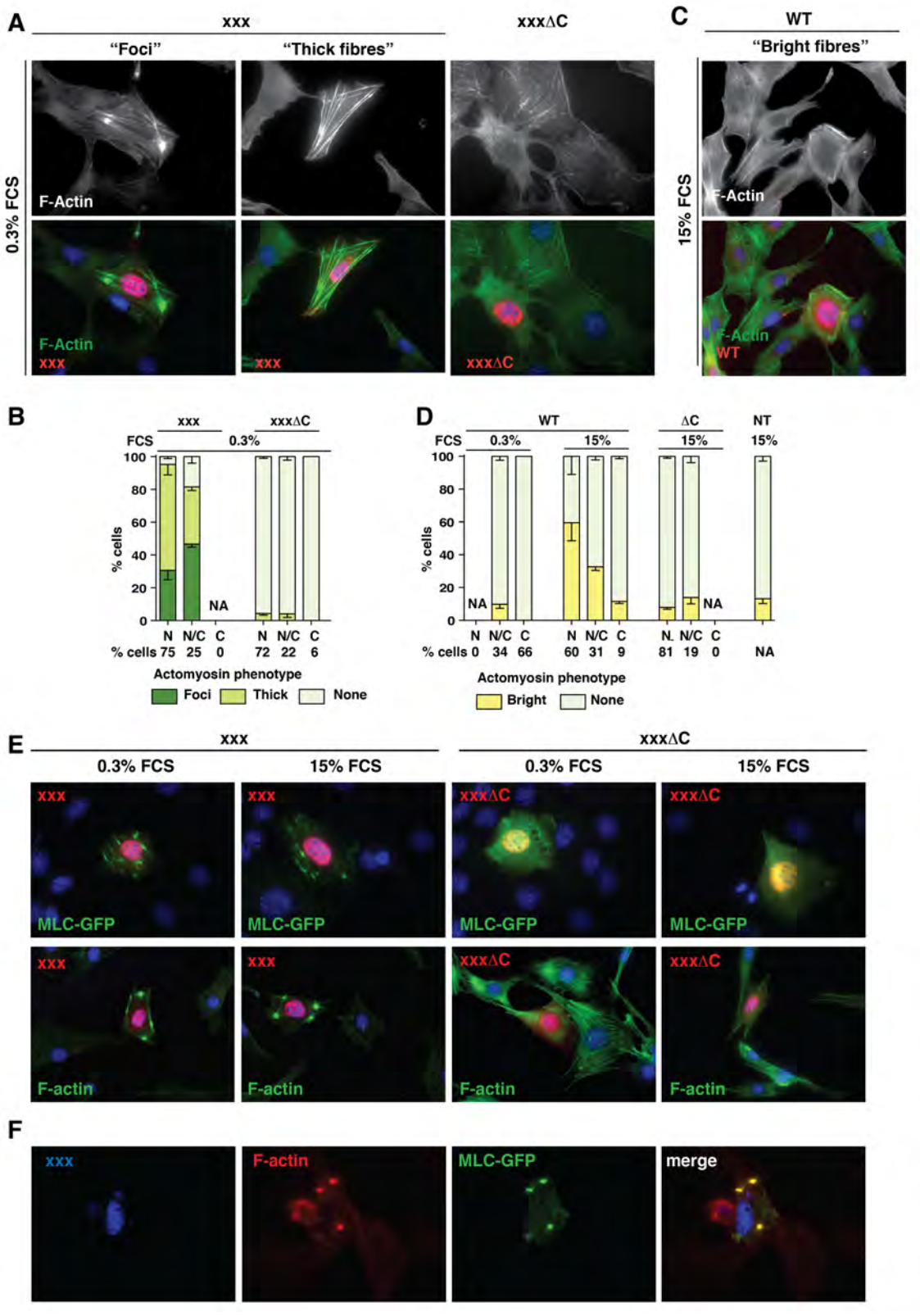
A
xxx
xxxΔC
"Foci"
"Thick fibres"
0.3% FCS
F-Actin
F-Actin
xxx
xxx
xxxΔC
C
WT
"Bright fibres"
15% FCS
F-Actin
F-Actin
WT
B
xxx
xxxΔC
FCS
0.3%
% cells
NA
N N/C C N N/C C
% cells 75 25 0 72 22 6
Actomyosin phenotype
Foci
Thick
None
D
WT
ΔC
NT
FCS
0.3%
15%
15%
15%
% cells
NA
NA
N N/C C N N/C C N N/C C
% cells 0 34 66 60 31 9 81 19 0 NA
Actomyosin phenotype
Bright
None
E
xxx
xxxΔC
0.3% FCS
15% FCS
0.3% FCS
15% FCS
MLC-GFP
F-actin
F
xxx
F-actin
MLC-GFP
merge

**Figure 3.14 Active Phactr1 induces actomyosin assembly in fibroblasts.**

**(A)** NIH3T3 cells transfected with the FLAG-tagged Phactr1-xxx and Phactr1-xxxΔC were maintained in 0.3% FCS for 20 hours before visualisation of Phactr1 and F-actin by fluorescence microscopy. The actomyosin phenotypes were scored as 'Foci', 'Thick Fibres' or 'none'; further examples of specimen phenotypes are shown in Figure 3.15. **(B)** Quantitation of cytoskeletal phenotypes in cells expressing Phactr1-xxx and Phactr1-xxxΔC scored according to Phactr1 subcellular localisation (N, N/C or C as in Figure 3.1; 100 cells per experiment; error bars, s.e.m. of three independent experiments; NA, not applicable). **(C)** 'Bright-fibre' F-actin phenotype in NIH3T3 cells expressing exogenously wild-type Phactr1 (WT) after 1 hour of serum stimulation. Further examples of specimen phenotypes are shown in Figure 7.1. **(D)** Quantitation of 'bright-fibre' phenotypes in cells expressing Phactr1-WT or Phactr1ΔC, scored as in B. Phenotypes of serum-stimulated untransfected cells (NT) are scored on the right. **(E)** MLC rearrangement upon expression of constitutively active Phactr1-xxx (xxx, shown on the left), but not C-terminal deletion mutants (xxxΔC, shown on the right). Cells were transfected with the indicated FLAG-tagged Phactr1 derivatives alone (bottom panel) or together with MLC-GFP (top panel) and maintained in 0.3% serum for 20h, with or without stimulation with 15% serum, before visualisation of Phactr1, MLC-GFP and/or F-actin. **(F)** For simultaneous view of F-actin, MLC and Phactr1-xxx, cells were transfected with FLAG-tagged Phactr1-xxx and GFP- MLC (as in top panel of part E) before visualization of Phactr1 (blue), F-actin (red), and MLC-GFP by fluorescence microscopy.

#### *3.4.4.2 Actomyosin rearrangements requires nuclear localisation of Phactr1*

We noted that formation of actomyosin structures in the cytoplasm of NIH3T3 cells was strictly linked to nuclear localisation of Phactr1 (Figure 3.14 B and D). We evaluated this association by quantifying the number of transfected cells containing each version of the phenotype ('foci', 'thick fibres' and 'bright fibres') and expressing Phactr1 in different compartments (Figure 3.14 B and D). Because (1) Phactr1-xxx is predominantly nuclear, (2) Phactr1-xxxΔC expression does not promote formation of actomyosin structures and (3) phenotype caused by wild-type Phactr1 is less pronounced, these constructs did not provide enough insight into the relationship between Phactr1 nuclear localisation and cytoskeletal rearrangements.

However, during the analysis of Phactr1 import, we designed a nuclear localisation mutant - Phactr1-xxxK3A,KRE/3A, which was nuclear in small proportion of cells (Figure 3.9 and 3.15 A). We therefore took advantage of this mutant to gain insight into the relationship between the occurrence of actomyosin phenotypes and Phactr1 nuclear localisation. Cells exhibiting predominantly nuclear Phactr1-xxxK3A,KRE/3A had a greater preponderance of actomyosin rearrangement than those in which this mutant was cytoplasmic (Figure 3.15 B and C). This data shows that actomyosin structures are formed when Phactr1 is localised in the nucleus.

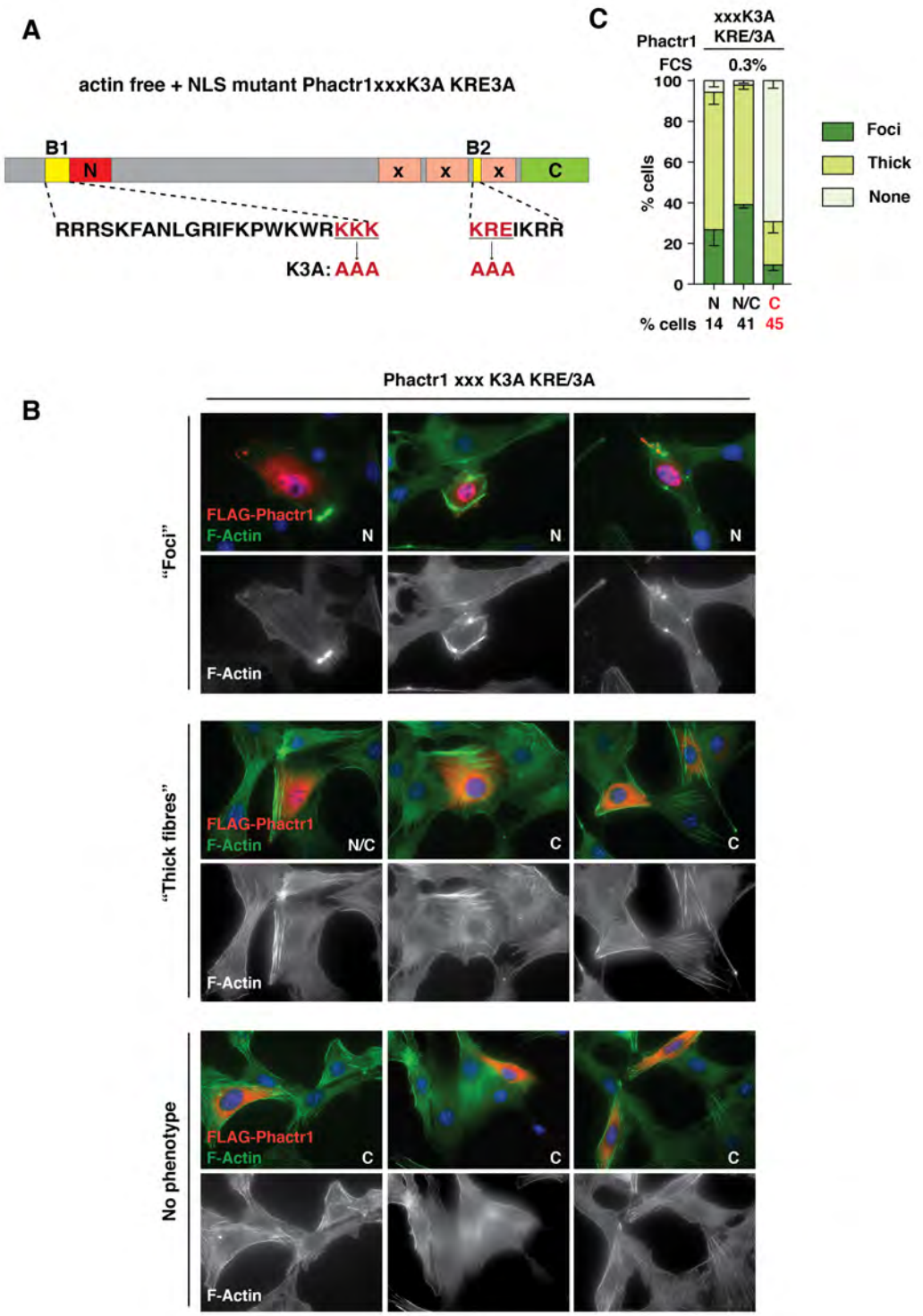
A
actin free + NLS mutant Phactr1xxxK3A KRE3A
B1
N
B2
x
x
x
C
RRRSKFANLGRIFKPWKWRKKK
K3A: AAA
KREIKRR
AAA
C
Phactr1
xxxK3A
KRE/3A
FCS
0.3%
100
80
60
40
20
0
% cells
Foci
Thick
None
N
N/C
C
% cells 14 41 45
B
Phactr1 xxx K3A KRE/3A
"Foci"
"Thick fibres"
No phenotype
FLAG-Phactr1
F-Actin
N
N/C
C
F-Actin

**Figure 3.15 Nuclear Phactr1 induces actomyosin rearrangements.**

Localisation of actin-free NLS mutant Phactr1-xxxK3A,KRE/3A in NIH3T3 cells reveals a correlation between nuclear localisation and aberrant actomyosin structures. **(A)** Schematic representation of Phactr1-xxxK3A,KRE/3A construct shown as in Figure 3.9. **(B)** Cells were transfected with FLAG-tagged Phactr1-xxxK3A,KRE/3A and maintained in 0.3% serum for 20h before visualisation of Phactr1 and F-actin. Subcellular localisation of Phactr1 in each transfected cell was scored as N (nuclear), N/C (pan-cellular) or C (cytoplasmic) and the actomyosin phenotypes were scored as 'foci', 'thick fibres' or 'no phenotype'. Three representative images for each phenotype are shown. **(C)** Summary of the data as in Figure 3.14 B.

#### *3.4.4.3 Phactr1 interacts with PP1 to induce MLC phosphorylation*

We have shown that PP1 binding to Phactr1 is required for the formation of actomyosin rearrangements in the cytoplasm of NIH 3T3 cells following Phactr1 over-expression. The thickened actomyosin fibres contained both F-actin and MLC, which might suggest a defect in the regulation of actomyosin contractility. To investigate this idea, we analysed the phosphorylation state of myosin II regulatory light chain (MLC) and the ATPase activity of Myosin II – two crucial aspects in the regulation of actomyosin contractility (Figure 3.16 A).

The activation of myosin II depends on the phosphorylation of its light chain (MLC). Several different kinases phosphorylate MLC at two highly conserved residues, T18 and S19, therefore promoting actomyosin contractility (Matsumura, 2005). The best-known kinases involved in this process include ROCK and MLCK (myosin light chain kinase). In addition, ROCK can inhibit myosin phosphatase activity, which leads to higher phosphorylation status of MLC on those two residues (for review, see (Ito et al., 2004) and section: 'Actomyosin contractility').

To investigate the role of Phactr1 in the regulation of actomyosin contractility, we evaluated the phosphorylation status of T18 and S19 upon expression of Phactr1-xxx. Because expression of Phactr1-xxx in NIH3T3 fibroblasts has a toxic effect on them and affects protein amounts, we quantified the phosphorylation state in relation to the expression of MLC-GFP. The proportion of co-expressed MLC-GFP phosphorylated at T18 and S19 was increased two-fold by the expression of Phactr1-xxx (Figure 3.16 B). This result suggests that Phactr1 interacts with PP1 to induce actomyosin phosphorylation.

Contractility in cells arises from the interaction between F-actin filaments, molecular motor Myosin II and crosslinkers. To become a part of the contractile machinery, Myosin II must form a multimer (Sellers, 2000). In addition, Myosin II achieves motor activity through its heavy chain (the N-terminal 'head' region), which contains ATP binding sites. The ATPase activity of myosin II is linked to the

continuous attachment and detachment of F-actin filaments (Rayment et al., 1993). ATPase activity is therefore crucial for actomyosin formation. Firstly, ATPase mediates hydrolysis of ATP and phosphate release to promote actin movement by conformational change. Secondly, it promotes ADP dissociation and facilitates detachment of the myosin motor from actin.

To better understand the role of Phactr1 in actomyosin assembly, we used a specific inhibitor of myosin II ATPase activity – blebbistatin (Straight et al., 2003) (Figure 3.16 A). Blebbistatin is widely used in the fields of cell motility and muscle physiology as it is permeable to cell membranes and can inhibit both muscle and non-muscle myosin II without targeting other myosins. The inhibitory effect of blebbistatin is achieved by binding to the myosin-ADP-$P_i$ complex, blocking phosphate release. Blebbistatin acts directly on ATPase activity, which has many implications in *in vivo* studies (Kovacs et al., 2004) (Figure 3.16 B). After expressing Phactr1-xxx in NIH3T3 cells, we treated the cells with blebbistatin. Actomyosin structures formed upon active Phactr1 expression rapidly dispersed upon treatment with blebbistatin (Figure 3.16 C). This result is consistent with the presence of MLC in the F-actin structures.

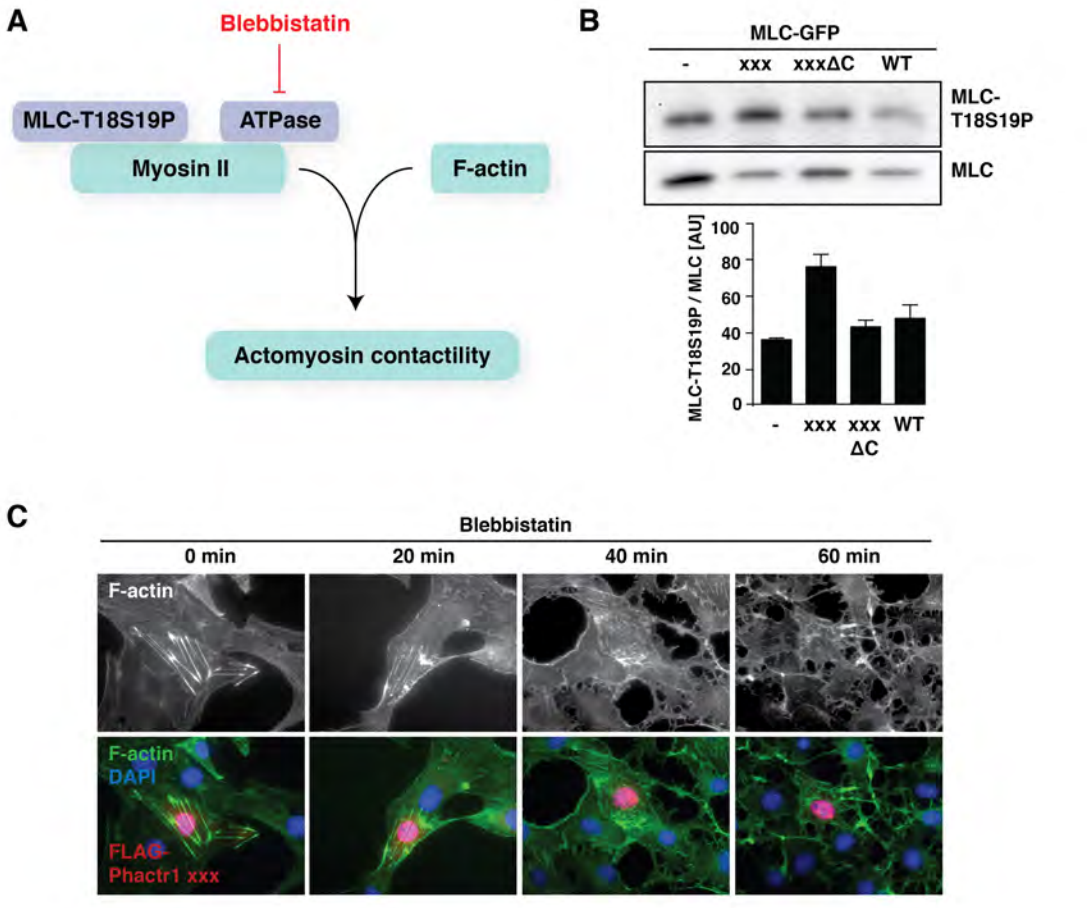


**Figure 3.16 Phactr1 interacts with PP1 to induce actomyosin contractility through MLC phosphorylation.**

**(A)** MLC-T18S19 phosphorylation and Myosin II ATPase activity are crucial for actomyosin crosslinking; blebbistatin specifically inhibits Myosin II ATPase activity (for details, see text). **(B)** Phactr1-xxx expression increases MLC-T18S19 phosphorylation. NIH3T3 cells expressing the indicated FLAG-tagged Phactr1 derivatives and MLC-GFP were maintained in 0.3% FCS, and cell lysates were analysed by quantitative immunoblotting using anti-Phospho-MLC2 (T18/S19) and anti-MLC2 antibodies (AU, arbitrary units). Note that Phactr1-xxx is expressed at a significantly lower level. Error bars represent the s.e.m. of three independent experiments. **(C)** Rapid dispersal of aberrant actomysin structures in Phactr1-xxx-expressing NIH3T3 cells following treatment with 20 μM blebbistatin.

## 3.5 Conclusions

In this chapter, I have presented the role of G-actin binding in the regulation of RPEL protein, Phactr1 in NIH3T3 fibroblasts. Rho-actin signalling induced nuclear accumulation of Phactr1, but not other Phactr family members. The RPEL domain in Phactr1 was required for the nuclear accumulation of Phactr1. I have uncovered a role for two basic sequences in Phactr1 and characterised them as nuclear localisation signals, an Importin α-β interaction sites. Actin effectively competed with Importin α-β for Phactr1 binding, therefore mediating its nuclear accumulation.

I also showed that Phactr1 binding to PP1 causes actomyosin rearrangement in NIH3T3 fibroblasts. Moreover, G-actin competes with PP1 for Phactr1 binding thus having regulatory function. The nuclear localisation of Phactr1 correlated with the appearance of actomyosin phenotypes and we suggest that Phactr1 binds PP1 in the nucleus of NIH3T3 cell, where PP1 is predominantly localised. Lastly, I showed that the expression of active Phactr1 promotes actomyosin contractility through phosphorylation of MLC at S19 and T18. Because the activity of Phactr1 depends on its association with G-actin, I will now present molecular details of this interaction.

# Chapter 4. Structural analysis of Phactr1 interaction with actin

## 4.1 Aims

The G-actin binding RPEL motifs play crucial roles in the regulation of Phactr1 localisation and activity. Having shown the molecular mechanism of Phactr1 nuclear accumulation and its interaction with PP1, we now sought to analyse structural details of Phactr1 interaction with G-actin. The structural approach to study RPEL motifs has previously proven to effectively illustrate how the nucleocytoplasmic shuttling of another RPEL protein, MRTF-A is regulated by actin (Mouilleron et al., 2008; Mouilleron et al., 2011).

In resting cells, MRTF-A is kept in the cytoplasm by actin and the Crm1-dependent nuclear export machinery, but it shuttles to the nucleus upon signal-induced depletion of the G-actin pool (Vartiainen et al., 2007). Transcriptional activity of MRTF-A is critically regulated by actin binding to three RPEL motifs located at the N-terminus of the protein (Guettler et al., 2008; Miralles et al., 2003; Vartiainen et al., 2007). In addition, artificial elevation of the G-actin concentration in the cell inhibits MRTF-A import. Structural studies showed that the RPEL domain from MRTF-A binds five G-actin molecules to form a pentavalent G-actin•$RPEL^{MRTF-A}$ complex with one actin binding to each of the three RPEL motifs and additional actins interacting with the intervening spacers. Within the pentavalent complex, the NLS sequences B2 and B3 are occluded by actin and not accessible to Importin α-β (Hirano and Matsuura, 2011; Mouilleron et al., 2011). The pentavalent G-actin•$RPEL^{MRTF-A}$ complex is unstable in solution, but a trivalent G-actin•$RPEL^{MRTF-A}$ complex, lacking G-actin binding to RPEL3 and Spacer2 is stable. Structural analysis of these complexes led to the proposal of the MRTF-A regulation model by G-actin (Figure 1.11).

We used X-ray crystallography to study Phactr1:G-actin interaction at a molecular level and to better understand the role of actin in Phactr1 regulation. Crystallography of G-actin•Phactr1 complexes and structural analyses shown here were performed in collaboration with Stephane Mouilleron, a postdoc form Neil McDonald's Structural Biology Laboratory at the LRI.

## 4.2 G-actin•RPEL$^{Phactr1}$ domain complex

To gain insight into the mechanism of G-actin binding by the RPEL motifs in Phactr1, we firstly focused on the C-terminal actin-binding site - the RPEL domain (referred to here as RPEL$^{Phactr1}$), which contains amino acids 414-528 from Phactr1 (Figure 4.1). This sequence is required to confer Phactr1 nuclear accumulation and is highly similar the RPEL domain from MRTF-A (Figure 4.1 B). We expressed RPEL$^{Phactr1}$ domain in bacteria and evaluated its ability to bind rabbit skeletal muscle α-actin / Mg•ATP / Latrunculin B (referred to here as G-actin). Before crystallization, G-actin-binding properties of RPEL$^{Phactr1}$ domain were assessed by size exclusion chromatography and multi-angle laser light scattering (SEC-MALLS).

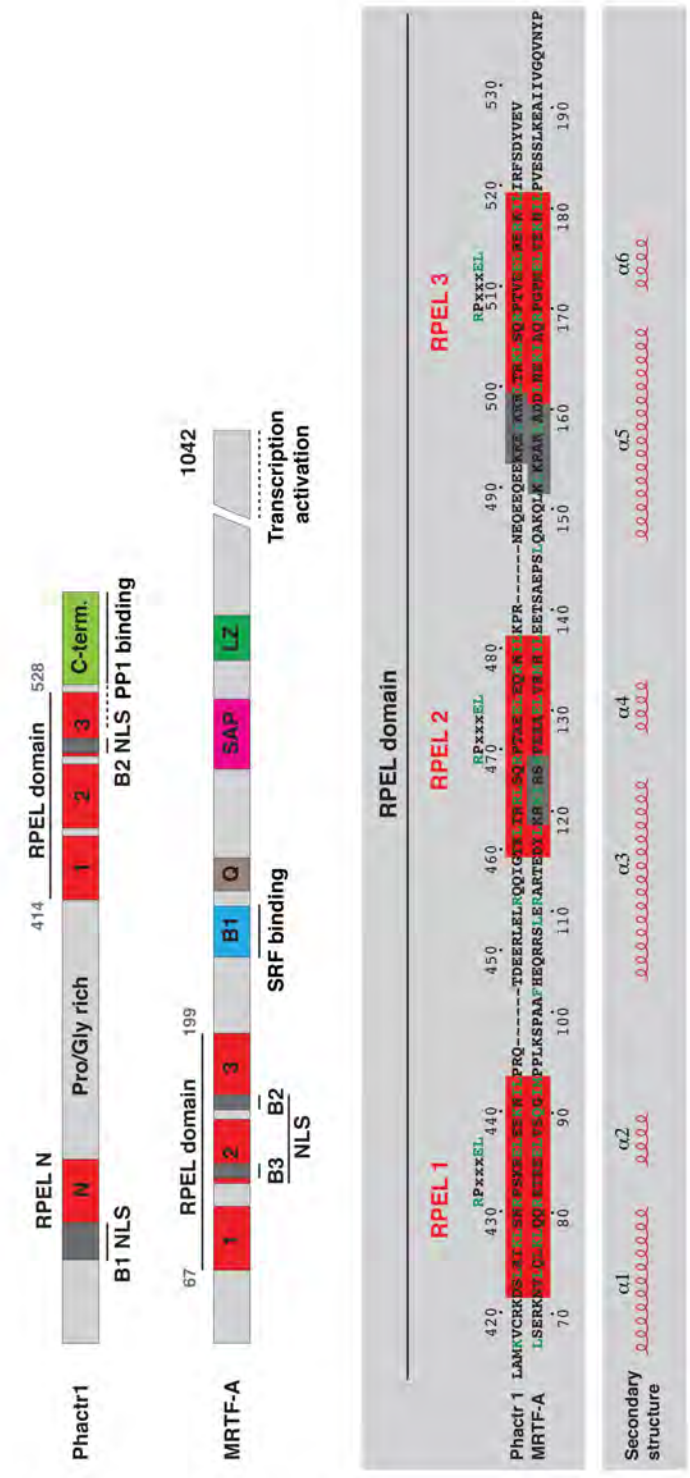
A
Phactr1
RPEL N
N
Pro/Gly rich
414
RPEL domain
528
1
2
3
C-term.
B1 NLS
B2 NLS PP1 binding
MRTF-A
67
RPEL domain
199
1042
1
2
3
B1
Q
SAP
LZ
B3
B2
NLS
SRF binding
Transcription activation
B
RPEL domain
RPEL 1
RPEL 2
RPEL 3
RPxxxEL
Phactr 1
MRTF-A
Secondary structure
α1
α2
α3
α4
α5
α6

**Figure 4.1 Phactr1 and MRTF-A RPEL domains.**

**(A)** Schematic representation of Phactr1 and MRTF-A conserved sequences, shown as in Figure 1.8 and Figure 1.16. **(B)** Domain structure of Phactr1 and MRTF-A RPEL domains; RPEL motifs are show as red boxes; NLS elements are shown as dark grey, secondary structure is indicated and shows helices α1- α6 (red).

### 4.2.1 Complex stoichiometry

#### *4.2.1.1 Size exclusion chromatography*

In order to form G-actin•RPEL$^{Phactr1}$ complex we employed size exclusion chromatography (SEC). This technique separates molecules based on their molecular weight by subsequent exclusion from the pores that form the core of the SEC packing material. The profile is compared to the chromatography of sample molecules with known molecular weights. Because bigger molecules have less access to the porous matrix, they are eluted from the column much quicker than the smaller molecules. Small molecules have access to the pores and need more time to be efficiently eluted. SEC is a technique widely used in the fields of proteomics, biochemistry and cell biology, especially a form of SEC used for the separation of molecules in aqueous solution, gel filtration chromatography.

#### *4.2.1.2 SEC-MALLS*

To precisely measure the molecular weight of the obtained complex, we coupled gel filtration to multi-angle laser light scattering (SEC-MALLS). This technique allows measurement of the average molecular weight of the complex in solution by detecting how particles scatter light. The scattered light is detected at multiple angles by an array of detectors, which allows fast and accurate measurement. This technique essentially differs form classical light scattering, which takes longer and is less precise, because single moving detector is used. SEC-MALLS readout is not affected by the shape of the complex and is therefore more accurate than gel filtration.

#### *4.2.1.3 How we obtained trivalent G-actin•RPEL$^{Phactr1}$ complex*

Studies of the RPEL domain from Phactr1 revealed that it was highly sensitive to proteolysis during affinity-tag purification. The protein was readily targeted by proteases to create a mixture of shorter fragments. Therefore, we could only form complexes containing full length RPEL domain under limiting actin conditions. This approach successfully generated G-actin•RPEL$^{Phactr1}$ complex of the experimental molecular weight of 127kDa ± 2 kDa by SEC-MALLS (Figure 4.2). This is consistent with the apparent approximate domain stoichiometry of 3:1 (G-actin:RPEL$^{Phactr1}$ domain), as the molecular weight of actin is 42kDa and of the RPEL$^{Phactr1}$ domain is 14kDa.

Previously obtained pentavalent G-actin•RPEL$^{MRTF-A}$ domain complex was present in solution only when 4 μM of G-actin were added to the gel filtration buffer. This was due to the instability of the pentavalent complex in solution and the dissociation of actin R3 (bound to RPEL3) and S2 (bound to Spacer2) (Mouilleron et al., 2011). In contrast, the trimeric G-actin•RPEL$^{Phactr1}$ domain complex is unaffected by the presence of G-actin in the buffer (Figure 4.2 B), suggesting that is does not respond to G-actin concentration in the same way as MRTF-A. Because we previously found that, like the RPEL$^{MRTF-A}$ domain, the RPEL$^{Phactr1}$ domain is required to mediate G-actin dependent nucleocytoplasmic shuttling, we sought to analyse the G-actin•RPEL$^{Phactr1}$ domain complex by X-ray crystallography.

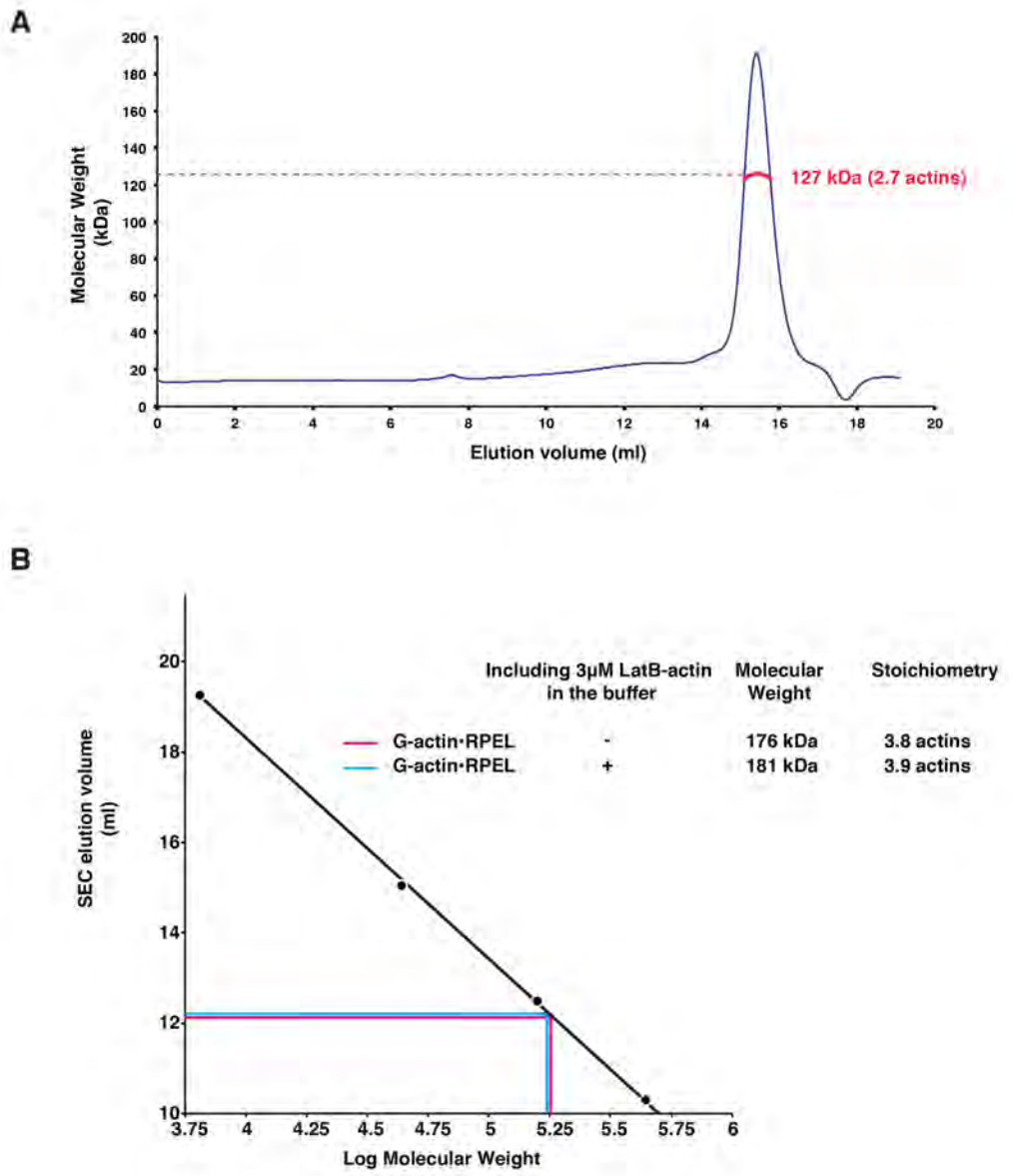


**Figure 4.2 Analysis of G-actin•RPELphactr1 complex stoichiometry.**

**(A)** Size exclusion chromatography (blue line, elution volume) coupled to multi-angle light scattering experiments (SEC-MALLS) indicate that the G-actin•RPEL$^{Phactr1}$ complex has an experimental molecular weight of 127kDa ± 2.0 kDa (red line). This is consistent with a 3:1 G-actin•RPEL$^{Phactr1}$ domain stoichiometry. **(B)** Size exclusion chromatography analysis of actin-RPEL$^{Phactr1}$ complex. Position of the peaks for G-actin•RPEL$^{Phactr1}$ migration in buffer alone and in buffer containing 3 µM LatB-actin are shown. The extended shape of the G-actin•RPEL$^{Phactr1}$ complex slows down its retention time and increases the apparent stoichiometry of the complex measured by size exclusion chromatography to 3.8:1. The apparent stoichiometry is unaffected by the presence of G-actin in the buffer. Stephane Mouilleron, adapted.

### 4.2.2 G-actin•RPEL $^{Phactr1}$ domain crystallisation

We crystallised the G-actin•RPEL$^{Phactr1}$ complex in sitting drop. Crystals reached maximum size in about two weeks and diffracted to 3.3 Å resolution using the Diamond synchrotron X-ray source (Oxford, UK). The structure was solved by molecular replacement using the high-resolution structures of each individual RPEL motifs 1, 2 and 3 bound to G-actin (structures of individual RPEL motifs are described further below). The final structure shows good geometry values with a final $R/R_{free}$ values of 22.2/25.0%. The structure indicates that one G-actin molecule interacts with each RPEL motif in Phactr1 forming a trivalent complex (Figure 4.3 A). Analysis of the structural data allowed establishing that G-actin•RPEL$^{Phactr1}$ crystals contained two trivalent complexes in the asymmetric unit (Figure 4.3 B). Both complexes had identical organization and a root mean square deviation (RMSD) of 1.04Å within the total of 103 RPEL domain Cα atoms (for data collection and refinement statistics see Table 7.3). To confirm the number of G-actin•RPEL$^{Phactr1}$ complexes in solution, small-angle X-ray scattering SAXS analysis was performed. Consistent with the SEC-MALLS analysis, it showed one trivalent G-actin•RPEL$^{Phactr1}$ in solution (Mouilleron et al., 2012) (Figure 7.2).

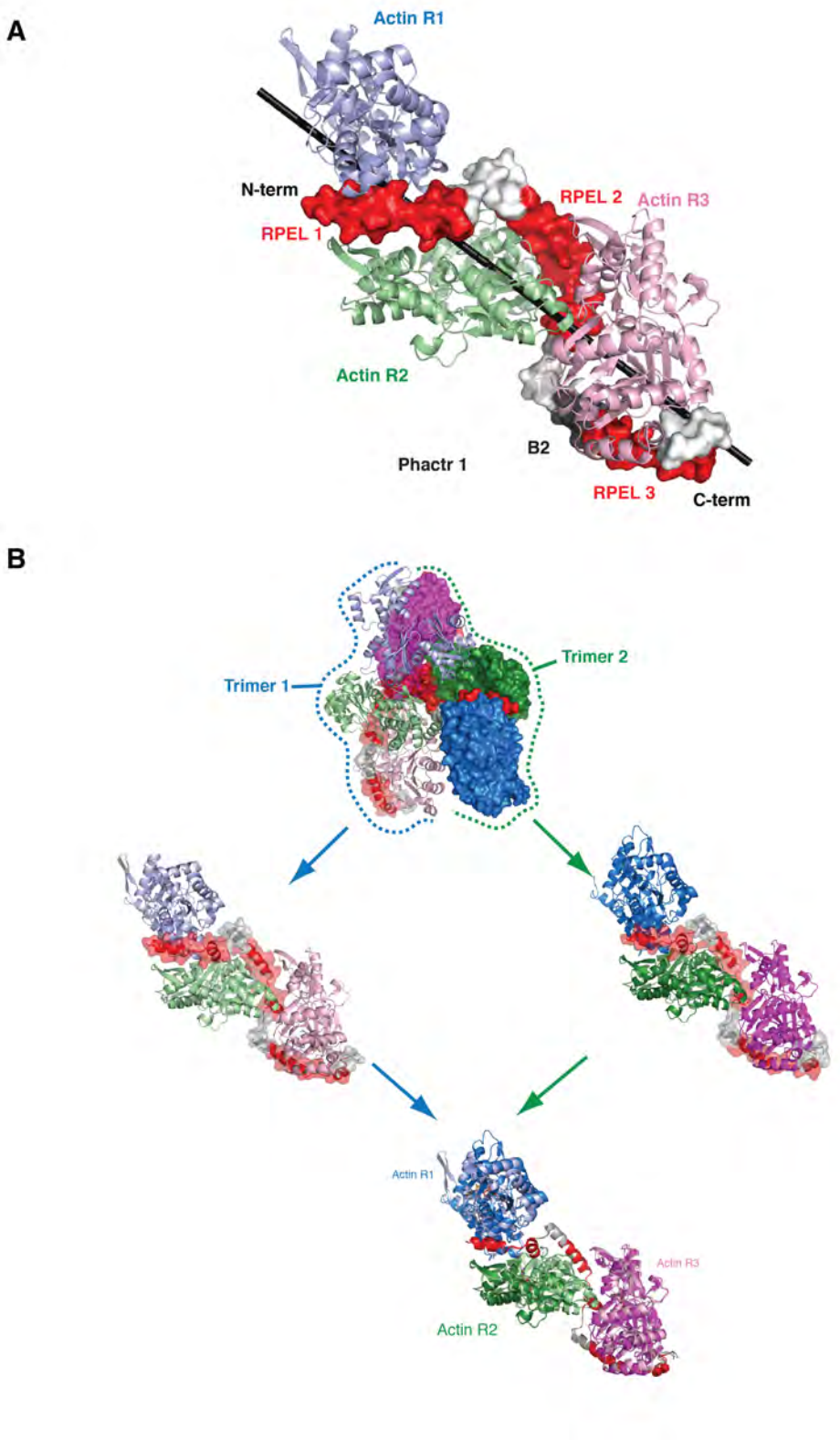
A
Actin R1
N-term
RPEL 2
Actin R3
RPEL 1
Actin R2
B2
Phactr 1
RPEL 3
C-term
B
Trimer 1
Trimer 2
Actin R1
Actin R3
Actin R2

**Figure 4.3 G-actin•RPEL$^{Phactr1}$ complex structure.**

**(C)** Structure of the Phactr1 RPEL domain crank (red and white solid rendering) bound to three G-actin molecules (actin R1- pale blue; actin R2 - green, and actin R3 - pink ribbon). The position of the screw axis is shown as a black line; RPEL motifs are shown in red and spacers in grey; the B2 NLS sequence is shown in dark grey. **(B)** The G-actin•RPEL$^{Phactr1}$ domain crystallographic asymmetric unit contains two nearly identical trivalent complexes. Upper panel shows the two trivalent complexes, one as ribbon, the other as a solid surface. Both trivalent complexes superpose closely (lower panel) with a root mean square deviation (RMSD) of 1.04 Å over 103 Cα atoms. Stephane Mouilleron, adapted.

### 4.2.3 G-actin•RPEL$^{Phactr1}$ domain complex assembly

After obtaining structural details of G-actin•RPEL$^{Phactr1}$ domain assembly, we characterised the unusual symmetry of the complex by comparison to known structural symmetries. Enantiomorphic symmetry allows for two proteins to be mirror images, which rotate the plane of polarized light in opposite directions, and therefore are not identical. Most oligomeric proteins, like alcohol dehydrogenase or glutamine synthetase possess rotational symmetry. When the translational symmetry is added to rotational symmetry, helical structures are formed. Helical non-hollow oligomers are built in a way that only several subunits form each turn of the helix. This is achieved by orienting the interacting sites of the monomers to form a tight and narrow filament. F-actin filaments and intermediate filaments are examples of such an assembly. This type of compilation of monomers is called 'open helical assembly', where the monomers can be efficiently added to the filament indefinitely. Because biomolecules are placed in a cellular environment, the filament will technically end when the boundary is met or when subunits run out (for review, see (Goodsell and Olson, 2000)).

#### *4.2.3.1 G-actin•RPEL$^{Phactr1}$ domain complex forms a closed helical assembly*

Assessment of the structural features of the trivalent G-actin•RPEL$^{Phactr1}$ complex indicates that G-actin interacts with the RPEL$^{Phactr1}$ domain to form a helical assembly. This type of complex cannot be categorised as an open assembly though, as it has defined length. It is rather a rare example of closed helical assembly, where two bordering monomers of G-actin flank the one in the middle.

Three G-actin molecules: actins R1, R2 and R3 are assembled around the helical axis of the left-handed RPEL$^{Phactr1}$ domain 'crank' (Figure 4.3 A). The complex has elongated shape and is very compact. The rigidity of the complex is not a result of the interactions between actins as they make little direct contact with each other. Actins

R1/R2 and R2/R3 have a very limited interface of 235 $Å^2$ and 250 $Å^2$, respectively. The trivalent complex is therefore formed through multiple contacts between RPEL motifs and actin. Below, I will describe interactions between $RPEL^{Phactr1}$ motifs and G-actin, based on the comparison to the G-actin•$RPEL^{MRTF-A}$ domain complex. Two classes of G-actin•RPEL interactions will be described, primary and secondary contacts.

### 4.2.4 G-actin•$RPEL^{MRTF-A}$ and G-actin•$RPEL^{Phactr1}$ domains adopt identical trajectories.

Analysis of the G-actin•$RPEL^{Phactr1}$ domain complex revealed similarities to the previously established G-actin•$RPEL^{MRTF-A}$ domain complex. Their comparison also highlights the differences in the length of spacers between RPEL motifs in MRTF-A and Phactr1 (Figure 4.4 A). Spacers that join RPEL motifs in MRTF-A are 22 amino acids long each, but in Phactr1 spacers are six amino acids shorter (Figure 4.1 B). It was previously shown that MRTF-A spacers bind G-actin molecules (Mouilleron et al., 2011). Spacer1 of MRTF-A (94-PPLKSPAA**F**HEQRRS**L**ERARTE-115) contains conserved residues that make crucial contacts with G-actin. $F102^{spacer1}$ and $L109^{spacer1}$ are engaged in hydrophobic interactions with the hydrophobic cleft of actin (Mouilleron et al., 2011). Similarly, in Spacer2 of MRTF-A (138-EETSAEPS**L**QAKQLK**L**KRARLA-159) $L146^{spacer2}$ and $L153^{spacer2}$ are engaged in hydrophobic interaction with the hydrophobic cleft of actin. Those conserved, hydrophobic residues are not conserved in the shorter Phactr1 spacers, which are than unable to bind G-actin (Figure 4.4 A). Taken together, interactions that are crucial for the recruitment of spacer actins in G-actin•$RPEL^{MRTF-A}$ domain complex, are missing in G-actin•$RPEL^{Phactr1}$ domain complex. Therefore, Phactr1 binds only three G-actin molecules and not five, like MRTF-A. Nevertheless, both $RPEL^{Phactr1}$ domain and $RPEL^{MRTF-A}$ cranks have very similar trajectories (Figure 4.4 B).

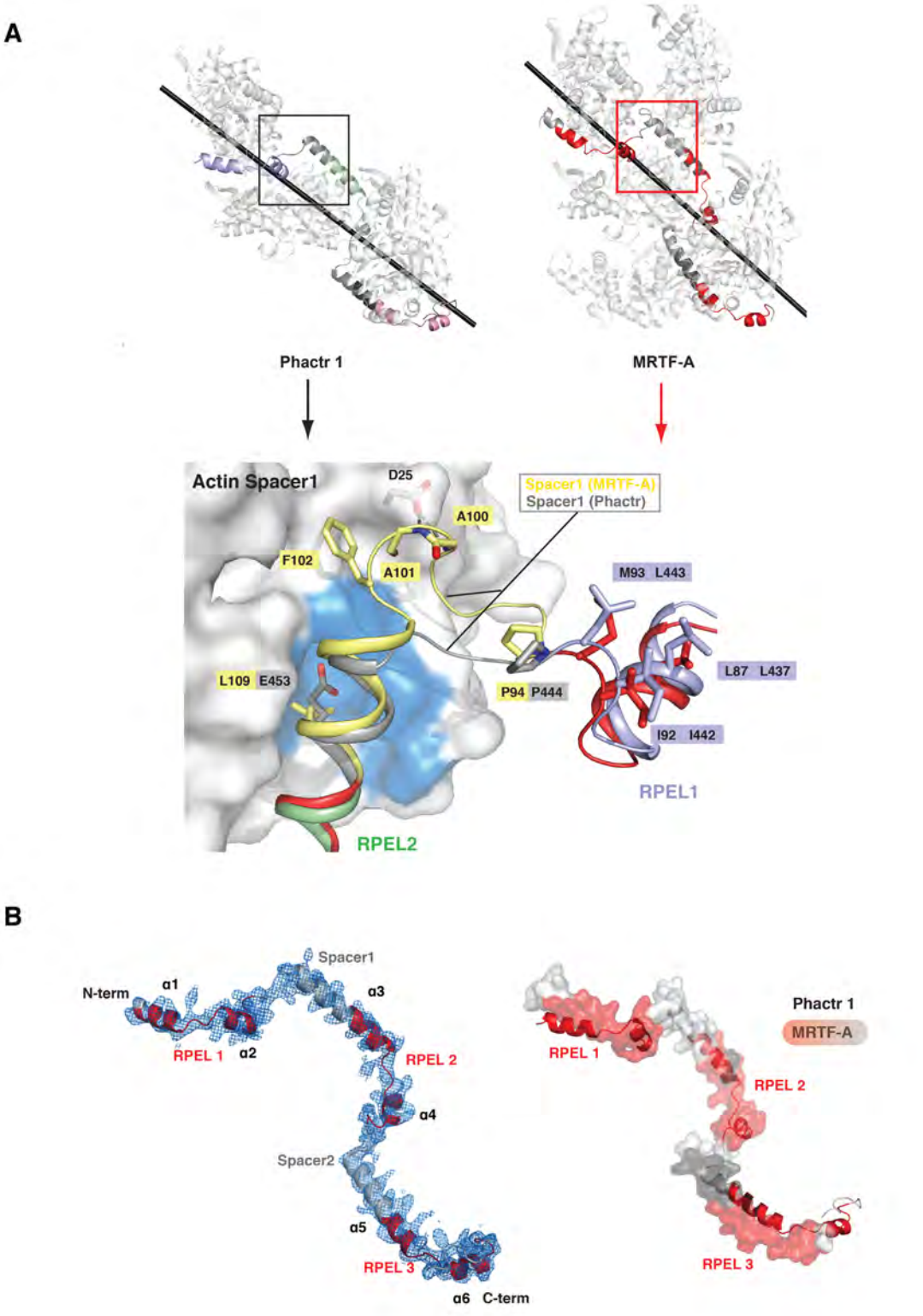
A
Phactr 1
MRTF-A
Actin Spacer1
D25
A100
F102
A101
Spacer1 (MRTF-A)
Spacer1 (Phactr)
M93 L443
L87 L437
L109 E453
P94 P444
I92 I442
RPEL1
RPEL2
B
Spacer1
N-term
α1
α2
α3
RPEL 1
RPEL 2
α4
Spacer2
α5
RPEL 3
α6 C-term
Phactr 1
MRTF-A
RPEL 1
RPEL 2
RPEL 3

**Figure 4.4 Similar trajectories of RPEL$^{Phactr1}$ domain and RPEL$^{MRTF-A}$ domains.**

**(A)** Top panel, schematic of the trivalent Phactr1 and pentavalent MRTF-A RPEL domain assemblies with G-actin indicating the location of the first 'spacer' actin bound to MRTF-A (red frame) and the first spacer in Phactr1 (black frame). Bottom panel, the short spacer sequences within Phactr1 (grey) linking RPEL1 (pale blue) and RPEL2 (green) preclude binding of a spacer G-actin. Comparison with the MRTF-A spacer (yellow) connecting RPEL1 and RPEL2 (red) shows the G-actin cleft binding residues (yellow sticks) are missing in Phactr1. G-actin S1 is shown as a surface rendering with its hydrophobic cleft indicated (blue patch). **(B)** Left, electron density map (shown in blue) for the Phactr1 RPEL domain prior to its inclusion in refinement, overlaid on the refined crank-shaped RPEL domain structure. Right, structural superposition of the RPEL domain crank from Phactr1 (ribbon) and MRTF-A (solid) and their very similar trajectories. Stephane Mouilleron, adapted.

There are two distinct groups of contacts that the RPEL motifs make with G-actins. 'Primary' actin contacts are formed between actin subdomains 1 and 3 hydrophobic clef and ledge and RPEL motif residues. Primary contacts were already observed in the structures of G-actin•RPEL$^{MRTF-A}$ peptides and defined elsewhere (Hirano and Matsuura, 2011; Mouilleron et al., 2008; Mouilleron et al., 2011). Additionally, the G-actin•RPEL$^{Phactr1}$ domain structure contains 'secondary' actin contacts, which RPEL1 and RPEL2 motifs make with their neighbouring actins R2 and R3. Those contacts were not previously observed within the G-actin•RPEL$^{MRTF-A}$ domain complex. Secondary contacts are centred on the interaction between the conserved RPEL glutamate, which points into the opposite direction from the primary contacts (described in detail further below).

Therefore, similar trajectory of the two complexes is based on the conserved interactions between RPEL motifs and G-actins. Screw axes of both complexes have strikingly similar rotational and translational elements with R=155.5°, t=39.5Å for Phactr1 and R=152.9°, t=38.7Å for MRTF-A (screw axes are represented by black lines) (Figure 4.4. A). This suggests that there is a spatial correspondence between the two complexes and that their overall organization is based on the interactions between one RPEL and one G-actin unit in each assembly.

### 4.2.5 Primary actin contacts within the G-actin•RPEL$^{Phactr1}$ domain complex

The primary RPEL contacts were already observed in MRTF-A (Mouilleron et al., 2008) (see section: 'The RPEL motif defines a G-actin binding element'). As predicted, RPEL motifs in Phactr1 engage the G-actin molecule in a similar manner to MRTF-A. The invariant arginines R431$^{RPEL1}$, R469$^{RPEL2}$ and R507$^{RPEL3}$ are all engaged in a salt bridge with the C-terminal carboxylate group of F375 in actin R1, R2 and R3 (Figure 4.5). The conserved L424$^{RPEL1}$/ L428$^{RPEL1}$, L462$^{RPEL2}$/ L466$^{RPEL2}$ and L500$^{RPEL3}$/L504$^{RPEL3}$ make hydrophobic contact with the actin hydrophobic cleft. Within the hydrophobic ledge, helix α2/α4/α6 interacts with G-actin subdomain 3

through L437$^{RPEL1}$/ L443$^{RPEL1}$, L475$^{RPEL2}$/ L481$^{RPEL2}$ and L513$^{RPEL3}$/ L519$^{RPEL3}$. Additional stabilising contacts are observed within the hydrophobic cleft and include I458$^{RPEL2}$ and I496$^{RPEL3}$ interactions with actin R2 and R3 respectively. Moreover, the nitrogen from K497$^{RPEL3}$ bonds with the sidechain of S348 in actin R3 and R516$^{RPEL3}$ docks onto Y166 in actin R3 (Figure 4.5). All those contacts are also present in the structures of individual RPEL$^{Phactr1}$ domain peptides with G-actin and will be discussed further below.

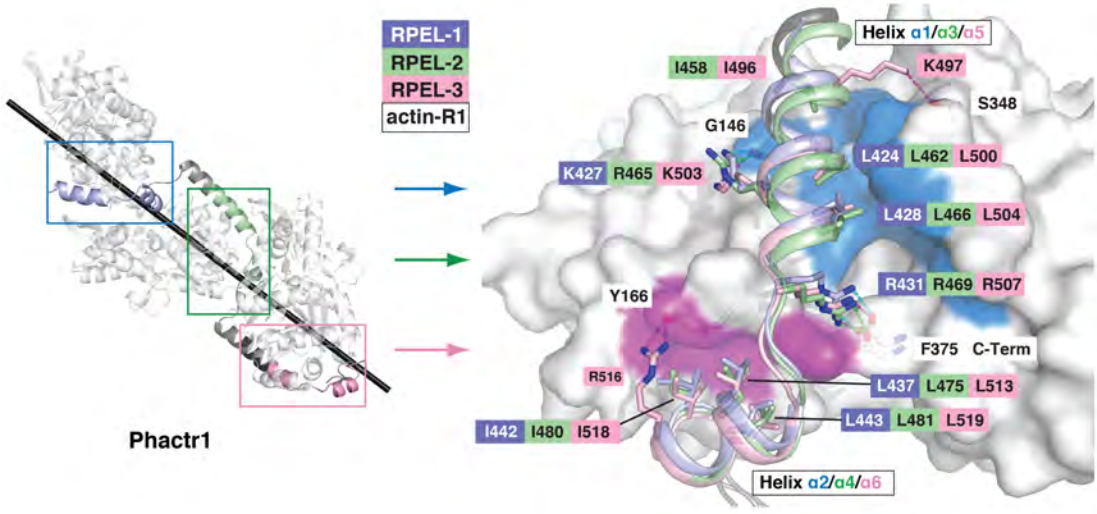


**Figure 4.5 Primary G-actin contacts within the G-actin•RPEL$^{Phactr1}$ domain complex.**
(Left) Schematic indicating the location of primary G-actin binding sites within the trivalent G-actin•RPEL$^{Phactr1}$ domain complex. (Right) Superposition of the three RPEL$^{Phactr1}$ motifs (coloured according to left panel) onto G-actin R1 (pale grey, solid rendering). The panel reveals highly conserved primary actin interactions made by each RPEL; RPEL motif specific contacts are indicated (hydrophobic cleft and ledge surfaces are colored as in Figure 1.10). Stephane Mouilleron, adapted.

### 4.2.6 Secondary G-actin binding sites within the G-actin•RPEL$^{Phactr1}$ domain complex

Structural study of the G-actin•RPEL$^{Phactr1}$ complex revealed additional interactions between RPEL motif and G-actin, which were not previously observed in the G-actin•RPEL$^{MRTF-A}$ domain complex and are referred to here as secondary contacts. Secondary contacts are mediating binding of RPEL1$^{Phactr1}$ to actin R2 and RPEL2$^{Phactr1}$ to actin R3 (Figure 4.3 A). It appears that secondary contacts are less extensive than the primary contacts, but play a critical role in forming the G-actin•RPEL$^{Phactr1}$ domain closed helical assembly.

Residues N430$^{RPEL1}$ and Q468$^{RPEL2}$, N-terminal to the conserved RPEL arginine, hydrogen-bond with the secondary actin S239 sidechain. The C-cap residues of helices $\alpha 2$ and $\alpha 4$, K440$^{RPEL1}$ and R478$^{RPEL2}$ hydrogen-bond secondary actin residue E214 and E214/K215 carbonyls respectively, N-terminal to the 203-216 helix (Figure 4.6). The following RPEL sidechains also closely approach the nucleotide-binding pocket of the adjacent actin, although detailed contacts were not observed at the 3.3Å resolution of the trivalent complex. At the center of the secondary binding site is the conserved RPEL glutamate, which shows a well-defined density despite the absence of any direct contact with neighbouring residues. This definition, and the similar orientation of both E436$^{RPEL1}$ and E474$^{RPEL2}$, is likely to reflect water-mediated hydrogen bonding with secondary actin (Figure 4.6) (Mouilleron et al., 2012). Further insight into secondary contacts was gained during the analysis of the G-actin•RPEL peptide$^{Phactr1}$ structures solved at high resolution (described in the following chapter).

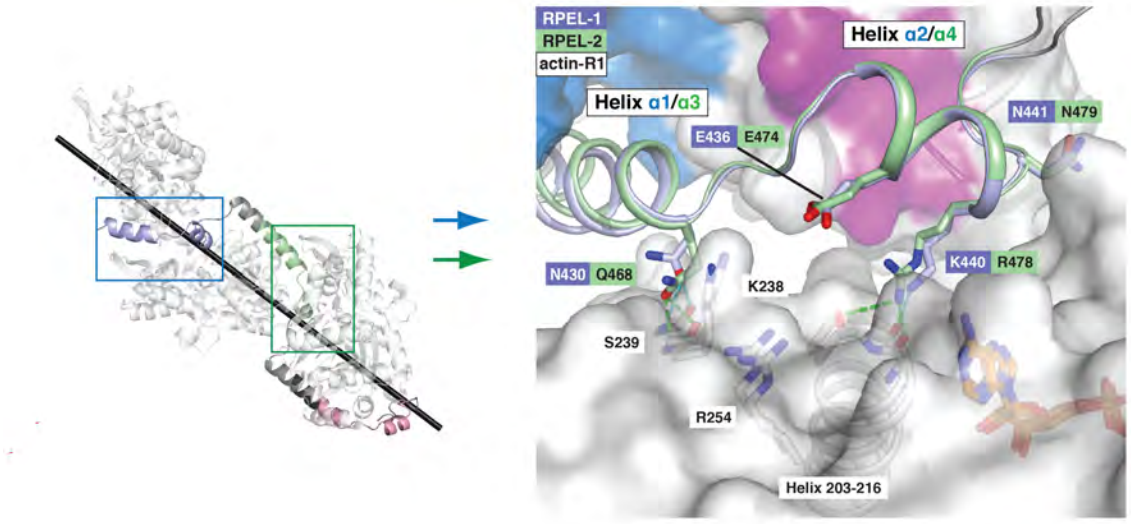


**Figure 4.6 Secondary actin contacts within the G-actin•RPEL $^{Phactr1}$ domain assembly.** (Left) Schematic showing the location of the secondary G-actin binding sites within the trivalent G-actin•RPEL $^{Phactr1}$ domain complex. (Right) Superposition of RPEL1 bound to actin R2 and RPEL2 bound to actin R3 showing selected secondary actin contacts (see text for details). RPEL1 (pale blue) and RPEL2 (green) are shown as cartoons and actins R1 and R2 are shown as pale grey surfaces (actin R1 hydrophobic cleft and ledge surfaces are colored as in Figure 1.10). Stephane Mouilleron, adapted.

## 4.3 G-actin•RPEL$^{Phactr1}$ peptide structures

We have previously shown in fluorescence polarisation assays that the RPEL motifs from Phactr1 bind G-actin with high affinity (Figure 3.5). Even though the homology between the motifs is very high, the affinities differ for each peptide. To better understand the differences in affinity, we solved the structure of each Phactr1 RPEL motif individually bound to G-actin at high resolution.

In order to crystallise G-actin•RPEL$^{Phactr1}$ peptide complexes we used 32 amino acid long peptides for each RPEL$^{Phactr1}$ motif. G-actin was again coupled to LatB in order to form G-actin monomers. Crystals were grown by vapour diffusion and reached the final size in two weeks. We were able to crystallise all four RPEL motifs from Phactr1 with G-actin (Figure 4.7). All crystals diffracted to high resolution, with G-actin•RPEL1$^{Phactr1}$ diffracting to 1.95Å, G-actin•RPEL2$^{Phactr1}$ to 1.7Å and G-actin•RPEL3$^{Phactr1}$ to 1.3Å. Crystals of the N-terminal RPEL-N with G-actin were represented by two distinct forms and diffracted to 1.95 Å for crystal form I and 1.75 Å for crystal form II (Figure 4.7) (for data collection and refinement statistics see Table 7.3).

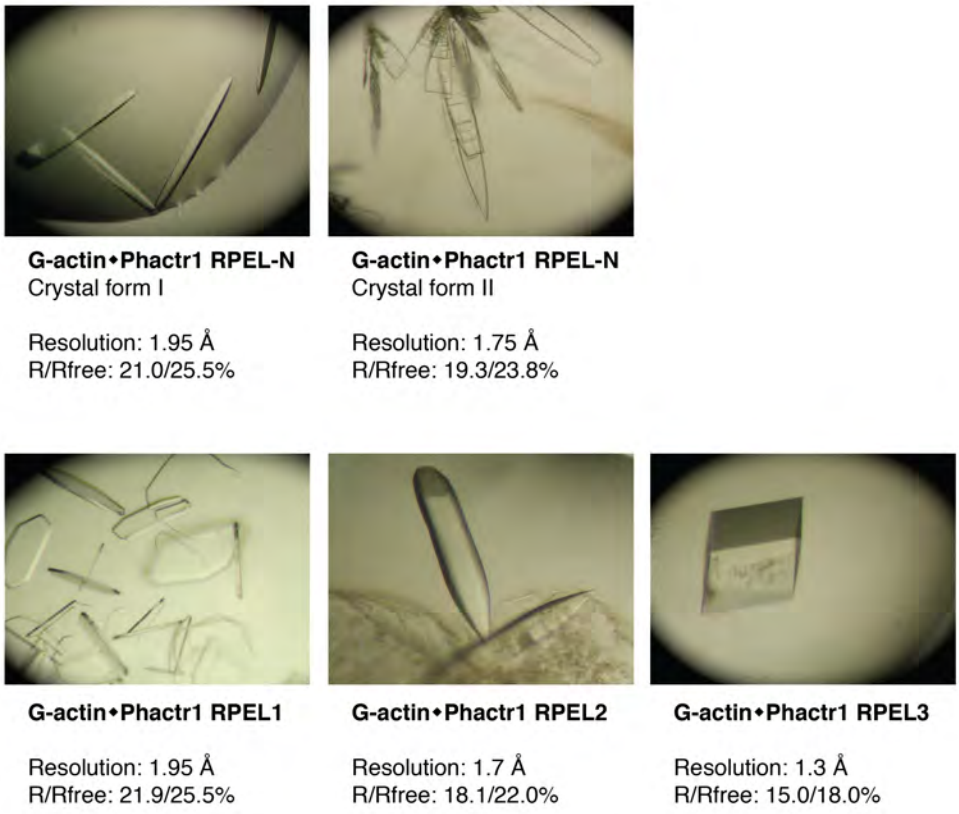


**Figure 4.7 G-actin•RPEL $^{Phactr1}$ peptide crystal forms.**

Top panel, G-actin•RPEL-N $^{Phactr1}$ crystallises in two distinct crystal forms, which diffract at 1.95 Å and 1.75 Å. Bottom panel, G-actin•RPEL-1$^{Phactr1}$ crystals diffract at 1.95Å, G-actin•RPEL-2$^{Phactr1}$ crystals diffract at 1.7 Å and G-actin•RPEL-1$^{Phactr1}$ crystals diffract at 1.3 Å. Images taken by Stephane Mouilleron.

As predicted, all G-actin•RPEL$^{Phactr1}$ peptide structures contained primary actin contacts, previously observed in the G-actin•RPEL$^{MRTF-A}$ peptide structures (Mouilleron et al., 2008), but also revealed additional primary contacts. Unexpectedly, high-resolution G-actin•RPEL-N$^{Phactr1}$ and G-actin•RPEL2$^{Phactr1}$ structures contained not only the primary but also the secondary actin contacts.

### 4.3.1 Primary actin interactions within the G-actin•RPEL$^{Phactr1}$ peptide complexes.

Primary actin contacts are observed within the structure of G-actin•RPEL$^{Phactr1}$ domain complex and in the high-resolution G-actin•RPEL$^{Phactr1}$ peptide structures (Figure 4.5 and Figure 4.8). However, additional primary contacts are observed in the peptide structures and some differences are apparent. For example, in the G-actin•RPEL2 peptide structure, I458$^{RPEL2}$ density is not defined, with the density for the N-terminal RPEL helix beginning only at G459$^{RPEL2}$. This is in contrast to the well-ordered helix α3 seen in the trivalent complex, suggesting that the unstable helix α3 is stabilized in the context of the trivalent complex (Figure 4.5).

We previously showed that RPEL motifs in Phactr1 bind G-actin with higher affinities than in MRTF-A. Higher RPEL-actin affinities were generally conserved in other Phactr family members. Because G-actin•RPEL$^{Phactr1}$ peptide structures revealed additional primary actin contacts, we sought to evaluate whether they contribute to higher binding affinity of Phactr1 RPEL motifs in comparison with MRTF-A. We performed fluorescence polarisation anisotropy assay to measure the binding affinity to G-actin.

Additional contacts in RPEL3, I496$^{RPEL3}$ and R516 $^{RPEL3}$ interact directly with primary actin, but are not highly conserved. Alanine substitution of I496$^{RPEL3}$ and R516$^{RPEL3}$ indeed reduced actin binding affinity two-fold (Figure 4.9). RPEL2 in Phactr1 has a relatively low affinity in Phactr1. Interestingly this is the case also for RPEL2 in Phacrtr2, 3, and 4, all of which have a glycine adjacent to the hydrophobic

contact residue I458. Substitution of this glycine (RPEL2 G459) by lysine, the equivalent residue in higher-affinity motif RPEL3, increased the RPEL2 actin binding affinity almost 10 fold (Figure 4.9)

Therefore, the binding affinity can be modified by supplementary actin contacts or by affecting secondary structure of the RPEL motifs, especially by the addition of stabilising forces.

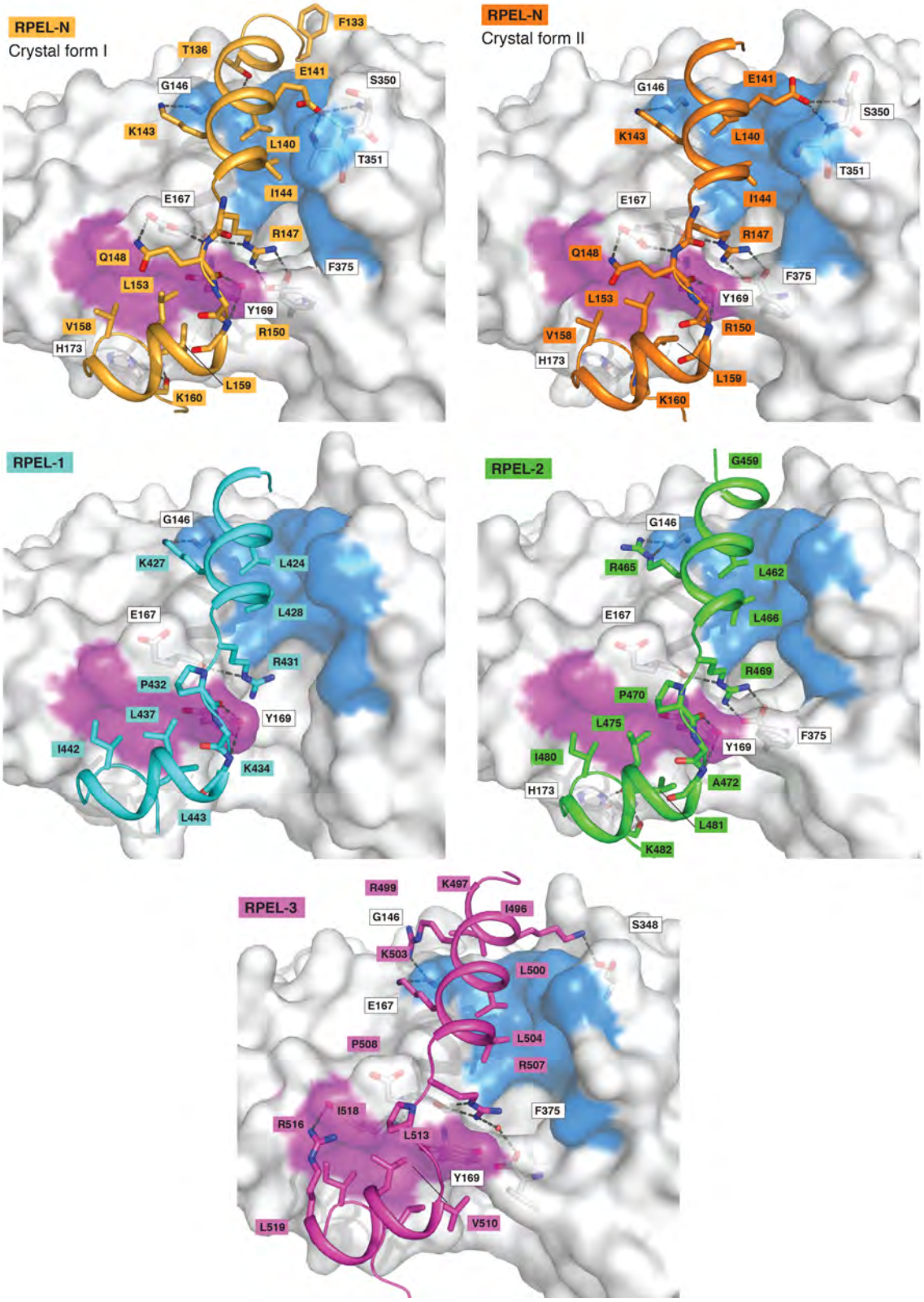
RPEL-N
Crystal form I
F133
T136
E141
S350
G146
K143
L140
T351
I144
E167
R147
Q148
F375
L153
Y169
V158
R150
H173
L159
K160
RPEL-N
Crystal form II
G146
E141
S350
K143
L140
T351
E167
I144
R147
Q148
F375
L153
Y169
V158
R150
H173
L159
K160
RPEL-1
G146
K427
L424
E167
L428
R431
P432
L437
Y169
I442
K434
L443
RPEL-2
G459
G146
R465
L462
E167
L466
R469
P470
L475
F375
Y169
I480
H173
A472
L481
K482
RPEL-3
R499
K497
G146
I496
S348
K503
L500
E167
P508
L504
R507
I518
F375
R516
L513
Y169
L519
V510

**Figure 4.8 Phactr1 RPEL peptide-actin complexes.**

Close-up of structures for individual RPEL peptides from Phactr1 bound to G-actin. RPEL peptide is shown as a cartoon and G-actin as a pale grey solid rendering. Contact surfaces made by each of the RPEL peptide to the G-actin hydrophobic cleft (blue) and ledge (pink) are indicated. Selected residues from the RPEL peptides are shown together with the corresponding G-actin interacting residues (hydrophobic cleft and ledge surfaces are colored as in Figure 1.10). Stephane Mouilleron, adapted.

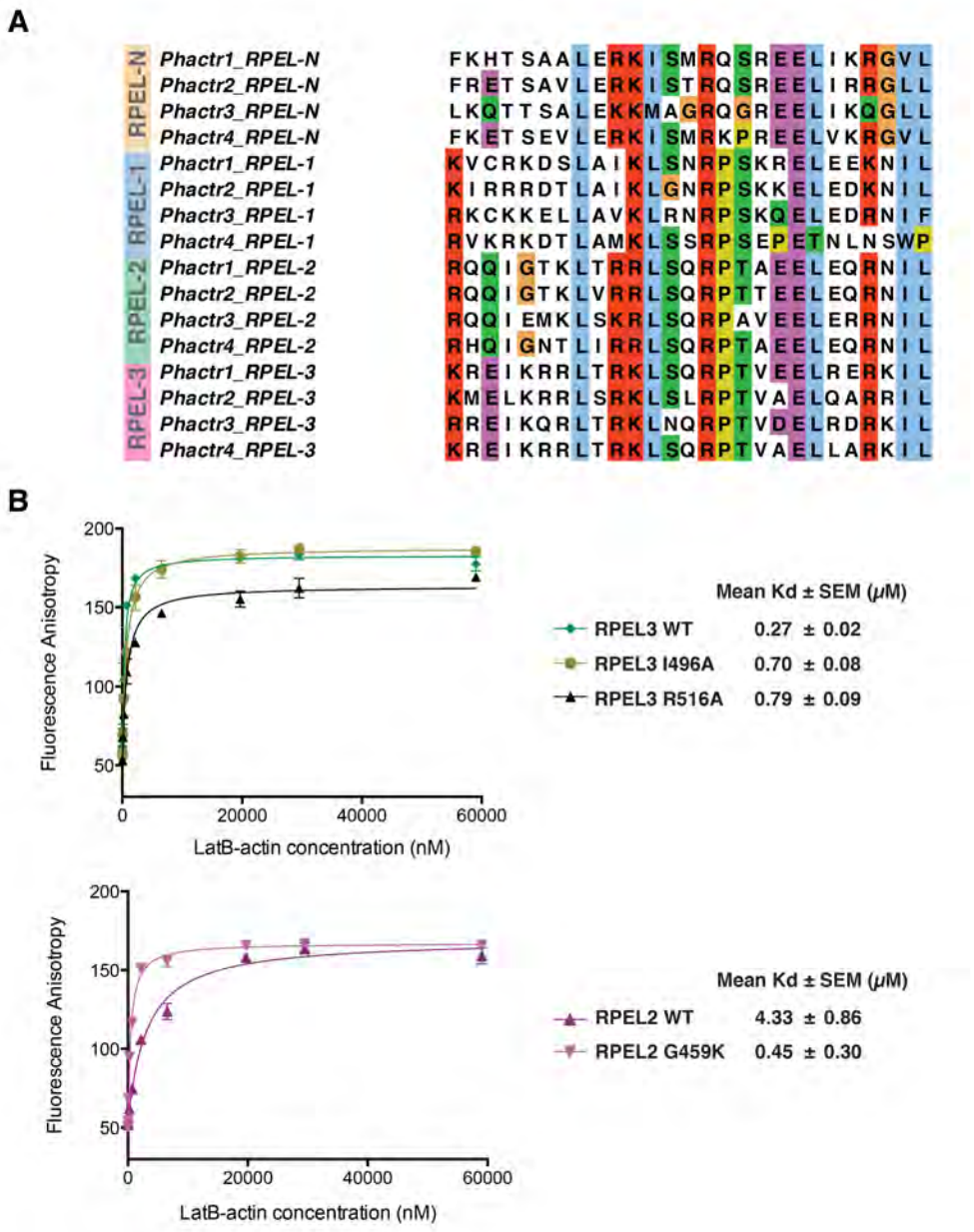


**Figure 4.9 RPEL motif primary contacts define actin affinities.**

**(A)** Alignment of RPEL motifs from Phactr1, 2, 3 and 4 indicating highly conserved residues, colour-coded using Clustal X alignment tool. **(B)** Fluorescence polarization assay indicating the role of primary contacts in high actin affinities. Top, RPEL3 wild-type (WT) peptide and two mutants I496A and R516A indicating a role of additional primary actin contacts. Bottom, RPEL2 G459K significantly increases RPEL2 actin binding affinity (K in this position is a conserved residue in RPEL3 motif, which exhibits higher affinity to actin).

### 4.3.2 G-actin•RPEL-N$^{Phactr1}$ and G-actin•RPEL2$^{Phactr1}$ peptide structures contain secondary actin contacts

Secondary actin contacts were observed within the G-actin•RPEL$^{Phactr1}$ domain complex (see previous sections). However, the resolution of the trivalent complex was not sufficient to fully observe the secondary actin binding surface. Crystallisation of G-actin•RPEL-N$^{Phactr1}$ and G-actin•RPEL2$^{Phactr1}$ peptides also revealed a secondary actin surface.

#### *4.3.2.1 G-actin•RPEL-N$^{Phactr1}$ and G-actin•RPEL2$^{Phactr1}$ peptide structures crystallise as open helical assemblies*

Complexes containing RPEL-N and RPEL-2 crystallised as open helical assemblies: filaments in which the primary G-actin•RPEL peptide within the asymmetric unit makes a secondary contact with the G-actin•RPEL peptide present in an adjacent asymmetric unit (Figure 4.10). Both crystal forms of G-actin•RPEL-N$^{Phactr1}$ peptide contained the same arrangement, which strongly suggests that these assemblies are not related to the crystal lattice, but are reflecting true properties of those RPEL motifs.

To better understand the arrangement of G-actin•RPEL-N$^{Phactr1}$ and G-actin•RPEL-2$^{Phactr1}$ complexes we compared their screw axes to the axis of G-actin•RPEL$^{Phactr1}$ domain complex (Figure 4.10 A and Figure 4.11). These axes by definition rotate a point within a flat surface while translating it parallel to the surface. It emerged that the screw operator relating subsequent actins in G-actin•RPEL-N$^{Phactr1}$ and G-actin•RPEL-2$^{Phactr1}$ complexes is crystallographic, with exactly 180° rotation (Figure 4.9 A). In contrast, the screw operator in the trivalent G-actin•RPEL$^{Phactr1}$ domain complex is non-crystallographic, with 155° rotation (Figure 4.11). There is no difference in the translational operator between the peptides structures and the trivalent domain, with both remaining at around 39Å. This variability in the rotational angle

might indicate a certain degree of flexibility within the complex arrangement during disassembly.

Another evidence that the open helical assemblies represent actual arrangement of RPEL motifs when bound actin molecules comes from the comparison of primary and secondary contacts with those observed in the trivalent complex. Despite the absence of fifteen amino acid-long spacer sequences, those two groups of interactions are very similar (Figure 4.11).

#### *4.3.2.2 Molecular details of the secondary actin contacts*

The high resolution of the G-actin•RPEL-N$^{Phactr1}$ and G-actin•RPEL-2$^{Phactr1}$ structures provides the molecular detail (direct and water-mediated) of the secondary actin interactions that are less well defined in the 3.3 Å resolution trivalent complex. We observed the same three RPEL residues at the secondary actin interface: (1) the residue preceding the conserved RPEL arginine, (2) the conserved RPEL glutamate, (3) and the basic residue from the C-cap (M146 $^{RPEL-N}$ / E152 $^{RPEL-N}$ / R156$^{RPEL-N}$ and Q468 $^{RPEL2}$ / E474 $^{RPEL2}$ / R478$^{RPEL2}$, Figure 4.10 B).

These residues act together to form a stable secondary interaction on the G-actin interface. R156$^{RPEL-N}$ and R478$^{RPEL2}$ each engage three carbonyl moieties from the C-terminus of helix 203–216 of the secondary actin through a network of hydrogen bonds. These arginine side chains also make two important water-mediated hydrogen bonds, one with the N8 atom of the ATP adenine moiety occupying the secondary actin nucleotide-binding cleft, the other with secondary actin R254. The invariant RPEL glutamate residue has a different side chain rotamer in each structure. E152$^{RPEL-N}$ interacts indirectly via a water molecule with R156$^{RPEL-N}$ and R254 of the secondary actin, while E474$^{RPEL2}$ interacts directly with K238 of the secondary actin (Figure 4.10 B).

Other secondary actin interactions include: $M146^{RPEL\text{-}N}$ with $V247^{G\text{-}actin}$, similarly the structurally equivalent $Q468^{RPEL2}$ contacts $E241^{G\text{-}actin}$, while side chains at equivalent positions to $G157^{RPEL\text{-}N}$ ($N440^{RPEL1}$; $N479^{RPEL2}$; and $K517^{RPEL3}$), all make a close approach to the secondary actin (Figure 4.10 B).

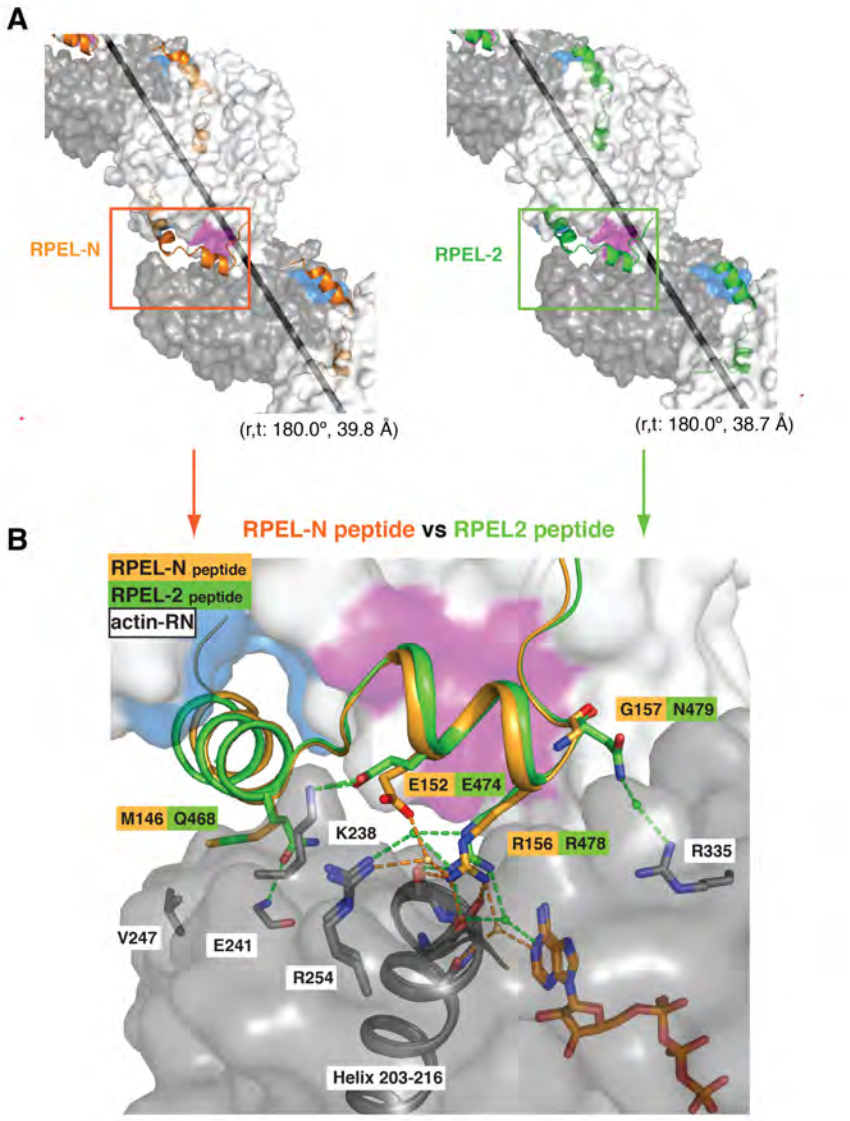


**Figure 4.10 G-actin•RPEL$^{Phactr1}$ peptide structures form open helical assemblies containing the secondary actin contacts.**

**(A)** Filamental structures formed by single RPEL motifs (RPEL-N, left panel; RPEL2, right panel) within a crystal lattice. Consecutive adjacent asymmetric units each containing a single G-actin•RPEL motif peptide complex generate an open helical assembly, where each RPEL motif (cartoon) bridges two actin molecules (pale grey and white, respectively); the crystallographic screw axis is shown as a black line. **(B)** Close-up of the secondary actin contacts within RPEL-N and RPEL2 helical assemblies, centered on the conserved RPEL glutamate. RPEL motifs are drawn as cartoons and actin molecules as pale grey surfaces. G-actin cleft and ledge surfaces are colored as in Figure 1.10. Stephane Mouilleron, adapted.

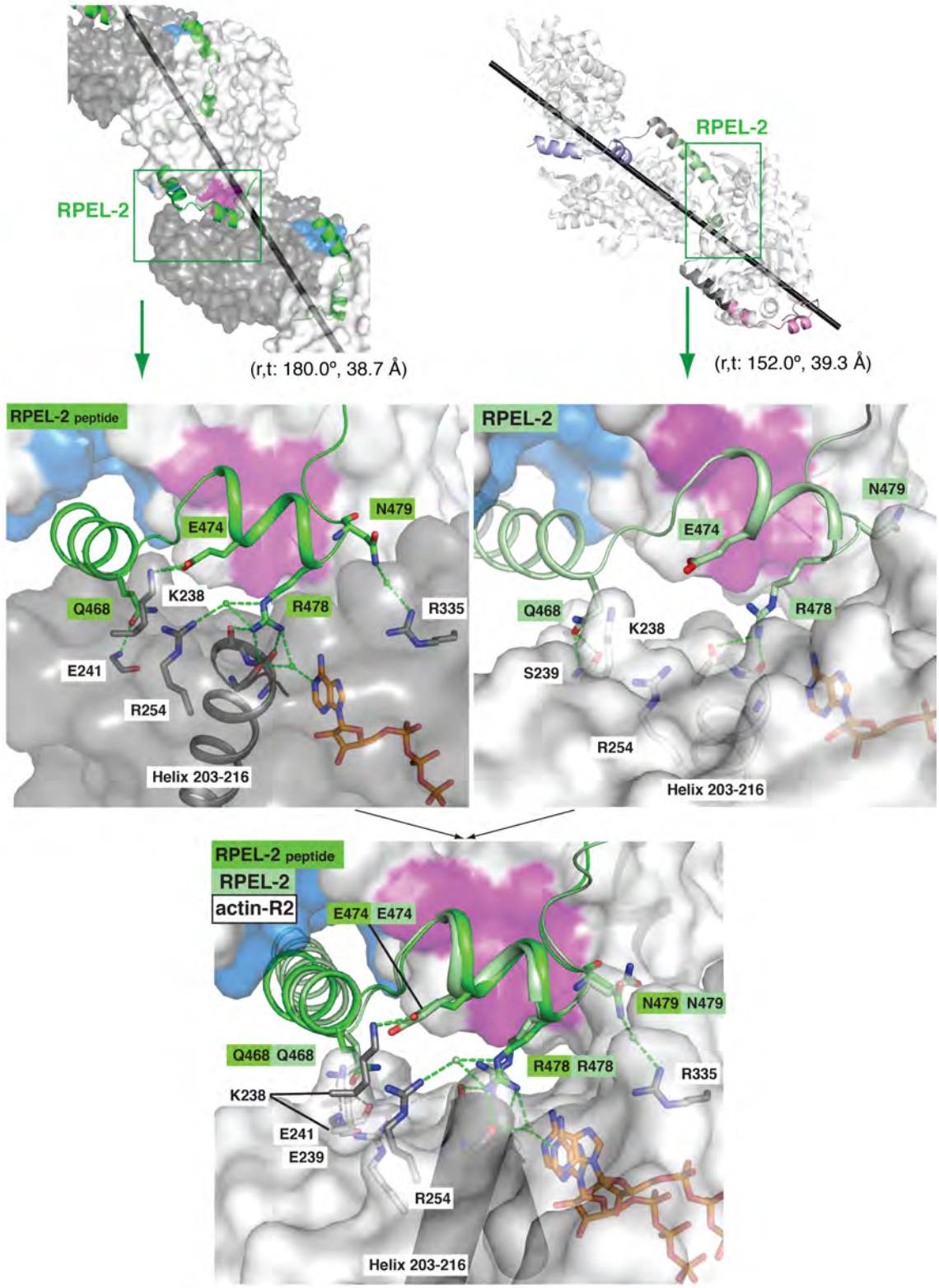
RPEL-2
(r,t: 180.0°, 38.7 Å)
RPEL-2
(r,t: 152.0°, 39.3 Å)
RPEL-2 peptide
E474
N479
K238
Q468
R478
R335
E241
R254
Helix 203-216
RPEL-2
N479
E474
Q468
K238
R478
S239
R254
Helix 203-216
RPEL-2 peptide
RPEL-2
actin-R2
E474 E474
N479 N479
Q468 Q468
R478 R478
R335
K238
E241
E239
R254
Helix 203-216

**Figure 4.11 Similar secondary contacts within G-actin•RPEL2$^{Phactr1}$ peptide complex and the trivalent G-actin•RPEL$^{Phactr1}$ complex.**

Comparison of RPEL2 from G-actin•RPEL2$^{Phactr1}$ peptide structure and from G-actin•RPEL$^{Phactr1}$ domain structure shows similar secondary actin contacts. The different rotation angles for each structure (180° compared to 152°) leads to interaction differences, in particular the disposition of G-actin-bound nucleotide and helix 203-216. Additional direct and indirect interactions with G-actin are observed in the higher resolution RPEL2 peptide structure. G-actin cleft and ledge surfaces are colored as in Figure 1.10. Stephane Mouilleron, adapted.

These observations show the molecular detail of the secondary actin contacts in the context of single peptide structures and the trivalent complex. The secondary actin contacts seen in the G-actin•RPEL-N$^{Phactr1}$ and G-actin•RPEL-2$^{Phactr1}$ assemblies may be perturbed compared with those in the trivalent G-actin•RPEL$^{Phactr1}$ domain complex as a result of crystal packing constraints. Nevertheless, the interactions described above are superimposable among the different structures, thus explain the conservation of secondary contact residues.

#### *4.3.2.3 The conservation of RPEL glutamate*

The RPEL glutamate is conserved within the Phactr family of proteins and within the MRTFs. Previous structural studies of MRTF-A have not clarified the rationale behind the strong conservation of this residue. Investigating the structures of G-actin•RPEL$^{Phactr1}$ peptide complexes and the trivalent complex explained the role of the glutamate. Superposition of the secondary actin contacts made by the RPEL domain from Phactr1 and MRTF-A showed strikingly similar contacts made by both proteins centered on the invariant RPEL motif glutamate (Figure 4.12). This residue is crucial for achieving higher order actin•RPEL assemblies on repeated RPEL motifs. It remains unclear why this glutamate is conserved in the last RPEL within the domain (RPEL3) both in Phactr family and in MRTF-A (see: 'Discussion'). Additionally, the RPEL glutamate contributes to the binding cooperativity of G-actin molecules on tandem RPEL motifs (see following section).

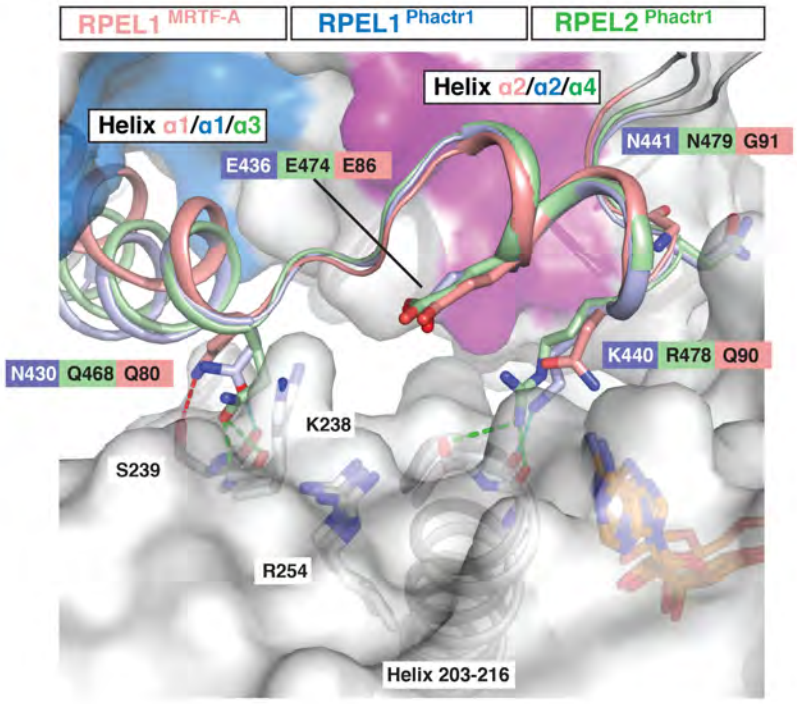


**Figure 4.12 Secondary actin contacts in Phactr1 and MRTF-A complexes with G-actin.** Superposition of the secondary actin contacts made by the RPEL domain from Phactr1 (RPEL1; blue and RPEL2; green) and MRTF-A (RPEL1; pink) showing the strikingly similar contacts made by both proteins centered on the invariant RPEL motif glutamate. Stephane Mouilleron, adapted.

## 4.4 Contribution of secondary actin contacts to Phactr1 regulation

We previously showed that the C-terminal RPEL domain is required for Phactr1 regulation by actin turnover. Alanine mutations of the invariant arginine abolished actin binding (Figure 3.5). The combinations of R/A mutations within the RPEL domain significantly reduce Phactr1 cytoplasmic retention, which suggests cooperative G-actin binding on the RPEL repeat (Figure 3.7 A). We hypothesised that in addition to defining the relationship between the G-actin molecules within the trivalent G-actin•RPEL$^{Phactr1}$ assembly, secondary actin contacts might contribute to cooperative G-actin binding to the C-terminal RPEL repeats. Moreover, actin overexpression studies showed that the integrity of both the RPEL domain and RPEL-N is required for effective inhibition of Phactr1 accumulation by actin (Figure 3.11). Therefore, we now sought to investigate the role of secondary contacts in actin binding cooperativity on Phactr1 RPEL domain and in maintaining the integrity of RPEL-N and the C-terminal repeat.

### 4.4.1 Secondary contacts facilitate cooperative actin binding

To test actin binding cooperativity on the C-terminal RPEL repeat we employed complex stoichiometry analysis. We used SEC-MALLS to assess the effects of RPEL mutations on the formation of multivalent G-actin•RPEL$^{Phactr1}$ complexes. We previously showed that the R/A mutation of the invariant arginine, a primary actin contact in Phactr1 (R431A$^{RPEL1}$, R496A$^{RPEL2}$, and R507A$^{RPEL3}$) effectively abolishes G-actin binding to individual RPEL motifs (Figure 3.5 A). We next introduced those mutations into the triple RPEL repeat and analysed G-actin binding property by SEC-MALLS.

The R431A$^{RPEL1}$ and R507A$^{RPEL3}$ mutations reduced the stoichiometry of the G-actin•RPEL$^{Phactr1}$ complex from 2.7 to 1.8 (actin molecules bound), consistent with loss

of the RPEL1 and RPEL3 associated actins. In contrast, the R469A$^{RPEL2}$ mutation had no effect G-actin binding (2.6 versus 2.7 actins bound) (Figure 4.13 B). Thus, in the context of the trivalent G-actin•RPEL$^{Phactr1}$ complex, loss of the ion-pair contact from RPEL2 with its primary actin by the conserved arginine is not sufficient to outweigh cooperative interactions maintaining the integrity of the complex (Mouilleron et al., 2012).

Theoretically, mutations of secondary actin contacts should not affect actin binding affinity in the fluorescence anisotropy assay, where affinity of one G-actin molecule to an RPEL peptide is measured. Indeed, the secondary actin contact mutations EK436,440AA$^{RPEL1}$; ER474,478AA$^{RPEL2}$; and ER512,516AA$^{RPEL3}$ decreased primary actin-binding affinity only 3, 4 and 2-fold, respectively (Figure 4.13 A). Introduction of these mutations into the RPEL$^{Phactr1}$ domain, either singly or in combination, did not affect its actin binding stoichiometry, as assessed by SEC-MALLS (Figure 4.13 B). However, their combination with the primary actin R469A$^{RPEL2}$ mutation led to a decrease in apparent stoichiometry from 2.7 to 1.6 (127kDa vs. 79kDa), consistent with loss of actin R2 (Mouilleron et al., 2012).

Taken together, these results provide evidence for the functional significance of the secondary actin binding sites during the assembly of the trivalent G-actin•RPEL$^{Phactr1}$ domain complex. These results are consistent with a view that the secondary actin contacts made by RPEL1 and RPEL2, as well as affinities of each individual RPEL motifs for primary actins, contribute to stabilization of the trivalent G-actin•RPEL$^{Phactr1}$ complex.

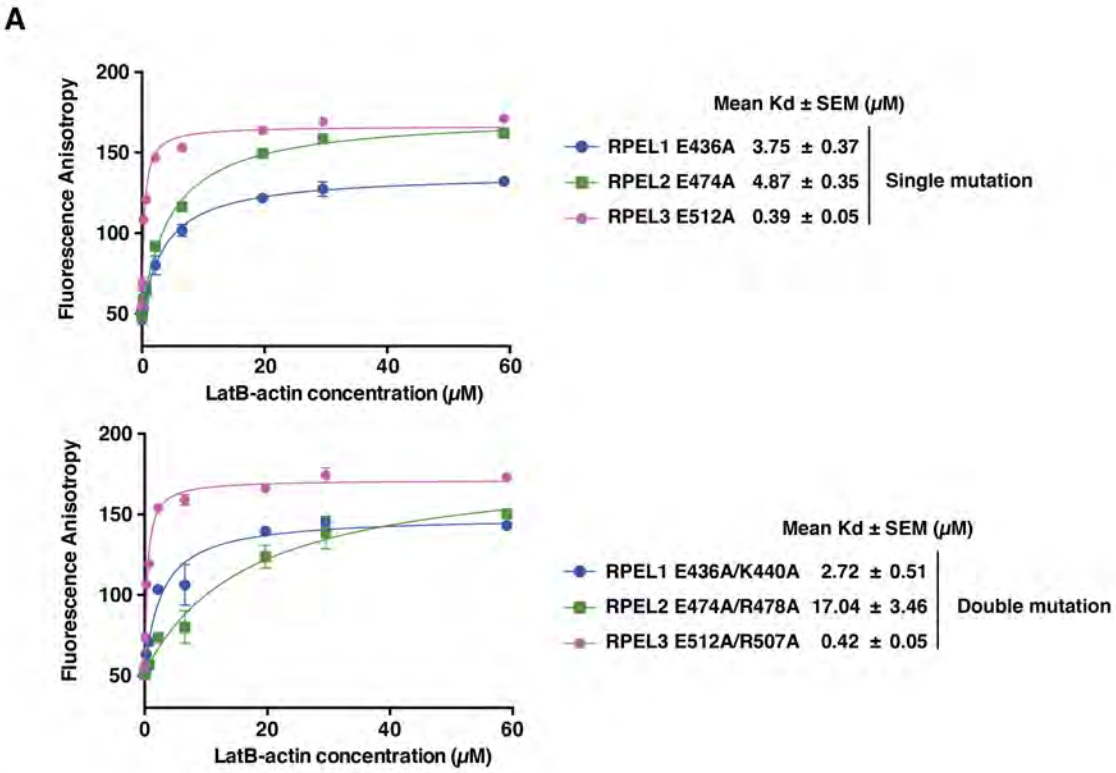
A
Fluorescence Anisotropy
200
150
100
50
0
20
40
60
LatB-actin concentration (μM)
Mean Kd ± SEM (μM)
RPEL1 E436A 3.75 ± 0.37
RPEL2 E474A 4.87 ± 0.35
RPEL3 E512A 0.39 ± 0.05
Single mutation
Fluorescence Anisotropy
200
150
100
50
0
20
40
60
LatB-actin concentration (μM)
Mean Kd ± SEM (μM)
RPEL1 E436A/K440A 2.72 ± 0.51
RPEL2 E474A/R478A 17.04 ± 3.46
RPEL3 E512A/R507A 0.42 ± 0.05
Double mutation

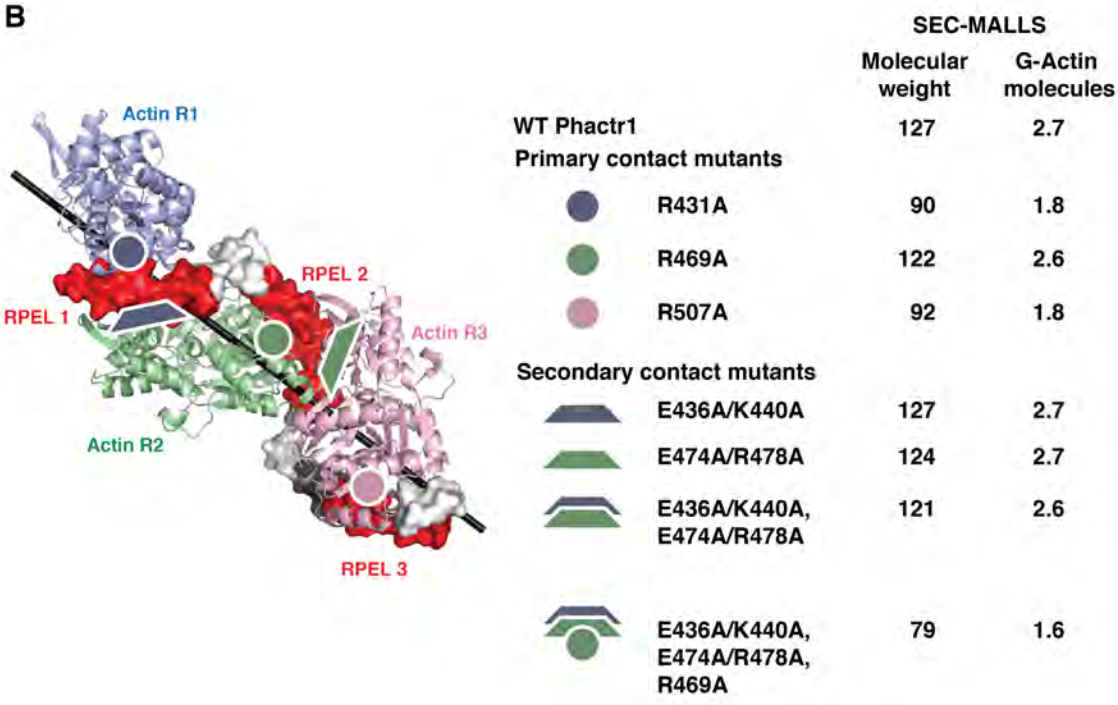
B
Actin R1
RPEL 2
RPEL 1
Actin R3
Actin R2
RPEL 3
SEC-MALLS
Molecular weight
G-Actin molecules
WT Phactr1 127 2.7
Primary contact mutants
R431A 90 1.8
R469A 122 2.6
R507A 92 1.8
Secondary contact mutants
E436A/K440A 127 2.7
E474A/R478A 124 2.7
E436A/K440A, E474A/R478A 121 2.6
E436A/K440A, E474A/R478A, R469A 79 1.6

**Figure 4.13 Secondary actin contacts are required for cooperative binding.**

**(A)** Effects of RPEL mutations on primary actin binding affinities. The dissociation constants ($K_D$) were determined by fluorescence polarization anisotropy assay. Data for wild-type RPEL motifs and primary actin contact mutants are presented in Figure 3.5 (RPEL1 0.9 μM, $R431A^{RPEL1}$ ND ; RPEL2 4.34 μM, $R469A^{RPEL2}$ ND; RPEL3 0.27 μM, and $R507A^{RPEL3}$ 18.4 μM; ND, not detectable). **(B)** Experimental molecular weights for $RPEL^{Phactr1}$ domain mutants bound to G-actin, derived from size exclusion chromatography coupled to multi-angle laser light scattering experiments (SEC-MALLS). Mutations within the RPEL domain are schematically shown on the left (for details, see text); apparent stoichiometries from the molecular weights are shown on the right.

### 4.4.2 Inhibition of actin-mediated nuclear accumulation of Phactr1 requires secondary contacts

Phactr1 accumulates in the nucleus upon serum activated Rho-actin signal (Wiezlak et al., 2012). I have shown that the C-terminal RPEL domain, but not RPEL-N was required to mediate Phactr1 regulation by G-actin (Figure 3.6). However, actin overexpression experiments suggest that the integrity of the C-terminal domain and the RPEL-N are required for the inhibition of Phactr1 accumulation by G-actin (Figure 3.11). Inhibition of Phactr1 nuclear accumulation by G-actin therefore arises from the saturation of all four RPEL motifs by G-actin. We speculated that secondary actin contacts might facilitate this process. To investigate this possibility we introduced secondary contact mutations into RPEL-N within the full length Phactr1 and performed actin overexpression assay.

First, we verified the secondary contact mutations in RPEL-N in fluorescence anisotropy assays. As predicted, substitution of conserved glutamate into alanine (E152A) had no effect on primary actin binding affinity (Figure 4.14 B). Subsequently, a 2-fold increase was observed for $M146A^{RPEL\text{-}N}$ and 3-fold for $R156A^{RPEL\text{-}N}$ mutations. We then tested two mutations that prevent close approach of secondary actin at previously position $G157^{RPEL\text{-}N}$. We substituted this glycine with either histidine or asparagine, residues containing long sidechains, which impede the approach of RPEL1 primary actin at this RPEL-N secondary binding site. As expected, $G157H^{RPEL\text{-}N}$ and $G157N^{157\ RPEL\text{-}N}$ reduced binding affinity of primary actin only 4-fold (Figure 4.14 B).

Next, we examined how those mutations affect Phactr1 regulation upon actin overexpression. We expressed Phactr1 wild-type or RPEL-N secondary contact mutants in NIH3T3 cells with or without non-polymerisable actin mutant R62D. Consistent with our previous results, nuclear accumulation of Phactr1 wild-type or secondary contact mutants was not affected when cells were stimulated with serum, and upon co-expression of R62D actin mutant the nuclear accumulation of wild-type Phactr1 was inhibited. However, Phactr1 RPEL-N secondary contact mutants M146A, E152A and R156A showed reduced susceptibility to actin R62D expression. G157H and G157N

mutations also reduced the inhibitory effect caused by actin overexpression (Figure 4.14 C). These findings demonstrate that RPEL-N secondary actin contacts are required for the inhibition of Phactr1 nuclear accumulation by G-actin (see: ‘Discussion’).

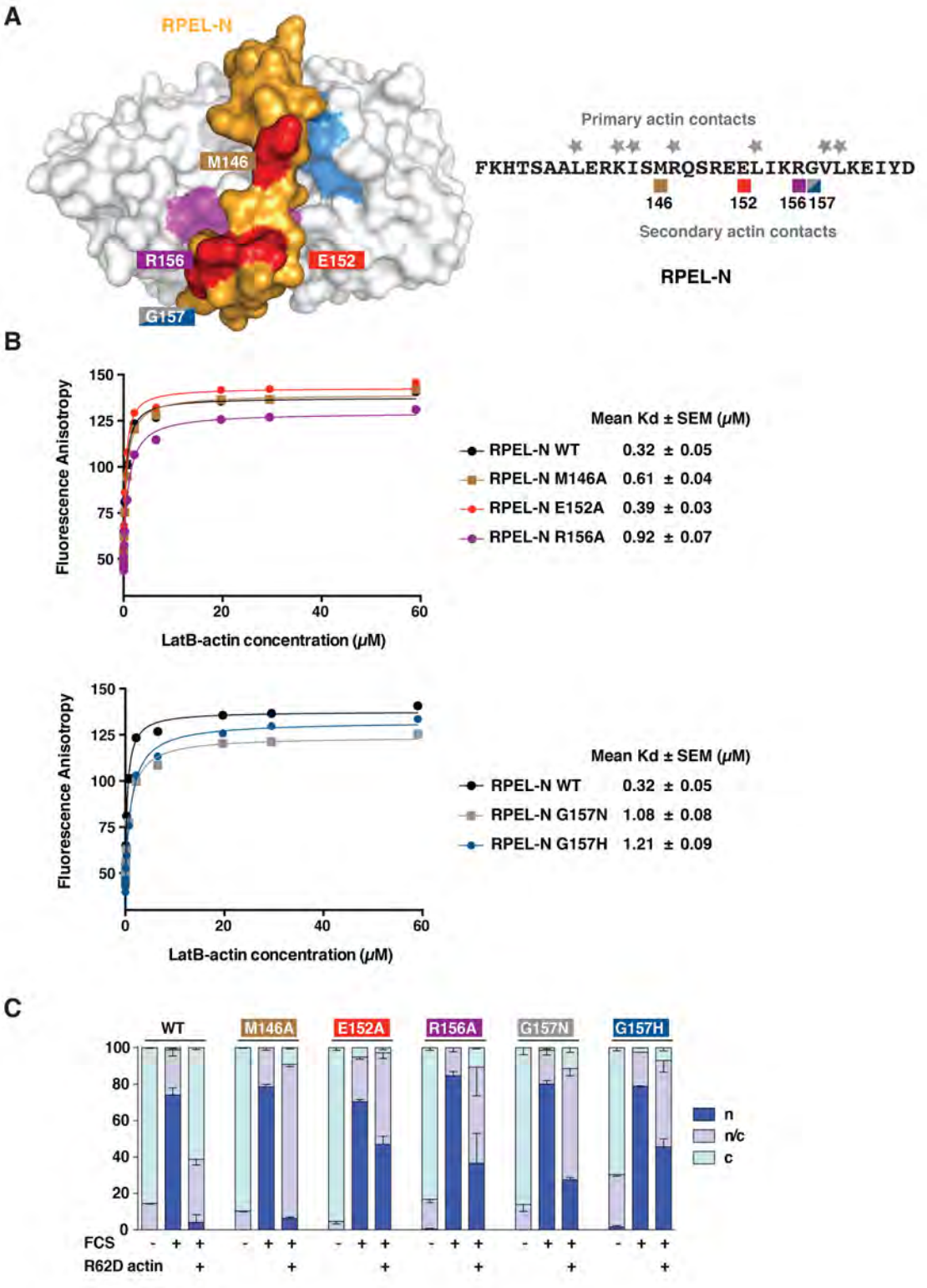
A
RPEL-N
M146
R156
E152
G157
Primary actin contacts
FKHTSAALERKISMRQSREELIKRGVLKEIYD
146
152
156 157
Secondary actin contacts
RPEL-N
B
Fluorescence Anisotropy
LatB-actin concentration (μM)
Mean Kd ± SEM (μM)
RPEL-N WT 0.32 ± 0.05
RPEL-N M146A 0.61 ± 0.04
RPEL-N E152A 0.39 ± 0.03
RPEL-N R156A 0.92 ± 0.07
Fluorescence Anisotropy
LatB-actin concentration (μM)
Mean Kd ± SEM (μM)
RPEL-N WT 0.32 ± 0.05
RPEL-N G157N 1.08 ± 0.08
RPEL-N G157H 1.21 ± 0.09
C
WT
M146A
E152A
R156A
G157N
G157H
n
n/c
c
FCS
R62D actin

**Figure 4.14 RPEL-N secondary contacts are required for actin-mediated inhibition of Phactr1 nuclear import.**

**(A)** Left, surface rendering of the RPEL-N peptide (orange surface) bound to the primary G-actin (white surface) highlighting the secondary actin contacts (red surfaces). Secondary contact residues are indicated and colour-labelled according to mutations (M146A, brown; E152A, red; R156A, purple; G157N, grey; G157H, blue). Actin hydrophobic cleft and ledge surfaces between actin subdomains 1 and 3 are coloured as in Figure 1.10. The secondary G-actin is not shown for clarity. Right, sequence of RPEL-N indicating primary (grey stars) and secondary (colour-labelled rectangles) actin contacts. **(B)** Effects of RPEL-N mutations on primary actin binding affinities. The dissociation constants ($K_D$) were determined by fluorescence polarization anisotropy assay. **(C)** The indicated FLAG-tagged Phactr1 derivatives (colour-labelled as in A) were co-expressed with the non-polymerisable actin R62D mutant in NIH 3T3 cells (to simplify quantification, Phactr1ΔC was used - protein expression levels remain unaffected by R62D actin overexpression upon Phactr1ΔC expression). The subcellular localisation before and after 1 hr serum (FCS) stimulation was scored by immunofluorescence (C, cytoplasmic; N/C, pan-cellular; N, nuclear; at least 75 cells counted per point, error bars represent the s.e.m. of three independent experiments).

## 4.5 Conclusions

In this this chapter, I have presented structural analysis of Phactr1 interaction with actin. This study elucidated previously unknown aspect of the RPEL motif interaction with G-actin, a secondary actin contact. Secondary actin surface is crucial for the formation of the higher order actin complexes with Phactr1. Binding of the primary actin to the RPEL motif induces a conformational change of the RPEL motif, which generates a secondary contact surface. The secondary actin surface comprise residues at the end of helix 1, conserved RPEL glutamate and an arginine in helix 2. These residues contribute to cooperative actin binding on tandem RPEL repeats and are involved in the inhibition of Phactr1 nuclear accumulation by G-actin.

Comparison of G-actin•RPEL$^{MRTF\text{-}A}$ complex with G-actin•RPEL$^{Phactr1}$ complex clarified how differences in actin spacers' length between the two proteins can be compensated by the fixed relative orientation of actins. Moreover, it explained the conservation of secondary contact RPEL glutamate in MRTFs.

# Chapter 5. Functional studies of Phactr1

## 5.1 Aims

In previous chapters we described the mechanism of Phactr1 nuclear accumulation and PP1 interaction. Through structural studies we better understood how G-actin interacts with Phactr1 and how this association differs from G-actin•MRTF-A complexes. Our next objective was to examine the role of Phactr1 in PP1 regulation and elucidate cellular function of Phactr1. Throughout our studies of Phactr1 we have shown its regulation in NIH3T3 fibroblasts, a cell line where Phactr1 is not endogenously expressed at high levels. Therefore, to study the function of Phactr1, we employed a cell line, where Phactr1 is highly expressed - a CHL-1 metastatic melanoma.

Consistent with our previous findings, we now uncover a function of Phactr1 in the regulation of actomyosin assembly in the endogenous setting. Consequently, we show a connection between Phactr1 expression and melanoma cell motile and invasive behaviours.

## 5.2 Phactr1 expression and regulation in CHL-1 melanoma cell line

It was previously shown, that Phactr1 is highly expressed in the cells of neuronal origin (Allen et al., 2004). However, subsequent studies showed high Phactr1 expression levels in malignant melanomas in comparison with nevi (Koh et al., 2009; Trufant, 2010). Melanomas are tumours that develop as a result of a malignant transformation of melanocytes, cells derived from the neural crest. Therefore consistently, Phactr1 high expression levels seem to be present in cells derived from a lineage in the nervous system.

We performed an oncogenomic analysis of Phactr1 mRNA expression levels using 'Oncomine', a cancer microarray database designed to facilitate discoveries from genome-wide expression data. This data-mining platform allowed us to characterise Phactr1 expression pattern in various malignant tumours and showed its consistently high levels in malignant melanomas (www.oncomine.org). To study Phactr1 function we thus took advantage of readily available melanoma cell line CHL-1.

CHL-1 cell line is a derivative of another melanoma cell line RPMI7932, a human melanoma cell line derived from the pleural effusion of a 36-year-old female patient with malignant melanoma. CHL-1 cell line was designed as a transfection host and can grow to a higher density (5 x $10^7$ cells/ml) in a suspension culture than RPMI7932. CHL-1 cells were engineered to contain specific plasmids, which contain several gene cassettes. Specific orientation of those cassettes enhances the growth of the cells by preventing mycoplasma contamination and by allowing high-density cell growth (Patent US5017478).

In order to study the function of Phactr1 in CHL-1 cell line, we first characterised its regulation. To begin with, we used a commercially available antibody against Phactr1 to examine the nuclear accumulation of Phactr1 upon serum stimulation. We also monitored the behaviour of exogenous Phactr1 in the context of serum stimulus. This allowed us to make comparisons with the previously obtained, fibroblasts based assays. Finally, we examined the interaction of Phactr1 with PP1 in melanoma cells. We then drew conclusions based on the results obtained in NIH3T3 fibroblasts and CHL-1 melanoma cells.

### 5.2.1 Serum stimulation of CHL-1 melanoma cells induces Phactr1 nuclear accumulation

Having previously found that transiently expressed Phactr1 accumulates in the nucleus of NIH3T3 cells upon serum stimulation, we now attempted to test the cellular localisation and dynamics of endogenous Phactr1. CHL-1 melanoma cells were grown in full medium until they reached desired density and then starved for 24 hours. After starvation, 15% serum was added onto the cells for up to one hour and localisation of Phactr1 was monitored by immunofluorescence. We could observe the rapid nuclear accumulation of endogenous Phactr1 upon serum stimulation (Figure 5.1 A). Phactr1 was nuclear after already 10 minutes of serum stimulation and remained in the nucleus for up to one hour. This experiment showed that, like in fibroblasts, endogenous Phactr1 accumulates in the nucleus of CHL-1 cells, but exhibits more rapid dynamics.

### 5.2.2 Transiently expressed Phactr1 responds to signal in CHL-1 cells

The preceding experiment showed, that endogenous Phactr1 behaves in a similar way to transiently expressed FLAG-tagged Phactr1 in NIH3T3 cells. We next sought to examine the regulation of FLAG-tagged Phactr1 and constitutively nuclear Phactr1-xxx in CHL-1 cells. Wild-type Phactr1 was cytoplasmic when cells were serum-starved, but accumulated in the nucleus upon serum stimulation. Consistent with previous findings, Phactr1-xxx exhibited constitutive nuclear localisation (Figure 5.1 B). These results suggest that Phactr1 nuclear accumulation in CHL-1 cells is based on the same mechanism as in NIH3T3 cells.

Previous studies of Phactr1-xxx interaction with PP1 allowed us to earlier propose that the contractile phenotype of actomyosin fibres is a consequence of Phactr1 interaction with PP1. As presented before, the appearance of actomyosin foci or thick fibres was observed when PP1-bound Phactr-xxx was expressed. In order to evaluate the formation of actomyosin structures in CHL-1 melanoma cells, we also visualised F-

actin in cells transfected with Phactr1-xxx. However, actomyosin structures were not as pronounced as in NIH3T3 cells (Figure 5.1 B). Instead of containing 'thick fibres' or 'foci', cells expressing Phactr1-xxx appear to exhibit brighter F-actin staining in comparison with untransfected cells.

### 5.2.3 Nuclear accumulation of endogenous Phactr1 is accompanied by increased PP1 binding

We previously showed by co-immunoprecipitation that interaction between PP1 and Phactr1 is enhanced upon serum stimulation in NIH3T3 fibroblasts (Figure 3.12 B). To evaluate the interaction between Phactr1 and PP1 in CHL-1 melanoma we performed immunoprecipitation assay of endogenous proteins. Consistent with our previous results, we could observe increased recovery of Phactr1 in PP1 immunoprecipitates following serum stimulation (Figure 5.1 C).

Taken together, these results allow us to conclude that Phactr1 exhibits actin-dependent nuclear accumulation and PP1 interaction in CHL-1 melanoma cells. Moreover, the nuclear accumulation of endogenous Phactr1 in CHL-1 cells is accompanied by enrichment of the PP1-Phactr1 interaction. These results are in agreement with our previous findings and establish CHL-1 melanoma cells as a suitable model for further studies of Phactr1.

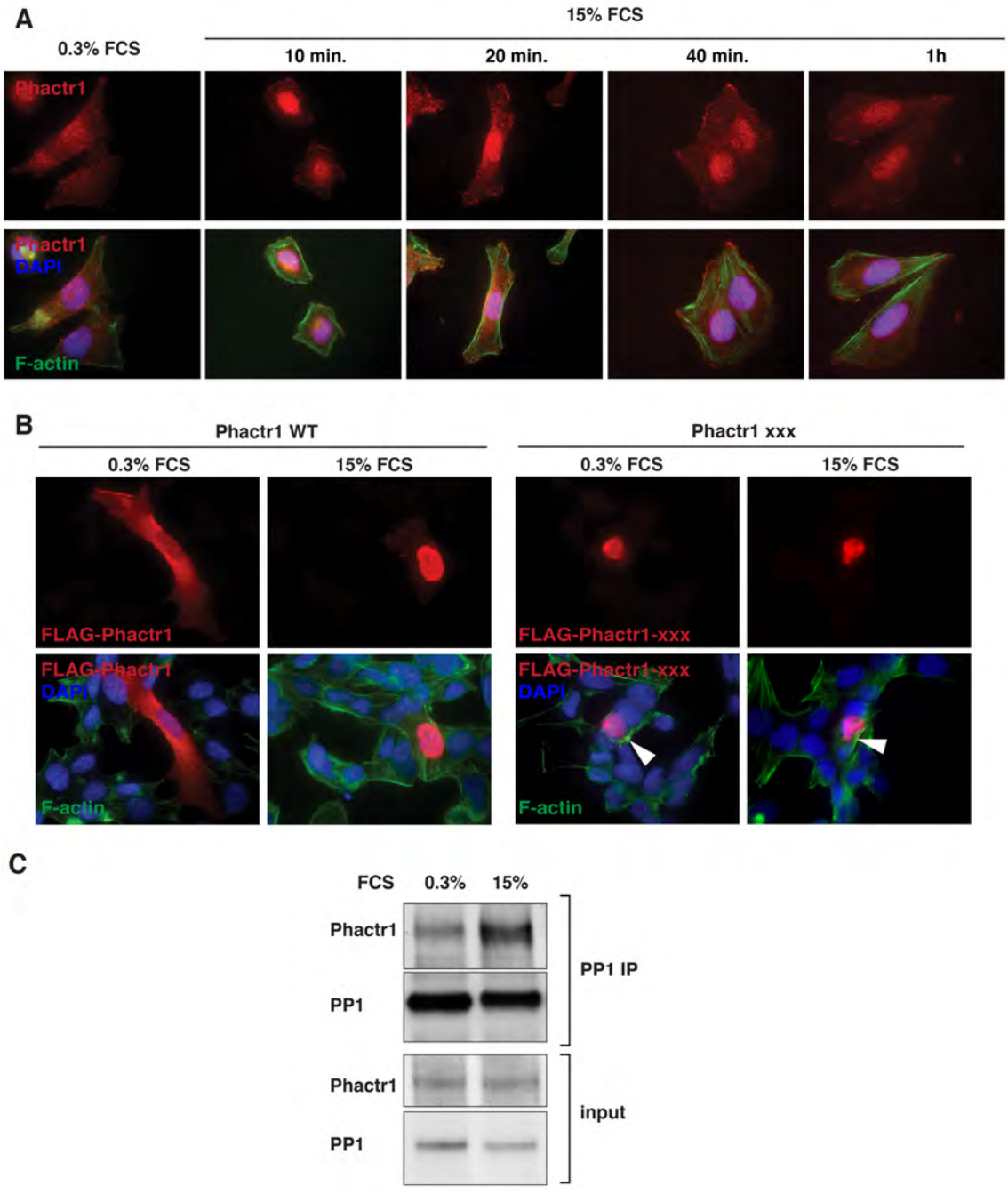
A
0.3% FCS
15% FCS
10 min.
20 min.
40 min.
1h
Phactr1
Phactr1
DAPI
F-actin
B
Phactr1 WT
Phactr1 xxx
0.3% FCS
15% FCS
0.3% FCS
15% FCS
FLAG-Phactr1
FLAG-Phactr1-xxx
FLAG-Phactr1
DAPI
F-actin
FLAG-Phactr1-xxx
DAPI
F-actin
C
FCS
0.3%
15%
Phactr1
PP1
PP1 IP
Phactr1
PP1
input

**Figure 5.1 Signal-induced Phactr1 nuclear accumulation and PP1 binding in CHL-1 melanoma cells.**

**(A)** Cells were maintained in 0.3% FCS for 20 hours, stimulated with 15% FCS, and endogenous Phactr1 visualised by fluorescence microscopy. **(B)** Cells were transfected with the FLAG-tagged Phactr-WT and Phactr-xxx and maintained in 0.3% FCS for 20 hours, with 1 hour serum stimulation, before visualisation of Phactr1 by fluorescence microscopy; white arrows indicate enhanced F-actin staining in cells transfected with Phactr1-xxx. **(C)** PP1 immunoprecipitates from CHL-1 cells maintained in 0.3% serum for 20 hours with or without a 1 hour serum stimulation were analysed by immunoblotting for endogenous Phactr1 and endogenous PP1. Immunoprecipitation was performed by Jasmine Abella.

## 5.3 Function of Phactr1 in CHL-1 melanoma cells

Having established a cell line for the studies of Phactr1 function, we next sought to characterise its role in the regulation of cytoskeletal dynamics. We have previously shown in NIH3T3 fibroblasts that the binding of PP1 to the C-terminal domain of Phactr1 can influence the actomyosin content of the cell (see section: 'Phactr1 interaction with PP1'). To examine the relevance of this finding and relate it to Phactr1 regulation in CHL-1 cells, we characterised cytoskeletal phenotypes arising from Phactr1 siRNA knock-down.

### 5.3.1 siRNA-mediated knockdown of Phactr1 expression

The siRNA-mediated knockdown of Phactr1 gene was initially performed using a pool of four siRNA oligos. The efficiency of the knockdown was assessed by immunoblotting, which showed very effective depletion of Phactr1 at 72 hours post-transfection with no protein detection at 64 kDa (Figure 5.2 A). To rule out off-target effects of the siRNA, deconvolution of the pooled siRNA was performed and three best oligos were used as a new siRNA pool (Figure 5.2 B). All experiments described below were carried out using the verified, pooled siRNA.

### 5.3.2 Phactr1 depletion induces morphological changes

To assess the effect of Phactr1 depletion in CHL-1 melanoma cells we firstly examined the morphology of the cells. Wild-type CHL-1 cells exhibit epithelial-like morphology with regular polygonal shapes and grow attached to the surface in discreet patches (Figure 5.2 C and Figure 5.3). Upon depletion of Phactr1 we could observe a significant change in the shape of the cells, which now became more rounded in comparison with the elongated wild-type cells (Figure 5.3). To assess changes in actin dynamics we visualised F-actin fibres with phalloidin. Phactr1 depletion led to the

reduction of transverse stress fibres and enhancement of F-actin staining on the cell periphery (Figure 5.3). This suggests an increase in the level of cortical actin versus transverse actin.

Intrigued by the alteration of cell morphology upon Phactr1 depletion, we hypothesised that knockdown cells might also exhibit defects in focal adhesion formation. In healthy cells, focal adhesions function as connectors of F-actin bundles with extracellular matrix. A variety of cytoskeletal proteins are involved in the formation of those connections, but many structural and signalling molecules are recruited to focal adhesions by an adaptor protein, paxillin (Brown and Turner, 2004). Paxillin binding partners include actin binding proteins like tubulin or vinculin and signalling proteins like FAK. Therefore, to evaluate the role of Phactr1 in the formation of focal adhesions we visualised paxillin in Phactr1-depleted CHL-1 cells. Diffuse paxillin staining in Phactr1-depleted cells indicated that F-actin associated focal adhesions were dispersed into smaller structures localising around the cell periphery (Figure 5.3). Consistently, all three deconvoluted siRNA oligos showed a very similar result to the pooled siRNA when used separately (Figure 5.2 C). This confirms the appropriate use of the siRNA pool and supports the view that Phactr1 is required for the formation of F-actin stress fibres and their attachment to the plasma membrane.

The interplay of actin polymerisation and the regulation of cell adhesion to extracellular matrix is necessary for proper regulation of cell migration. The analysis of Phactr1-depleted CHL-1 cells by immunofluorescence showed not only defects in F-actin localisation and content, but also disruption of focal adhesion formation as shown by paxillin staining. As described in the introduction, the spatiotemporal regulation of actin cytoskeleton by Rho-GTPases is essential for the proper control of cell motility. Because we observed defects in cytoskeletal organisation upon Phactr1 depletion, we next examined motility defects in those cells.

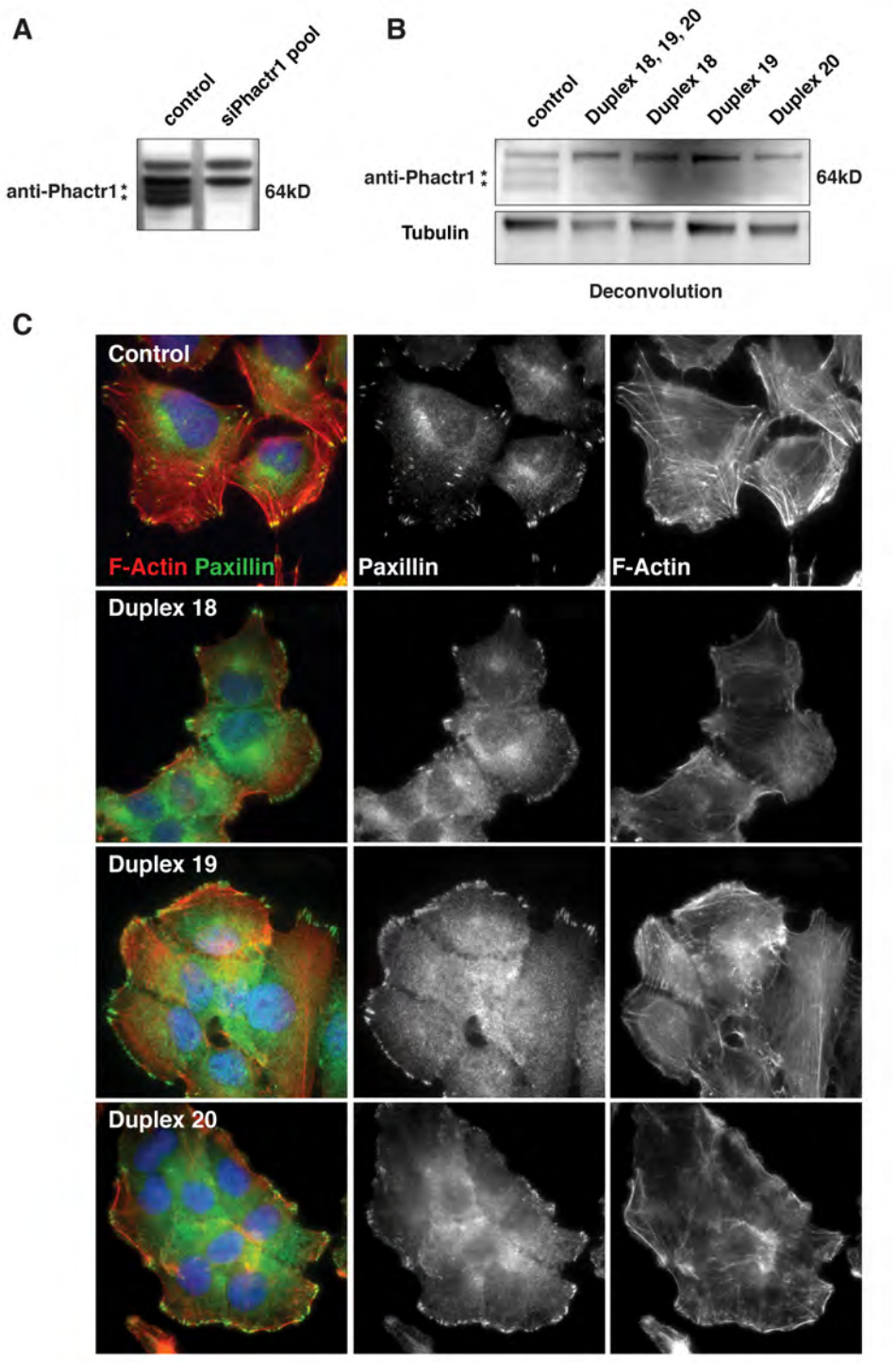
A
control
siPhactr1 pool
anti-Phactr1
64kD
B
control
Duplex 18, 19, 20
Duplex 18
Duplex 19
Duplex 20
anti-Phactr1
64kD
Tubulin
Deconvolution
C
Control
F-Actin Paxillin
Paxillin
F-Actin
Duplex 18
Duplex 19
Duplex 20

**Figure 5.2 siRNA-mediated knockdown of Phactr1 expression in CHL-1 cells.**

**(A)** CHL-1 cells treated with Dharmacon Phactr1 siRNA pool (for sequences see: 'Materials and methods') or control siRNA were analysed by immunoblotting with anti-Phactr1 antibody, detecting a Phactr1 doublet at 64kDa (*). **(B)** Three siRNAs from the siPhactr1 pool. Cells were treated with the Phactr1 oligonucleotides 18, 19, and 20 individually, or in combination, and analysed by immunoblotting with anti-Phactr1 antibody. **(C)** Morphological changes and actin stress fibre dispersal following Phactr1 knockdown by oligonucleotides 18, 19 or 20. Cells were stained for F-actin and paxillin. Images were taken by Jasmine Abella.

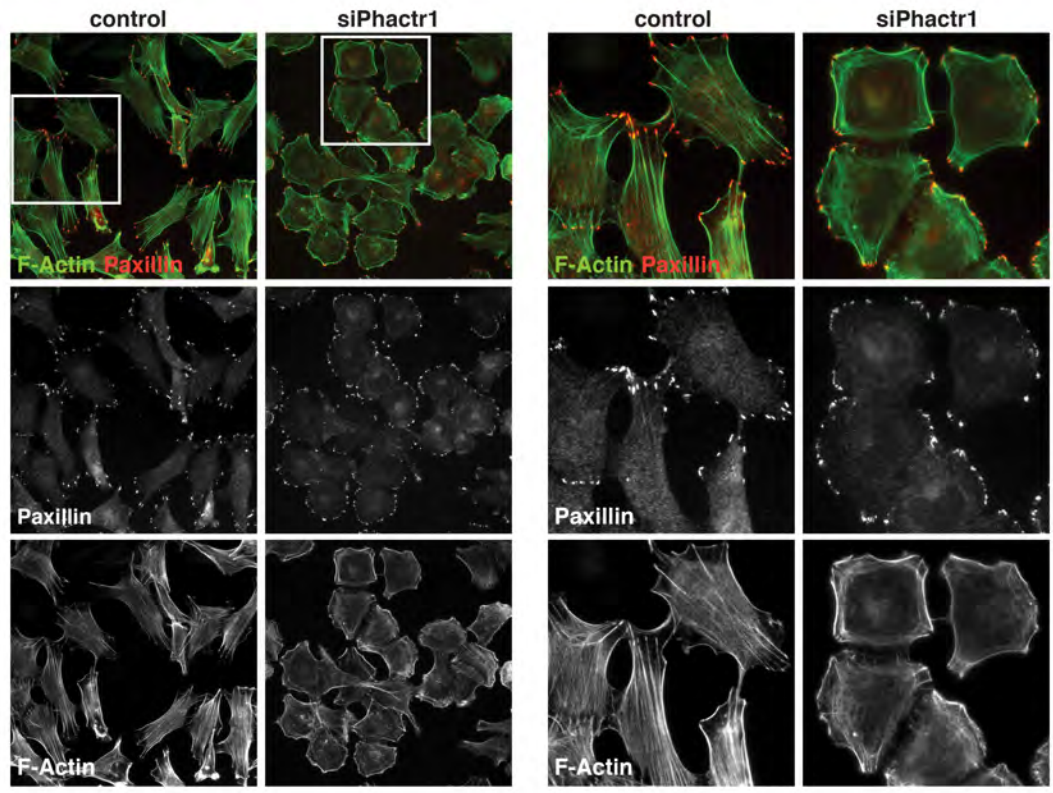


**Figure 5.3 Phactr1 depletion induces morphological changes.**

Morphological changes and actin stress fibre dispersal following Phactr1 knockdown. F-actin and paxillin were visualised by immunofluorescence in cells treated with control siRNA or the three active Phactr1 siRNA oligonucleotides used in combination. Panels on the right show single cell fields (65x) from the larger fields (25x) in the left panels. Images were taken by Jasmine Abella.

### 5.3.3 Phactr1 is required for the motility of CHL-1 cells

The scratch wound healing assay is a sensitive method for the evaluation of cell migration defects. Therefore, we used this technique to characterise the role of Phactr1 in cell motility. We seeded control and Phactr1-depleted CHL-1 melanoma cells on 96-well plates and applied a scratch when cells reached desired confluency. The closure of the scratch wound was monitored for 45 hours. Cells transfected with the control siRNA closed 90% of the wound in 45 hours, but Phactr1-depleted cells only reached 40% wound closure during that time (Figure 5.4 A).

Cell migration is essential for wound repair in this model, but to be productive it must proceed with directionality. Therefore, we next evaluated the directionality of CHL-1 melanoma cells upon Phactr1-depletion. Cells at the leading edge of the scratch were tracked using the Tracker software. Upon Phactr1 knockdown, CHL-1 cells lost their directionality in comparison to control cells (Figure 5.4 B). Moreover, Phactr-1 depletion caused a significant decrease in cell speed. Cells expressing control siRNA moved with the speed of around 13 μm/min, but Phactr1-depleted cells with only 8 μm/min and were less persistent (Figure 5.4 C).

### 5.3.4 Phactr1 activity is required for invasiveness

Some types of cancers, like melanoma, exhibit more invasive behaviour than other cancers. It has been proposed that melanoma cells invasiveness is related to the specific capability of those cells to migrate from the neural crest to the epidermis (Gupta et al., 2005; Vance and Goding, 2004). Several genes whose expression correlates with the metastatic melanoma behaviour have been identified. Some of them have been associated with the cytoskeletal organisation of melanoma cells, like NEDD9, an adaptor for focal adhesion kinase (Kim et al., 2006). Microphthalmia-associated transcription factor (MITF), crucial for melanocyte development was also linked to the

regulation of mDia1, which controls actin polymerisation (Carreira et al., 2006; Opdecamp et al., 1997).

Given the effects of Phactr1 depletion on stress fibre assembly, focal adhesions formation and cell motility, we hypothesised that the knockdown of Phactr1 might also affect the invasiveness of those cells. In order to metastasize, cells must be able to not only efficiently migrate but also secrete proteases to break down barriers on their way. Matrigel contains a complex mixture of proteins secreted by mouse sarcoma cells, which resembles extracellular environment of many tissues (Hughes et al., 2010). The use of matrigel as a system for studying the invasive behaviour of cells is now considered as a method of choice for quantitative measurement of cellular metastatic potential. Therefore, we performed a matrigel-based invasion assay in the Matrigel Invasion Chambers (for details see: 'Materials and Methods').

Phactr-1 depleted cells showed a significant decrease in their invasive behaviour when compared to the control cells (Figure 5.4 E). Consistent with our previous results, all three siRNA oligos showed decreased invasion into matrigel. This result indicates that Phactr1 activity is required for the invasiveness of CHL-1 melanoma cells and suggests that it might play a role in their metastatic behaviour.

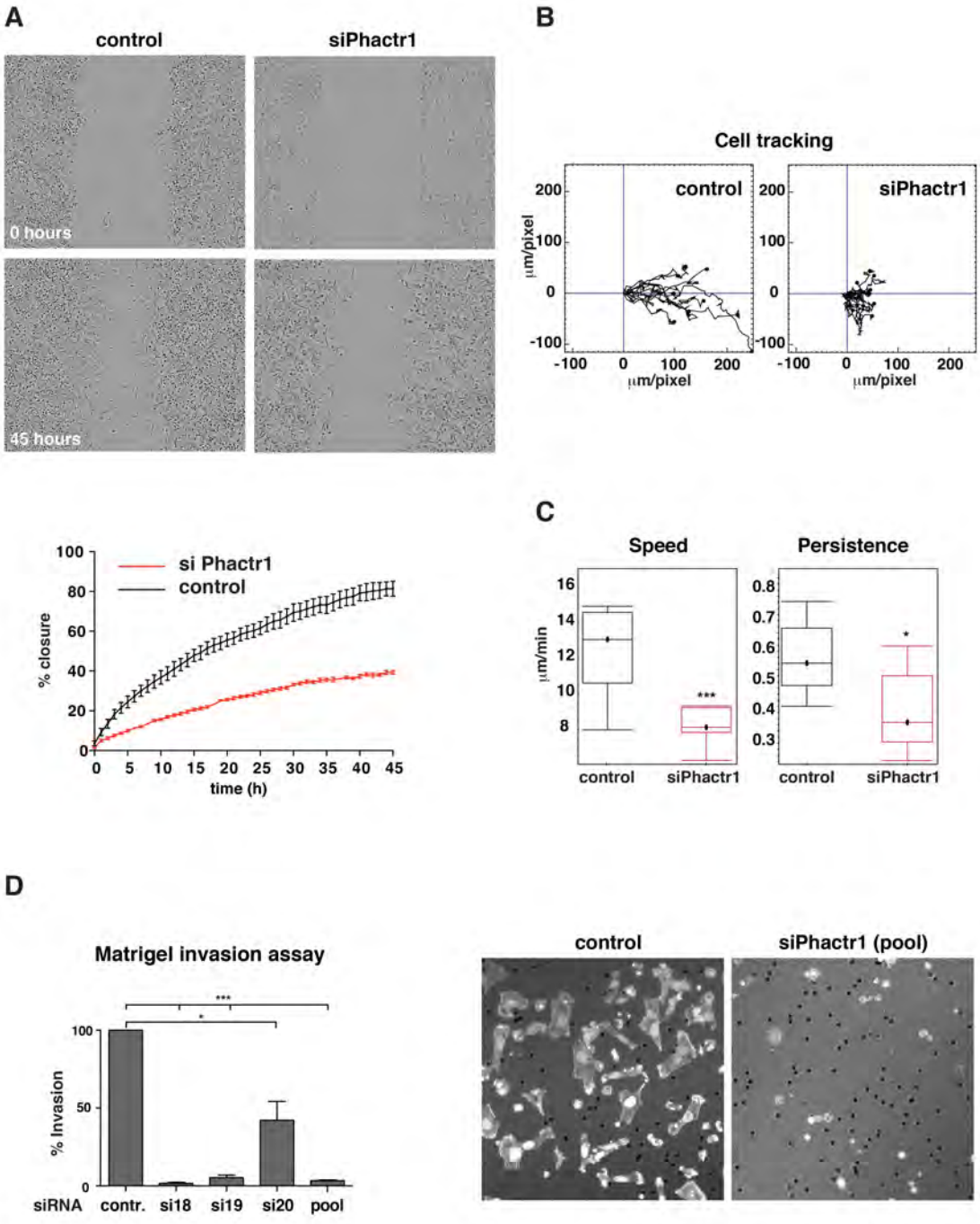
A
control
siPhactr1
0 hours
45 hours
B
Cell tracking
control
siPhactr1
µm/pixel
C
Speed
Persistence
µm/min
control
siPhactr1
si Phactr1
control
% closure
time (h)
D
Matrigel invasion assay
% Invasion
siRNA
contr.
si18
si19
si20
pool
control
siPhactr1 (pool)

**Figure 5.4 Phactr1 is required for motility and invasiveness in CHL-1 melanoma cells.**
**(A)** Phactr1 knockdown impairs cell motility. Cells were treated with control or the Phactr1 siRNA pool and grown to confluence. A scratch was made across the monolayer and migration of individual cells tracked over 45 hours using video microscopy. Top, microscopy images at 0 hours and 45 hours time points; bottom, time course of wound closure. **(B)** Tracks of 10 individual cells from the scratch wound shown for each population. **(C)** Migration speed and persistence calculated from cell tracking. Statistical significance was assessed by ANOVA (*P,0.05; ***P,0.001) (**D**) Phactr1 knockdown reduces CHL-1 melanoma invasiveness. Cells treated with control, individual Phactr1 siRNAs or the Phactr1 siRNA pool were allowed to migrate through a matrigel-coated filter towards serum-containing medium for 22 hours, and cells that had traversed the filter were then imaged. Efficiency of migration was expressed relative to control cells. Error bars represent the s.e.m. of three independent experiments, 16 images per experiment. Statistical significance was assessed by paired t-test (*P,0.05; ***P,0.001); right, examples of control and siPhactr1 (pool) microscopy images. Invasion assay was performed by Jasmine Abella.

## 5.4 Conclusions

In this chapter I have presented a study of Phactr1 in the endogenous setting. Because previous results in NIH3T3 fibroblasts indicated a role of Phactr1 in the assembly of actomyosin, we sought to elucidate the effect of Phactr1 depletion in CHL-1 cells melanoma cells.

We firstly showed that endogenous Phactr1 accumulates in the nucleus upon serum stimulation of CHL-1 cells. Subsequently, we showed that Phactr1 nuclear localisation correlates with the increase of PP1 binding to Phactr1. We then revealed a role of Phactr1 in the cytoskeletal dynamics, including focal adhesions formation and stress fibre assembly. Lastly, we elucidated the effect of Phactr1 depletion on the motility and invasiveness of melanoma cells.

We previously showed that Phactr1-PP1 interaction promotes MLC phosphorylation, which leads to actomyosin contractility. In contrast, upon Phactr1 depletion we observe loss of stress fibres. Taken together, this reveals a clear role of Phactr1 in cytoskeletal dynamics and we propose that this function is associated with Phactr1 interaction with PP1. However, a direct mechanism of Phactr1 interaction with PP1 and its downstream role in regulating MLC phosphorylation remains unclear and requires further analysis (see: ‘Discussion’).

# Chapter 6. Discussion

The aim of this thesis was to elucidate the molecular mechanism of Phactr1 interaction with actin and to explore its function. I have shown that Phactr1, like MRTF-A, responds to serum-induced activation of the Rho-actin signalling pathway. Depletion of the G-actin pool caused Phactr1 nuclear accumulation in fibroblasts and melanoma cells. Other members of Phactr family did not accumulate in the nucleus of NIH3T3 cell upon serum stimulation. The nuclear import of Phactr1 depends on Importin α-β binding to two nuclear localisation signals located within conserved domains at the N-terminus and C-terminus of Phactr1 and actin competed with Importin α-β for Phactr1 binding.

Structural analysis of Phactr1-actin complexes showed that the RPEL domain from Phactr1 binds three G-actin molecules, and not five like the RPEL domain of MRTF-A. We uncovered a new actin-RPEL interaction surface, crucial for the formation of higher-order complexes with actin, a secondary actin surface. We showed that secondary contacts, centered on the conserved glutamate, facilitate cooperative binding of G-actin molecules on tandem RPEL repeats and are required for the inhibition of Phactr1 nuclear accumulation by actin overexpression.

We showed that actin competes with PP1 binding for Phactr1 C-terminal region. Phactr1 binding to PP1 promoted actomyosin formation, dependent on Phactr1 nuclear localisation. In melanoma cells, Phactr1 depletion decreased stress fibre formation, cell motility and invasiveness. My data suggest that Rho-actin signalling to Phactr1 has an important role in controlling invasive and motile behaviour.

## 6.1 Mechanisms of Phactr1 regulation

### 6.1.1 Actin binding property of Phactr1

It was previously shown that Phactr proteins interact with actin (Allen et al., 2004; Sagara et al., 2009; Sagara et al., 2003), but the molecular mechanism of actin binding was not understood. It was suggested that actin binding occurs at the C-terminal RPEL domain of Phactr1 and Phactr3. I showed that serum-induced depletion of G-actin pool induces nuclear accumulation of Phactr1 (Figure 6.1). I then showed by fluorescence anisotropy that Phactr1 binds G-actin through all four RPEL motifs and mutation of the invariant arginine into an alanine abolished or significantly decreased actin binding. Cytoplasmic retention of Phactr1 is dependent on actin binding to its C-terminal RPEL domain. Within the C-terminal RPEL domain, RPEL1 and RPEL3 bind G-actin with high affinities and RPEL2 binds with lower affinity. These affinities reflect specific G-actin sensing property of the RPEL domain.

In MRTF-A, another RPEL protein, RPEL1 and 2 bind actin with higher affinity and RPEL3 binds with lower affinity (Guettler et al., 2008). Differences in RPEL-actin affinities signify regulatory properties of MRTF-A. RPEL domain in MRTF-A binds five actin molecules, but this complex is not stable and upon depletion of the G-actin pool two actin molecules dissociate. This allows Importin α-β binding and nuclear accumulation of MRTF-A (Mouilleron et al., 2011).

We showed by complex stoichiometry analysis that Phactr1 RPEL domain stably binds three G-actin molecules and not five. This is because the spacers between RPEL motifs in Phactr1 are shorter than in MRTF-A and not compatible with actin binding (see section ‘Structural analysis of Phactr1 interaction with G-actin’). Regulatory G-actin binding to the RPEL domain in Phactr1 depends on competitive Importin α-β binding to the NLS within the domain and on specific affinity of each

RPEL motif to actin. Therefore relative affinities of RPEL motifs to G-actin contribute to the regulation of Phactr1.

### 6.1.2 Phactr1 shuttling

#### *6.1.2.1 Response to signal*

Phactr1 accumulates in the nucleus upon serum stimulation and this response depends on Rho signalling, as co-expression of Phactr1 with a specific Rho inhibitor - C3 transferase, inhibits nuclear accumulation of Phactr1. Latrunculin B, an inhibitor of actin polymerisation induced constitutively cytoplasmic localisation of Phactr1. Cytochalasin D, an actin polymerisation inhibitor found to inhibit actin-RPEL interaction in MRTF-A (Miralles et al., 2003; Sotiropoulos et al., 1999) promoted nuclear accumulation of Phactr1 in unstimulated cells. These results show that Phactr1, like MRTF-A, responds to Rho-actin signalling.

Rho kinase, ROCK, also partially impairs the accumulation of Phactr1, as shown by Y-27632 treatment. Because inhibition of ROCK only partially impairs accumulation of Phactr1, it is conceivable that activity of another Rho effector – mDia might also contribute to this mechanism. Formins nucleate and elongate actin filaments and this mechanism effectively decreases the pool of G-actin (Chesarone and Goode, 2009). Activation of MRTF-SRF requires actin polymerisation and the ROCK-LIMK-cofilin signalling pathway. Dominant mDia1 derivatives inhibit serum and LIMK-induced SRF activation and reduce ability of LIMK to induce F-actin formation. This shows functional cooperation between RhoA-controlled LIMK and mDia effector pathways in MRTF-A-SRF pathway (Geneste et al., 2002). Consequently, Phactr1 localisation might as well be influenced by the activity of formins and future experiments could address this issue by co-expressing active mDia with Phactr1 and evaluating its subcellular localisation.

The basal level of Rho signalling is higher in MDA-MB-231 breast cancer cell line than in fibroblasts, which essentially changes the output of F-actin in those cells (Medjkane et al., 2009). MDA-MB-231 exhibit predominantly nuclear localisation of MRTF-A and Phactr1, which indicates similar G-actin sensing properties of both proteins. However, the dynamics of Phactr1 translocation to the nucleus in NIH3T3 cells is somewhat slower than of MRTF-A (Vartiainen et al., 2007). We observe Phactr1 accumulation in the nucleus after around 20 minutes of serum stimulation, but MRTF-A accumulates within few minutes. This difference might be a reflection of a relatively stronger G-actin interaction of Phactr1 RPEL motifs.

#### *6.1.2.2 Actin overexpression*

We have shown that G-actin sensing by Phactr1 is dependent on actin binding to the C-terminal RPEL repeat. Deletion of the triple RPEL domain or mutation of invariant arginines results in constitutive nuclear localisation of Phactr1. However, we found that either deletion or mutation of RPEL-N did not affect nuclear accumulation of Phactr1 upon serum stimulation. However, upon artificial elevation of G-actin levels, the integrity of both RPEL-N and the RPEL domain was required to inhibit the nuclear accumulation of Phactr1. The saturation of all actin binding sites and the effective occlusion of Importin α-β binding sites is therefore required to achieve the inhibition of Phactr1 by actin. This shows that RPEL-N is an additional sensor of G-actin, which registers upon high G-actin levels. This suggests that Phactr1 might form a tetravalent complex with G-actin in this context. The discovery of secondary actin surface supports this model (see following section: ‘Structural analysis of Phactr1 interaction with actin’).

This regulatory mechanism is distinct from MRTFs and supports a model in which the two protein families are regulated differentially. However, actin overexpression is an *in vitro* system and we do not know under what physiological circumstances it would occur. Nevertheless, the finding that both RPEL families respond to Rho-actin signal and exhibit G-actin mediated inhibition of nuclear

accumulation shows that actin overexpression assay reflects a real regulatory phenomenon.

#### *6.1.2.3 Export*

There are many similarities in the mechanism of shuttling by MRTF-A and Phactr1. However, we still do not understand if Phactr1 is continuously shuttling between the nucleus and the cytoplasm, like MRTF-A. MRTF-A is continuously exported from the nucleus via exportin Crm1 and serum stimulation reduces binding of G-actin to MRTF-A, which in turn reduces its export (Vartiainen et al., 2007). We show by LMB treatment that Phactr1 is not exported from the nucleus via Crm1, which indicates a distinct export mechanism for MRTF-A.

Finding an export pathway of Phactr1 would not only help to understand molecular mechanism of its export, but would also serve a tool for studying the continuous shuttling of Phactr1. Future studies should address this issue by employing siRNA screen of export factors inhibitors in NIH3T3 cells or CHL-1 melanoma cells. Inhibition of Phactr1 export pathway would also help to better understand its function in the nucleus.

#### *6.1.2.4 Import*

We show that import of Phactr1 is mediated by Importin α-β (Figure 6.1). We performed detailed mutational analysis of Phactr1 NLS sequences to show that both the B1 and B2 regions are mediating Phactr1 import. As expected, mutations of the basic residues within the B1 sequence abolished Phactr1 nuclear accumulation. Our studies of actin binding to the RPEL domain uncovered the B2 region, sensitive to mutagenesis even when the B1 region was active. However, combination of the B1 and B2 mutations together with abolishing actin binding to the RPEL domain (xxxK3A KRE/3A) showed that, to a small extent, nuclear import is still active. Interestingly, the actin-binding-

defective NLS mutant of Phactr1 (xxxK3A KRE/3A) was pan-cellular in unstimulated cells suggesting a strong contribution of the B2 region to the regulation of Phactr1. It is hard to evaluate why this mutant is not fully cytoplasmic, and one possibility is that to achieve full cytoplasmic retention of Phactr1 in the absence of actin, the whole B2 sequence might have to be deleted. Another possibility is that additional nuclear localisation signals are present in Phactr1.

Import mechanisms of Phactr1 and MRTF-A are very similar. Both proteins bind Importin α-β to their conserved NLS sequences and in both cases actin competes with Importin α-β for binding. However, the RPEL domain from Phactr1 cannot functionally replace the RPEL domain in MRTF-A. This might be caused by the insufficient nuclear localisation signal within the domain of Phactr1, as Phactr1 import is mediated by two NLSs. This experiment also showed that apparent LMB sensitization by the chimera is decreased, which might suggest that the RPEL domain in MRTF-A determines Crm1 signal.

Similar, actin-dependent import mechanism was recently shown for Junction-mediating and regulatory protein (JMY). JMY was first identified as a WH2-domain transcriptional co-activator that promotes cell death in response to DNA damage. However, in the cytoplasm JMY promotes actin filament assembly and cell migration (Coutts et al., 2007; Shikama et al., 1999; Zuchero et al., 2009). It was recently proposed that JMY shuttles to the nucleus to mediate its nuclear function, but it is not clear if JMY actually continuously shuttles between the nucleus and the cytoplasm as its export factor was not identified (Zuchero et al., 2012). However, like in RPEL proteins, the interaction of G-actin with JMY blocks Importin α-β binding to the NLS sequence and prevents its import. Genome analysis showed that besides MRTF and Phactr families, some other proteins contain putative actin-binding domains and Importin α-β binding sites (Zuchero et al., 2012). It would be interesting to test whether those proteins also confer actin-dependent nucleocytoplasmic shuttling.

### 6.1.3 Other Phactr family members

Phactr1 is the only Phactr family member that accumulates in the nucleus upon serum stimulation in NIH3T3 fibroblasts. Given sequences similarity between the four proteins, it is somewhat surprising that Phactr2, 3 and 4 are not responding to cellular G-actin levels in the same way. This distinct behaviour might be related to several factors.

Firstly, regulation of nuclear import might be different due to the properties of nuclear import signal elements and export machinery in other Phactr family members. This issue was not addressed in this study and analysis of NLS sequences in Phactr2, 3 and 4 might explain this variability. Indeed, Huet and colleagues recently suggested that the N-terminal domain in Phactr4 might be a membrane-targeting unit (Huet et al., 2012), but no specific myristoylation motif was shown. Surely, more mutational analysis is needed to fully understand behaviour of Phactr4 and location of membrane targeting sequences.

Secondly, the affinity of Phactr1 to G-actin is high for all four RPEL motifs, but this is not the case for the rest of the Phactr family members, which each contain one RPEL that does not bind G-actin. Therefore, we might expect that those proteins would form different higher-order assemblies with G-actin. Future experiments should address differential behaviour of other Phactr family members. Determining the localisation of different Phactr family chimeric proteins, containing for example NLS sequences form Phactr1, could provide more insight about the functionality of these regions in other family members.

### 6.1.4 Phactr1 interaction with PP1

Previous studies indicated multiple interaction sites between PP1 and Phactr family members. It was shown that last ten amino acids of Phactr proteins were required

for PP1 binding in co-immunoprecipitation assays, with F577 and H578 playing crucial roles (Allen et al., 2004; Sagara et al., 2009) (Figure 1.16). R650 in Phactr4 was also shown to play a role in the PP1 interaction (Kim et al., 2007). Additionally, one study suggests that RPEL3 might also be involved in a PP1 interaction, as a construct containing this sequence was more effective in PP1 inhibition assays (Sagara et al., 2003).

We confirmed that truncation of the whole C-terminal region was indeed required for the interaction with PP1, as it was effective in abolishing PP1 binding in co-immunoprecipitation assays. We also found that the RPEL domain in Phactr1 is required for PP1 binding, suggesting that the PP1 binding site extends and overlaps with RPEL3 within the RPEL domain. In a direct binding assay, we later showed that actin competes with PP1 for Phactr1 C-terminal region. However, the exact interaction points of PP1 and Phactr1 are not shown.

Considering, that Phactr1 possesses a version of the PP1 binding consensus (R/K)$x_{0-1}$(V/I)x(F/W) at the C-terminal end of RPEL3 (represented by $^{517}$KILIRF$^{522}$), it might be interesting to perform additional mutational analysis of KILIRF region to address this question. Mutations of the I520 and F522 into alanines within this sequence in Phactr1 might answer questions about the presence of PP1 binding consensus in Phactr family of proteins. These mutations in yeast homologs of Phactr proteins, Afr1 and Bni4 inhibit their interaction with yeast PP1, Glc7 (Bharucha et al., 2008; Larson et al., 2008). According to a recent view of PP1 binding mode, this consensus in Phactr1 might serve as a docking region for PP1 binding (Roy and Cyert, 2009). Therefore, either the region encompassing the conserved R536 (R650 in Phactr4) or the conserved F577 would be the PP1 activity-modulating site (Allen et al., 2004; Kim et al., 2007). I hypothesise that Phactr1 might therefore exhibit similar PP1 binding mode to MYPT1, which has several PP1 interaction points and structurally wraps around PP1 (Figure 1.13). Ultimately, only the structural analysis of PP1 binding to Phactr1 could fully explain the molecular mechanism of PP1 binding to Phactr1.

We found that PP1 binding site in Phactr1 is not required for its translocation to the nucleus. It was somewhat puzzling for us, why Phactr1 translocates to the nucleus in the first place, and the initial hypothesis was that Phactr1 is required in the nucleus as a PP1 binding partner. Because PP1 can be differentially expressed within the cell, we examined the localisation of endogenous PP1 in NIH3T3 cells to find that it was indeed nuclear. Consistent with our view, Phactr-xxx was constitutively nuclear and also bound PP1 all the time. However, deletion mutant of the PP1 binding site (Phactr1-xxxΔC) was also nuclear, but did not bind PP1. Therefore, Phactr1 is targeted to the nucleus to interact with PP1, but PP1 is not dictating the localisation of Phactr1 (Figure 6.1). It was suggested that other Phactr family member, Phactr4 interacts with PP1 in the cytoplasm, which also suggests that PP1 is not required for Phactr1 nuclear localisation (Huet et al., 2012).

In our study we analysed Phactr1 interaction with PP1α, an isoform of PP1 initially found to bind Phactr1 by Allen and colleagues (Allen et al., 2004). We assume that Phactr1 is equally competent to bind other isoforms of PP1, as this was recently shown for Phactr4 (Kim et al., 2007). However, given some of the differences between Phactr proteins, a direct test should be performed to confirm our assumption.

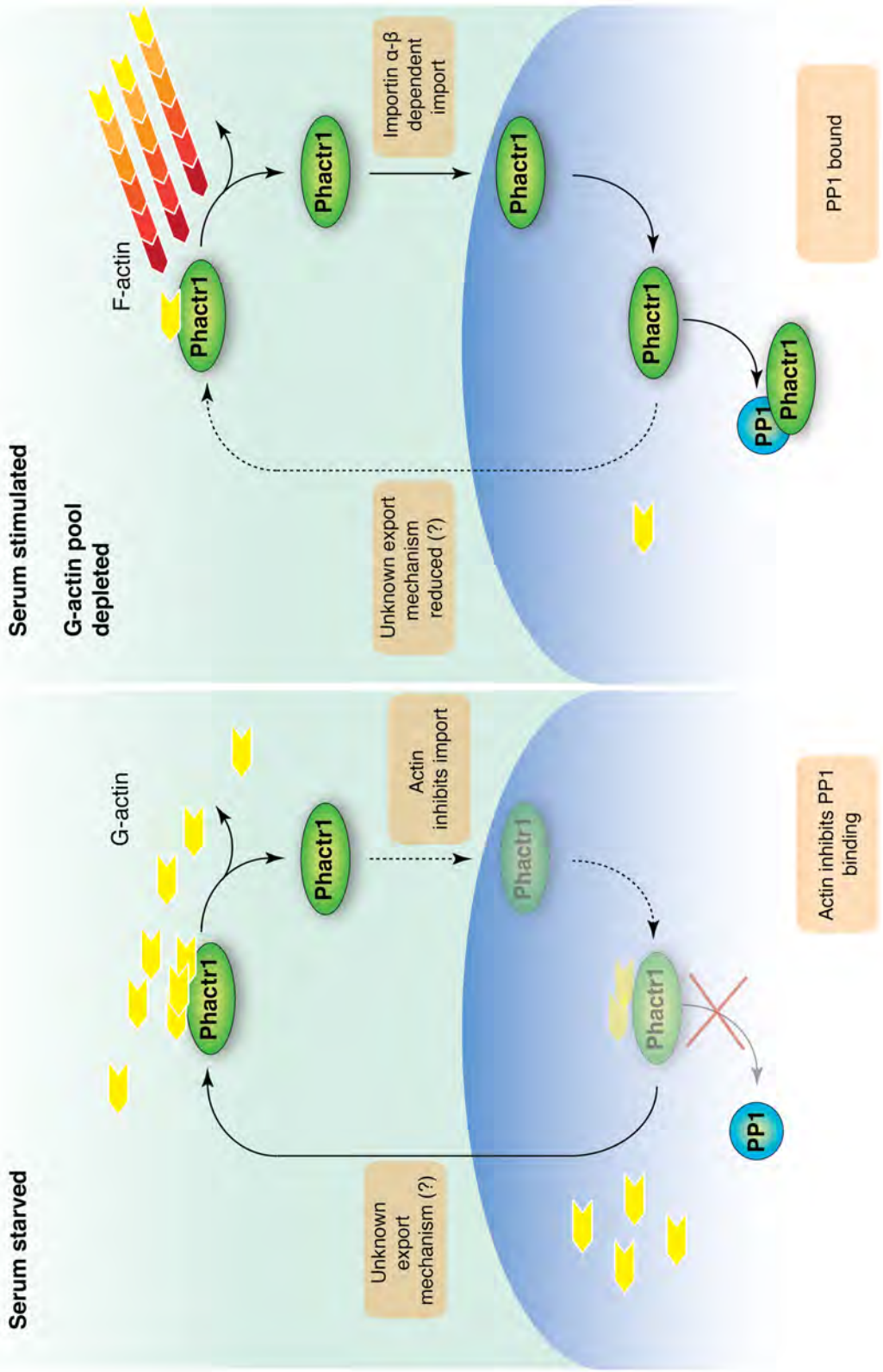
Serum stimulated
G-actin pool depleted
F-actin
Phactr1
Importin α-β dependent import
Unknown export mechanism reduced (?)
PP1
PP1 bound
Serum starved
G-actin
Actin inhibits import
Unknown export mechanism (?)
Actin inhibits PP1 binding

**Figure 6.1 Molecular mechanism of Phactr1 nuclear accumulation upon serum stimulation.**

In starved cells, Phactr1 is predominantly cytoplasmic and binds G-actin. Actin inhibits Importin α-β dependent import of Phactr1 and PP1 binding. It is not known whether Phactr1 is actively exported from the nucleus. Upon serum stimulation, G-actin pool in the cell decreases, which allows Importin α-β to bind Phactr1 and promotes its import. Subsequently, PP1 is now competent for the interaction with Phactr1 in the nucleus.

## 6.2 Structural analysis of Phactr1 interaction with G-actin

### 6.2.1 RPEL motif interactions with G-actin

It was previously shown that individual RPEL motifs from MRTF-A interact with actin monomers through primary contacts between the helices in RPEL motifs and hydrophobic cleft and ledge in G-actin (Mouilleron et al., 2008). Highly conserved RPEL motif G-actin contacts are predominantly hydrophobic and in RPEL2$^{MRTF-A}$ involve L131, I136 and L137 in helix-α2, and L118 and I122 in helix-α1 (Figure 1.10 C). The invariant R-loop arginine, critical for G-actin binding, forms a salt bridge with the C-terminus of G-actin (Mouilleron et al., 2008). We showed by X-ray crystallography that primary actin contacts are also present in the high-resolution structures of Phactr1 RPEL motifs with G-actin. We observed additional primary contacts, which contribute to the high affinity of Phacr1 RPEL motifs, as shown by fluorescence anisotropy analysis.

G-actin•RPEL-N and G-actin•RPEL2 structures revealed the presence of secondary actin interaction surface, also observed in the trivalent G-actin•RPEL$^{Phactr1}$ domain complex structure (see further below). These contacts are highly conserved in all RPEL motifs form Phactr1 and in RPEL motifs in MRTF-A. We observed the same three RPEL residues at the secondary actin interface in both structures: the residue preceding the conserved RPEL arginine, the conserved RPEL glutamate, and the basic residue from the C-cap (M146/ E152/ R156$^{RPEL-N}$ and Q468/ E474/ R478$^{RPEL2}$) (Figure 4.9 B). We show that these residues act together to form a stable secondary interaction on the G-actin interface. The basic C-cap residue represented by R156$^{RPEL-N}$ and R478$^{RPEL2}$ each interact with the C-terminus of helix 203–216 of the secondary actin through hydrogen bonds. The invariant RPEL glutamate residue (E152$^{RPEL-N}$ and E474$^{RPEL2}$ ) interacts either indirectly via a water molecule or directly with secondary actin.

Secondary contacts were not observed previously in MRTF-A due to the lower resolution of multivalent G-actin•MRTF-A complexes. Superposition of the secondary actin contacts made by RPEL domain from Phactr1 and MRTF-A revealed a strikingly similar interaction surface, centred on the invariant glutamate. Therefore, RPEL motif interactions with G-actin are based of two groups of interactions, primary and secondary actin contacts (Figure 6.2).

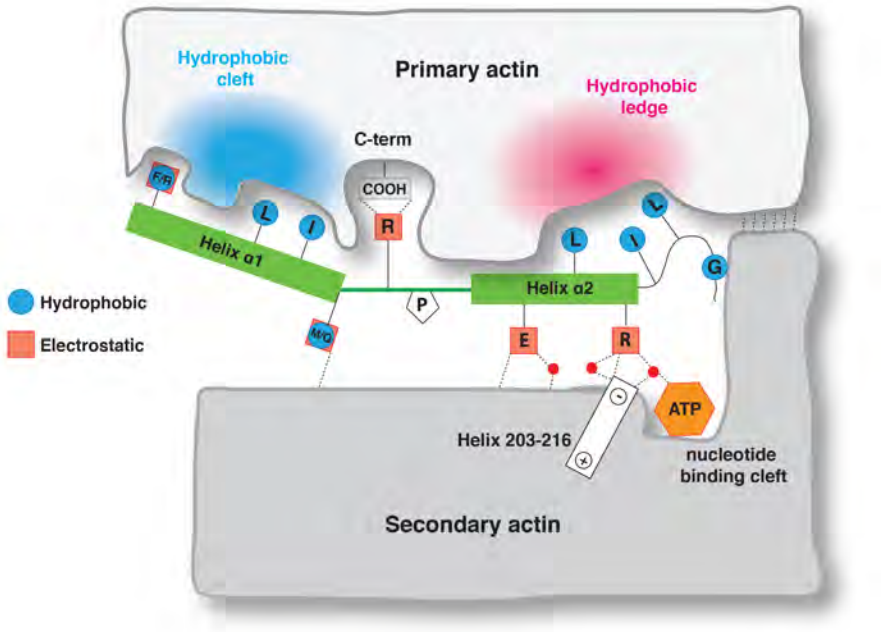


**Figure 6.2 Schematic model of Phactr1 RPEL motifs interaction with actin monomers.** Primary and secondary G-actin contacts made by RPEL motif (green) in Phactr1. Primary G-actin contacts are based on the interaction of hydrophobic cleft and hydrophobic ledge of G-actin with helix-α1 and helix-α2 of the RPEL motif. Secondary G-actin contacts are centred on the conserved glutamate and a conserved basic C-cap residue (here represented by an arginine). Helix 203-216 in G-actin and the nucleotide binding cleft are crucial points of G-actin secondary interaction surface with RPEL motif. Adapted from figure by Stephane Mouilleron.

### 6.2.2 Trivalent G-actin•RPEL domain complex

We show by X-ray crystallography that the RPEL domain form Phactr1 binds three G-actin molecules to form a trivalent complex. Analysis of the structural data shows that G-actin•RPEL$^{Phactr1}$ crystals contained two trivalent complexes in the asymmetric unit. However, in solution a single trivalent complex is present, as shown by SEC-MALLS and SAXS analysis (Mouilleron et al., 2012).

The trivalent G-actin•RPEL domain $^{Phactr1}$ complex is a rare example of a closed helical assembly and is distinct from the pentavalent G-actin•RPEL domain $^{MRTF-A}$ assembly. In MRTF-A, primary actin contacts are conserved not only within the RPEL motifs, but also within the intervening spacers, which also bind G-actin and they are crucial for the formation of a pentavalent G-actin•RPEL domain $^{MRTF-A}$ assembly (Mouilleron et al., 2011). The trimeric G-actin•RPEL domain$^{Phactr1}$ complex spacers are shorter and incompetent for the interaction with G-actin. Therefore, the main difference between the two complexes is the lack of spacer actins within the G-actin•RPEL domain$^{Phactr1}$ complex. However, both complexes adopt strikingly similar trajectories and the shape of both RPEL domain cranks is virtually the same. This similarity is due to the presence of the secondary actin contacts, present in both complexes.

We showed by mutational and complex stoichiometry analysis that secondary actin interface within the G-actin•RPEL domain$^{Phactr1}$ complex facilitates cooperative actin binding within the RPEL domain of Phactr1 and contribute to the rigidity of this assembly. This analysis explained the lower affinity of RPEL2$^{Phactr1}$ to G-actin (actin R2). Within the trivalent complex, the binding of actin R2 is supported by secondary interactions with RPEL1$^{Phactr1}$ and by the rigidity of the complex.

We also show that secondary contacts are present in the pentavalent G-actin•RPEL domain $^{MRTF-A}$ complex. Therefore, to explain the striking similarities between shapes of the two cranks, we suggest that the secondary contact surface contributes to the arrangement of the pentavalent G-actin•RPEL domain$^{MRTF-A}$ complex.

However, mutational analysis of these interactions in MRTF-A should be performed to address this issue.

We now understand the conservation of the secondary surface contact, glutamate in RPEL-N $^{Phactr1}$, RPEL1 $^{Phactr1}$, RPEL2 $^{Phactr1}$ and in RPEL1 $^{MRTF-A}$ and RPEL2 $^{MRTF-A}$. However, it remains hard to understand the conservation of this residue in the C-terminal RPEL3 motif. Perhaps it is involved in the intramolecular interactions with other binding partners. In Phactr1, residues implicated in the maintenance of secondary actin interactions are essentially overlapping with PP1 binding sites. Structural analysis of PP1 interaction with Phactr1 could help to understand the conservation of secondary actin contacts in RPEL3.

Although significant progress has been made in the understanding of actin-RPEL interactions within higher-order assemblies in both MRTF-A and Phactr1, we still struggle to fully understand the dynamics of actin loading onto tandem RPEL motifs. Indeed, we observe actin binding cooperativity within the RPEL domain, but we do not distinguish the order of actin monomers assembly and disassembly onto the domain. Analysis of secondary contacts within the MRTF-A RPEL domain might help to answer this intriguing question.

### 6.2.3 Significance of the secondary actin surface

Studies of Phactr1 regulation revealed that C-terminal RPEL domain, but not RPEL-N was required to mediate Phactr1 regulation by G-actin. However, actin overexpression experiments showed that the integrity of the C-terminal domain and RPEL-N is required for the inhibition of Phactr1 accumulation by G-actin, which arises from the saturation of all four RPEL motifs by G-actin. By mutational analysis we showed that secondary actin contacts facilitate this process. Mutagenesis of the secondary contact residues in RPEL-N showed that they are required for actin-mediated inhibition of Phactr1 nuclear accumulation in localisation assays.

We hypothesise that under conditions of elevated actin concentration *in vivo,* Phactr1 might form a tetravalent G-actin•RPEL domain$^{Phactr1}$ complex through secondary contacts between the actin-bound RPEL-N and the RPEL1 primary actin (Figure 6.3). We assume that within this tetravalent assembly, the access to both B1 and B2 import signals would be impaired. This state can be considered equivalent to the pentavalent G-actin•RPEL domain$^{MRTF\text{-}A}$ assembly, in which Importin α-β binding sites are occluded by actin.

A recently reported crystal structure of MRTF-A RPEL domain in complex with the ARM-repeat domain of Importin-α showed that upon this interaction MRTF-A adopts an extended conformation (Hirano and Matsuura, 2011). The folding of MRTF-A in the pentavalent actin complex is entirely different from its conformation within the MRTF-A:Importin-α complex. The NLS residues in MRTF-A engage in a α-helical conformation upon actin binding, which is incompatible with Importin-α binding. The structural study of Phactr1 complex with Importin-α was not yet reported, but it is probable that the structure of RPEL motifs and NLS sequences in Phactr1 also engages in an extended conformation, or simply a different conformation to the actin-bound state. This would suggest that the actin-binding state and Importin α-β -binding states are indeed mutually exclusive.

In theory, secondary actin contacts would induce the interaction between the N-terminal and the C-terminal parts of Phactr1 and future experiments should establish if this interaction occurs. This can be investigated *in vivo* by fluorescence resonance energy transfer (FRET) between the donor and acceptor fluorofores fused to the ends of Phactr1.

The question of generality of the RPEL motif in conferring nucleocytoplasmic shuttling was somewhat intriguing. We learned that Phactr1 and MRTF-A use very similar molecular mechanisms to be targeted to the nucleus. It would be interesting to find and study other proteins, which contain tandem RPEL repeats to further expand the analysis of RPEL generality. Because those motifs seem to play roles in targeting proteins to perform important biological roles, the discovery of new RPEL proteins

could lead to the discovery of new functions. Moreover, the presence of a secondary interaction surface supports a view that the actin-RPEL interaction promotes the formation of higher-order actin assemblies on tandem repeats, which could have actin-sequestering cytoskeletal roles.

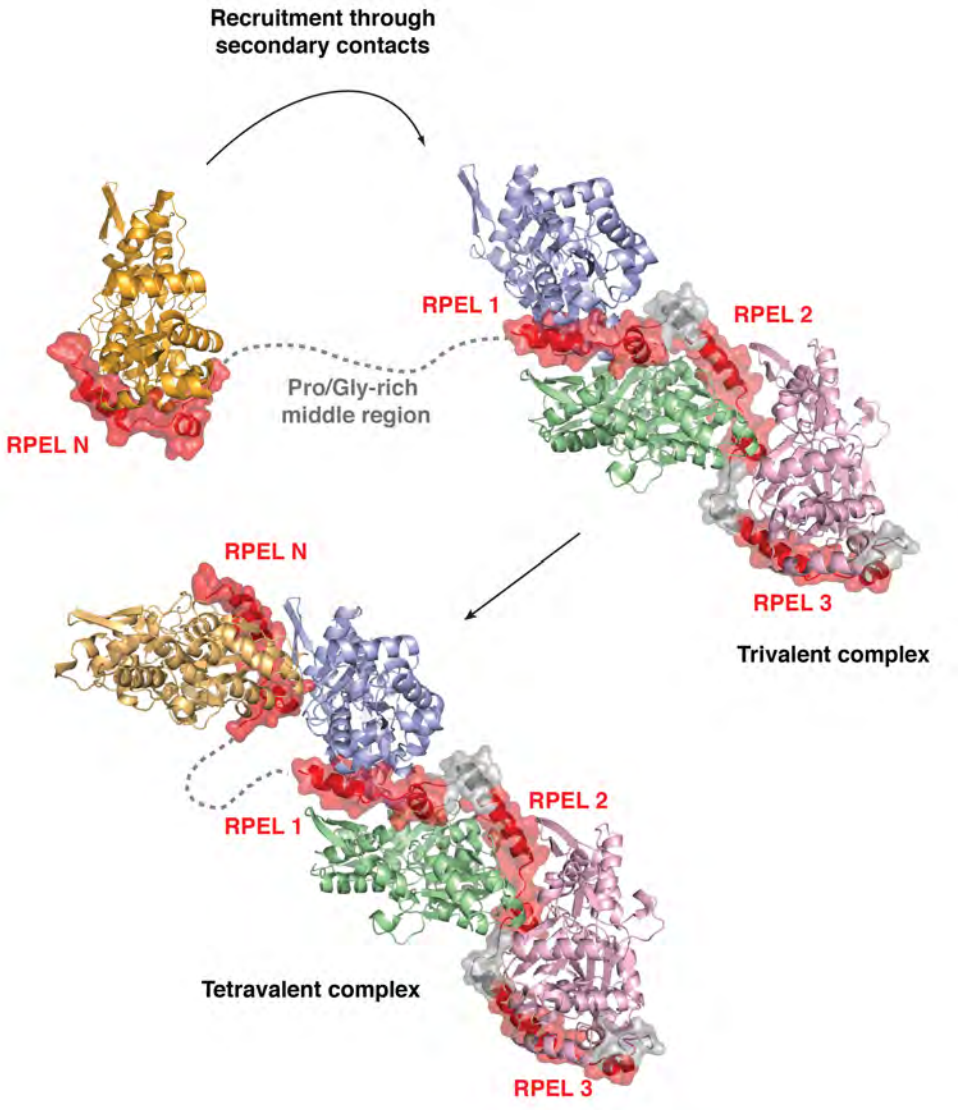


**Figure 6.3 Model of tetravalent G-actin•Phactr1 assembly.**

Model for the recruitment of G-actin•RPEL-N to the trivalent G-actin•RPEL domain$^{Phactr1}$ complex through RPEL-N secondary actin contacts. This nuclear-import-inhibited tetravalent assembly might be present upon high G-actin concentrations. Adapted from figure by Stephane Mouilleron.

## 6.3 Function of Phactr1

### 6.3.1 Actomyosin rearrangements induced by active Phactr1

We showed that the expression of PP1-bound Phactr1-xxx promotes striking cytoskeletal rearrangements in NIH3T3 cells. These rearrangements depend on PP1 binding to the C-terminal region of Phactr1, because deletion of this domain abolished the phenotype. Phactr1-xxx expression showed either condensed foci of actomyosin or thickened stress fibres. It is intriguing to understand why cells expressing Phactr1-xxx exhibit two forms of similar rearrangements. A simple assumption is that the two phenotypes reflect populations of cells with different levels of Phactr1-PP1 activity. A similar phenotype was also noticed during the expression of wild-type Phactr1, but only upon serum stimulation. Wild-type Phactr1 induced milder effect, as PP1-Phactr1 interaction is weaker in comparison to PP1-Phactr1-xxx, as shown in co-immunoprecipitation assays.

We show by quantitative immunofluorescence and localisation analysis that Phactr1 needs to be localised in the nucleus to induce the actomyosin phenotype. We used actin-binding defective NLS mutant of Phactr1 (xxxK3A KRE/3A) to evaluate a link between Phactr1 nuclear localisation and actomyosin rearrangements. However, this mutant is not fully cytoplasmic and can still bind PP1 in the nucleus. Therefore, to ultimately show that nuclear localisation is required for PP1 binding, it would be best to use a mutant, which is (1) localised exclusively in the cytoplasm, (2) does not bind actin and (3) is able to interact with PP1. Nevertheless, our results strongly suggest that only nuclear Phactr1 binds PP1 as only Phactr1-xxx and stimulated wild-type Phactr1 induce rearrangements.

Expression of ROCK was previously implicated in the promotion of actin rearrangements (Leung et al., 1996; Sahai et al., 1998), which are reminiscent of those induced by the expression of non-actin binding Phactr1 mutant (Phactr1-xxx). One of

the main functions of ROCK is the control of actomyosin crosslinking by regulation of MLC phosphorylation at S19 and T18 (see 'Actomyosin contractility' and (Somlyo and Somlyo, 2000)). We found that rearrangements observed in cells expressing Phactr1-xxx exhibit enhanced MLC phosphorylation at S19 and T18. Moreover, the phenotype rapidly dispersed upon blebbistatin treatment, a specific inhibitor of MLC ATPase.

This indicates that Phactr1 might regulate MLC phosphorylation by interacting with PP1. To dephosphorylate MLC, PP1 associates with MYPT1 to form active MLC phosphatase (MLCP) (for review, see (Ito et al., 2004)). Therefore, Phactr1 binding to PP1 might prevent the formation of active MLCP, which would lead to increase in MLC phosphorylation and actomyosin crosslinking. However, we do not know if the role of Phactr1 is directly linked to MLCP of if Phactr1 is involved in promoting MLC phosphorylation indirectly, for example through gene expression. A direct role is hard to evaluate, because nuclear localisation of Phactr1 is required to promote MLC phosphorylation and MLC is localised in the cytoplasm (see following section 'Phactr1 function in cytoskeletal homeostasis').

### 6.3.2 Cytoskeletal phenotypes induced by Phactr1 depletion.

To better understand function of Phactr1 we examined its roles in the context of malignant melanoma cells, where it is highly expressed (Koh et al., 2009; Trufant, 2010). In CHL-1 cells, Phactr1 also translocates to the nucleus and exhibits enhanced interaction with PP1 upon serum stimulation, as shown by fluorescence microscopy and co-immunoprecipitation. However, expression of non-actin binding Phactr1-xxx did not induce similar degree of cytoskeletal rearrangements as in NIH3T3 cells. This might be due to different relative levels of G- and F-actin in the two cell lines. Taken together, these findings confirmed that Phactr1 regulation is a more general mechanism and established CHL-1 as a relevant cell line to study Phactr1 function.

Upon Phactr1 depletion in CHL-1 cells, stress fibres become severely dispersed, cell spreading and motility is significantly decreased and cells loose persistence in

scratch wound assays. Moreover, Phactr1-depleted cells fail to invade into the matrigel. Therefore, in CHL-1 melanoma cells Phactr1 is required for the maintenance of cell morphology, cell motility and invasiveness. This finding is in agreement with previous studies, which showed that Phactr1 is involved in promoting motility of endothelial cells (Allain et al., 2011; Jarray et al., 2011). Phactr3 was also shown to have a role in cell morphology, as disruption of PP1 interaction induced cell rounding and shrinkage (Sagara et al., 2009). We have shown in NIH3T3 cells that Phactr1-induced phenotypes are directly linked to the interaction with PP1. We therefore suggest that Phactr1 binding to PP1 is required for the maintenance of stress fibre assembly and actomyosin crosslinking in CHL-1 melanoma cells.

### 6.3.3 Phactr1 function in cytoskeletal homeostasis

Here, we present a model, where Phactr1 binds and sequesters PP1 in the nucleus, therefore impairing the formation of MLCP complex in the cytoplasm. This is supported by the observation that the expression of nuclear Phactr1-xxx causes the enhancement of PP1 nuclear staining in NIH3T3 fibroblasts. Because there is less available PP1 in the cytoplasm, MLCP complex becomes less active, which leads to hyper-phosphorylation of MLC and the observed contractile phenotype (Figure 6.4). Our results suggest that the regulation of Phactr1 activity by G-actin provide a homeostatic feedback loop serving to coordinate levels of phosphorylated MLC, and hence actomyosin crosslinking, with F-actin assembly (Figure 6.4). This model is reminiscent of the role of MRTFs homeostatic control of cytoskeletal gene expression (Medjkane et al., 2009; Olson and Nordheim, 2010).

We have not directly tested if Phactr1 is an inhibitor of PP1. It was previously shown that Phactr proteins can modulate activity of PP1, but some of those studies were inconsistent (Allen et al., 2004; Huet et al., 2012; Sagara et al., 2003). These variations might be related to the differences between Phactr family members. PP1 holoenzymes can either encompass regulatory subunits that act positively to enhance PP1 substrate specificity or as substrate-independent inhibitory cofactors (for review, see (Ceulemans

and Bollen, 2004)). We propose that Phactr1 directly regulates phosphorylation of MLC through the inhibition of MLCP complex, consisting of MYPT1 and PP1. The role of MYPT1-PP1 complex is to specifically sense MLC as a substrate, therefore enabling its dephosphorylation. The role of Phactr1 might be to specifically target PP1 and block its interaction with MYPT1. It was shown that MYPT1 interacts with PP1 through multiple sites, and the docking 'RVxF' channel in PP1 is crucially engaged during this interaction (Terrak et al., 2004). It is also possible that the 'RVxF' motif is indeed present in Phactr1 (Bharucha et al., 2008; Larson et al., 2008). If this was the case PP1-Phactr1 interaction would be incompatible with MYPT1 binding, and PP1-MYTP1 or PP1-Phactr1 complexes would be mutually exclusive. However, this hypothesis was not directly tested and we cannot exclude that PP1 would form a ternary complex with Phactr1 and MYPT1.

We suggest that Phactr1 is a negative regulator of PP1 activity, which is consistent with previous findings (Allen et al., 2004). Phactr3 was also shown to inhibit PP1 activity (Sagara et al., 2003). Phactr4-PP1 complex however was recently proposed to act positively to dephosphorylate Rb and cofilin but no direct demonstration of these findings was shown (Kim et al., 2007; Zhang et al., 2012). Huet and colleagues performed an *in vitro* assay to test the activity of PP1 upon Phactr4 and suggest that Phactr4 binding increases PP1 activity (Huet et al., 2012). Therefore, it is possible that Phactr1 and Phacr4 might affect PP1 activity in a different way. More studies are necessary to understand the activity of PP1-Phactr complexes and differences that those complexes might exhibit between Phactr family members. Structural analysis of Phactr1-PP1 interaction would certainly help to understand how Phactr1 modulates PP1 activity.

Lastly, the phenotypes described upon Phactr1 depletion in CHL-1 melanoma cell line allow us to suggest that Phactr1 has a role in cancer cell motility and invasion. This is consistent with high expression levels of Phactr1 in malignant melanoma cancers (Koh et al., 2009; Trufant, 2010). In contrast, Phactr4 was shown to act as a tumour suppressor in variety of cancers, again indicating its distinct function (Solimini et al.,

2013). More biochemical and functional studies are needed to understand those differences.

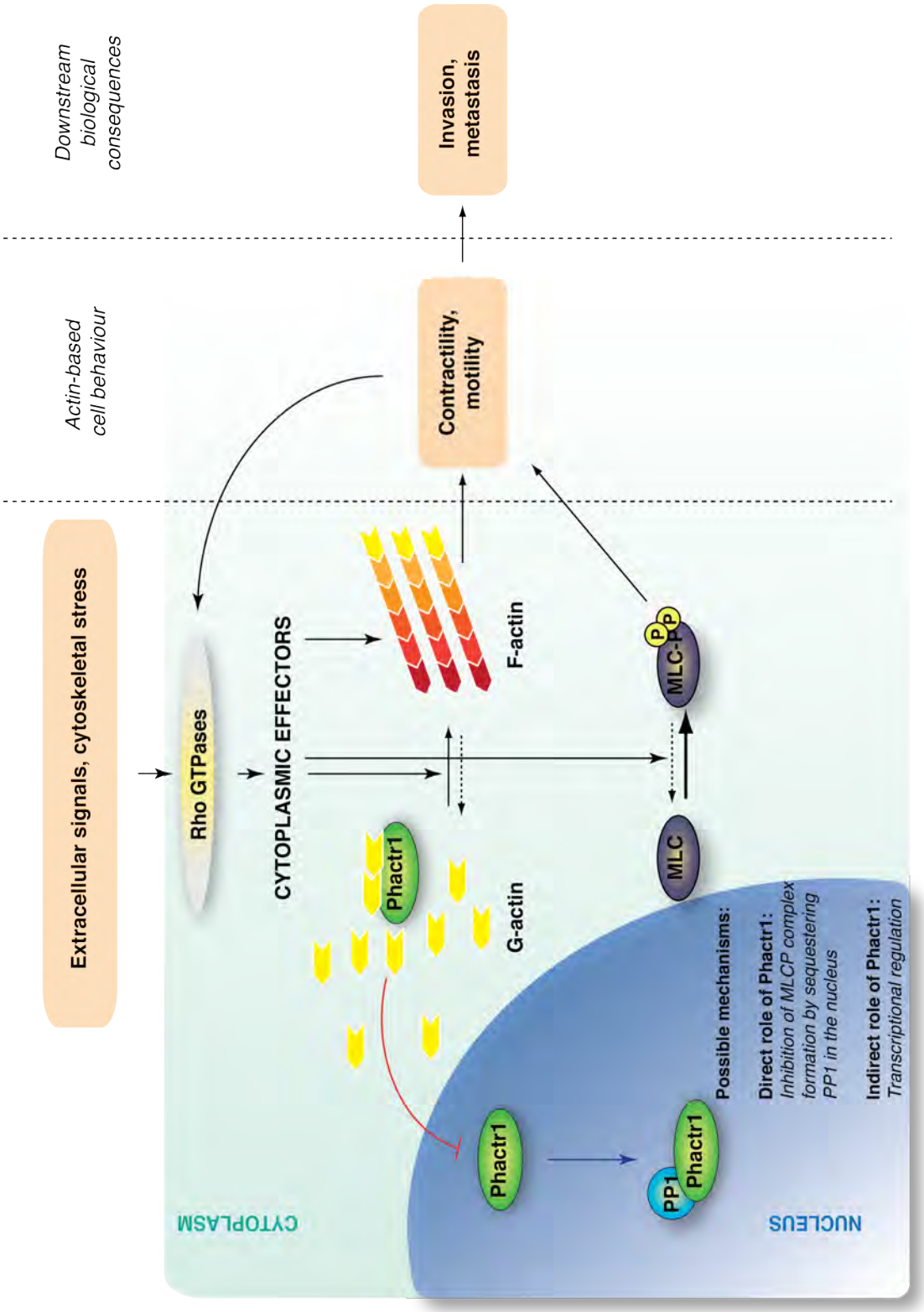
Downstream biological consequences
Actin-based cell behaviour
Invasion, metastasis
Contractility, motility
Extracellular signals, cytoskeletal stress
Rho GTPases
CYTOPLASMIC EFFECTORS
F-actin
G-actin
Phactr1
MLC
MLC-P
P
Possible mechanisms:
Direct role of Phactr1:
Inhibition of MLCP complex formation by sequestering PP1 in the nucleus
Indirect role of Phactr1:
Transcriptional regulation
PP1
CYTOPLASM
NUCLEUS

**Figure 6.4 Model of Phactr1 function in cytoskeletal homeostasis.**

Upon activation of Rho-GTPases and Rho effectors, G-actin assembles into filaments (F-actin). G-actin inhibits Phactr1 nuclear translocation and upon depletion of G-actin pool Phactr1 accumulates in the nucleus. Phactr1 binds PP1 in the nucleus and this association promotes MLC phosphorylation at T18 S19. Potential mechanism involves sequestering of PP1 in the nucleus by Phactr1 and consequent inhibition of MLCP complex formation. Mechanism of MLC phosphorylation by Phactr1 is not fully understood, but might be either direct (inhibition through competition with MYPT1) or indirect (through transcriptional regulation). Cell invasion and metastatic potential are important biological consequences of this mechanism.

## 6.4 Conclusions

In this thesis, I have described the molecular mechanism of Phactr1 nuclear accumulation, its association with PP1 and its potential roles in cytoskeletal dynamics. My studies revealed a functional role of G-actin in control of Phactr1 nucleocytoplasmic shuttling and PP1 interaction. Biochemical analysis of Phactr1 showed that its nuclear accumulation is dependent on the direct competition between G-actin and Importin α-β binding. Mutational studies allowed us to further characterise the domains of Phactr1, involved in its regulation. In collaboration with Stephane Mouilleron, I performed a structural analysis of Phactr-actin complexes. This approach allowed us to better explain the mechanism of Phactr1 nuclear accumulation. It also showed crucial similarities as well as differences compared to MRTF-actin complexes. Most importantly however, it enabled us to characterise a new actin interaction surface in RPEL proteins, which is involved in the formation of higher-order assemblies with G-actin. The analysis of these interactions indicates a conformational switch upon actin binding. These findings emphasise the significance of RPEL motif in modulation of protein interactions according to G-actin concentration. Lastly, through a functional analysis we suggest a role of Phactr1 in the motility and invasiveness of malignant melanoma cells. We propose that this function of Phactr1 depends on its association with PP1 and consequent cytoskeletal changes.

# Appendix

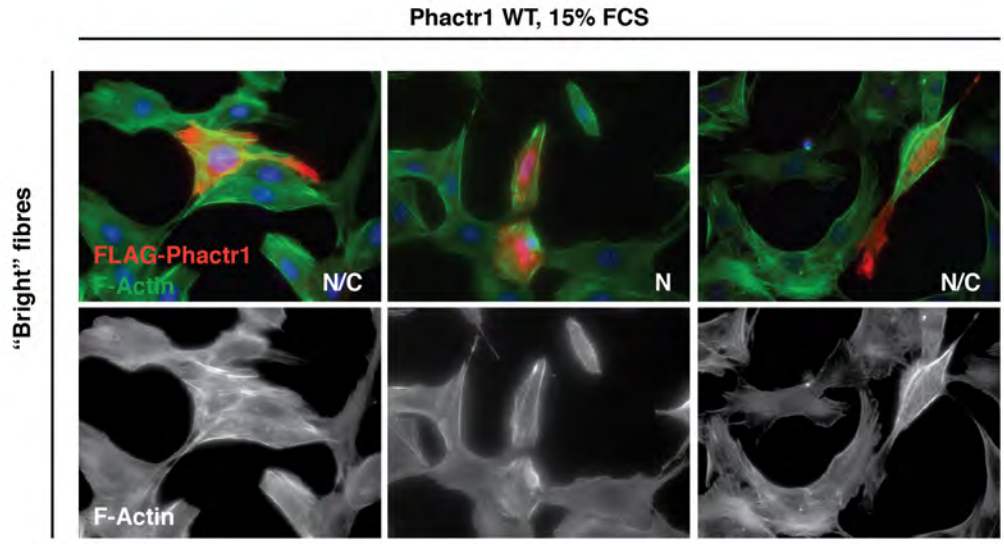


**Figure 7.1 Expression of wild-type Phactr1 induces 'bright fibre' formation upon serum stimulation.**

'Bright-fibre' F-actin phenotype in NIH3T3 cells expressing wild-type Phactr1 (WT) after 1 hour of serum stimulation. Subcellular localisation of Phactr1 was scored as N (nuclear), N/C (pan-cellular) or C (cytoplasmic). Three representative images are shown.

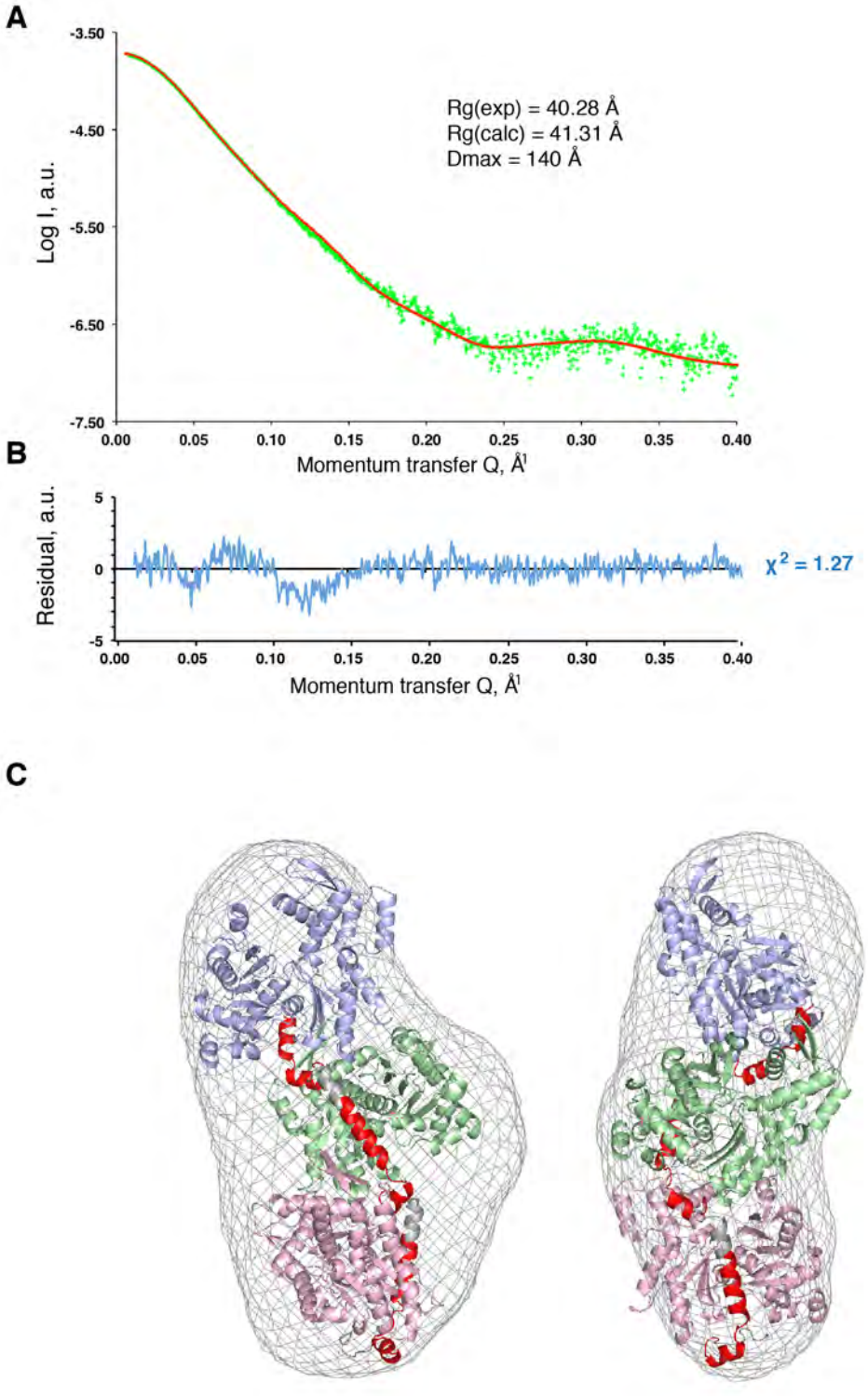
A
Rg(exp) = 40.28 Å
Rg(calc) = 41.31 Å
Dmax = 140 Å
Log I, a.u.
-3.50
-4.50
-5.50
-6.50
-7.50
0.00
0.05
0.10
0.15
0.20
0.25
0.30
0.35
0.40
Momentum transfer Q, Å¹
B
Residual, a.u.
5
0
-5
χ² = 1.27
Momentum transfer Q, Å¹
C

**Figure 7.2 SAXS analysis of the G-actin•RPEL$^{Phactr1}$ complex.**

SAXS analysis indicates that the G-actin•RPEL$^{Phactr1}$ complex is trivalent in solution. **(A)** Experimental X-ray scattering intensities for the G-actin•RPEL$^{Phactr1}$ complex as a function of the maximum momentum transfer Qmax= $4\pi\sin(\theta)/\lambda$ of 0.40 Å-1 (green). Computed scattering patterns derived from the trivalent G-actin•RPEL$^{Phactr1}$ complex are shown in red. The radius of gyration ($R_g$) derived from the scattering curves and representing the average size of the particle in solution was $R_{g(exp)}$ = 40.3Å. This value is in agreement with the expected value for a single trivalent G-actin•RPEL$^{Phactr1}$ complex ($R_g$=41.3Å). **(B)** Residuals for the least-square fits (($I_{exp} - I_{calc}$)/ $\sigma_{exp}$) are shown for a linear scale. **(C)** Fit of the computed scattering patterns of the model to the experimental scattering curves over the entire Q range (Mouilleron et al., 2012).

| | RPEL domain | RPEL-N Crystal form I | RPEL-N Crystal form II | | RPEL1 | RPEL2 | RPEL3 |
|---|---|---|---|---|---|---|---|
| **Data collection** | | | | | | | |
| Space group | P $2_1$ $2_1$ $2_1$ | P $3_2$ 2 | P $2_1$ | I 4 2 2 | P $3_1$ 2 | P $2_1$ |
| Cell dimensions | | | | | | | |
| a, b, c (Å) | 127.0, 142.9, 184.3 | 77.5, 77.5, 128.2 | 44.1, 75.9, 122.4 | 128.2, 128.2, 135.4 | 77.3, 77.3, 130.8 | 52.5, 63.5, 62.5 |
| a, b, g (°) | 90.0, 90.0, 90.0 | 90.0, 90.0, 120.0 | 90.0, 97.0, 90.0 | 90.0, 90.0, 90.0 | 90.0, 90.0, 120.0 | 90.0, 108.8, 90.0 |
| $Z_a$ (G-actin : RPEL motif) | 2 | 1 | 2 | 1 | 1 | 1 |
| Resolution (Å) | 40 – 3.30 | 30.00 – 2.00 | 40.00 – 1.80 | 40.00 – 2.00 | 40 – 1.80 | 30.00 – 1.29 |
| (Outer resolution shell) Å | (3.48 – 3.30) | (2.11 – 2.00) | (1.90 – 1.80) | (2.11 – 2.00) | (1.90 – 1.80) | (1.36 – 1.29) |
| $R_{sym}$ (%) | 14.5 (59.9) | 9.6 (55.9) | 10.8 (44.1) | 15.2 (55.6) | 6.5 (69.0) | 7.5 (42.4) |
| $R_{p.i.m.}$ (%) | 6.6 (26.9) | 3.9 (22.0) | 7.8 (33.1) | 6.4 (23.4) | 2.9 (32.9) | 5.1 (28.6) |
| I/sI | 4.6 (1.3) | 5.6 (1.3) | 4.0 (1.5) | 4.0 (1.3) | 7.7 (1.1) | 5.5 (1.8) |
| Completeness (%) | 99.6 (100.0) | 98.4 (98.9) | 96.4 (97.5) | 97.8 (98.6) | 98.7 (99.7) | 99.7 (99.7) |
| Redundancy | 5.6 (5.7) | 6.6 (6.8) | 2.6 (2.5) | 6.2 (6.2) | 5.6 (5.3) | 3.1 (3.1) |
| **Refinement** | | | | | | | |
| Resolution (Å) | | | | | | | |
| (Outer resolution shell) Å | | | | | | | |
| No. unique reflections | 51 065 | 30 822 | 80 937 | 38 647 | 69 989 | 98 023 |
| $R_{work}$ [a] | 22.2 (31.4) | 20.7 (30.0) | 18.9 (33.3) | 19.3 (29.4) | 18.1 (30.2) | 15.2 (25.9) |
| $R_{free}$ [a] | 25.0 (31.6) | 25.3 (35.5) | 23.3 (39.0) | 23.5 (35.4) | 22.0 (36.5) | 17.8 (29.9) |
| No. atoms | | | | | | |
| Wilson B factor | 78.8 | 25.2 | 16.8 | 20.2 | 27.9 | 10.8 |
| Average isotropic *B*-factors ($Å^2$) | 81.1 | 33.8 | 20.5 | 22.8 | 36.4 | 17.1 |
| R.m.s. deviations | | | | | | |
| bonds (Å) | 0.004 | 0.0078 | 0.007 | 0.007 | 0.007 | 0.01 |
| angles (°) | 1.05 | 1.20 | 1.15 | 1.06 | 1.07 | 1.45 |
| Ramachandran plot (%) | | | | | | |
| (favoured. allowed. disallowed) | 98.4 /1.5/0.1 | 98.1/1.6/0.3 | 98.3/1.7/0 | 98.7/1.3/0 | 97.4/2.6/0 | 98.4/1.6/0 |

**Table 7.1 Data collection and refinement statistics.**

Table assembled according to Mouilleron and colleagues (Mouilleron et al., 2012).

A

| Peptide name | sequence | Mean Kd ± SEM (μM) |
|---|---|---|
| MRTF-A RPEL3 | RARLADDLNEKIAQRPGPMELVEKNILPVESS | 18.8±1.0 |
| Phactr1 RPEL3 | KREIKRRLTRKLSQRPTVEELRERKILIRFSD | 0.27±0.02 |
| MRTF-A RPEL3-Phactr1 chimeric peptide (B1) | RARLARRLTRKLSQRPTVEELRERKILPVESS | 0.15 |
| chimeric peptide A1 | RARLKRRLTRKLSQRPTVEELRERKILPVESS | 0.038 |
| chimeric peptide C1 | RARLADRLTRKLSQRPTVEELRERKILPVESS | 0.137 |
| chimeric peptide A | RARLKRRLTRKLSQRPTVEELRERKILIRFSD | 0.079 |
| chimeric peptide B | RARLARRLTRKLSQRPTVEELRERKILIRFSD | 0.193 |
| chimeric peptide B | RARLADRLTRKLSQRPTVEELRERKILIRFSD | 0.217 |

B

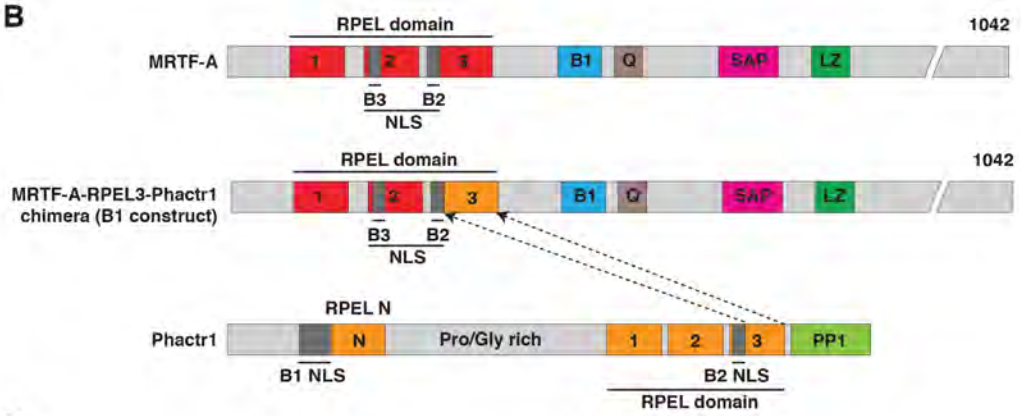


C

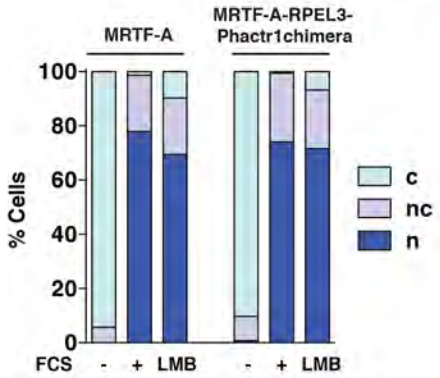

**Figure 7.3 MRTF-A RPEL3-Phactr1 chimera.**

**(A)** Affinities ($K_D$) obtained in fluorescence polarisation anisotropy experiments for MRTF-A RPEL3 peptide (sequence is shown in red), Phactr1 RPEL3 (sequence is shown in blue), and chimeric peptides (replaced sequences are colour-coded); chimeric peptide B1 sequence (MRTF-A RPEL3-Phactr1 chimera) was introduced into full length MRTF-A. **(B)** Schematic representation of chimeric construct used in C. **(C)** Introduction of B1 chimera into the full-length MRTF-A does not affect its regulation upon serum stimulation or LMB treatment; C, cytoplasmic; N/C, pan-cellular; N, nuclear; at least 100 cells were counted per point (preliminary observations)

# Reference List

Adelman, M.R., and Taylor, E.W. (1969). Isolation of an actomyosin-like protein complex from slime mold plasmodium and the separation of the complex into actin- and myosin-like fractions. Biochemistry *8*, 4964-4975.

Adelstein, R.S., Conti, M.A., Daniel, J.L., and Anderson, W., Jr. (1975). The interaction of platelet actin, myosin and myosin light chain kinase. Ciba Foundation symposium *35*, 101-109.

Adelstein, R.S., and Sellers, J.R. (1987). Effects of calcium on vascular smooth muscle contraction. The American journal of cardiology *59*, 4B-10B.

Alessi, D., MacDougall, L.K., Sola, M.M., Ikebe, M., and Cohen, P. (1992). The control of protein phosphatase-1 by targetting subunits. The major myosin phosphatase in avian smooth muscle is a novel form of protein phosphatase-1. Eur J Biochem *210*, 1023-1035.

Allain, B., Jarray, R., Borriello, L., Leforban, B., Dufour, S., Liu, W.Q., Pamonsinlapatham, P., Bianco, S., Larghero, J., Hadj-Slimane, R.*, et al.* (2011). Neuropilin-1 regulates a new VEGF-induced gene, Phactr-1, which controls tubulogenesis and modulates lamellipodial dynamics in human endothelial cells. Cell Signal.

Allen, P.B., Greenfield, A.T., Svenningsson, P., Haspeslagh, D.C., and Greengard, P. (2004). Phactrs 1-4: A family of protein phosphatase 1 and actin regulatory proteins. Proc Natl Acad Sci U S A *101*, 7187-7192.

Amano, M., Chihara, K., Kimura, K., Fukata, Y., Nakamura, N., Matsuura, Y., and Kaibuchi, K. (1997). Formation of actin stress fibers and focal adhesions enhanced by Rho-kinase. Science *275*, 1308-1311.

Amano, M., Ito, M., Kimura, K., Fukata, Y., Chihara, K., Nakano, T., Matsuura, Y., and Kaibuchi, K. (1996). Phosphorylation and activation of myosin by Rho-associated kinase (Rho-kinase). J Biol Chem *271*, 20246-20249.

Amano, M., Nakayama, M., and Kaibuchi, K. (2010). Rho-kinase/ROCK: A key regulator of the cytoskeleton and cell polarity. Cytoskeleton (Hoboken) *67*, 545-554.

Ammosova, T., Jerebtsova, M., Beullens, M., Lesage, B., Jackson, A., Kashanchi, F., Southerland, W., Gordeuk, V.R., Bollen, M., and Nekhai, S. (2005). Nuclear targeting of protein phosphatase-1 by HIV-1 Tat protein. J Biol Chem *280*, 36364-36371.

Ammosova, T., Yedavalli, V.R., Niu, X., Jerebtsova, M., Van Eynde, A., Beullens, M., Bollen, M., Jeang, K.T., and Nekhai, S. (2011). Expression of a protein phosphatase 1 inhibitor, cdNIPP1, increases CDK9 threonine 186 phosphorylation and inhibits HIV-1 transcription. J Biol Chem *286*, 3798-3804.

Ampe, C., Markey, F., Lindberg, U., and Vandekerckhove, J. (1988). The primary structure of human platelet profilin: reinvestigation of the calf spleen profilin sequence. FEBS Lett *228*, 17-21.

Andreassen, P.R., Lacroix, F.B., Villa-Moruzzi, E., and Margolis, R.L. (1998). Differential subcellular localization of protein phosphatase-1 alpha, gamma1, and delta isoforms during both interphase and mitosis in mammalian cells. J Cell Biol *141*, 1207-1215.

Aravind, L., and Koonin, E.V. (2000). SAP - a putative DNA-binding motif involved in chromosomal organization. Trends in biochemical sciences *25*, 112-114.

Armitage P, B.G. (1994). Statistical Methods in Medical Research.

Aspenstrom, P., Fransson, A., and Saras, J. (2004). Rho GTPases have diverse effects on the organization of the actin filament system. The Biochemical journal *377*, 327-337.

Badour, K., Zhang, J., Shi, F., Leng, Y., Collins, M., and Siminovitch, K.A. (2004). Fyn and PTP-PEST-mediated regulation of Wiskott-Aldrich syndrome protein (WASp) tyrosine phosphorylation is required for coupling T cell antigen receptor engagement to WASp effector function and T cell activation. The Journal of experimental medicine *199*, 99-112.

Bamburg, J.R., and Bray, D. (1987). Distribution and cellular localization of actin depolymerizing factor. J Cell Biol *105*, 2817-2825.

Bamburg, J.R., Harris, H.E., and Weeds, A.G. (1980). Partial purification and characterization of an actin depolymerizing factor from brain. FEBS Lett *121*, 178-182.

Bankovic, J., Stojsic, J., Jovanovic, D., Andjelkovic, T., Milinkovic, V., Ruzdijic, S., and Tanic, N. (2010). Identification of genes associated with non-small-cell lung cancer promotion and progression. Lung Cancer *67*, 151-159.

Berezney, R., and Coffey, D.S. (1975). Nuclear protein matrix: association with newly synthesized DNA. Science *189*, 291-293.

Berndt, N., Dohadwala, M., and Liu, C.W. (1997). Constitutively active protein phosphatase 1alpha causes Rb-dependent G1 arrest in human cancer cells. Current biology : CB *7*, 375-386.

Bernstein, B.W., and Bamburg, J.R. (2010). ADF/cofilin: a functional node in cell biology. Trends in cell biology *20*, 187-195.

Bharucha, J.P., Larson, J.R., Konopka, J.B., and Tatchell, K. (2008). Saccharomyces cerevisiae Afr1 protein is a protein phosphatase 1/Glc7-targeting subunit that regulates the septin cytoskeleton during mating. Eukaryotic cell *7*, 1246-1255.

Bliss, T.V., and Collingridge, G.L. (1993). A synaptic model of memory: long-term potentiation in the hippocampus. Nature *361*, 31-39.

Bloecher, A., and Tatchell, K. (2000). Dynamic localization of protein phosphatase type 1 in the mitotic cell cycle of Saccharomyces cerevisiae. J Cell Biol *149*, 125-140.

Bollen, M. (2001). Combinatorial control of protein phosphatase-1. Trends in biochemical sciences *26*, 426-431.

Bollen, M., and Beullens, M. (2002). Signaling by protein phosphatases in the nucleus. Trends in cell biology *12*, 138-145.

Bollen, M., Peti, W., Ragusa, M.J., and Beullens, M. (2010). The extended PP1 toolkit: designed to create specificity. Trends in biochemical sciences *35*, 450-458.

Bollen, M., and Stalmans, W. (1992). The structure, role, and regulation of type 1 protein phosphatases. Critical reviews in biochemistry and molecular biology *27*, 227-281.

Bosch, L.J., Oort, F.A., Neerincx, M., Khalid-de Bakker, C.A., Terhaar sive Droste, J.S., Melotte, V., Jonkers, D.M., Masclee, A.A., Mongera, S., Grooteclaes, M.*, et al.* (2012). DNA methylation of phosphatase and actin regulator 3 detects colorectal cancer in stool and complements FIT. Cancer Prev Res (Phila) *5*, 464-472.

Brown, M.C., and Turner, C.E. (2004). Paxillin: adapting to change. Physiol Rev *84*, 1315-1339.

Bryksin, A.V., and Matsumura, I. (2010). Overlap extension PCR cloning: a simple and reliable way to create recombinant plasmids. BioTechniques *48*, 463-465.

Bu, W., Lim, K.B., Yu, Y.H., Chou, A.M., Sudhaharan, T., and Ahmed, S. (2010). Cdc42 interaction with N-WASP and Toca-1 regulates membrane tubulation, vesicle formation and vesicle motility: implications for endocytosis. PloS one *5*, e12153.

Buchwalter, G., Gross, C., and Wasylyk, B. (2004). Ets ternary complex transcription factors. Gene *324*, 1-14.

Burbelo, P.D., Drechsel, D., and Hall, A. (1995). A conserved binding motif defines numerous candidate target proteins for both Cdc42 and Rac GTPases. J Biol Chem *270*, 29071-29074.

Carlier, M.F., Pantaloni, D., and Korn, E.D. (1984). Evidence for an ATP cap at the ends of actin filaments and its regulation of the F-actin steady state. J Biol Chem *259*, 9983-9986.

Carlier, M.F., Ressad, F., and Pantaloni, D. (1999). Control of actin dynamics in cell motility. Role of ADF/cofilin. J Biol Chem *274*, 33827-33830.

Carmody, L.C., Baucum, A.J., 2nd, Bass, M.A., and Colbran, R.J. (2008). Selective targeting of the gamma1 isoform of protein phosphatase 1 to F-actin in intact cells requires multiple domains in spinophilin and neurabin. FASEB journal : official publication of the Federation of American Societies for Experimental Biology *22*, 1660-1671.

Carreira, S., Goodall, J., Denat, L., Rodriguez, M., Nuciforo, P., Hoek, K.S., Testori, A., Larue, L., and Goding, C.R. (2006). Mitf regulation of Dia1 controls melanoma proliferation and invasiveness. Genes & development *20*, 3426-3439.

Ceulemans, H., and Bollen, M. (2004). Functional diversity of protein phosphatase-1, a cellular economizer and reset button. Physiol Rev *84*, 1-39.

Ceulemans, H., Stalmans, W., and Bollen, M. (2002a). Regulator-driven functional diversification of protein phosphatase-1 in eukaryotic evolution. BioEssays : news and reviews in molecular, cellular and developmental biology *24*, 371-381.

Ceulemans, H., Vulsteke, V., De Maeyer, M., Tatchell, K., Stalmans, W., and Bollen, M. (2002b). Binding of the concave surface of the Sds22 superhelix to the alpha 4/alpha 5/alpha 6-triangle of protein phosphatase-1. J Biol Chem *277*, 47331-47337.

Chan, C., Beltzner, C.C., and Pollard, T.D. (2009). Cofilin dissociates Arp2/3 complex and branches from actin filaments. Current biology : CB *19*, 537-545.

Chander, H., Truesdell, P., Meens, J., and Craig, A.W. (2012). Transducer of Cdc42-dependent actin assembly promotes breast cancer invasion and metastasis. Oncogene.

Chen, X.Q., Tan, I., Ng, C.H., Hall, C., Lim, L., and Leung, T. (2002). Characterization of RhoA-binding kinase ROKalpha implication of the pleckstrin homology domain in ROKalpha function using region-specific antibodies. J Biol Chem *277*, 12680-12688.

Cheng, X.C., Kihara, T., Kusakabe, H., Magae, J., Kobayashi, Y., Fang, R.P., Ni, Z.F., Shen, Y.C., Ko, K., Yamaguchi, I.*, et al.* (1987). A new antibiotic, tautomycin. The Journal of antibiotics *40*, 907-909.

Chesarone, M.A., DuPage, A.G., and Goode, B.L. (2010). Unleashing formins to remodel the actin and microtubule cytoskeletons. Nature reviews Molecular cell biology *11*, 62-74.

Chesarone, M.A., and Goode, B.L. (2009). Actin nucleation and elongation factors: mechanisms and interplay. Curr Opin Cell Biol *21*, 28-37.

Chik, J.K., Lindberg, U., and Schutt, C.E. (1996). The structure of an open state of beta-actin at 2.65 A resolution. J Mol Biol *263*, 607-623.

Christofidou-Solomidou, M., Scherpereel, A., Solomides, C.C., Muzykantov, V.R., Machtay, M., Albelda, S.M., and DiNubile, M.J. (2002). Changes in plasma gelsolin concentration during acute oxidant lung injury in mice. Lung *180*, 91-104.

Chua, B.T., Volbracht, C., Tan, K.O., Li, R., Yu, V.C., and Li, P. (2003). Mitochondrial translocation of cofilin is an early step in apoptosis induction. Nature cell biology *5*, 1083-1089.

Cohen, P.T. (2002). Protein phosphatase 1--targeted in many directions. Journal of cell science *115*, 241-256.

Coleman, M.L., Sahai, E.A., Yeo, M., Bosch, M., Dewar, A., and Olson, M.F. (2001). Membrane blebbing during apoptosis results from caspase-mediated activation of ROCK I. Nature cell biology *3*, 339-345.

Connor, J.H., Kleeman, T., Barik, S., Honkanen, R.E., and Shenolikar, S. (1999). Importance of the beta12-beta13 loop in protein phosphatase-1 catalytic subunit for inhibition by toxins and mammalian protein inhibitors. J Biol Chem *274*, 22366-22372.

Connor, J.H., Weiser, D.C., Li, S., Hallenbeck, J.M., and Shenolikar, S. (2001). Growth arrest and DNA damage-inducible protein GADD34 assembles a novel signaling complex containing protein phosphatase 1 and inhibitor 1. Molecular and cellular biology *21*, 6841-6850.

Conti, M.A., and Adelstein, R.S. (2008). Nonmuscle myosin II moves in new directions. Journal of cell science *121*, 11-18.

Coso, O.A., Chiariello, M., Yu, J.C., Teramoto, H., Crespo, P., Xu, N., Miki, T., and Gutkind, J.S. (1995). The small GTP-binding proteins Rac1 and Cdc42 regulate the activity of the JNK/SAPK signaling pathway. Cell *81*, 1137-1146.

Coue, M., Brenner, S.L., Spector, I., and Korn, E.D. (1987). Inhibition of actin polymerization by latrunculin A. FEBS Lett *213*, 316-318.

Coutts, A.S., Boulahbel, H., Graham, A., and La Thangue, N.B. (2007). Mdm2 targets the p53 transcription cofactor JMY for degradation. EMBO reports *8*, 84-90.

Cunningham, C.C., Stossel, T.P., and Kwiatkowski, D.J. (1991). Enhanced motility in NIH 3T3 fibroblasts that overexpress gelsolin. Science *251*, 1233-1236.

Dalton, S., and Treisman, R. (1992). Characterization of SAP-1, a protein recruited by serum response factor to the c-fos serum response element. Cell *68*, 597-612.

Derivery, E., and Gautreau, A. (2010). Generation of branched actin networks: assembly and regulation of the N-WASP and WAVE molecular machines. BioEssays : news and reviews in molecular, cellular and developmental biology *32*, 119-131.

Descot, A., Hoffmann, R., Shaposhnikov, D., Reschke, M., Ullrich, A., and Posern, G. (2009). Negative regulation of the EGFR-MAPK cascade by actin-MAL-mediated Mig6/Errfi-1 induction. Molecular cell *35*, 291-304.

Didry, D., Carlier, M.F., and Pantaloni, D. (1998). Synergy between actin depolymerizing factor/cofilin and profilin in increasing actin filament turnover. J Biol Chem *273*, 25602-25611.

Dingwall, C., and Laskey, R.A. (1991). Nuclear targeting sequences--a consensus? Trends in biochemical sciences *16*, 478-481.

Dominguez, R. (2007). The beta-thymosin/WH2 fold: multifunctionality and structure. Annals of the New York Academy of Sciences *1112*, 86-94.

Dominguez, R., and Holmes, K.C. (2011). Actin structure and function. Annu Rev Biophys *40*, 169-186.

Dopie, J., Skarp, K.P., Rajakyla, E.K., Tanhuanpaa, K., and Vartiainen, M.K. (2012). Active maintenance of nuclear actin by importin 9 supports transcription. Proc Natl Acad Sci U S A *109*, E544-552.

dos Remedios, C.G., Chhabra, D., Kekic, M., Dedova, I.V., Tsubakihara, M., Berry, D.A., and Nosworthy, N.J. (2003). Actin binding proteins: regulation of cytoskeletal microfilaments. Physiol Rev *83*, 433-473.

Dounay, A.B., and Forsyth, C.J. (2002). Okadaic acid: the archetypal serine/threonine protein phosphatase inhibitor. Current medicinal chemistry *9*, 1939-1980.

Druckenbrod, N.R., and Epstein, M.L. (2005). The pattern of neural crest advance in the cecum and colon. Developmental biology *287*, 125-133.

Durfee, T., Becherer, K., Chen, P.L., Yeh, S.H., Yang, Y., Kilburn, A.E., Lee, W.H., and Elledge, S.J. (1993). The retinoblastoma protein associates with the protein phosphatase type 1 catalytic subunit. Genes & development *7*, 555-569.

Eden, S., Rohatgi, R., Podtelejnikov, A.V., Mann, M., and Kirschner, M.W. (2002). Mechanism of regulation of WAVE1-induced actin nucleation by Rac1 and Nck. Nature *418*, 790-793.

Edgar, R.C. (2004). MUSCLE: multiple sequence alignment with high accuracy and high throughput. Nucleic acids research *32*, 1792-1797.

Egloff, M.P., Cohen, P.T., Reinemer, P., and Barford, D. (1995). Crystal structure of the catalytic subunit of human protein phosphatase 1 and its complex with tungstate. J Mol Biol *254*, 942-959.

Egloff, M.P., Johnson, D.F., Moorhead, G., Cohen, P.T., Cohen, P., and Barford, D. (1997). Structural basis for the recognition of regulatory subunits by the catalytic subunit of protein phosphatase 1. The EMBO journal *16*, 1876-1887.

Ellerbroek, S.M., Wennerberg, K., and Burridge, K. (2003). Serine phosphorylation negatively regulates RhoA in vivo. J Biol Chem *278*, 19023-19031.

Erickson-Viitanen, S., Ruggieri, S., Natalini, P., and Horecker, B.L. (1983). Distribution of thymosin beta 4 in vertebrate classes. Arch Biochem Biophys *221*, 570-576.

Etienne-Manneville, S., and Hall, A. (2002). Rho GTPases in cell biology. Nature *420*, 629-635.

Eto, M. (2009). Regulation of cellular protein phosphatase-1 (PP1) by phosphorylation of the CPI-17 family, C-kinase-activated PP1 inhibitors. J Biol Chem *284*, 35273-35277.

Farghaian, H., Chen, Y., Fu, A.W., Fu, A.K., Ip, J.P., Ip, N.Y., Turnley, A.M., and Cole, A.R. (2011). Scapinin-induced inhibition of axon elongation is attenuated by phosphorylation and translocation to the cytoplasm. J Biol Chem *286*, 19724-19734.

Favot, L., Gillingwater, M., Scott, C., and Kemp, P.R. (2005). Overexpression of a family of RPEL proteins modifies cell shape. FEBS Lett *579*, 100-104.

Fernandez, A., Brautigan, D.L., Mumby, M., and Lamb, N.J. (1990). Protein phosphatase type-1, not type-2A, modulates actin microfilament integrity and myosin light chain phosphorylation in living nonmuscle cells. J Cell Biol *111*, 103-112.

Ferrai, C., Naum-Ongania, G., Longobardi, E., Palazzolo, M., Disanza, A., Diaz, V.M., Crippa, M.P., Scita, G., and Blasi, F. (2009). Induction of HoxB transcription by retinoic acid requires actin polymerization. Molecular biology of the cell *20*, 3543-3551.

Ferrara, N. (2004). Vascular endothelial growth factor: basic science and clinical progress. Endocrine reviews *25*, 581-611.

Firat-Karalar, E.N., and Welch, M.D. (2011). New mechanisms and functions of actin nucleation. Curr Opin Cell Biol *23*, 4-13.

Flores-Delgado, G., Liu, C.W., Sposto, R., and Berndt, N. (2007). A limited screen for protein interactions reveals new roles for protein phosphatase 1 in cell cycle control and apoptosis. Journal of proteome research *6*, 1165-1175.

Friend, S.H., Bernards, R., Rogelj, S., Weinberg, R.A., Rapaport, J.M., Albert, D.M., and Dryja, T.P. (1986). A human DNA segment with properties of the gene that predisposes to retinoblastoma and osteosarcoma. Nature *323*, 643-646.

Fujii, T., Iwane, A.H., Yanagida, T., and Namba, K. (2010). Direct visualization of secondary structures of F-actin by electron cryomicroscopy. Nature *467*, 724-728.

Gallagher, E.D., Gutowski, S., Sternweis, P.C., and Cobb, M.H. (2004). RhoA binds to the amino terminus of MEKK1 and regulates its kinase activity. J Biol Chem *279*, 1872-1877.

Gandhi, M., Smith, B.A., Bovellan, M., Paavilainen, V., Daugherty-Clarke, K., Gelles, J., Lappalainen, P., and Goode, B.L. (2010). GMF is a cofilin homolog that binds Arp2/3 complex to stimulate filament debranching and inhibit actin nucleation. Current biology : CB *20*, 861-867.

Gautreau, A., Ho, H.Y., Li, J., Steen, H., Gygi, S.P., and Kirschner, M.W. (2004). Purification and architecture of the ubiquitous Wave complex. Proc Natl Acad Sci U S A *101*, 4379-4383.

Geneste, O., Copeland, J.W., and Treisman, R. (2002). LIM kinase and Diaphanous cooperate to regulate serum response factor and actin dynamics. J Cell Biol *157*, 831-838.

Geuss, U., Mayr, G.W., and Heilmeyer, L.M., Jr. (1985). Steady-state kinetics of skeletal muscle myosin light chain kinase indicate a strong down regulation by products. Eur J Biochem *153*, 327-334.

Gille, H., Sharrocks, A.D., and Shaw, P.E. (1992). Phosphorylation of transcription factor p62TCF by MAP kinase stimulates ternary complex formation at c-fos promoter. Nature *358*, 414-417.

Gilmore, T.D. (2006). Introduction to NF-kappaB: players, pathways, perspectives. Oncogene *25*, 6680-6684.

Goldberg, J., Huang, H.B., Kwon, Y.G., Greengard, P., Nairn, A.C., and Kuriyan, J. (1995). Three-dimensional structure of the catalytic subunit of protein serine/threonine phosphatase-1. Nature *376*, 745-753.

Goley, E.D., and Welch, M.D. (2006). The ARP2/3 complex: an actin nucleator comes of age. Nature reviews Molecular cell biology *7*, 713-726.

Gong, M.C., Fuglsang, A., Alessi, D., Kobayashi, S., Cohen, P., Somlyo, A.V., and Somlyo, A.P. (1992). Arachidonic acid inhibits myosin light chain phosphatase and sensitizes smooth muscle to calcium. J Biol Chem *267*, 21492-21498.

Gonsior, S.M., Platz, S., Buchmeier, S., Scheer, U., Jockusch, B.M., and Hinssen, H. (1999). Conformational difference between nuclear and cytoplasmic actin as detected by a monoclonal antibody. Journal of cell science *112 ( Pt 6)*, 797-809.

Goodsell, D.S., and Olson, A.J. (2000). Structural symmetry and protein function. Annual review of biophysics and biomolecular structure *29*, 105-153.

Gould, C.J., Maiti, S., Michelot, A., Graziano, B.R., Blanchoin, L., and Goode, B.L. (2011). The formin DAD domain plays dual roles in autoinhibition and actin nucleation. Current biology : CB *21*, 384-390.

Grana, X., Garriga, J., and Mayol, X. (1998). Role of the retinoblastoma protein family, pRB, p107 and p130 in the negative control of cell growth. Oncogene *17*, 3365-3383.

Guettler, S., Vartiainen, M.K., Miralles, F., Larijani, B., and Treisman, R. (2008). RPEL motifs link the serum response factor cofactor MAL but not myocardin to Rho signaling via actin binding. Molecular and cellular biology *28*, 732-742.

Gupta, P.B., Kuperwasser, C., Brunet, J.P., Ramaswamy, S., Kuo, W.L., Gray, J.W., Naber, S.P., and Weinberg, R.A. (2005). The melanocyte differentiation program predisposes to metastasis after neoplastic transformation. Nature genetics *37*, 1047-1054.

Hager, J., Kamatani, Y., Cazier, J.B., Youhanna, S., Ghassibe-Sabbagh, M., Platt, D.E., Abchee, A.B., Romanos, J., Khazen, G., Othman, R.*, et al.* (2012). Genome-wide association study in a Lebanese cohort confirms PHACTR1 as a major determinant of coronary artery stenosis. PloS one *7*, e38663.

Han, L., Stope, M.B., de Jesus, M.L., Oude Weernink, P.A., Urban, M., Wieland, T., Rosskopf, D., Mizuno, K., Jakobs, K.H., and Schmidt, M. (2007). Direct stimulation of

receptor-controlled phospholipase D1 by phospho-cofilin. The EMBO journal *26*, 4189-4202.

Hanson, J., and Lowy, J. (1964). The Structure of Actin Filaments and the Origin of the Axial Periodicity in the I-Substance of Vertebrate Striated Muscle. Proc R Soc Lond B Biol Sci *160*, 449-460.

Harper, S.J., and Bates, D.O. (2008). VEGF-A splicing: the key to anti-angiogenic therapeutics? Nature reviews Cancer *8*, 880-887.

Hartshorne, D.J., Ito, M., and Erdodi, F. (1998). Myosin light chain phosphatase: subunit composition, interactions and regulation. Journal of muscle research and cell motility *19*, 325-341.

Hatano, S., and Oosawa, F. (1966). Isolation and characterization of plasmodium actin. Biochim Biophys Acta *127*, 488-498.

Hayashi, K., and Morita, T. (2013). Differences in the Nuclear Export Mechanism between Myocardin and Myocardin-related Transcription Factor A. J Biol Chem *288*, 5743-5755.

He, W.Q., Peng, Y.J., Zhang, W.C., Lv, N., Tang, J., Chen, C., Zhang, C.H., Gao, S., Chen, H.Q., Zhi, G.*, et al.* (2008). Myosin light chain kinase is central to smooth muscle contraction and required for gastrointestinal motility in mice. Gastroenterology *135*, 610-620.

Heanue, T.A., and Pachnis, V. (2007). Enteric nervous system development and Hirschsprung's disease: advances in genetic and stem cell studies. Nature reviews Neuroscience *8*, 466-479.

Heasman, S.J., and Ridley, A.J. (2008). Mammalian Rho GTPases: new insights into their functions from in vivo studies. Nature reviews Molecular cell biology *9*, 690-701.

Helps, N.R., Luo, X., Barker, H.M., and Cohen, P.T. (2000). NIMA-related kinase 2 (Nek2), a cell-cycle-regulated protein kinase localized to centrosomes, is complexed to protein phosphatase 1. The Biochemical journal *349*, 509-518.

Hendrickx, A., Beullens, M., Ceulemans, H., Den Abt, T., Van Eynde, A., Nicolaescu, E., Lesage, B., and Bollen, M. (2009). Docking motif-guided mapping of the interactome of protein phosphatase-1. Chemistry & biology *16*, 365-371.

Herman, I.M. (1993). Actin isoforms. Curr Opin Cell Biol *5*, 48-55.

Herrera, R.E., Shaw, P.E., and Nordheim, A. (1989). Occupation of the c-fos serum response element in vivo by a multi-protein complex is unaltered by growth factor induction. Nature *340*, 68-70.

Hertzog, M., van Heijenoort, C., Didry, D., Gaudier, M., Coutant, J., Gigant, B., Didelot, G., Preat, T., Knossow, M., Guittet, E.*, et al.* (2004). The beta-thymosin/WH2 domain; structural basis for the switch from inhibition to promotion of actin assembly. Cell *117*, 611-623.

Heyduk, T., and Lee, J.C. (1990). Application of fluorescence energy transfer and polarization to monitor Escherichia coli cAMP receptor protein and lac promoter interaction. Proc Natl Acad Sci U S A *87*, 1744-1748.

Hill, C.S., and Treisman, R. (1995). Transcriptional regulation by extracellular signals: mechanisms and specificity. Cell *80*, 199-211.

Hill, C.S., Wynne, J., and Treisman, R. (1994). Serum-regulated transcription by serum response factor (SRF): a novel role for the DNA binding domain. The EMBO journal *13*, 5421-5432.

Hill, C.S., Wynne, J., and Treisman, R. (1995). The Rho family GTPases RhoA, Rac1, and CDC42Hs regulate transcriptional activation by SRF. Cell *81*, 1159-1170.

Hirano, H., and Matsuura, Y. (2011). Sensing actin dynamics: Structural basis for G-actin-sensitive nuclear import of MAL. Biochemical and biophysical research communications *414*, 373-378.

Hirschi, A., Cecchini, M., Steinhardt, R.C., Schamber, M.R., Dick, F.A., and Rubin, S.M. (2010). An overlapping kinase and phosphatase docking site regulates activity of the retinoblastoma protein. Nature structural & molecular biology *17*, 1051-1057.

Ho, H.Y., Rohatgi, R., Lebensohn, A.M., Le, M., Li, J., Gygi, S.P., and Kirschner, M.W. (2004). Toca-1 mediates Cdc42-dependent actin nucleation by activating the N-WASP-WIP complex. Cell *118*, 203-216.

Holmes, K.C., Popp, D., Gebhard, W., and Kabsch, W. (1990). Atomic model of the actin filament. Nature *347*, 44-49.

Hong, F., Haldeman, B.D., Jackson, D., Carter, M., Baker, J.E., and Cremo, C.R. (2011). Biochemistry of smooth muscle myosin light chain kinase. Arch Biochem Biophys *510*, 135-146.

Hong, F., Haldeman, B.D., John, O.A., Brewer, P.D., Wu, Y.Y., Ni, S., Wilson, D.P., Walsh, M.P., Baker, J.E., and Cremo, C.R. (2009). Characterization of tightly

associated smooth muscle myosin-myosin light-chain kinase-calmodulin complexes. J Mol Biol *390*, 879-892.

Honkanen, R.E., Dukelow, M., Zwiller, J., Moore, R.E., Khatra, B.S., and Boynton, A.L. (1991). Cyanobacterial nodularin is a potent inhibitor of type 1 and type 2A protein phosphatases. Molecular pharmacology *40*, 577-583.

Hsieh-Wilson, L.C., Allen, P.B., Watanabe, T., Nairn, A.C., and Greengard, P. (1999). Characterization of the neuronal targeting protein spinophilin and its interactions with protein phosphatase-1. Biochemistry *38*, 4365-4373.

Hu, J., Mukhopadhyay, A., and Craig, A.W. (2011). Transducer of Cdc42-dependent actin assembly promotes epidermal growth factor-induced cell motility and invasiveness. J Biol Chem *286*, 2261-2272.

Hu, X.D., Huang, Q., Roadcap, D.W., Shenolikar, S.S., and Xia, H. (2006). Actin-associated neurabin-protein phosphatase-1 complex regulates hippocampal plasticity. Journal of neurochemistry *98*, 1841-1851.

Huang, J., Min Lu, M., Cheng, L., Yuan, L.J., Zhu, X., Stout, A.L., Chen, M., Li, J., and Parmacek, M.S. (2009). Myocardin is required for cardiomyocyte survival and maintenance of heart function. Proc Natl Acad Sci U S A *106*, 18734-18739.

Hubbard, M.J., and Cohen, P. (1989). Regulation of protein phosphatase-1G from rabbit skeletal muscle. 2. Catalytic subunit translocation is a mechanism for reversible inhibition of activity toward glycogen-bound substrates. Eur J Biochem *186*, 711-716.

Huet, G., Rajakyla, E.K., Viita, T., Skarp, K.P., Crivaro, M., Dopie, J., and Vartiainen, M.K. (2012). Actin-regulated feedback loop based on Phactr4, PP1 and cofilin maintains the actin monomer pool. Journal of cell science.

Hughes, C.S., Postovit, L.M., and Lajoie, G.A. (2010). Matrigel: a complex protein mixture required for optimal growth of cell culture. Proteomics *10*, 1886-1890.

Hurley, T.D., Yang, J., Zhang, L., Goodwin, K.D., Zou, Q., Cortese, M., Dunker, A.K., and DePaoli-Roach, A.A. (2007). Structural basis for regulation of protein phosphatase 1 by inhibitor-2. J Biol Chem *282*, 28874-28883.

Husson, C., Cantrelle, F.X., Roblin, P., Didry, D., Le, K.H., Perez, J., Guittet, E., Van Heijenoort, C., Renault, L., and Carlier, M.F. (2010). Multifunctionality of the beta-thymosin/WH2 module: G-actin sequestration, actin filament growth, nucleation, and severing. Annals of the New York Academy of Sciences *1194*, 44-52.

Huttenlocher, A., Sandborg, R.R., and Horwitz, A.F. (1995). Adhesion in cell migration. Curr Opin Cell Biol *7*, 697-706.

Huxley, H.E. (1969). The mechanism of muscular contraction. Science *164*, 1356-1365.

Innocenti, M., Zucconi, A., Disanza, A., Frittoli, E., Areces, L.B., Steffen, A., Stradal, T.E., Di Fiore, P.P., Carlier, M.F., and Scita, G. (2004). Abi1 is essential for the formation and activation of a WAVE2 signalling complex. Nature cell biology *6*, 319-327.

Ishizaki, T., Naito, M., Fujisawa, K., Maekawa, M., Watanabe, N., Saito, Y., and Narumiya, S. (1997). p160ROCK, a Rho-associated coiled-coil forming protein kinase, works downstream of Rho and induces focal adhesions. FEBS Lett *404*, 118-124.

Ito, M., Nakano, T., Erdodi, F., and Hartshorne, D.J. (2004). Myosin phosphatase: structure, regulation and function. Molecular and cellular biochemistry *259*, 197-209.

Jaffe, A.B., and Hall, A. (2005). Rho GTPases: biochemistry and biology. Annual review of cell and developmental biology *21*, 247-269.

Jaffe, A.B., Hall, A., and Schmidt, A. (2005). Association of CNK1 with Rho guanine nucleotide exchange factors controls signaling specificity downstream of Rho. Current biology : CB *15*, 405-412.

Janknecht, R., Ernst, W.H., Pingoud, V., and Nordheim, A. (1993). Activation of ternary complex factor Elk-1 by MAP kinases. The EMBO journal *12*, 5097-5104.

Jarray, R., Allain, B., Borriello, L., Biard, D., Loukaci, A., Larghero, J., Hadj-Slimane, R., Garbay, C., Lepelletier, Y., and Raynaud, F. (2011). Depletion of the novel protein PHACTR-1 from human endothelial cells abolishes tube formation and induces cell death receptor apoptosis. Biochimie *93*, 1668-1675.

Kabsch, W., Mannherz, H.G., Suck, D., Pai, E.F., and Holmes, K.C. (1990). Atomic structure of the actin:DNase I complex. Nature *347*, 37-44.

Kameyama, K., Lee, H.K., Bear, M.F., and Huganir, R.L. (1998). Involvement of a postsynaptic protein kinase A substrate in the expression of homosynaptic long-term depression. Neuron *21*, 1163-1175.

Kathiresan, S., Voight, B.F., Purcell, S., Musunuru, K., Ardissino, D., Mannucci, P.M., Anand, S., Engert, J.C., Samani, N.J., Schunkert, H.*, et al.* (2009). Genome-wide association of early-onset myocardial infarction with single nucleotide polymorphisms and copy number variants. Nature genetics *41*, 334-341.

Katoh, K., Kano, Y., Amano, M., Onishi, H., Kaibuchi, K., and Fujiwara, K. (2001). Rho-kinase--mediated contraction of isolated stress fibers. J Cell Biol *153*, 569-584.

Kelker, M.S., Page, R., and Peti, W. (2009). Crystal structures of protein phosphatase-1 bound to nodularin-R and tautomycin: a novel scaffold for structure-based drug design of serine/threonine phosphatase inhibitors. J Mol Biol *385*, 11-21.

Kheradmand, F., Werner, E., Tremble, P., Symons, M., and Werb, Z. (1998). Role of Rac1 and oxygen radicals in collagenase-1 expression induced by cell shape change. Science *280*, 898-902.

Kim, J.Y., Choi, S.Y., Moon, Y., Kim, H.J., Chin, J.H., Kim, H., and Sun, W. (2012). Different expression patterns of Phactr family members in normal and injured mouse brain. Neuroscience *221*, 37-46.

Kim, M., Gans, J.D., Nogueira, C., Wang, A., Paik, J.H., Feng, B., Brennan, C., Hahn, W.C., Cordon-Cardo, C., Wagner, S.N.*, et al.* (2006). Comparative oncogenomics identifies NEDD9 as a melanoma metastasis gene. Cell *125*, 1269-1281.

Kim, T.H., Goodman, J., Anderson, K.V., and Niswander, L. (2007). Phactr4 regulates neural tube and optic fissure closure by controlling PP1-, Rb-, and E2F1-regulated cell-cycle progression. Developmental cell *13*, 87-102.

Kimura, K., Ito, M., Amano, M., Chihara, K., Fukata, Y., Nakafuku, M., Yamamori, B., Feng, J., Nakano, T., Okawa, K.*, et al.* (1996). Regulation of myosin phosphatase by Rho and Rho-associated kinase (Rho-kinase). Science *273*, 245-248.

Kita, A., Matsunaga, S., Takai, A., Kataiwa, H., Wakimoto, T., Fusetani, N., Isobe, M., and Miki, K. (2002). Crystal structure of the complex between calyculin A and the catalytic subunit of protein phosphatase 1. Structure *10*, 715-724.

Kitagawa, M., Higashi, H., Jung, H.K., Suzuki-Takahashi, I., Ikeda, M., Tamai, K., Kato, J., Segawa, K., Yoshida, E., Nishimura, S.*, et al.* (1996). The consensus motif for phosphorylation by cyclin D1-Cdk4 is different from that for phosphorylation by cyclin A/E-Cdk2. The EMBO journal *15*, 7060-7069.

Kitazawa, T., Eto, M., Woodsome, T.P., and Khalequzzaman, M. (2003). Phosphorylation of the myosin phosphatase targeting subunit and CPI-17 during Ca2+ sensitization in rabbit smooth muscle. The Journal of physiology *546*, 879-889.

Klamt, F., Zdanov, S., Levine, R.L., Pariser, A., Zhang, Y., Zhang, B., Yu, L.R., Veenstra, T.D., and Shacter, E. (2009). Oxidant-induced apoptosis is mediated by oxidation of the actin-regulatory protein cofilin. Nature cell biology *11*, 1241-1246.

Koh, S.S., Opel, M.L., Wei, J.P., Yau, K., Shah, R., Gorre, M.E., Whitman, E., Shitabata, P.K., Tao, Y., Cochran, A.J.*, et al.* (2009). Molecular classification of melanomas and nevi using gene expression microarray signatures and formalin-fixed and paraffin-embedded tissue. Mod Pathol *22*, 538-546.

Kolupaeva, V., and Janssens, V. (2013). PP1 and PP2A phosphatases - cooperating partners in modulating retinoblastoma protein activation. The FEBS journal *280*, 627-643.

Koronakis, V., Hume, P.J., Humphreys, D., Liu, T., Horning, O., Jensen, O.N., and McGhie, E.J. (2011). WAVE regulatory complex activation by cooperating GTPases Arf and Rac1. Proc Natl Acad Sci U S A *108*, 14449-14454.

Kovacs, M., Toth, J., Hetenyi, C., Malnasi-Csizmadia, A., and Sellers, J.R. (2004). Mechanism of blebbistatin inhibition of myosin II. J Biol Chem *279*, 35557-35563.

Kovacs, M., Wang, F., Hu, A., Zhang, Y., and Sellers, J.R. (2003). Functional divergence of human cytoplasmic myosin II: kinetic characterization of the non-muscle IIA isoform. J Biol Chem *278*, 38132-38140.

Kreivi, J.P., Trinkle-Mulcahy, L., Lyon, C.E., Morrice, N.A., Cohen, P., and Lamond, A.I. (1997). Purification and characterisation of p99, a nuclear modulator of protein phosphatase 1 activity. FEBS Lett *420*, 57-62.

Kunda, P., Craig, G., Dominguez, V., and Baum, B. (2003). Abi, Sra1, and Kette control the stability and localization of SCAR/WAVE to regulate the formation of actin-based protrusions. Current biology : CB *13*, 1867-1875.

Lange, A., Mills, R.E., Lange, C.J., Stewart, M., Devine, S.E., and Corbett, A.H. (2007). Classical nuclear localization signals: definition, function, and interaction with importin alpha. J Biol Chem *282*, 5101-5105.

Larson, J.R., Bharucha, J.P., Ceaser, S., Salamon, J., Richardson, C.J., Rivera, S.M., and Tatchell, K. (2008). Protein phosphatase type 1 directs chitin synthesis at the bud neck in Saccharomyces cerevisiae. Molecular biology of the cell *19*, 3040-3051.

Lebensohn, A.M., and Kirschner, M.W. (2009). Activation of the WAVE complex by coincident signals controls actin assembly. Molecular cell *36*, 512-524.

Lesage, B., Qian, J., and Bollen, M. (2011). Spindle checkpoint silencing: PP1 tips the balance. Current biology : CB *21*, R898-903.

Leung, T., Chen, X.Q., Manser, E., and Lim, L. (1996). The p160 RhoA-binding kinase ROK alpha is a member of a kinase family and is involved in the reorganization of the cytoskeleton. Molecular and cellular biology *16*, 5313-5327.

Li, L., Kozlowski, K., Wegner, B., Rashid, T., Yeung, T., Holmes, C., and Ballermann, B.J. (2007). Phosphorylation of TIMAP by glycogen synthase kinase-3beta activates its associated protein phosphatase 1. J Biol Chem *282*, 25960-25969.

Li, S., Chang, S., Qi, X., Richardson, J.A., and Olson, E.N. (2006). Requirement of a myocardin-related transcription factor for development of mammary myoepithelial cells. Molecular and cellular biology *26*, 5797-5808.

Li, S., Wang, D.Z., Wang, Z., Richardson, J.A., and Olson, E.N. (2003). The serum response factor coactivator myocardin is required for vascular smooth muscle development. Proc Natl Acad Sci U S A *100*, 9366-9370.

Liepina, I., Czaplewski, C., Janmey, P., and Liwo, A. (2003). Molecular dynamics study of a gelsolin-derived peptide binding to a lipid bilayer containing phosphatidylinositol 4,5-bisphosphate. Biopolymers *71*, 49-70.

Lodish H, B.A., Zipursky S L, Matsudaira P, Baltimore D , Darnell J (2000). The Dynamics of Actin Assembly, Vol 4th edition (New York).

Low, T.L., Hu, S.K., and Goldstein, A.L. (1981). Complete amino acid sequence of bovine thymosin beta 4: a thymic hormone that induces terminal deoxynucleotidyl transferase activity in thymocyte populations. Proc Natl Acad Sci U S A *78*, 1162-1166.

Lu, X., Wang, L., Chen, S., He, L., Yang, X., Shi, Y., Cheng, J., Zhang, L., Gu, C.C., Huang, J.*, et al.* (2012). Genome-wide association study in Han Chinese identifies four new susceptibility loci for coronary artery disease. Nature genetics *44*, 890-894.

Lymn, R.W., and Taylor, E.W. (1971). Mechanism of adenosine triphosphate hydrolysis by actomyosin. Biochemistry *10*, 4617-4624.

Ma, H., Siegel, A.J., and Berezney, R. (1999). Association of chromosome territories with the nuclear matrix. Disruption of human chromosome territories correlates with the release of a subset of nuclear matrix proteins. J Cell Biol *146*, 531-542.

Ma, X., Kovacs, M., Conti, M.A., Wang, A., Zhang, Y., Sellers, J.R., and Adelstein, R.S. (2012). Nonmuscle myosin II exerts tension but does not translocate actin in vertebrate cytokinesis. Proc Natl Acad Sci U S A *109*, 4509-4514.

Ma, Z., Morris, S.W., Valentine, V., Li, M., Herbrick, J.A., Cui, X., Bouman, D., Li, Y., Mehta, P.K., Nizetic, D.*, et al.* (2001). Fusion of two novel genes, RBM15 and MKL1, in the t(1;22)(p13;q13) of acute megakaryoblastic leukemia. Nature genetics *28*, 220-221.

Mabuchi, Y., Mabuchi, K., Stafford, W.F., and Grabarek, Z. (2010). Modular structure of smooth muscle Myosin light chain kinase: hydrodynamic modeling and functional implications. Biochemistry *49*, 2903-2917.

Mahoney, N.M., Rozwarski, D.A., Fedorov, E., Fedorov, A.A., and Almo, S.C. (1999). Profilin binds proline-rich ligands in two distinct amide backbone orientations. Nature structural biology *6*, 666-671.

Malenka, R.C., and Bear, M.F. (2004). LTP and LTD: an embarrassment of riches. Neuron *44*, 5-21.

Maraganore, D.M., de Andrade, M., Lesnick, T.G., Strain, K.J., Farrer, M.J., Rocca, W.A., Pant, P.V., Frazer, K.A., Cox, D.R., and Ballinger, D.G. (2005). High-resolution whole-genome association study of Parkinson disease. American journal of human genetics *77*, 685-693.

Marais, R., Wynne, J., and Treisman, R. (1993). The SRF accessory protein Elk-1 contains a growth factor-regulated transcriptional activation domain. Cell *73*, 381-393.

Matsumura, F. (2005). Regulation of myosin II during cytokinesis in higher eukaryotes. Trends in cell biology *15*, 371-377.

Mayol, X., Garriga, J., and Grana, X. (1995). Cell cycle-dependent phosphorylation of the retinoblastoma-related protein p130. Oncogene *11*, 801-808.

McCallion, A.S., Emison, E.S., Kashuk, C.S., Bush, R.T., Kenton, M., Carrasquillo, M.M., Jones, K.W., Kennedy, G.C., Portnoy, M.E., Green, E.D.*, et al.* (2003). Genomic variation in multigenic traits: Hirschsprung disease. Cold Spring Harb Symp Quant Biol *68*, 373-381.

McDonald, D., Carrero, G., Andrin, C., de Vries, G., and Hendzel, M.J. (2006). Nucleoplasmic beta-actin exists in a dynamic equilibrium between low-mobility polymeric species and rapidly diffusing populations. J Cell Biol *172*, 541-552.

McGough, A.M., Staiger, C.J., Min, J.K., and Simonetti, K.D. (2003). The gelsolin family of actin regulatory proteins: modular structures, versatile functions. FEBS Lett *552*, 75-81.

Medjkane, S., Perez-Sanchez, C., Gaggioli, C., Sahai, E., and Treisman, R. (2009). Myocardin-related transcription factors and SRF are required for cytoskeletal dynamics and experimental metastasis. Nature cell biology *11*, 257-268.

Mercher, T., Coniat, M.B., Monni, R., Mauchauffe, M., Nguyen Khac, F., Gressin, L., Mugneret, F., Leblanc, T., Dastugue, N., Berger, R.*, et al.* (2001). Involvement of a human gene related to the Drosophila spen gene in the recurrent t(1;22) translocation of acute megakaryocytic leukemia. Proc Natl Acad Sci U S A *98*, 5776-5779.

Miki, H., Suetsugu, S., and Takenawa, T. (1998). WAVE, a novel WASP-family protein involved in actin reorganization induced by Rac. The EMBO journal *17*, 6932-6941.

Miki, H., Yamaguchi, H., Suetsugu, S., and Takenawa, T. (2000). IRSp53 is an essential intermediate between Rac and WAVE in the regulation of membrane ruffling. Nature *408*, 732-735.

Miki, T., Okawa, K., Sekimoto, T., Yoneda, Y., Watanabe, S., Ishizaki, T., and Narumiya, S. (2009). mDia2 shuttles between the nucleus and the cytoplasm through the importin-{alpha}/{beta}- and CRM1-mediated nuclear transport mechanism. J Biol Chem *284*, 5753-5762.

Millard, T.H., Sharp, S.J., and Machesky, L.M. (2004). Signalling to actin assembly via the WASP (Wiskott-Aldrich syndrome protein)-family proteins and the Arp2/3 complex. The Biochemical journal *380*, 1-17.

Minden, A., Lin, A., Claret, F.X., Abo, A., and Karin, M. (1995). Selective activation of the JNK signaling cascade and c-Jun transcriptional activity by the small GTPases Rac and Cdc42Hs. Cell *81*, 1147-1157.

Miralles, F., Posern, G., Zaromytidou, A.I., and Treisman, R. (2003). Actin dynamics control SRF activity by regulation of its coactivator MAL. Cell *113*, 329-342.

Mirkovitch, J., Mirault, M.E., and Laemmli, U.K. (1984). Organization of the higher-order chromatin loop: specific DNA attachment sites on nuclear scaffold. Cell *39*, 223-232.

Miyamoto, K., Pasque, V., Jullien, J., and Gurdon, J.B. (2011). Nuclear actin polymerization is required for transcriptional reprogramming of Oct4 by oocytes. Genes & development *25*, 946-958.

Mooren, O.L., Galletta, B.J., and Cooper, J.A. (2012). Roles for actin assembly in endocytosis. Annual review of biochemistry *81*, 661-686.

Morii, N., and Narumiya, S. (1995). Preparation of native and recombinant Clostridium botulinum C3 ADP-ribosyltransferase and identification of Rho proteins by ADP-ribosylation. Methods in enzymology *256*, 196-206.

Morrison, D.K., and Davis, R.J. (2003). Regulation of MAP kinase signaling modules by scaffold proteins in mammals. Annual review of cell and developmental biology *19*, 91-118.

Mouilleron, S., Guettler, S., Langer, C.A., Treisman, R., and McDonald, N.Q. (2008). Molecular basis for G-actin binding to RPEL motifs from the serum response factor coactivator MAL. The EMBO journal *27*, 3198-3208.

Mouilleron, S., Langer, C.A., Guettler, S., McDonald, N.Q., and Treisman, R. (2011). Structure of a pentavalent G-actin*MRTF-A complex reveals how G-actin controls nucleocytoplasmic shuttling of a transcriptional coactivator. Sci Signal *4*, ra40.

Mouilleron, S., Wiezlak, M., O'Reilly, N., Treisman, R., and McDonald, N.Q. (2012). Structures of the Phactr1 RPEL domain and RPEL motif complexes with G-actin reveal the molecular basis for actin binding cooperativity. Structure *20*, 1960-1970.

Munton, R.P., Vizi, S., and Mansuy, I.M. (2004). The role of protein phosphatase-1 in the modulation of synaptic and structural plasticity. FEBS Lett *567*, 121-128.

Murata-Hori, M., Suizu, F., Iwasaki, T., Kikuchi, A., and Hosoya, H. (1999). ZIP kinase identified as a novel myosin regulatory light chain kinase in HeLa cells. FEBS Lett *451*, 81-84.

Nagaoka, R., Abe, H., Kusano, K., and Obinata, T. (1995). Concentration of cofilin, a small actin-binding protein, at the cleavage furrow during cytokinesis. Cell motility and the cytoskeleton *30*, 1-7.

Nagaoka, R., Abe, H., and Obinata, T. (1996). Site-directed mutagenesis of the phosphorylation site of cofilin: its role in cofilin-actin interaction and cytoplasmic localization. Cell motility and the cytoskeleton *35*, 200-209.

Nair, U.B., Joel, P.B., Wan, Q., Lowey, S., Rould, M.A., and Trybus, K.M. (2008). Crystal structures of monomeric actin bound to cytochalasin D. J Mol Biol *384*, 848-864.

Nelson, D.A., Krucher, N.A., and Ludlow, J.W. (1997). High molecular weight protein phosphatase type 1 dephosphorylates the retinoblastoma protein. J Biol Chem *272*, 4528-4535.

Neufeld, G., Cohen, T., Shraga, N., Lange, T., Kessler, O., and Herzog, Y. (2002). The neuropilins: multifunctional semaphorin and VEGF receptors that modulate axon guidance and angiogenesis. Trends in cardiovascular medicine *12*, 13-19.

Niiro, N., Koga, Y., and Ikebe, M. (2003). Agonist-induced changes in the phosphorylation of the myosin- binding subunit of myosin light chain phosphatase and CPI17, two regulatory factors of myosin light chain phosphatase, in smooth muscle. The Biochemical journal *369*, 117-128.

Nobes, C.D., and Hall, A. (1995). Rho, rac, and cdc42 GTPases regulate the assembly of multimolecular focal complexes associated with actin stress fibers, lamellipodia, and filopodia. Cell *81*, 53-62.

Norman, C., Runswick, M., Pollock, R., and Treisman, R. (1988). Isolation and properties of cDNA clones encoding SRF, a transcription factor that binds to the c-fos serum response element. Cell *55*, 989-1003.

O'Donnell, C.J., Kavousi, M., Smith, A.V., Kardia, S.L., Feitosa, M.F., Hwang, S.J., Sun, Y.V., Province, M.A., Aspelund, T., Dehghan, A.*, et al.* (2011). Genome-wide association study for coronary artery calcification with follow-up in myocardial infarction. Circulation *124*, 2855-2864.

Oda, T., Iwasa, M., Aihara, T., Maeda, Y., and Narita, A. (2009). The nature of the globular- to fibrous-actin transition. Nature *457*, 441-445.

Oh, J., Richardson, J.A., and Olson, E.N. (2005). Requirement of myocardin-related transcription factor-B for remodeling of branchial arch arteries and smooth muscle differentiation. Proc Natl Acad Sci U S A *102*, 15122-15127.

Oikawa, T., and Yamada, T. (2003). Molecular biology of the Ets family of transcription factors. Gene *303*, 11-34.

Ojala, P.J., Paavilainen, V.O., Vartiainen, M.K., Tuma, R., Weeds, A.G., and Lappalainen, P. (2002). The two ADF-H domains of twinfilin play functionally distinct roles in interactions with actin monomers. Molecular biology of the cell *13*, 3811-3821.

Oliver, C.J., Terry-Lorenzo, R.T., Elliott, E., Bloomer, W.A., Li, S., Brautigan, D.L., Colbran, R.J., and Shenolikar, S. (2002). Targeting protein phosphatase 1 (PP1) to the actin cytoskeleton: the neurabin I/PP1 complex regulates cell morphology. Molecular and cellular biology *22*, 4690-4701.

Olson, E.N., and Nordheim, A. (2010). Linking actin dynamics and gene transcription to drive cellular motile functions. Nature reviews Molecular cell biology *11*, 353-365.

Olson, M.F., and Sahai, E. (2009). The actin cytoskeleton in cancer cell motility. Clinical & experimental metastasis *26*, 273-287.

Opdecamp, K., Nakayama, A., Nguyen, M.T., Hodgkinson, C.A., Pavan, W.J., and Arnheiter, H. (1997). Melanocyte development in vivo and in neural crest cell cultures: crucial dependence on the Mitf basic-helix-loop-helix-zipper transcription factor. Development *124*, 2377-2386.

Paavilainen, V.O., Oksanen, E., Goldman, A., and Lappalainen, P. (2008). Structure of the actin-depolymerizing factor homology domain in complex with actin. J Cell Biol *182*, 51-59.

Paddison, P.J., Silva, J.M., Conklin, D.S., Schlabach, M., Li, M., Aruleba, S., Balija, V., O'Shaughnessy, A., Gnoj, L., Scobie, K.*, et al.* (2004). A resource for large-scale RNA-interference-based screens in mammals. Nature *428*, 427-431.

Padrick, S.B., Cheng, H.C., Ismail, A.M., Panchal, S.C., Doolittle, L.K., Kim, S., Skehan, B.M., Umetani, J., Brautigam, C.A., Leong, J.M.*, et al.* (2008). Hierarchical regulation of WASP/WAVE proteins. Molecular cell *32*, 426-438.

Pardee, J.D., Simpson, P.A., Stryer, L., and Spudich, J.A. (1982). Actin filaments undergo limited subunit exchange in physiological salt conditions. J Cell Biol *94*, 316-324.

Patel, R.S., Morris, A.A., Ahmed, Y., Kavtaradze, N., Sher, S., Su, S., Zafari, A.M., Din-Dzietham, R., Waddy, S.P., Vaccarino, V.*, et al.* (2012). A genetic risk variant for myocardial infarction on chromosome 6p24 is associated with impaired central hemodynamic indexes. American journal of hypertension *25*, 797-803.

Paul, A.S., and Pollard, T.D. (2009). Energetic requirements for processive elongation of actin filaments by FH1FH2-formins. J Biol Chem *284*, 12533-12540.

Pawlowski, R., Rajakyla, E.K., Vartiainen, M.K., and Treisman, R. (2010). An actin-regulated importin alpha/beta-dependent extended bipartite NLS directs nuclear import of MRTF-A. The EMBO journal *29*, 3448-3458.

Pechlivanis, S., Muhleisen, T.W., Mohlenkamp, S., Schadendorf, D., Erbel, R., Jockel, K.H., Hoffmann, P., Nothen, M.M., Scherag, A., and Moebus, S. (2013). Risk loci for coronary artery calcification replicated at 9p21 and 6q24 in the Heinz Nixdorf Recall Study. BMC medical genetics *14*, 23.

Pederson, T. (2008). As functional nuclear actin comes into view, is it globular, filamentous, or both? J Cell Biol *180*, 1061-1064.

Pellegrin, S., and Mellor, H. (2007). Actin stress fibres. Journal of cell science *120*, 3491-3499.

Pellegrini, L., Tan, S., and Richmond, T.J. (1995). Structure of serum response factor core bound to DNA. Nature *376*, 490-498.

Percipalle, P. (2012). Co-transcriptional nuclear actin dynamics. Nucleus *4*.

Perona, R., Montaner, S., Saniger, L., Sanchez-Perez, I., Bravo, R., and Lacal, J.C. (1997). Activation of the nuclear factor-kappaB by Rho, CDC42, and Rac-1 proteins. Genes & development *11*, 463-475.

Philippar, U., Schratt, G., Dieterich, C., Muller, J.M., Galgoczy, P., Engel, F.B., Keating, M.T., Gertler, F., Schule, R., Vingron, M.*, et al.* (2004). The SRF target gene Fhl2 antagonizes RhoA/MAL-dependent activation of SRF. Molecular cell *16*, 867-880.

Polet, D., Lambrechts, A., Vandepoele, K., Vandekerckhove, J., and Ampe, C. (2007). On the origin and evolution of vertebrate and viral profilins. FEBS Lett *581*, 211-217.

Pollard, T.D. (2010). Mechanics of cytokinesis in eukaryotes. Curr Opin Cell Biol *22*, 50-56.

Pollard, T.D., and Borisy, G.G. (2003). Cellular motility driven by assembly and disassembly of actin filaments. Cell *112*, 453-465.

Pollard, T.D., and Cooper, J.A. (2009). Actin, a central player in cell shape and movement. Science *326*, 1208-1212.

Posern, G., Miralles, F., Guettler, S., and Treisman, R. (2004). Mutant actins that stabilise F-actin use distinct mechanisms to activate the SRF coactivator MAL. The EMBO journal *23*, 3973-3983.

Posern, G., Sotiropoulos, A., and Treisman, R. (2002). Mutant actins demonstrate a role for unpolymerized actin in control of transcription by serum response factor. Molecular biology of the cell *13*, 4167-4178.

Posern, G., and Treisman, R. (2006). Actin' together: serum response factor, its cofactors and the link to signal transduction. Trends in cell biology *16*, 588-596.

Pring, M., Evangelista, M., Boone, C., Yang, C., and Zigmond, S.H. (2003). Mechanism of formin-induced nucleation of actin filaments. Biochemistry *42*, 486-496.

Puls, A., Eliopoulos, A.G., Nobes, C.D., Bridges, T., Young, L.S., and Hall, A. (1999). Activation of the small GTPase Cdc42 by the inflammatory cytokines TNF(alpha) and IL-1, and by the Epstein-Barr virus transforming protein LMP1. Journal of cell science *112 ( Pt 17)*, 2983-2992.

Qi, L., Parast, L., Cai, T., Powers, C., Gervino, E.V., Hauser, T.H., Hu, F.B., and Doria, A. (2011). Genetic susceptibility to coronary heart disease in type 2 diabetes: 3 independent studies. Journal of the American College of Cardiology *58*, 2675-2682.

Qian, L., Huang, Y., Spencer, C.I., Foley, A., Vedantham, V., Liu, L., Conway, S.J., Fu, J.D., and Srivastava, D. (2012). In vivo reprogramming of murine cardiac fibroblasts into induced cardiomyocytes. Nature *485*, 593-598.

Rayment, I., Holden, H.M., Whittaker, M., Yohn, C.B., Lorenz, M., Holmes, K.C., and Milligan, R.A. (1993). Structure of the actin-myosin complex and its implications for muscle contraction. Science *261*, 58-65.

Rebrikov, D.V., Desai, S.M., Siebert, P.D., and Lukyanov, S.A. (2004). Suppression subtractive hybridization. Methods Mol Biol *258*, 107-134.

Ridley, A.J., and Hall, A. (1992). The small GTP-binding protein rho regulates the assembly of focal adhesions and actin stress fibers in response to growth factors. Cell *70*, 389-399.

Ridley, A.J., Paterson, H.F., Johnston, C.L., Diekmann, D., and Hall, A. (1992). The small GTP-binding protein rac regulates growth factor-induced membrane ruffling. Cell *70*, 401-410.

Riento, K., and Ridley, A.J. (2003). Rocks: multifunctional kinases in cell behaviour. Nature reviews Molecular cell biology *4*, 446-456.

Robbins, J., Dilworth, S.M., Laskey, R.A., and Dingwall, C. (1991). Two interdependent basic domains in nucleoplasmin nuclear targeting sequence: identification of a class of bipartite nuclear targeting sequence. Cell *64*, 615-623.

Rost, B., Yachdav, G., and Liu, J. (2004). The PredictProtein server. Nucleic acids research *32*, W321-326.

Rothenbach, P.A., Dahl, B., Schwartz, J.J., O'Keefe, G.E., Yamamoto, M., Lee, W.M., Horton, J.W., Yin, H.L., and Turnage, R.H. (2004). Recombinant plasma gelsolin infusion attenuates burn-induced pulmonary microvascular dysfunction. J Appl Physiol *96*, 25-31.

Rouiller, I., Xu, X.P., Amann, K.J., Egile, C., Nickell, S., Nicastro, D., Li, R., Pollard, T.D., Volkmann, N., and Hanein, D. (2008). The structural basis of actin filament branching by the Arp2/3 complex. J Cell Biol *180*, 887-895.

Roy, J., and Cyert, M.S. (2009). Cracking the phosphatase code: docking interactions determine substrate specificity. Sci Signal *2*, re9.

Sagara, J., Arata, T., and Taniguchi, S. (2009). Scapinin, the protein phosphatase 1 binding protein, enhances cell spreading and motility by interacting with the actin cytoskeleton. PloS one *4*, e4247.

Sagara, J., Higuchi, T., Hattori, Y., Moriya, M., Sarvotham, H., Shima, H., Shirato, H., Kikuchi, K., and Taniguchi, S. (2003). Scapinin, a putative protein phosphatase-1 regulatory subunit associated with the nuclear nonchromatin structure. J Biol Chem *278*, 45611-45619.

Sahai, E., Alberts, A.S., and Treisman, R. (1998). RhoA effector mutants reveal distinct effector pathways for cytoskeletal reorganization, SRF activation and transformation. The EMBO journal *17*, 1350-1361.

Sahai, E., and Marshall, C.J. (2002). ROCK and Dia have opposing effects on adherens junctions downstream of Rho. Nature cell biology *4*, 408-415.

Sakisaka, T., Nakanishi, H., Takahashi, K., Mandai, K., Miyahara, M., Satoh, A., Takaishi, K., and Takai, Y. (1999). Different behavior of l-afadin and neurabin-II during the formation and destruction of cell-cell adherens junction. Oncogene *18*, 1609-1617.

Satoh, A., Nakanishi, H., Obaishi, H., Wada, M., Takahashi, K., Satoh, K., Hirao, K., Nishioka, H., Hata, Y., Mizoguchi, A*., et al.* (1998). Neurabin-II/spinophilin. An actin filament-binding protein with one pdz domain localized at cadherin-based cell-cell adhesion sites. J Biol Chem *273*, 3470-3475.

Schillace, R.V., Voltz, J.W., Sim, A.T., Shenolikar, S., and Scott, J.D. (2001). Multiple interactions within the AKAP220 signaling complex contribute to protein phosphatase 1 regulation. J Biol Chem *276*, 12128-12134.

Schlabach, M.R., Luo, J., Solimini, N.L., Hu, G., Xu, Q., Li, M.Z., Zhao, Z., Smogorzewska, A., Sowa, M.E., Ang, X.L*., et al.* (2008). Cancer proliferation gene discovery through functional genomics. Science *319*, 620-624.

Schratt, G., Philippar, U., Berger, J., Schwarz, H., Heidenreich, O., and Nordheim, A. (2002). Serum response factor is crucial for actin cytoskeletal organization and focal adhesion assembly in embryonic stem cells. J Cell Biol *156*, 737-750.

Sellers, J.R. (2000). Myosins: a diverse superfamily. Biochim Biophys Acta *1496*, 3-22.

Selvaraj, A., and Prywes, R. (2004). Expression profiling of serum inducible genes identifies a subset of SRF target genes that are MKL dependent. BMC molecular biology *5*, 13.

Sen, R., and Baltimore, D. (1986). Multiple nuclear factors interact with the immunoglobulin enhancer sequences. Cell *46*, 705-716.

Senger, D.R., Galli, S.J., Dvorak, A.M., Perruzzi, C.A., Harvey, V.S., and Dvorak, H.F. (1983). Tumor cells secrete a vascular permeability factor that promotes accumulation of ascites fluid. Science *219*, 983-985.

Shaw, P.E., Schroter, H., and Nordheim, A. (1989). The ability of a ternary complex to form over the serum response element correlates with serum inducibility of the human c-fos promoter. Cell *56*, 563-572.

Shikama, N., Lee, C.W., France, S., Delavaine, L., Lyon, J., Krstic-Demonacos, M., and La Thangue, N.B. (1999). A novel cofactor for p300 that regulates the p53 response. Molecular cell *4*, 365-376.

Shimizu, Y., Thumkeo, D., Keel, J., Ishizaki, T., Oshima, H., Oshima, M., Noda, Y., Matsumura, F., Taketo, M.M., and Narumiya, S. (2005). ROCK-I regulates closure of the eyelids and ventral body wall by inducing assembly of actomyosin bundles. J Cell Biol *168*, 941-953.

Shin, H.M., Je, H.D., Gallant, C., Tao, T.C., Hartshorne, D.J., Ito, M., and Morgan, K.G. (2002). Differential association and localization of myosin phosphatase subunits during agonist-induced signal transduction in smooth muscle. Circulation research *90*, 546-553.

Shirato, H., Shima, H., Sakashita, G., Nakano, T., Ito, M., Lee, E.Y., and Kikuchi, K. (2000). Identification and characterization of a novel protein inhibitor of type 1 protein phosphatase. Biochemistry *39*, 13848-13855.

Shore, P., and Sharrocks, A.D. (1995). The MADS-box family of transcription factors. Eur J Biochem *229*, 1-13.

Silacci, P., Mazzolai, L., Gauci, C., Stergiopulos, N., Yin, H.L., and Hayoz, D. (2004). Gelsolin superfamily proteins: key regulators of cellular functions. Cellular and molecular life sciences : CMLS *61*, 2614-2623.

Silva, J.M., Li, M.Z., Chang, K., Ge, W., Golding, M.C., Rickles, R.J., Siolas, D., Hu, G., Paddison, P.J., Schlabach, M.R.*, et al.* (2005). Second-generation shRNA libraries covering the mouse and human genomes. Nature genetics *37*, 1281-1288.

Small, E.M., Warkman, A.S., Wang, D.Z., Sutherland, L.B., Olson, E.N., and Krieg, P.A. (2005). Myocardin is sufficient and necessary for cardiac gene expression in Xenopus. Development *132*, 987-997.

Solimini, N.L., Liang, A.C., Xu, C., Pavlova, N.N., Xu, Q., Davoli, T., Li, M.Z., Wong, K.K., and Elledge, S.J. (2013). STOP gene Phactr4 is a tumor suppressor. Proc Natl Acad Sci U S A *110*, E407-414.

Solimini, N.L., Xu, Q., Mermel, C.H., Liang, A.C., Schlabach, M.R., Luo, J., Burrows, A.E., Anselmo, A.N., Bredemeyer, A.L., Li, M.Z.*, et al.* (2012). Recurrent hemizygous deletions in cancers may optimize proliferative potential. Science *337*, 104-109.

Somlyo, A.P., and Somlyo, A.V. (2000). Signal transduction by G-proteins, rho-kinase and protein phosphatase to smooth muscle and non-muscle myosin II. The Journal of physiology *522 Pt 2*, 177-185.

Somlyo, A.V., Bradshaw, D., Ramos, S., Murphy, C., Myers, C.E., and Somlyo, A.P. (2000). Rho-kinase inhibitor retards migration and in vivo dissemination of human prostate cancer cells. Biochemical and biophysical research communications *269*, 652-659.

Sotiropoulos, A., Gineitis, D., Copeland, J., and Treisman, R. (1999). Signal-regulated activation of serum response factor is mediated by changes in actin dynamics. Cell *98*, 159-169.

Spector, I., Shochet, N.R., Kashman, Y., and Groweiss, A. (1983). Latrunculins: novel marine toxins that disrupt microfilament organization in cultured cells. Science *219*, 493-495.

Steffen, A., Rottner, K., Ehinger, J., Innocenti, M., Scita, G., Wehland, J., and Stradal, T.E. (2004). Sra-1 and Nap1 link Rac to actin assembly driving lamellipodia formation. The EMBO journal *23*, 749-759.

Strack, S., Barban, M.A., Wadzinski, B.E., and Colbran, R.J. (1997). Differential inactivation of postsynaptic density-associated and soluble Ca2+/calmodulin-dependent protein kinase II by protein phosphatases 1 and 2A. Journal of neurochemistry *68*, 2119-2128.

Straight, A.F., Cheung, A., Limouze, J., Chen, I., Westwood, N.J., Sellers, J.R., and Mitchison, T.J. (2003). Dissecting temporal and spatial control of cytokinesis with a myosin II Inhibitor. Science *299*, 1743-1747.

Stuven, T., Hartmann, E., and Gorlich, D. (2003). Exportin 6: a novel nuclear export receptor that is specific for profilin.actin complexes. The EMBO journal *22*, 5928-5940.

Suetsugu, S., and Takenawa, T. (2003). Translocation of N-WASP by nuclear localization and export signals into the nucleus modulates expression of HSP90. J Biol Chem *278*, 42515-42523.

Sun, H., Lin, K., and Yin, H.L. (1997). Gelsolin modulates phospholipase C activity in vivo through phospholipid binding. J Cell Biol *138*, 811-820.

Sun, H.Q., Yamamoto, M., Mejillano, M., and Yin, H.L. (1999). Gelsolin, a multifunctional actin regulatory protein. J Biol Chem *274*, 33179-33182.

Tan, S.L., Tareen, S.U., Melville, M.W., Blakely, C.M., and Katze, M.G. (2002). The direct binding of the catalytic subunit of protein phosphatase 1 to the PKR protein kinase is necessary but not sufficient for inactivation and disruption of enzyme dimer formation. J Biol Chem *277*, 36109-36117.

Tapon, N., Nagata, K., Lamarche, N., and Hall, A. (1998). A new rac target POSH is an SH3-containing scaffold protein involved in the JNK and NF-kappaB signalling pathways. The EMBO journal *17*, 1395-1404.

Teramoto, H., Coso, O.A., Miyata, H., Igishi, T., Miki, T., and Gutkind, J.S. (1996). Signaling from the small GTP-binding proteins Rac1 and Cdc42 to the c-Jun N-terminal kinase/stress-activated protein kinase pathway. A role for mixed lineage kinase 3/protein-tyrosine kinase 1, a novel member of the mixed lineage kinase family. J Biol Chem *271*, 27225-27228.

Terrak, M., Kerff, F., Langsetmo, K., Tao, T., and Dominguez, R. (2004). Structural basis of protein phosphatase 1 regulation. Nature *429*, 780-784.

Terry-Lorenzo, R.T., Roadcap, D.W., Otsuka, T., Blanpied, T.A., Zamorano, P.L., Garner, C.C., Shenolikar, S., and Ehlers, M.D. (2005). Neurabin/protein phosphatase-1 complex regulates dendritic spine morphogenesis and maturation. Molecular biology of the cell *16*, 2349-2362.

Treisman, R. (1986). Identification of a protein-binding site that mediates transcriptional response of the c-fos gene to serum factors. Cell *46*, 567-574.

Treisman, R. (1994). Ternary complex factors: growth factor regulated transcriptional activators. Current opinion in genetics & development *4*, 96-101.

Trinkle-Mulcahy, L., Ajuh, P., Prescott, A., Claverie-Martin, F., Cohen, S., Lamond, A.I., and Cohen, P. (1999). Nuclear organisation of NIPP1, a regulatory subunit of protein phosphatase 1 that associates with pre-mRNA splicing factors. Journal of cell science *112 ( Pt 2)*, 157-168.

Trufant, J.W. (2010). Phactr1 as a novel biomarker to distinguish malignant melanoma from nevus. Yale University School of Medicine *M.D. thesis*.

Tsuji, T., Ishizaki, T., Okamoto, M., Higashida, C., Kimura, K., Furuyashiki, T., Arakawa, Y., Birge, R.B., Nakamoto, T., Hirai, H*., et al.* (2002). ROCK and mDia1 antagonize in Rho-dependent Rac activation in Swiss 3T3 fibroblasts. J Cell Biol *157*, 819-830.

Vale, R.D., and Milligan, R.A. (2000). The way things move: looking under the hood of molecular motor proteins. Science *288*, 88-95.

Vance, K.W., and Goding, C.R. (2004). The transcription network regulating melanocyte development and melanoma. Pigment cell research / sponsored by the European Society for Pigment Cell Research and the International Pigment Cell Society *17*, 318-325.

Vartiainen, M.K., Guettler, S., Larijani, B., and Treisman, R. (2007). Nuclear actin regulates dynamic subcellular localization and activity of the SRF cofactor MAL. Science *316*, 1749-1752.

Vartiainen, M.K., and Machesky, L.M. (2004). The WASP-Arp2/3 pathway: genetic insights. Curr Opin Cell Biol *16*, 174-181.

Vietri, M., Bianchi, M., Ludlow, J.W., Mittnacht, S., and Villa-Moruzzi, E. (2006). Direct interaction between the catalytic subunit of Protein Phosphatase 1 and pRb. Cancer cell international *6*, 3.

Wang, D., Chang, P.S., Wang, Z., Sutherland, L., Richardson, J.A., Small, E., Krieg, P.A., and Olson, E.N. (2001). Activation of cardiac gene expression by myocardin, a transcriptional cofactor for serum response factor. Cell *105*, 851-862.

Wang, D.Z., Li, S., Hockemeyer, D., Sutherland, L., Wang, Z., Schratt, G., Richardson, J.A., Nordheim, A., and Olson, E.N. (2002). Potentiation of serum response factor activity by a family of myocardin-related transcription factors. Proc Natl Acad Sci U S A *99*, 14855-14860.

Wang, F., Kovacs, M., Hu, A., Limouze, J., Harvey, E.V., and Sellers, J.R. (2003a). Kinetic mechanism of non-muscle myosin IIB: functional adaptations for tension generation and maintenance. J Biol Chem *278*, 27439-27448.

Wang, L.E., Gorlova, O.Y., Ying, J., Qiao, Y., Weng, S.F., Lee, A.T., Gregersen, P.K., Spitz, M.R., Amos, C.I., and Wei, Q. (2013). Genome-wide association study reveals novel genetic determinants of DNA repair capacity in lung cancer. Cancer research *73*, 256-264.

Wang, Z., Wang, D.Z., Pipes, G.C., and Olson, E.N. (2003b). Myocardin is a master regulator of smooth muscle gene expression. Proc Natl Acad Sci U S A *100*, 7129-7134.

Washington, K., Ammosova, T., Beullens, M., Jerebtsova, M., Kumar, A., Bollen, M., and Nekhai, S. (2002). Protein phosphatase-1 dephosphorylates the C-terminal domain of RNA polymerase-II. J Biol Chem *277*, 40442-40448.

Watanabe, N., Kato, T., Fujita, A., Ishizaki, T., and Narumiya, S. (1999). Cooperation between mDia1 and ROCK in Rho-induced actin reorganization. Nature cell biology *1*, 136-143.

Wegner, A. (1976). Head to tail polymerization of actin. J Mol Biol *108*, 139-150.

Weinberg, R.A. (1995). The retinoblastoma protein and cell cycle control. Cell *81*, 323-330.

Weiner, O.D., Rentel, M.C., Ott, A., Brown, G.E., Jedrychowski, M., Yaffe, M.B., Gygi, S.P., Cantley, L.C., Bourne, H.R., and Kirschner, M.W. (2006). Hem-1 complexes are essential for Rac activation, actin polymerization, and myosin regulation during neutrophil chemotaxis. PLoS biology *4*, e38.

Weston, C.R., and Davis, R.J. (2007). The JNK signal transduction pathway. Curr Opin Cell Biol *19*, 142-149.

Westphal, R.S., Tavalin, S.J., Lin, J.W., Alto, N.M., Fraser, I.D., Langeberg, L.K., Sheng, M., and Scott, J.D. (1999). Regulation of NMDA receptors by an associated phosphatase-kinase signaling complex. Science *285*, 93-96.

Wider, C., Lincoln, S.J., Heckman, M.G., Diehl, N.N., Stone, J.T., Haugarvoll, K., Aasly, J.O., Gibson, J.M., Lynch, T., Rajput, A*., et al.* (2009). Phactr2 and Parkinson's disease. Neuroscience letters *453*, 9-11.

Wiezlak, M., Diring, J., Abella, J., Mouilleron, S., Way, M., McDonald, N.Q., and Treisman, R. (2012). G-actin regulates the shuttling and PP1 binding of the RPEL protein Phactr1 to control actomyosin assembly. Journal of cell science *125*, 5860-5872.

Wilkinson, S., Paterson, H.F., and Marshall, C.J. (2005). Cdc42-MRCK and Rho-ROCK signalling cooperate in myosin phosphorylation and cell invasion. Nature cell biology *7*, 255-261.

Wilson, D.P., Sutherland, C., Borman, M.A., Deng, J.T., Macdonald, J.A., and Walsh, M.P. (2005). Integrin-linked kinase is responsible for Ca2+-independent myosin diphosphorylation and contraction of vascular smooth muscle. The Biochemical journal *392*, 641-648.

Wu, D.Y., Tkachuck, D.C., Roberson, R.S., and Schubach, W.H. (2002). The human SNF5/INI1 protein facilitates the function of the growth arrest and DNA damage-inducible protein (GADD34) and modulates GADD34-bound protein phosphatase-1 activity. J Biol Chem *277*, 27706-27715.

Wyckoff, J.B., Pinner, S.E., Gschmeissner, S., Condeelis, J.S., and Sahai, E. (2006). ROCK- and myosin-dependent matrix deformation enables protease-independent tumor-cell invasion in vivo. Current biology : CB *16*, 1515-1523.

Xiao, Z.X., Ginsberg, D., Ewen, M., and Livingston, D.M. (1996). Regulation of the retinoblastoma protein-related protein p107 by G1 cyclin-associated kinases. Proc Natl Acad Sci U S A *93*, 4633-4637.

Yamaguchi, H., Kasa, M., Amano, M., Kaibuchi, K., and Hakoshima, T. (2006). Molecular mechanism for the regulation of rho-kinase by dimerization and its inhibition by fasudil. Structure *14*, 589-600.

Yoneda, A., Multhaupt, H.A., and Couchman, J.R. (2005). The Rho kinases I and II regulate different aspects of myosin II activity. J Cell Biol *170*, 443-453.

Yonezawa, N., Nishida, E., Iida, K., Yahara, I., and Sakai, H. (1990). Inhibition of the interactions of cofilin, destrin, and deoxyribonuclease I with actin by phosphoinositides. J Biol Chem *265*, 8382-8386.

Young, H.M., Bergner, A.J., Anderson, R.B., Enomoto, H., Milbrandt, J., Newgreen, D.F., and Whitington, P.M. (2004). Dynamics of neural crest-derived cell migration in the embryonic mouse gut. Developmental biology *270*, 455-473.

Yuen, S.L., Ogut, O., and Brozovich, F.V. (2009). Nonmuscle myosin is regulated during smooth muscle contraction. American journal of physiology Heart and circulatory physiology *297*, H191-199.

Zambetti, G., Ramsey-Ewing, A., Bortell, R., Stein, G., and Stein, J. (1991). Disruption of the cytoskeleton with cytochalasin D induces c-fos gene expression. Experimental cell research *192*, 93-101.

Zarkowska, T., and Mittnacht, S. (1997). Differential phosphorylation of the retinoblastoma protein by G1/S cyclin-dependent kinases. J Biol Chem *272*, 12738-12746.

Zaromytidou, A.I., Miralles, F., and Treisman, R. (2006). MAL and ternary complex factor use different mechanisms to contact a common surface on the serum response factor DNA-binding domain. Molecular and cellular biology *26*, 4134-4148.

Zeng, Q., Lagunoff, D., Masaracchia, R., Goeckeler, Z., Cote, G., and Wysolmerski, R. (2000). Endothelial cell retraction is induced by PAK2 monophosphorylation of myosin II. Journal of cell science *113 ( Pt 3)*, 471-482.

Zhang, W.C., Peng, Y.J., Zhang, G.S., He, W.Q., Qiao, Y.N., Dong, Y.Y., Gao, Y.Q., Chen, C., Zhang, C.H., Li, W.*, et al.* (2010). Myosin light chain kinase is necessary for tonic airway smooth muscle contraction. J Biol Chem *285*, 5522-5531.

Zhang, Y., Kim, T.H., and Niswander, L. (2012). Phactr4 regulates directional migration of enteric neural crest through PP1, integrin signaling, and cofilin activity. Genes & development *26*, 69-81.

Zhao, S., and Lee, E.Y. (1997). Targeting of the catalytic subunit of protein phosphatase-1 to the glycolytic enzyme phosphofructokinase. Biochemistry *36*, 8318-8324.

Zheng, B., Han, M., Bernier, M., and Wen, J.K. (2009). Nuclear actin and actin-binding proteins in the regulation of transcription and gene expression. The FEBS journal *276*, 2669-2685.

Zhou, G.P. (2011). The structural determinations of the leucine zipper coiled-coil domains of the cGMP-dependent protein kinase Ialpha and its interaction with the myosin binding subunit of the myosin light chains phosphase. Protein and peptide letters *18*, 966-978.

Zigmond, S.H. (2004). Formin-induced nucleation of actin filaments. Curr Opin Cell Biol *16*, 99-105.

Zuchero, J.B., Belin, B., and Mullins, R.D. (2012). Actin binding to WH2 domains regulates nuclear import of the multifunctional actin regulator JMY. Molecular biology of the cell *23*, 853-863.

Zuchero, J.B., Coutts, A.S., Quinlan, M.E., Thangue, N.B., and Mullins, R.D. (2009). p53-cofactor JMY is a multifunctional actin nucleation factor. Nature cell biology *11*, 451-459.